A New Target for Pain: Development of Tools to Study Human Histidine Triad Nucleotide Binding proteins

A DISSERTATION
SUBMITTED TO THE FACULTY OF
UNIVERSITY OF MINNESOTA
BY

Rachit Shah

IN PARTIAL FULFILLMENT OF THE REQUIREMENTS
FOR THE DEGREE OF
DOCTOR OF PHILOSOPHY

Dr. Carston Rick Wagner, Adviser

September 2017

© RACHIT SHAH (2017)

Acknowledgements

I would first like to extend my sincerest thanks to my thesis advisor Dr. Carston R. Wagner. I am very greatful for his patience, encouragement and guidance. His enthusiasm for science, patience as a mentor has and will always keep inspiring me.

I am very grateful to my committee members, Dr. Courtney Aldrich, Dr. Carrie-Haskell Leuvano and Dr. Mark Distefano for their valuable suggestion and feedback throughout my graduate studies. I would like to thank my colloborators Dr. Javier Garzon, Dr. Barry Finzel and Dr. George Wilcox. I want to thank Dr. Brock Matter and Dr. Peter Villata for help with LC-MS studies.

I want to specially thank former members of Dr. Wagner's laboratory, Dr. Adrian Fegan, Dr. Sidharth Kumaraperuma and Dr. Amit Ganger for their support and help. I would like to thank Jing Jing Shen, Anieken Okon, Trent West, Alex Strom, Ozgun Kullic, Clifford Czimar and other members in the Wagner laboratory for their generous help and friendship.

I owe my special thanks to my most important friends Nayan Patel, Kalpit Patel, Vimal Patel and Manish Gandhi for their strong support and encouragement that had carried me all through difficult times during my graduate study.

Lastly I owe my deepest gratitude to my parents and my loving younger brother Rahul Shah. This dissertation is dedicated to my family and my friends.

Table of Contents

List of Tables

Chapter 6

List of Figures

Chapter 1

Chapter 2

Chapter 3

Chapter 4

Chapter 5

Chapter 6

List of Abbreviations

HIT	Histidine Triad
HINT	Histidine Triad Nucleotide Binding Protein
AMP	Adenosine 5′-Monophosphate
PKC	Protein Kinase C
PKCI-1	Protein Kinase C Inhibitor -1
GPCRs	G-Protein Coupled Receptors
MOR	μ-Opioid Receptor
RGSZ1	Regulator of G-protein signaling Z1
NMDAR	N-Methyl-D-Aspartate Receptors
PKA	Protein Kinase A
DLFC	Dorsolateral Frontal Cortex
VTA	Ventral Trigeminal Area
NMBA	N-Nitroso Benzylamine
MITF	Micropthalmia-associated Transcription Factor
AP_4A	Diadenosine P_1-P_4-Tetraphosphate
LysRs	Lysine t-RNA synthetases
LTP	Long-term Synaptic Potentiation
PAG	Periaqueductal Gray Area
DAMGO	[D-Ala^2, N-$MePhe^4$, Gly-ol]-Enkephalin
ITC	Isothermal Titration Calorimetry
CCI	Chronic Constriction Injury
AMPA	α-amino-3-hydroxy-5-methyl-4-isoxazolepropionic acid receptor
DMSO	Dimethyl sulfoxide

EDTA	Ethylenediaminetetraacetic acid
DTT	Dithiothreitol
MPE	Maximum Possible Effect
i.c.v	Intracerebro ventricular
i.t	Intrathecal
TFA	Triflouroacetic acid
Bio-AMS	5′-amino-5′-N-(biotinyl)sulfamoyl-5′-Deoxyadenosine
TrpGc	Tryptamine-5′-Guanosine Carbamate
GMP	Guanosine 5′-Monophosphate
TEA	Tri Ethyl Amine
ACN	Acetonitrile
FRET	Forster Resonance Energy Transfer
PNS	Peripheral Nervous System
CMT1	Charcot Marie Tooth 1
MBP	Maltose Binding Protein
TEV	Tobacco Etch Virus
CD	Circular Dichroism
HEPES	4-(2-Hydroxyethyl)piperazine-1-ethanesulfonic acid
His	Histidine
HPLC	High Performance Liquid Chromatography
IPTG	Isopropylthiogalactoside
LB	Lauria Bertani
NMR	Nuclear Magnetic Resonance

PAGE	Polyacrylamide Gel Electrophoresis
PDB	Protein Data Bank
SDS	Sodium Dodecyl Sulfate
SDS-PAGE	Sodium Dodecyl Sulfate Polyacrylamide Gel Electrophoresis
SEC	Size Exclusion Chromatography
Trp	Tryptophan
Tris	Tris(hydroxylmethyl)aminomthane
WT	Wild Type

Chapter 1

Literature Review

Histidine Nucleotide Binding proteins (Hint's)

Histidine Nucleotide Binding Proteins are classified as members of the HIT superfamily proteins, which contain a His-Ø-His-Ø-His-Ø-Ø nucleoside-binding motif, where Ø is a hydrophobic amino acid (**Figure 1**). Based on the enzymatic activity, Hint proteins are classified as acyl-adenylate hydrolases and nucleoside phosphoramidases.[1] The motif positions the substrate in such a way that enables attack of the α-phosphate via nucleophilic histidine (**Figure 2**). The Nucleotidylated-Histidine intermediate undergoes hydrolysis via water-mediated attack to subsequently release of the product, nucleoside monophosphate, from the active site.[2] Mutation of the nucleophilic Histidine abolishes the hydrolase activity of Hint proteins.

I. History of nucleoside phosphoramidases

In 1959, Smith et al. first reported enzymatic hydrolysis of the phosphoramidic acid (**Figure 3A**) to monophosphate and ammonia in *E.coli* lysate.[3] In addition to the hydrolytic reaction, an enzymatic phosphoryl transfer from phosphoramidate to glucose or hexose sugars was observed (**Figure 3B**).[4] Three years later they isolated two fractions containing the enzymatic activity.[5] The phosphoramidic activity in the fraction I was dependent on divalent metal ions and reducing substances (cysteine and glutathione) to achieve the maximum rate of ammonia release, while the activity in fraction III was found to be independent. No nucleoside phosphoramidase activity was observed in either of these fractions. In 1981, Rossomando et al. performed cold chase radiolabeling experiments [^{3}H-ATP] on *Dictyostelium Discoideum* lysate.[6] They observed that a

Figure 1: Alignment of the amino acid sequences of Human Hint proteins. Highlighted in red are the conserved Histidine residues that form part of the nucleotide binding motif of HINT1, HINT2, HINT3 and echinT proteins. The middle Histidine of the motif is essential for the hydrolase activity.

```
HINT1   ----------------------------------------------------MADEIAKAQVARP-GGD --TIFGKIIRKEIP---AKIIFE
HINT2   MAAAVVLAAGLRAARRAVAATGVRGGQVRG AAGVTDGNEVAKAQQATP-GGAAPTIFSRILDKSLP--ADILYE
HINT3   ----------MAEEQVNRSAGLAPDCEASATAETTVSSVGTCEAAGKSPEPKDYDSTCVFCRIAGRQDPGTELLHCE
echinT  ----------------------------------------------------MAEE--------------------TIFSKIIRREIPSDIVYQ--

HINT1   DDRCLAFHDISPQAPTHFLVIPKKHISQISVAEDDDESLLGHLMIVGKKCAADLGLNKGYRMVVNEGSDGGQSVY
HINT2   DQQCLVFRDVAPQAPVHFLVIPKKPIPRISQAEEEDQQLLGHLLLVAKQTAKAEGLGDGYRLVINDGKLGAQSVY
HINT3   NEDLICFKDIKPAATHHYLVVPKKHIGNCRTLRKDQVELVENMVTVGKTILERNNFTDFTNVRMGFHMPPFCSIS
echinT  DDLVTAFRDISPQAPTHILIIPNILIPTVNDVSAEHEQALGRMITVAAKIAEQEGIAEDGYRLIMNTNRH---GGQEVY

HINT1   HVHLHVL---GGRQMHWPPG---------------------------------------------------------------------- 126
HINT2   HLHIHVL --- GGRQLQWPPG---------------------------------------------------------------------- 163
HINT3   HLHLHVLP--VDQLGFLSKLVYRVNSY---------------------------------WFITADHLIEKLRT----------182
echinT  HIHMHLL --- GGRPLG -- PM -----LAHKGL-------------------------------------------------------119
```

Figure 2: Adenosine Monophosphate (AMP) (PDB: 3tw2) bound X-ray crystal structure of Human Hint1[7]

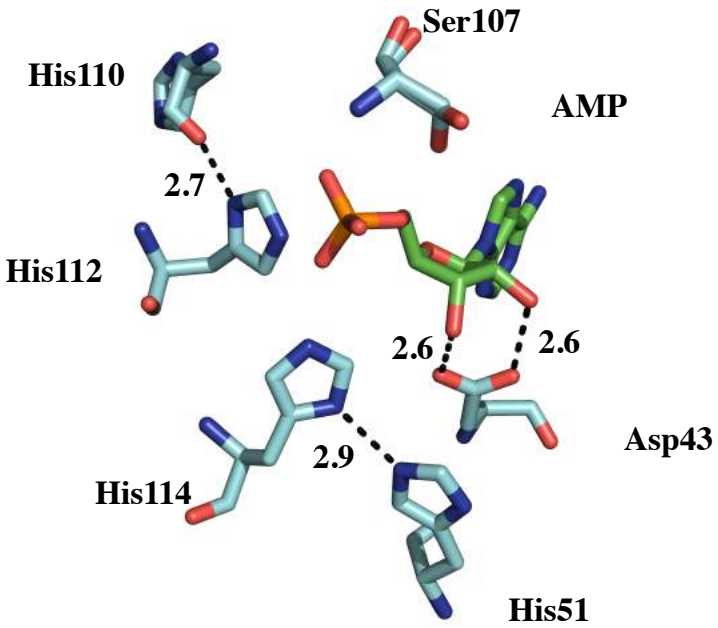

Figure 3: Classification of phosohoramidases and transphosphorylase. In the scheme; A) Hydrolysis of phosphoramidic acid via phosphoramidases and B) Transfer of an phosphoryl group from phosphoramidic acid to hexose sugar via transphosphorylase in *E.coli* lysate

A)

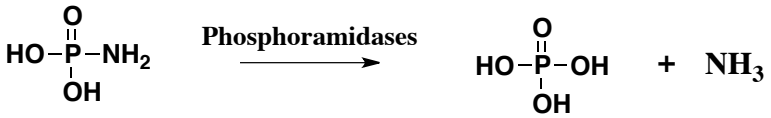

Phosphoramidic acid

B)

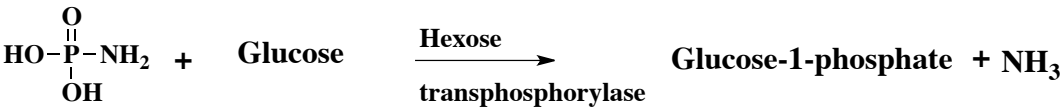

Phosphoramidic acid

significant level of radioactivity was retained following cold precipitation and isolation of the membrane extract. Treatment of the of the extract with a base did not reduce the amount of radiolabeling, indicating formation of a covalent nucleotidylated-protein complex with a phosphoramidate linkage (**Figure 4**). Isolation and characterization of the phosphoramidated proteins found the apparent molecular weight to be 13.5 and 1.5 kDa.[8] Since the formation of the phosphoramidated protein is likely via coupling of lysine or N-terminus residues, substrates such as lysyl-(N-ϵ-5′-phospho) adenosyl phosphoramidate conjugated to different tetrapeptides was synthesized (**Figure 5**). Hydrolysis of these substrates was observed in the presence of the isolated phosphoramidases and was sensitive to inhibition by divalent metal ions such as copper (II) and zinc (II).

The first mammalian phosphoramidase was isolated from bovine brain tissue extracts. The protein was identified as an inhibitor of Protein Kinase C (PKC) and hence was named as protein kinase c inhibitor interacting protein-1 (PKCI-1).[9] However, subsequent studies demonstrated that, while Hint binds to PKC, it is a modulator of PKC function and not a PKC inhibitor. Hence, the protein was later renamed Histidine Triad Nucleotide Binding Protein 1 based on its structural ligand-binding motif. Enzymatic and chemical degradation followed by mass spectrometric analysis found that bovine Hint1 consists of 125 amino acids with a molecular weight of 13.7 kDa.[10] The apparent molecular weight of the target protein on size exclusion chromatography was observed to be 36 kDa, indicating that Hint1 is a dimeric protein. Primary amino acid sequence did not indicate the presence of a zinc finger domain, however radiolabeling studies demonstrated that Hint1 could bind to $^{65}Zn^{+2}$ ions.[10] Subsequently, Lima et al. performed the first *in vitro* characterization and solved the first X-ray crystal structure of Hint1.

Figure 4: Adenyltansferases and Nucleoside phosphoramidase activity on protein phosphoramidates

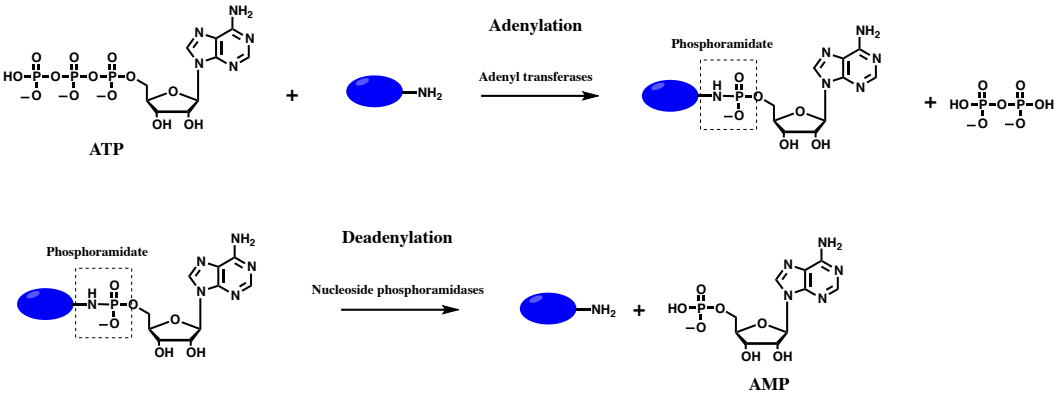

Figure 5: Structure of lysyl-(N-ϵ-5′-phospho) adenosine phosphoramidate tetrapeptide, tuftsin (thr-lys-pro-arg) as substrates for phosphoramidase activity in *D. discoideum*

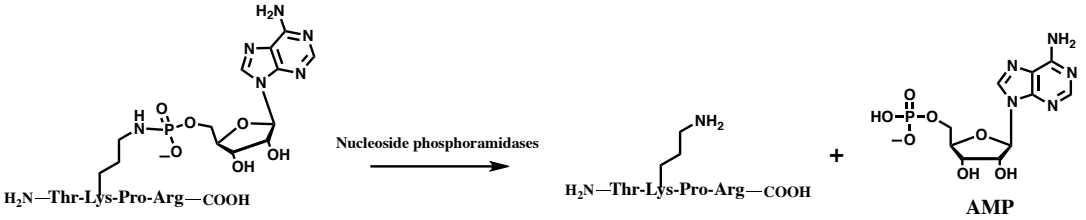

They also attempted X-ray crystallographic studies of Human PKCI-1 in the presence of Zn^{+2} ions.[11] Nevertheless, they could not detect the presence of zinc ions in their x-ray crystal structure.[11] They speculated that the x-ray crystallographic conditions were forcing the proteins to crystallize mainly in the Apo form. In addition, they also observed a decrease in the stability of Hint1 in the presence of zinc. Immunofluorescence studies on a human fibroblast cell line indicated localization of Hint1 to be mainly restricted to the cytoskeletal structures in the cytoplasm.[12]

To date, Hint proteins have been identified across several species such as cyanobacteria,[13] yeast,[14] plants,[15] *C. Elegans*[16] and a variety of mammalian species, which suggest their important role in cellular functions. The human genome consists of three isoforms namely, HINT1, HINT2 and HINT3 gene products. The physiological role and functions of Human Hint proteins are described below.

II. Physiological roles of Eukaryotic Histidine Nucleotide Binding Proteins

A. Neuronal cell biology

Evidence of the biological role of Hint1 in neuronal cells emerged from a yeast two-hybrid study designed to screen and identify μ-opioid receptor (MOR) interacting proteins. Hint1 was identified as an MOR interacting protein. Genetic knockout of Hint1 in mice shown to increase the analgesic response as well as reduced tolerance towards opioids in mice (**Figure 6**).[17] Later on, Young and co-workers demonstrated that the interaction of Hint1 with N-terminus of Regulator of G-protein signaling Z1 (RGSZ1)

Figure 6: Hot plate assay for opioid's analgesic response in Hint1$^{-/-}$ and Hint1$^{+/+}$ mice. A) Time course: Morphine produced elevated analgesic response in Hint1$^{-/-}$ mice over 4-h period. Hot plate latencies were recorded at 15, 30, 45, 60, 75, 90, 120, 150, 180 and 240 min after single injection of morphine (10 mg/kg). B) Chronic tolerance, time course of tolerance development in Hint1$^{-/-}$ and Hint1$^{+/+}$ mice treated daily with morphine (10 mg/kg, s.c.) for 7 days. Hot plate latencies were recorded 30 min after the injection on the days indicated. Analgesic response is reported as the percentage of maximum possible effect (MPE). [17]

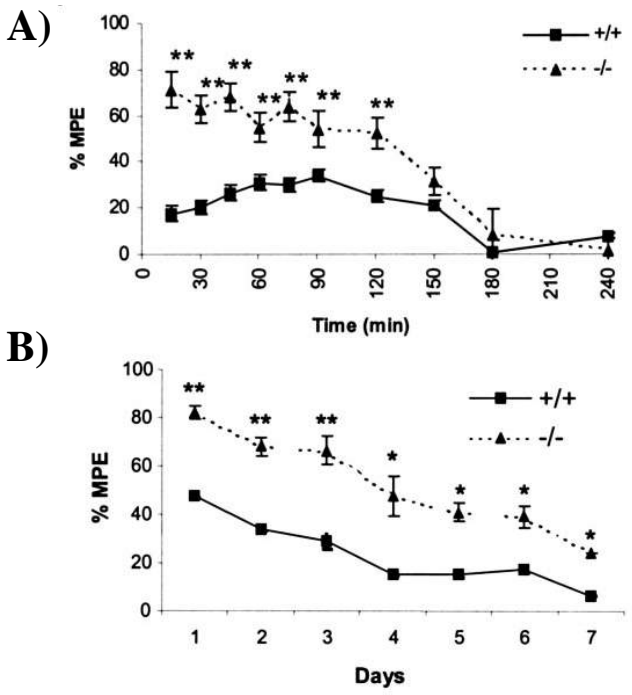

Scheme 1: Proposed schematic pathway for the mechanism of opioid signaling and cross talk of mu-opioid receptor with NMDAR in the central nervous system. Hint1 plays an important regulatory protein via unknown mechanism regulating its active site in governing this cross talk. In the basal state Hint1 is associated with NMDAR, upon morphine challenge the analgesic response is obtained via G-protein signaling and NOS pathway. This activation helps Hint1 to co-associate NMDAR with MOR and recruit PKCγ onto the membrane. PKCγ and PKA mediated phosphorylation onto the C-terminus of NMDAR results into the negative feedback via phosphorylation onto the mu-opioid receptor by CaMKII signaling pathway leads to the development of tolerance.

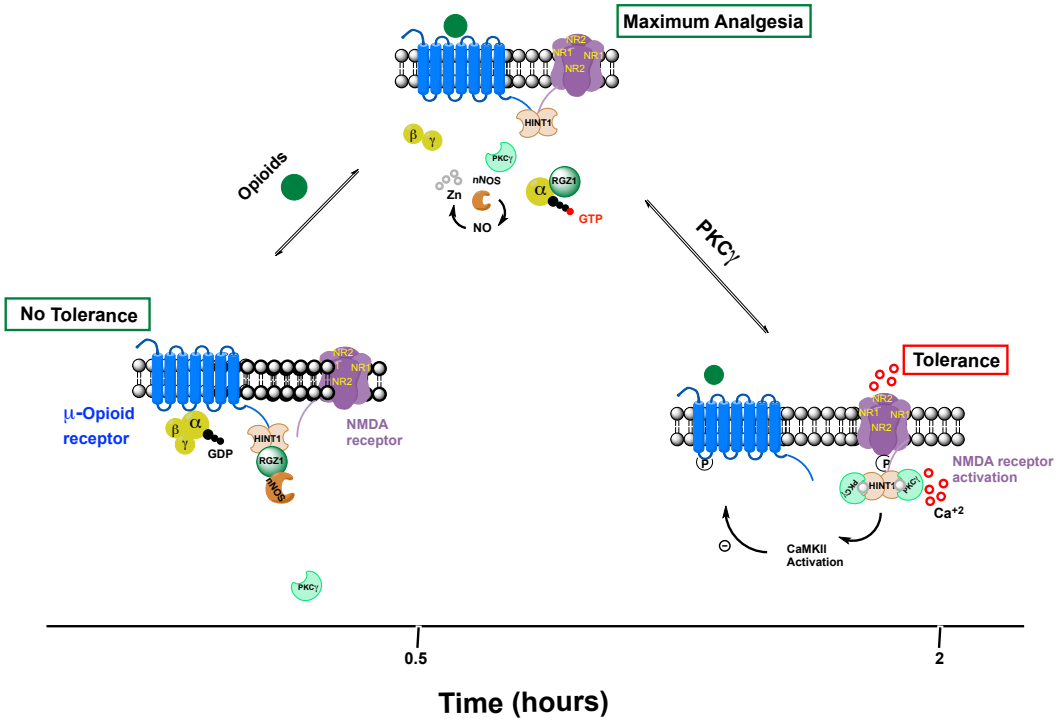

protein with Hint1 is critical in regulating the opioids analgesic response.[18] Further molecular and pharmacological studies by Garzon et al. demonstrated that Hint1-RGSZ complex along with zinc is critical in recruiting PKCγ to the neuronal membrane for the activation of N-Methyl-D-Aspartate Receptors (NMDAR) following the activation of MOR (**Scheme 1**).[19] Recently, they also demonstrated a similar role of Hint1 in mediating crosstalk between cannabinoid and NMDA receptors.[20]

Immunohistochemical analysis indicated that intracellular localization of Hint1 is restricted mainly to cell bodies and dendritic projections of the neuronal cells.[21] Interestingly, very little or no expression of Hint1 was observed in the astrocytes and dopaminergic regions, indicating tight regulation of Hint1 expression in CNS. Expression of Hint1 in the brain is evident within 14 days of embryonic development of mice (**Figure 7**). In adult mice, abundant expression is observed within the dorsolateral frontal cortex regions (DLFC), such as the olfactory system, amygdala, cerebral cortex and hippocampus regions of the CNS. The olfactory system is known to be well-connected with DLFC regions of the brain that are associated with affective and mnemonic functions such as behavioral mood, associative learning, and episodic memory. Hint1$^{-/-}$ mice do exhibit behavioral symptoms associated with mood disorders such as an increase in anxiety and depression.[22] Genetic mutations in Hint1 have been also shown to impact behavioral learning associated with odors in *C. Elegans*.[16] Interestingly, such symptoms are very common among schizophrenic patients[23] and a decrease in the mRNA levels of Hint1 within the dorsolateral frontal cortex (DLFC) region of schizophrenic patients has

Figure 7: Brain tissue distribution of Hint1 across CNS. A) and B) Western blot analysis of PKCI-1/Hint1 in different ages of mouse brain tissue as well as in different regions of adult mouse brain. Whole brain tissue extract of 30μg protein was loaded into each lane. E14, embryonic day 14; n.b., new born; m, months; (B and D) Western blot quantifications show the densities of ratio between Hint1 and Actin in the same lane.[21]

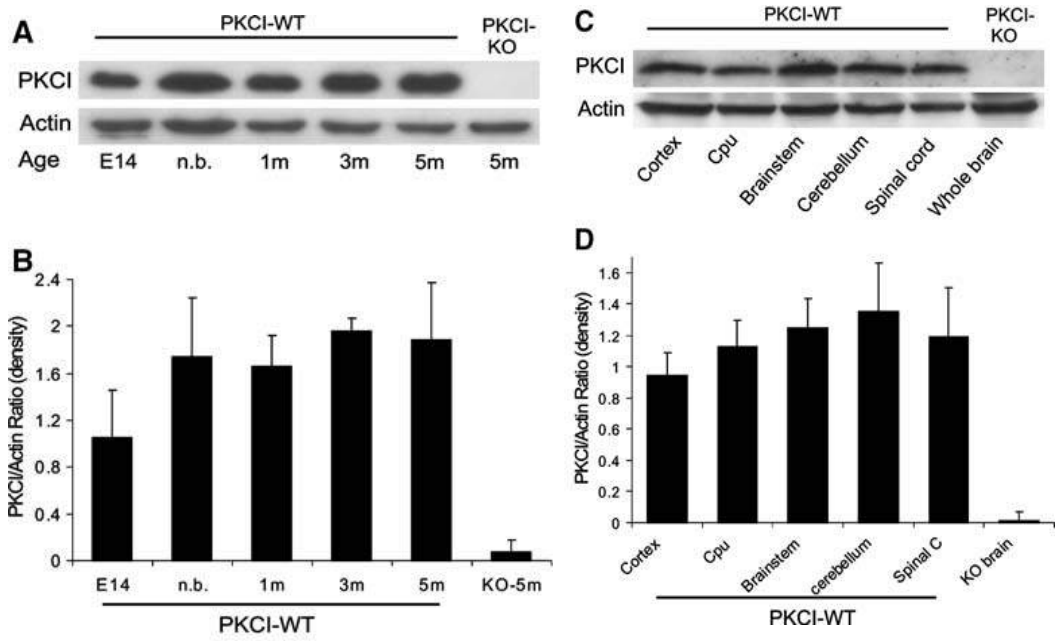

been reported.[24] Additionally, genetic variants of Hint1 were also found to be associated with nicotine dependence, which is a frequent cause of comorbidity in schizophrenic patients.[25, 26] The neuronal circuitry of the ventral trigeminal area (VTA) connecting the hippocampus and nucleus acummbens plays a major role in the hippocampal dependent formation of behavioral memory associated with repeated exposure of substances of abuse. A dynamic change in the expression of Hint1 is observed within the nucleus acummbens upon chronic administration of nicotine, which further indicates a critical role of Hint1 in regulating behavioral memory. [25]

Synaptic facilitation between peripheral nociceptors and spinal dorsal horn pain-transmitting neurons is one of the key hallmarks in the development of neuropathic pain. NMDAR plays a significant role in the sensitization of spinal pain transmitting neurons. Abundant expression of Hint1 is also reported in the spinal cord especially in the peripheral sciatic nerve,[21, 27] This observation is consistent with the study that Hint1$^{-/-}$ mice experience enhanced supraspinal nociceptive sensitivity.[28] Neuropathic pain is commonly observed among patients suffering from peripheral neuropathies. Recently, several point mutations in Hint1 have been identified as one of the most frequent cause of peripheral neuropathy.[27] It is evident from these observations that Hint1 is potentially critical in driving the long-term cellular fate of neuronal cells and regulating brain adaptations involved in the development of tolerance, neuropathic pain, and addiction.

B. Cancer cell biology

Cellular differentiation, in which one cell type transit to another, is a key hallmark in the embryonic development of multicellular organisms. Once differentiated, cells undergo programmed cellular senescence or cell cycle arrest to control embryonic patterning and development. Embryonic senescent cells are non-proliferative and are often compared to the mechanism of oncogene-induced senescence observed in tumor suppression. Genetic knockout of Hint1 in mice results in normal fetal and adult development. However, fibroblast cultivated from day 14 of the embryonic mice displayed increased growth rate and spontaneous immortalization.[29] In contrast, fibroblast from wild-type Hint1 mice underwent cellular senescence (**Figure 8**). Furthermore, it was demonstrated that N-Nitroso Benzylamine (NMBA) treatment induced squamous tumor formation with higher frequency in Hint1$^{-/-}$ mice than in wild type. These observations were the first demonstration of the role of Hint1 as a potential tumor suppressor protein.[30] Consistent with tumor suppression function, methylation-dependent down regulation of Hint1 was observed in human non-small lung cancer cell line, NCI-H522.[31] Overexpression of Hint1 in this cell line resulted in reduced cell growth and inhibition of tumorogenesis. In this context, a mechanistic investigation discovered that Hint1 interacts with the ATP/GTP binding motif of Pontin and Reptin, which is essential to disrupt their homo and heteromeric interactions.[32] Both Pontin and Reptin are known to repress transcriptional activity of β-catenin in Wnt signaling pathways and are associated with a variety of chromatin-remodeling complexes.[33] Consistent with a role on transcriptional regulation, overexpression of Hint1 in MCF-7 and SW480 cells resulted in the upregulation of pro-apoptotic factor Bax and down-regulation of anti-apoptotic factor Bcl-2. In similar fashion, expression of Hint1 was shown to be critical in the epigenetic silencing of genes

Figure 8: The dependence of the growth of fibroblast cells on Hint1 expression. MEF cultures established from both Hint1$^{+/+}$ and Hint1$^{-/-}$ mice from 13.5-day embryos. Number of cells was measured at passage day (p) 2, 10, 20 and 25.[29]

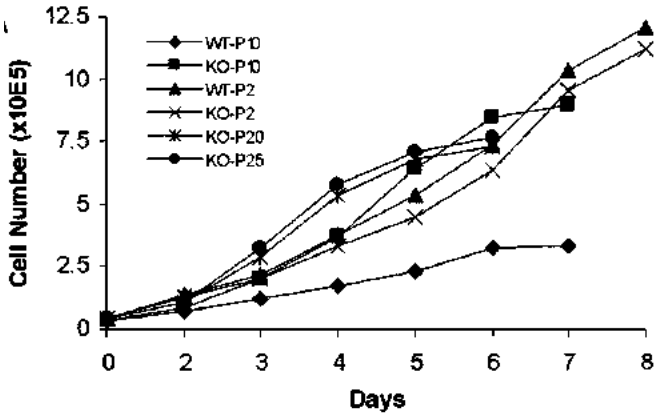

associated with human colon and hepatocellular carcinomas.[34] A catalytically inactive Hint1 mutant (H112N) was unable to block induction of apoptosis in the SW480 cell line, suggesting that Hint1 apoptotic function is independent of the Hint1 enzymatic activity.[32] Finally, some recent evidence has emerged indicating potential role of Hint2 in hepatocellular carcinomas. [35]

C. Mast cell biology

Evidence for the biological function of Hint1 in mast cells emerged with the identification of its interaction with Micropthalmia-associated transcription factor (MITF) in a yeast two hybrid screening study.[36] MITF is a transcription factor containing a helix-loop-helix leucine zipper DNA-binding protein and is mainly associated with regulatory functions in mast, melanocyte and osteoclast cells. In quiescent mast cells, the activity of MITF is repressed in part via its interaction with Hint1. Upon activation of mast cells, dissociation of Hint1 is driven by the antigen-stimulated production of signaling molecules such as diadenosine tetraphosphate (AP_4A). The production of AP_4A is regulated via non-canonical function of Lysine t-RNA synthetases (LysRs) (**Scheme 2**). Activation of mast cells induces the translocation of LysRs from the cytoplasm to the nucleus, which binds to MITF, generates AP_4A and dissociates Hint1 to activate transcription functions (**Scheme 3**).[37, 38] However, whether AP_4A mediated regulation of Hint1 is a general mechanism in other physiological roles is not yet clear.

Scheme 2: Canonical and non-canonical catalytic processes of Lysine t-RNA Synthetase

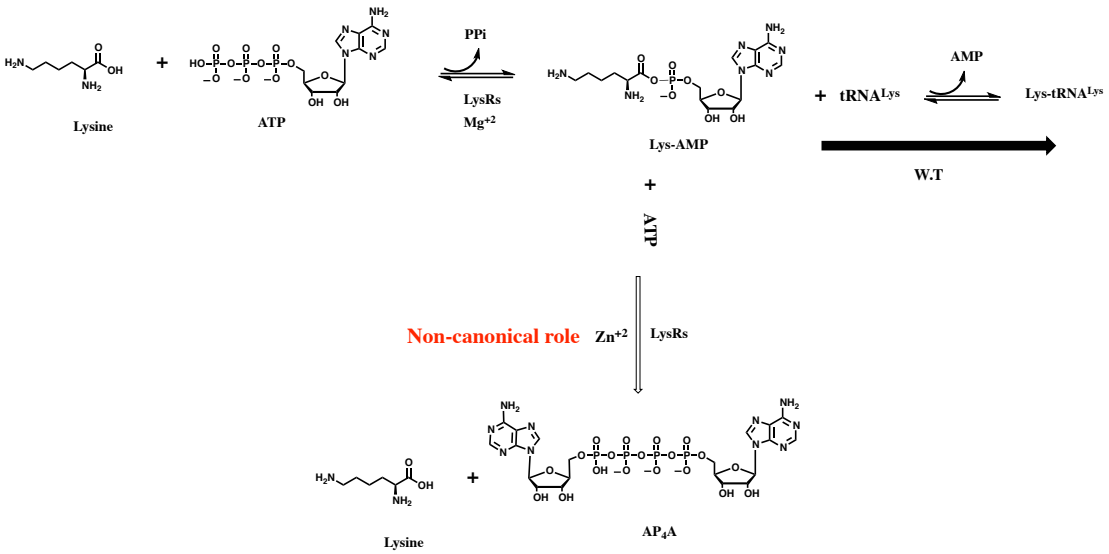

Scheme 3: Proposed model for the regulation of micropthalmia transcription factor (MITF) in the quiescent and activated mast cells via Hint1 and LysRs[37]

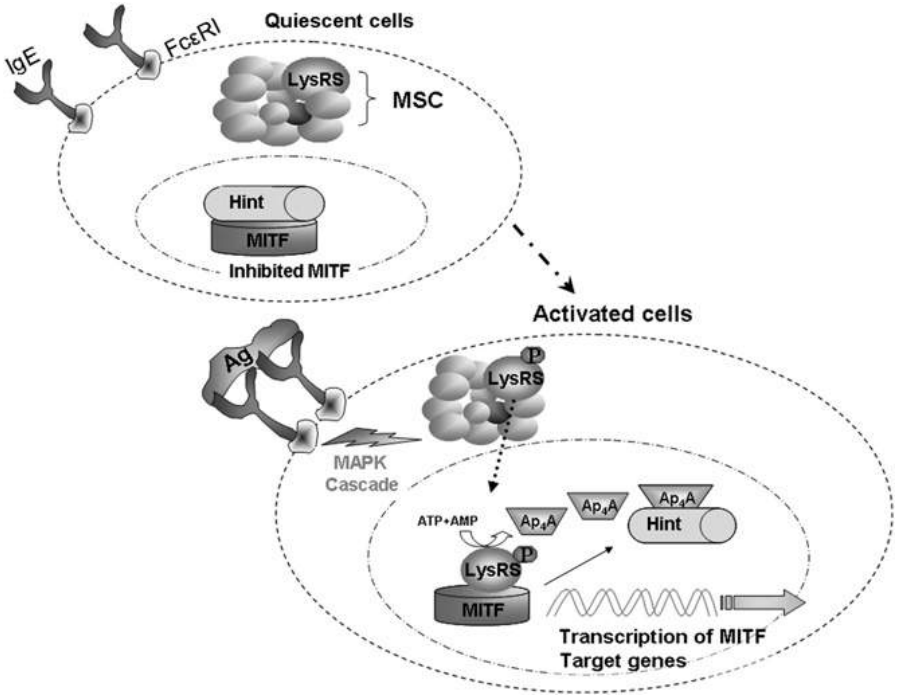

Figure 9: Tissue distribution of Hint2 mRNA (left) and protein expression levels (right). mRNA levels were assessed by real-time quantitative PCR and normalized to skeletal muscle expression levels. Protein expression analysis was performed using immunoblot analysis.[35]

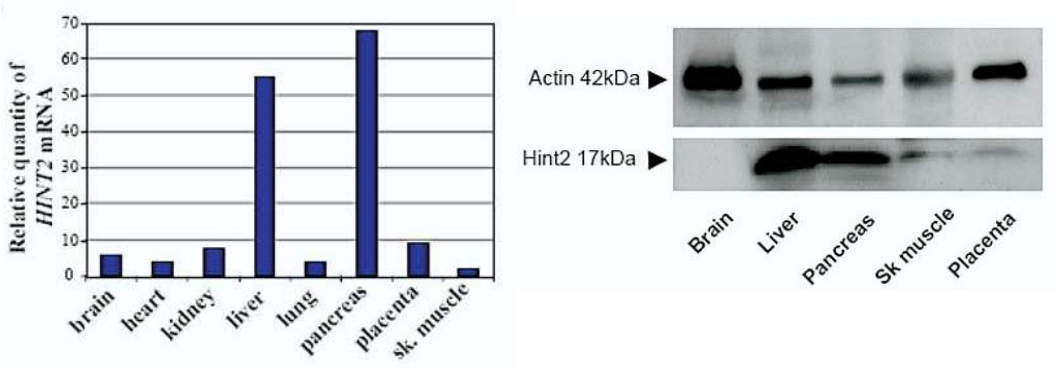

Figure 10: Regulation of glucose homeostasis by Hint2. A) Insulin tolerance test, Hint2$^{-/-}$ mice showed impaired recovery from hypoglycemia after insulin injection. B) Secretion of counter regulatory hormone glucagon after 2 hours of insulin injection was significantly lower in Hint2$^{-/-}$ mice, whereas higher levels of corticosterone were observed in Hint2$^{-/-}$ mice.[39]

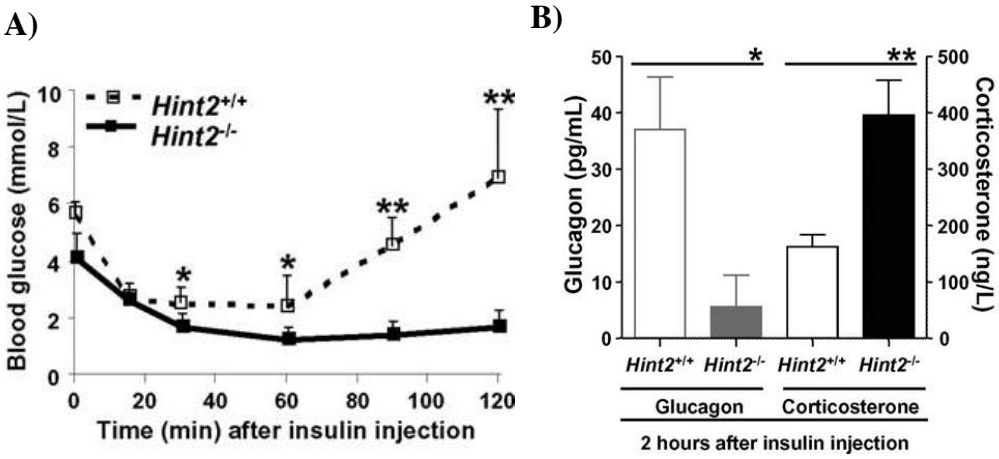

D. Mitochondrial function

Mitochondria are known as the powerhouse of the cell. They regulate many critical functions of cells such as apoptosis, calcium homeostasis, steroid biosynthesis, as well as carbohydrate and lipid metabolism. Tissue expression and mRNA analysis by Dufour and co-workers first demonstrated that Hint2 is primarily expressed in the liver and pancreas. Unlike Hint1, little or no expression was observed in brain tissue or skeletal muscles (**Figure 9**).[35] Immunocytochemistry studies on Huh-7 cells indicated that Hint2 is primarily localized in the mitochondria.[35] Genetic knockdown of Hint2 in H295R cells with siRNA resulted in a marked reduction in the angiotensin stimulated steroidal response.[40] Recently, phenotypic studies on Hint2$^{-/-}$ mice suggested a significant alteration in the accumulation of hepatic triglycerides, decreased glucose tolerance, abnormal regulation of insulin (**Figure 10**) and altered mitochondrial calcium dynamics.[39, 41] Mitochondria isolated from the hepatocytes of KO animals indicated a significant increase in the reactive oxygen species and altered membrane potential. This change was accompanied by a decrease in glutamate dehydrogenase activity and an increase in acetylation of mitochondrial proteins. Overexpression of Hint2 in Huh-7 cells resulted in an increase in the apoptotic-signaling pathway, which was found to be dependent on the catalytic activity of Hint2. However, the regulation of protein-protein interactions or posttranslational modifications by Hint2 in mitochondrial functions has remained elusive.

Figure 11: A) Overlay of the X-ray crystal structures of Human Hint1 (Blue, PDB: 1AV5) and Hint 2 (Orange, PDB: 4INC)[42]

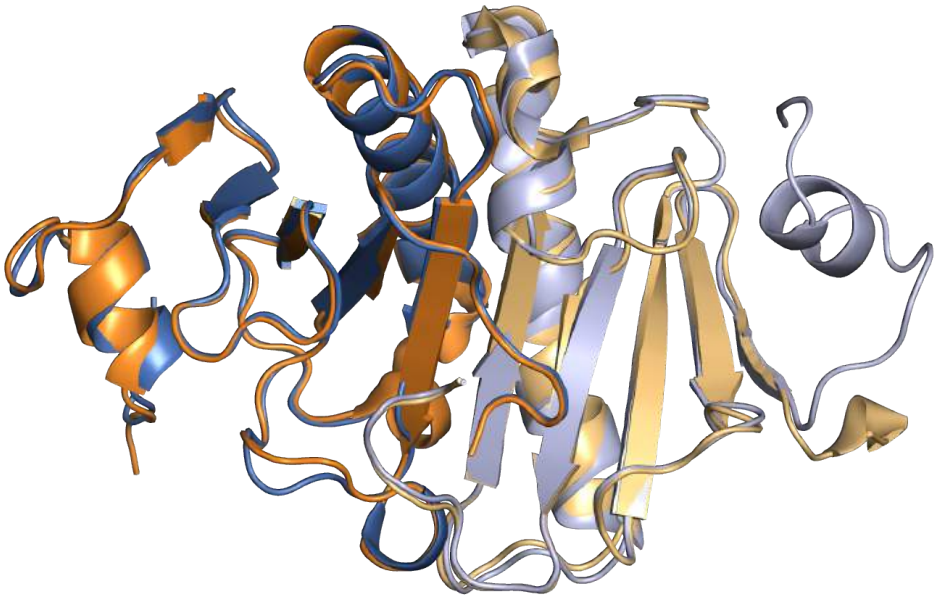

B) Hydrophobic residues in the nucleoside-binding pocket of Human Hint1 (PDB: 3tw2)

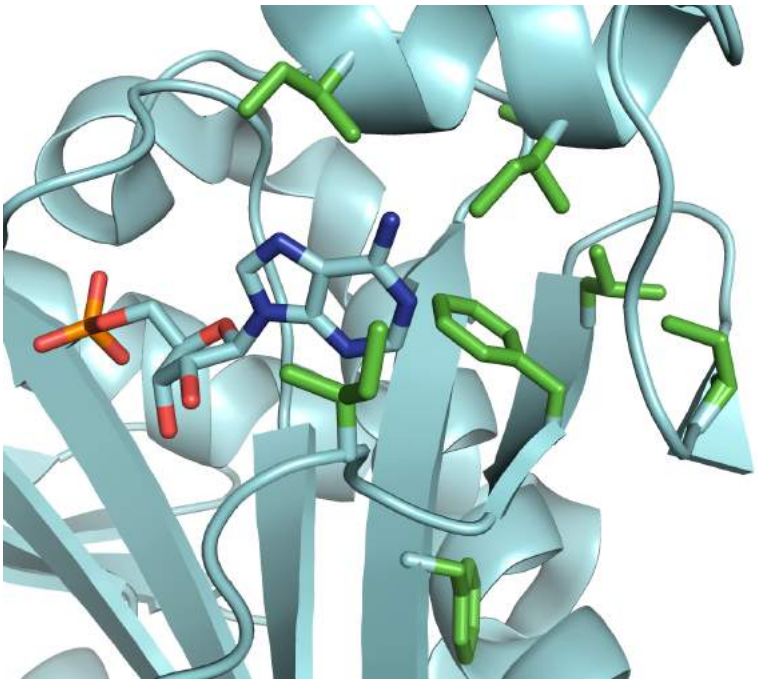

III. Structural characterization of Human Hint proteins

To date several x-ray crystal structures of Hint proteins have been reported as apo, AMP or GMP-bound complexes. Hint1 exist as a homodimeric protein with $\alpha + \beta$ overall folding topology (**Figure 11**). Each monomer consists of five anti-parallel sheet and two-helices. Both the monomers are brought together to form ten anti-parallel sheets, with the central helix of each monomer packed against the central helix of the other monomer. A set of conserved hydrophobic residues form the binding pocket for the purine base, while polar residues form the binding pocket of the ribose sugar. A string of histidine residues occupies the active site, particularly His-112, which functions as a catalytic nucleophile. Human Hint2 shares a sequence similarity of 61% to Hint1 and also exists as a homodimer. Recently, Maize et al solved the first X-ray crystal structure of Human Hint 2 protein.[42] The overall structure of Human Hint2 was found to be nearly identical to Human Hint1 (**Figure 11**). In comparison to Hint1 and Hint2, very little is known about the structure and function of Human Hint3. Comparison of the primary amino acid sequence reveals less than 31% homology, and hence Hint3 is classified as a distinct branch of HIT family proteins.[43]

To study the importance of homodimerization on the catalytic activity of Hint1, Wagner and coworkers designed a monomeric version of Hint1 by destabilizing the dimerization interface with point mutations.[44] This mutations were characterized by a combination of size-exclusion chromatography, static light scattering, and chemically induced dimerization studies.[44] Molecular dynamics simulations of the monomeric hHint1 did not detect significant perturbations of the active-site residues. The combined

kinetic and structural results demonstrate that, for monomeric hHint1, the catalytic efficiency (k_{cat}/K_m) of substrate hydrolysis is dependent on homodimerization. However, the underlying dynamics governing the catalysis or protein interactions of Hint1 remain unknown.

IV. Intracellular regulators/substrates of Human Hint proteins

Physiological evidence of the function of Hint1 across variety of cellular processes and interactions indicate an important role of its structural motif or catalytic activity in the regulation of *in vivo* functions. X-ray crystallographic and NMR studies have clearly indicated that the nucleotide-binding motif is an inextricable part of Hint1 in the molecular recognition of ligands. However, the identity of the natural regulatory substrate or ligand has remained elusive. Previous studies have indicated that the nucleoside phosphoramidase activity of Hint1 may act as part of a novel regulatory mechanism of protein adenylation or guanidylation. Wagner and Chou et al. have (unpublished results) performed pulse-chase radiolabeling experiments with $\boldsymbol{\alpha}$-^{32}P [ATP/GTP] on mammalian and *E.coli* lysates. Results from these studies indicated a preference for the formation of guanylate over adenylated proteins in the lysates. However, stability studies indicated that formation of a phosphoramidate linkage was unlikely, since treatment with base efficiently removed such linkages. We also found labeling to be independent of the Hint proteins catalytic activity. Hence, our results demonstrate that Hints are unlikely to be direct protein nucleotidylases.

Figure 12: Adenyl sulfate: Ammonia adenyltransferase synthesized AMP-NH_2

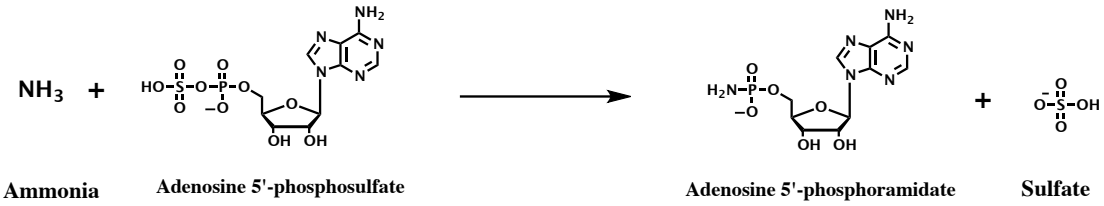

Ammonia **Adenosine 5'-phosphosulfate** **Adenosine 5'-phosphoramidate** **Sulfate**

Table 1: Substrate specificity of nucleoside phosphoramidates by Hint1[1]

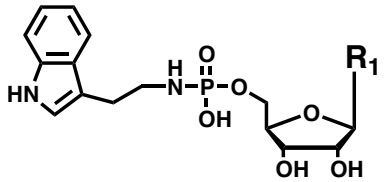

R_1	k_{cat} (s^{-1})	k_m (μM)	k_{cat}/k_m (x 10^{-3} s^{-1} M^{-1})
Adenine	2.1 ± 0.1	0.13 ± 0.02	15000 ± 3000
Guanine	2.3 ± 0.7	0.21 ± 0.02	11000 ± 1000
Hypoxanthine	2.6 ± 0.04	0.71 ± 0.03	3700 ± 300
Uracil	2.5 ± 0.3	2.2 ± 0.4	42 ± 15
Thymidine	0.10 ± 0.01	32 ± 5	3 ± 1
Cytosine	1.2 ± 0.1	2.3 ± 0.4	600 ± 200

Scheme 4: A) Catalytic mechanism of Hint1

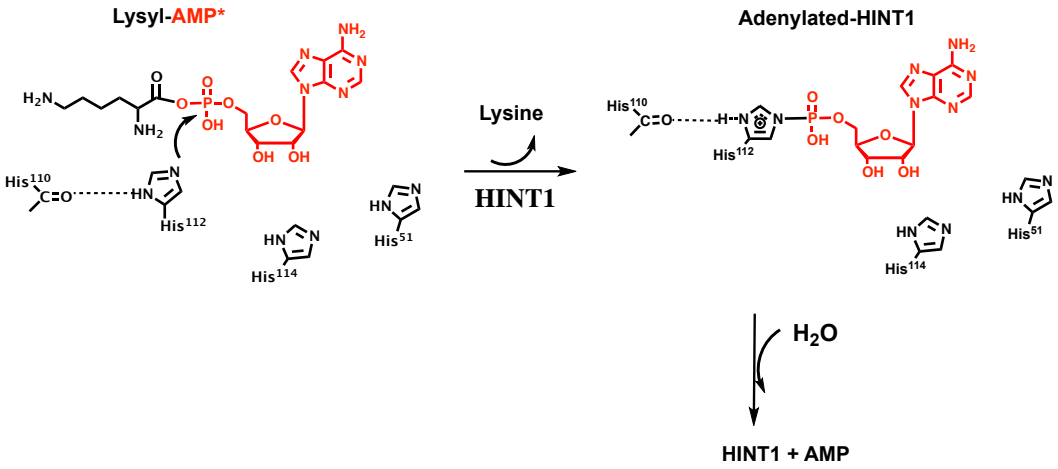

B) Scheme of the Kinetic mechanism of Hint1[2]

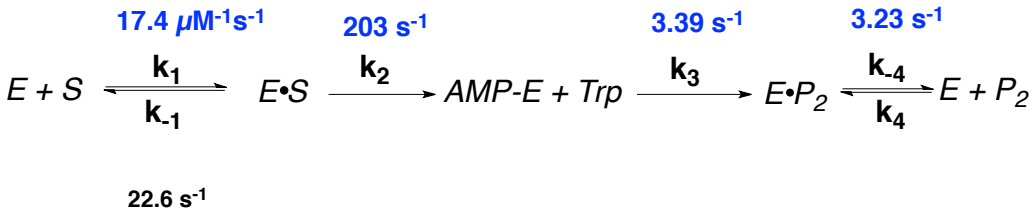

It is likely that small molecule adenylates with acyl-phosphate or phosphoramidate linkage are intracellular regulators of Hint proteins. Brenner and co-workers first performed a detailed analysis on a variety of endogenous nucleotidylated amino acids, sugars, and dinucleotides as possible substrates for Hint1. They discovered that Hint1 could efficiently hydrolyze adenosine monophosphoramidate (AMP-NH_2), an intracellular solute synthesized from AMP-Sulfate (AMP-SO_4) in prokaryotic and eukaryotic organisms (**Figure 12**).[14] They also demonstrated efficient hydrolysis of adenylated amino acids, such as AMP-N-acetyl-lysine-N-methyl ester phosphoramidate, by Hint1. However, little cleavage of cellular metabolites, such as nucleoside disphosphates, dinucleotides or adenylated sugars, by Hint1 was observed. Wagner and coworkers performed a detailed nucleoside phosphoramidate substrate specificity study on Hint proteins, which clearly demonstrated a preference for purine over pyrimidine nucleosides (**Table 1**). They further demonstrated Hint1 hydrolyzed the Lysyl-AMP generated by t-RNA synthetase *in vitro* (**Scheme 4**). However, the physiological role of Lysyl-AMP or other endogenous substrates to regulate Hint function *in vivo* has remained elusive.

IV. Trends

- Hint1$^{-/-}$ mice exhibit a variety of CNS phenotypes such as an increase in opioid analgesia, nicotine dependence and anxiety.
- Hint1 is essential for modulating the cross talk between μ-opioid and NMDA receptor *in vivo*.

- Genetic point mutations in Hint1 have been identified in clinical patients to be the leading cause of peripheral neuropathy.
- Hint1 interacts with a variety of transcription factors to regulate tumor suppression function, which is independent of its catalytic activity.
- AP_4A dissociates Hint1 from microphthalmia transcription factor complex to regulate the immunomodulatory function in mast cells.
- Hint $2^{-/-}$ mice exhibit phenotypes associated with deregulation of mitochondrial functions such as carbohydrate metabolism, apoptosis, and oxidative phosphorylation.
- Hint 2 dependent apoptosis in cancer cells is dependent on the catalytic activity.
- Hint 3 is oligomeric in structure and very little is known about its function.

V. Outstanding questions

- What is the role of the Hint1 active site or activity in regulating CNS functions or phenotypes?
- What is the endogenous substrate of Hint proteins *in vivo*?
- What are the critical structural features or dynamics associated with catalysis that may regulate Hint-protein or Hint-ligand interactions *in vivo*?
- What is the role of the dimeric/oligomeric structures of Hint proteins in regulating its function *in vivo*?
- What are the critical structural features of Hint proteins that are essential for interactions with transcription factors and proteins involved in the NMDAR signaling pathway?

VI. Current Research:

The research described in the current thesis elucidates the contributions to the characterization of Hint1 from the aspect of function, mechanism, and structural

determinants. To do so, we describe development of variety of tools to study Human Hint proteins. The first two chapters provide the first strong evidence of the role of Hint1 active site in the CNS using chemical genetics, medicinal chemistry and neuropharmacological studies. In Chapter 3, we describe the covalent capture of the Hint1-adenylated intermediate using an alternate substrate and time-lapse crystallographic studies as part of our efforts to elucidate reaction trajectory of Hint1. In Chapter 4, we describe the development of switch-on fluorescent probes as tools for monitoring the active site and detection of Hint proteins. Chapter 5 describes the structural and functional characterization of genetic mutations of Hint1 associated with peripheral neuropathy as well as structural determinants of Hint1.

References:

1. Chou, T. F.; Baraniak, J.; Kaczmarek, R.; Zhou, X.; Cheng, J.; Ghosh, B.; Wagner, C. R., Phosphoramidate pronucleotides: a comparison of the phosphoramidase substrate specificity of human and Escherichia coli histidine triad nucleotide binding proteins. *Mol Pharm* **2007,** *4* (2), 208-17.
2. Zhou, X.; Chou, T. F.; Aubol, B. E.; Park, C. J.; Wolfenden, R.; Adams, J.; Wagner, C. R., Kinetic mechanism of human histidine triad nucleotide binding protein 1. *Biochemistry* **2013,** *52* (20), 3588-600.
3. SMITH, R. A.; BURROW, D. J., Enzymic cleavage of phosphoramidic acid. *Biochim Biophys Acta* **1959,** *34*, 274-6.
4. FUJIMOTO, A.; SMITH, R. A., Metabolism of phosphoramidates. II. Further studies on the Escherichia coli phosphoramidate phosphoryl transfer enzyme. *Biochim Biophys Acta* **1962,** *56*, 501-11.
5. HOLZER, M. E.; BURROW, D. J.; SMITH, R. A., Metabolism of phosphoramidates. I. Enzymic hydrolysis and transfer reactions. *Biochim Biophys Acta* **1962,** *56*, 491-501.
6. Rossomando, E. F.; Crean, E. V.; Kestler, D. P., Isolation and characterization of an adenylyl-protein complex formed during the incubation of membranes from Dictyostelium discoideum with ATP. *Biochim Biophys Acta* **1981,** *675* (3-4), 386-91.
7. Dolot, R.; Ozga, M.; Włodarczyk, A.; Krakowiak, A.; Nawrot, B., A new crystal form of human histidine triad nucleotide-binding protein 1 (hHINT1) in complex with adenosine 5'-monophosphate at 1.38 Å resolution. *Acta Crystallogr Sect F Struct Biol Cryst Commun* **2012,** *68* (Pt 8), 883-8.
8. Rossomando, E. F.; Hadjimichael, J., Characterization and cAMP inhibition of a lysyl-(N-epsilon-5'-phospho) adenosyl phosphoamidase in Dictyostelium discoideum. *Int J Biochem* **1986,** *18* (5), 481-4.
9. McDonald, J. R.; Walsh, M. P., Ca2+-binding proteins from bovine brain including a potent inhibitor of protein kinase C. *Biochem J* **1985,** *232* (2), 559-67.
10. Pearson, J. D.; DeWald, D. B.; Mathews, W. R.; Mozier, N. M.; Zürcher-Neely, H. A.; Heinrikson, R. L.; Morris, M. A.; McCubbin, W. D.; McDonald, J. R.; Fraser, E. D., Amino acid sequence and characterization of a protein inhibitor of protein kinase C. *J Biol Chem* **1990,** *265* (8), 4583-91.
11. Lima, C. D.; Klein, M. G.; Weinstein, I. B.; Hendrickson, W. A., Three-dimensional structure of human protein kinase C interacting protein 1, a member of the HIT family of proteins. *Proc Natl Acad Sci U S A* **1996,** *93* (11), 5357-62.
12. Brzoska, P. M.; Chen, H.; Levin, N. A.; Kuo, W. L.; Collins, C.; Fu, K. K.; Gray, J. W.; Christman, M. F., Cloning, mapping, and in vivo localization of a human member of the PKCI-1 protein family (PRKCNH1). *Genomics* **1996,** *36* (1), 151-6.
13. Bustos, S. A.; Schaefer, M. R.; Golden, S. S., Different and rapid responses of four cyanobacterial psbA transcripts to changes in light intensity. *J Bacteriol* **1990,** *172* (4), 1998-2004.

14. Bieganowski, P.; Garrison, P. N.; Hodawadekar, S. C.; Faye, G.; Barnes, L. D.; Brenner, C., Adenosine monophosphoramidase activity of Hint and Hnt1 supports function of Kin28, Ccl1, and Tfb3. *J Biol Chem* **2002,** *277* (13), 10852-60.
15. Zhang, X.; Zhai, C.; Hua, C.; Qiu, M.; Hao, Y.; Nie, P.; Ye, W.; Wang, Y., PsHint1, associated with the G-protein α subunit PsGPA1, is required for the chemotaxis and pathogenicity of Phytophthora sojae. *Mol Plant Pathol* **2016,** *17* (2), 272-85.
16. Priscilla S. An, L. E. D., Yuan Luo and Jia Bei Wang, *Enhanced odorant preference associative learning in C. Elegans with protein kinase C-interactive protein (PKCI)/HINT1 mutation*. Nova science: Trends in cognitive sciences, 2012.
17. Guang, W.; Wang, H.; Su, T.; Weinstein, I. B.; Wang, J. B., Role of mPKCI, a novel mu-opioid receptor interactive protein, in receptor desensitization, phosphorylation, and morphine-induced analgesia. *Mol Pharmacol* **2004,** *66* (5), 1285-92.
18. Ajit, S. K.; Ramineni, S.; Edris, W.; Hunt, R. A.; Hum, W. T.; Hepler, J. R.; Young, K. H., RGSZ1 interacts with protein kinase C interacting protein PKCI-1 and modulates mu opioid receptor signaling. *Cell Signal* **2007,** *19* (4), 723-30.
19. Rodríguez-Muñoz, M.; Garzón, J., Nitric oxide and zinc-mediated protein assemblies involved in mu opioid receptor signaling. *Mol Neurobiol* **2013,** *48* (3), 769-82.
20. Sánchez-Blázquez, P.; Rodríguez-Muñoz, M.; Garzón, J., The cannabinoid receptor 1 associates with NMDA receptors to produce glutamatergic hypofunction: implications in psychosis and schizophrenia. *Front Pharmacol* **2014,** *4*, 169.
21. Liu, Q.; Puche, A. C.; Wang, J. B., Distribution and expression of protein kinase C interactive protein (PKCI/HINT1) in mouse central nervous system (CNS). *Neurochem Res* **2008,** *33* (7), 1263-76.
22. Varadarajulu, J.; Lebar, M.; Krishnamoorthy, G.; Habelt, S.; Lu, J.; Bernard Weinstein, I.; Li, H.; Holsboer, F.; Turck, C. W.; Touma, C., Increased anxiety-related behaviour in Hint1 knockout mice. *Behav Brain Res* **2011,** *220* (2), 305-11.
23. Turetsky, B. I.; Hahn, C. G.; Borgmann-Winter, K.; Moberg, P. J., Scents and nonsense: olfactory dysfunction in schizophrenia. *Schizophr Bull* **2009,** *35* (6), 1117-31.
24. Varadarajulu, J.; Schmitt, A.; Falkai, P.; Alsaif, M.; Turck, C. W.; Martins-de-Souza, D., Differential expression of HINT1 in schizophrenia brain tissue. *Eur Arch Psychiatry Clin Neurosci* **2012,** *262* (2), 167-72.
25. Jackson, K. J.; Wang, J. B.; Barbier, E.; Damaj, M. I.; Chen, X., The histidine triad nucleotide binding 1 protein is involved in nicotine reward and physical nicotine withdrawal in mice. *Neurosci Lett* **2013,** *550*, 129-33.
26. Jackson, K. J.; Chen, Q.; Chen, J.; Aggen, S. H.; Kendler, K. S.; Chen, X., Association of the histidine-triad nucleotide-binding protein-1 (HINT1) gene variants with nicotine dependence. *Pharmacogenomics J* **2011,** *11* (4), 251-7.
27. Zimoń, M.; Baets, J.; Almeida-Souza, L.; De Vriendt, E.; Nikodinovic, J.; Parman, Y.; Battaloğlu, E.; Matur, Z.; Guergueltcheva, V.; Tournev, I.; Auer-Grumbach, M.; De Rijk, P.; Petersen, B. S.; Müller, T.; Fransen, E.; Van Damme, P.; Löscher, W. N.; Barišić, N.; Mitrovic, Z.; Previtali, S. C.; Topaloğlu, H.; Bernert, G.; Beleza-Meireles, A.;

Todorovic, S.; Savic-Pavicevic, D.; Ishpekova, B.; Lechner, S.; Peeters, K.; Ooms, T.; Hahn, A. F.; Züchner, S.; Timmerman, V.; Van Dijck, P.; Rasic, V. M.; Janecke, A. R.; De Jonghe, P.; Jordanova, A., Loss-of-function mutations in HINT1 cause axonal neuropathy with neuromyotonia. *Nat Genet* **2012,** *44* (10), 1080-3.
28. Liu, F.; Ma, J.; Liu, P.; Chu, Z.; Lei, G.; Jia, X. D.; Wang, J. B.; Dang, Y. H., Hint1 gene deficiency enhances the supraspinal nociceptive sensitivity in mice. *Brain Behav* **2016,** *6* (8), e00496.
29. Su, T.; Suzui, M.; Wang, L.; Lin, C. S.; Xing, W. Q.; Weinstein, I. B., Deletion of histidine triad nucleotide-binding protein 1/PKC-interacting protein in mice enhances cell growth and carcinogenesis. *Proc Natl Acad Sci U S A* **2003,** *100* (13), 7824-9.
30. Li, H.; Zhang, Y.; Su, T.; Santella, R. M.; Weinstein, I. B., Hint1 is a haplo-insufficient tumor suppressor in mice. *Oncogene* **2006,** *25* (5), 713-21.
31. Zhang, Y. J.; Li, H.; Wu, H. C.; Shen, J.; Wang, L.; Yu, M. W.; Lee, P. H.; Bernard Weinstein, I.; Santella, R. M., Silencing of Hint1, a novel tumor suppressor gene, by promoter hypermethylation in hepatocellular carcinoma. *Cancer Lett* **2009,** *275* (2), 277-84.
32. Weiske, J.; Huber, O., The histidine triad protein Hint1 triggers apoptosis independent of its enzymatic activity. *J Biol Chem* **2006,** *281* (37), 27356-66.
33. Gallant, P., Control of transcription by Pontin and Reptin. *Trends Cell Biol* **2007,** *17* (4), 187-92.
34. Wang, L.; Zhang, Y.; Li, H.; Xu, Z.; Santella, R. M.; Weinstein, I. B., Hint1 inhibits growth and activator protein-1 activity in human colon cancer cells. *Cancer Res* **2007,** *67* (10), 4700-8.
35. Martin, J.; Magnino, F.; Schmidt, K.; Piguet, A. C.; Lee, J. S.; Semela, D.; St-Pierre, M. V.; Ziemiecki, A.; Cassio, D.; Brenner, C.; Thorgeirsson, S. S.; Dufour, J. F., Hint2, a mitochondrial apoptotic sensitizer down-regulated in hepatocellular carcinoma. *Gastroenterology* **2006,** *130* (7), 2179-88.
36. Razin, E.; Zhang, Z. C.; Nechushtan, H.; Frenkel, S.; Lee, Y. N.; Arudchandran, R.; Rivera, J., Suppression of microphthalmia transcriptional activity by its association with protein kinase C-interacting protein 1 in mast cells. *J Biol Chem* **1999,** *274* (48), 34272-6.
37. Yannay-Cohen, N.; Carmi-Levy, I.; Kay, G.; Yang, C. M.; Han, J. M.; Kemeny, D. M.; Kim, S.; Nechushtan, H.; Razin, E., LysRS serves as a key signaling molecule in the immune response by regulating gene expression. *Mol Cell* **2009,** *34* (5), 603-11.
38. Ofir-Birin, Y.; Fang, P.; Bennett, S. P.; Zhang, H. M.; Wang, J.; Rachmin, I.; Shapiro, R.; Song, J.; Dagan, A.; Pozo, J.; Kim, S.; Marshall, A. G.; Schimmel, P.; Yang, X. L.; Nechushtan, H.; Razin, E.; Guo, M., Structural switch of lysyl-tRNA synthetase between translation and transcription. *Mol Cell* **2013,** *49* (1), 30-42.
39. Martin, J.; Maurhofer, O.; Bellance, N.; Benard, G.; Graber, F.; Hahn, D.; Galinier, A.; Hora, C.; Gupta, A.; Ferrand, G.; Hoppeler, H.; Rossignol, R.; Dufour, J. F.; St-Pierre, M. V., Disruption of the histidine triad nucleotide-binding hint2 gene in mice affects glycemic control and mitochondrial function. *Hepatology* **2013,** *57* (5), 2037-48.

40. Lenglet, S.; Antigny, F.; Vetterli, L.; Dufour, J. F.; Rossier, M. F., Hint2 is expressed in the mitochondria of H295R cells and is involved in steroidogenesis. *Endocrinology* **2008,** *149* (11), 5461-9.
41. Ndiaye, D.; Collado-Hilly, M.; Martin, J.; Prigent, S.; Dufour, J. F.; Combettes, L.; Dupont, G., Characterization of the effect of the mitochondrial protein Hint2 on intracellular Ca(2+) dynamics. *Biophys J* **2013,** *105* (5), 1268-75.
42. Maize, K. M.; Wagner, C. R.; Finzel, B. C., Structural characterization of human histidine triad nucleotide-binding protein 2, a member of the histidine triad superfamily. *FEBS J* **2013,** *280* (14), 3389-98.
43. Chou, T. F.; Cheng, J.; Tikh, I. B.; Wagner, C. R., Evidence that human histidine triad nucleotide binding protein 3 (Hint3) is a distinct branch of the histidine triad (HIT) superfamily. *J Mol Biol* **2007,** *373* (4), 978-89.
44. Chou, T. F.; Tikh, I. B.; Horta, B. A.; Ghosh, B.; De Alencastro, R. B.; Wagner, C. R., Engineered monomeric human histidine triad nucleotide-binding protein 1 hydrolyzes fluorogenic acyl-adenylate and lysyl-tRNA synthetase-generated lysyl-adenylate. *J Biol Chem* **2007,** *282* (20), 15137-47.

Chapter 2

A New Target For Pain: **Inhibition of Hint1 as a novel strategy to modulate the cross talk between μ-Opioid and NMDA receptor in the central nervous system**

INTRODUCTION:

The transition of nociceptive signals into chronic pain is dependent on key cellular signaling events that modulate synaptic plasticity of the central nervous system.[1-3] The duration or frequency of the input signal is critical in mediating long-term neuronal cellular fate. Two layers of regulation mediate such neuronal processes: first an upstream rapid activation of the transient signaling filters high-frequency signals, which ultimately transmits to downstream signaling events leading to stable alterations such as receptor localization, gene expression, morphological changes or synaptic remodeling.[4, 5] Such changes are described as long-term synaptic potentiation (LTP),[6] which often relies on the activation of the postsynaptic N-methyl-D-aspartate (NMDA) receptors by neurotransmitter such as glutamate. Development of neuropathic is induced primary via sensitization of the primary sensory neurons (peripheral sensitization) following subsequent sensitization of the spinal cord neurons (central sensitization).[1, 2] Activation of the NMDA receptors in the spinal dorsal horn nociceptive neurons plays an essential role in the development of hypersensitivity to pain.[7, 8] Administration of NMDA, an agonist of NMDA receptor, intrathecally exhibits biting, scratching and licking nociceptive hyperalgesic behavior in mice. Opioids such as morphine are known to alleviate such behavior (**Scheme 1**).[9-11]

According to "control gate theory" the nociceptive signals originated in the peripheral nervous system encounter "nerve gates" before reaching the cortical region of the brain.[1] Certain discrete regions of the brain, including periaqueductal gray area (PAG) of brain, negatively regulate the nerve gates. Studies have demonstrated that direct

electric stimulation of PAG region inhibits opening of the nerve gates and hence produces an analgesic effect. Most clinically used opioids act by activating MOR (possibly in the PAG region, where they are densely expressed) to produce analgesic effect. It is also known that repeated exposure of opioids leads to the development of acute tolerance via activation of NMDAR signaling pathway in both PAG and dorsal horn of the spinal cord.[12, 13] Such events have been described to be essential for the transition of an acute pain into chronic state. Although this phenomenon is well known, the molecular mechanism governing the cross-talk between MOR and NMDAR has remained unclear.

In 2004, Wang and coworkers demonstrated that genetic disruption of Human histidine triad nucleotide binding protein 1 (hHint1) in mice results into increased morphine analgesia as well as reduced development of tolerance.[14] It has been proposed that upon morphine challenge, the interplay of different protein assemblies (including PKCγ) at MOR results in the activation of NMDAR, leading to the development of acute morphine tolerance.[15-17] Hint1 plays an essential role in recruiting these protein assemblies at MOR.[18] As a result, NMDAR fails to exert any negative regulation on MOR signaling in Hint1$^{-/-}$ mice, resulting into enhanced analgesic effect of morphine (**Scheme 1, Chapter 1**). One of the limitations associated with genetic knockout studies is that they cannot differentiate whether the role of Hint1-protein interactions or enzymatic activity is associated with the phenotypic response.

Chemical genetics is a powerful approach to elucidate biological functions of genes or proteins of interest using screens of diverse and targeted small molecules.

Scheme 1. Proposed schematic pathway for the mechanism of NMDA evoked nociceptive (scratching and biting) behavior and effect of morphine in antagonizing this effect in spinal cord. Hint1 plays an important regulatory protein via unknown mechanism regulating its active site in governing this cross talk. In the basal state Hint1 is associated with NMDAR, upon NMDA challenge the scratching behavior is observed via NMDAR activation and calcium influx. Administration of morphine leads to a negative feed back on NMDAR signaling and hence blocking this effect via co associating with NMDAR. Administration of TrpGc prevents this cross talk and antagonizes the effect of morphine in vivo.

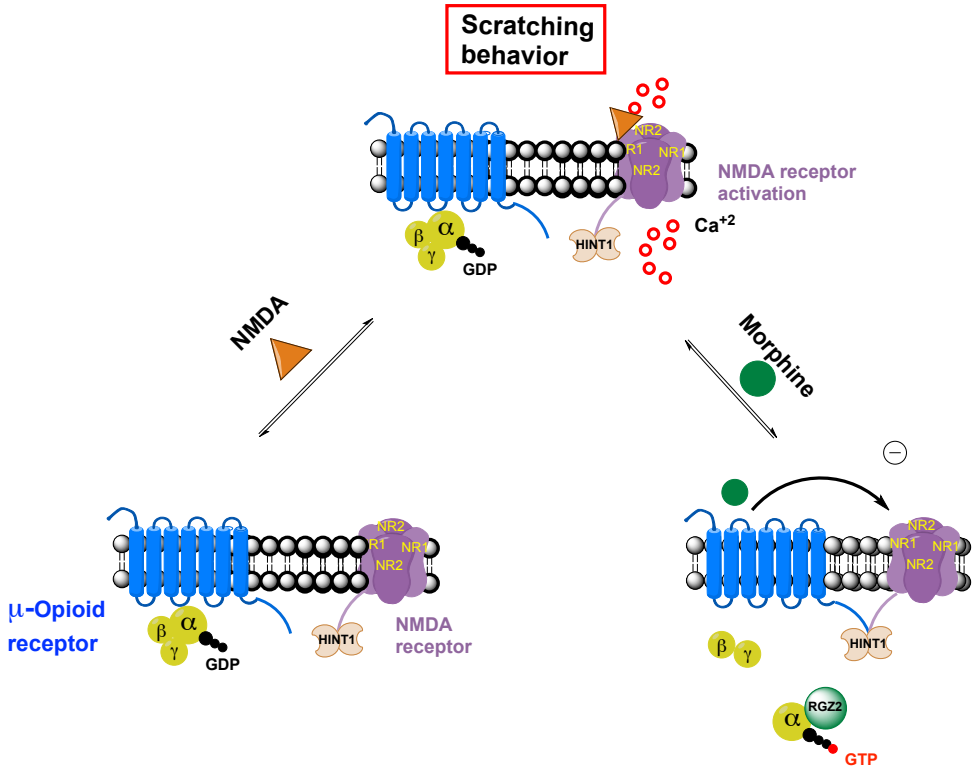

Screening small molecule libraries for a compound that induces phenotype of interest represents forward chemical genetics, whereas reverse approach uses small molecules targeted to a protein or gene of interest, to probe their biological function.[19] Both approaches offer particular advantages of reversibility and potential to modulate protein function *in vivo*. In the current work, we describe reverse chemical genetic approach in combination with neuropharmacological studies to investigate the role of Hint1 active site in modulating opioid analgesia and neuropathic pain.

RESULTS

Synthesis and *in vitro* characterization of an nucleoside carbamate inhibitor of Hint1

We have previously developed an inhibitor of Hint1 by replacing the phosphoramidate backbone of the substrate with a non-hydrolysable carbamate linker (**Figure 1**). The designed inhibitor contains tryptamine coupled to 5′-OH of the guanosine with a carbamate linker (**TrpGc**). We chose guanosine instead of adenosine in order to avoid off-target effects associated with inhibiting other adenosine triphosphate (**ATP**) utilizing enzymes. The reported synthesis of **TrpGc** proceeds via isolation of the activated ester and subsequent coupling to an amine side chain.[20] Nevertheless, our attempts to isolate the intermediate proved futile due to high reactivity and instability of the activated ester (data not shown). To circumvent this problem, we revised the synthesis under one-pot reaction without need for the isolation of the intermediate (**Scheme 2**). Activation of the protected guanosine (**2**) with 1.2 equivalents of chloroformate followed by subsequent

addition of an excess amount of tryptamine (**4.0 eqv**) resulted in the coupled product (**3**). Isolation and deprotection of **3** with an aqueous TFA resulted in the final product with 70% yield.[17] Next, we investigated the effect of TrpGc on the activity of hHint1 using a fluorescence assay described previously.[21] Under fixed saturating substrate concentration, a dose-dependent decrease in the activity of hHint1 was observed upon addition of TrpGc. The half maximum inhibitory concentration (IC_{50}) value of TrpGc was calculated to be 25.5 ± 6.0 μM (**Figure 2**, Bottom). Next, we employed isothermal titration calorimetric (ITC) studies to investigate the thermodynamic forces behind the non-covalent association of TrpGc with hHint1 (**Figure 2**, Top). Thermodynamic studies indicated that enthalpic but not entropic forces are primarily responsible for the binding of TrpGc to hHint1 (**Table 1**). The dissociation constant (K_d) value was calculated to be 3.65 ± 1.0 μM and with an n value of 0.98 ± 0.5, indicating single-site binding event per monomer (**Table 1**).[17]

TrpGc increases the analgesic effect of opioids in mice

To perform reverse chemical genetic studies with TrpGc, we established collaboration with the neuropharmacological laboratory of Dr. Javier Garzon at the Cajal Institute in Spain. We began by evaluating morphine analgesia using a tail flick assay on two different strains of mice. The ED_{80} value for morphine in 129S1 mice was calculated to be 1 nmol, whereas a value of 10 nmol was found for CD1 mice. This result is consistent with the fact that opioids produce a stronger analgesic response in 129S1 strains than CD1 mice. We used the respective ED_{80} values for the dosing of morphine in our animal studies. Upon pretreatment of mice with TrpGc (20 nmoles i.c.v) an increased in

Figure 1. Chemical structures of the substrates and an inhibitor of Human Hint1

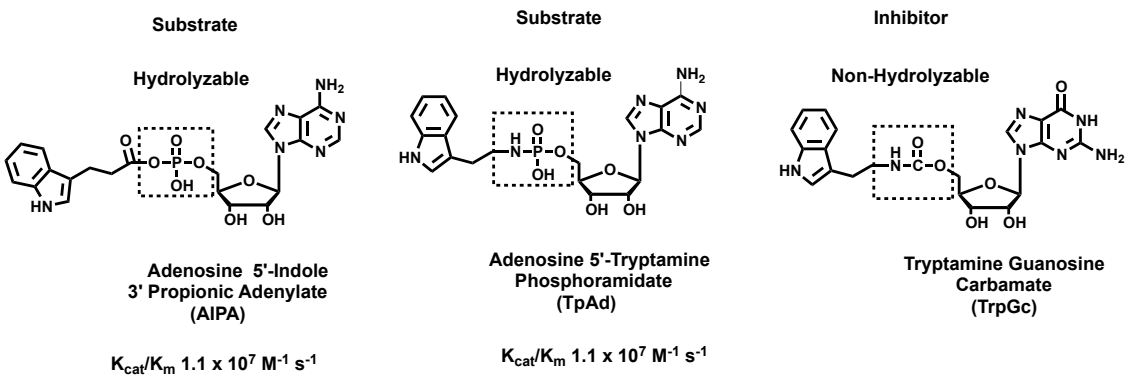

Scheme 2: Synthetic scheme for TrpGc.

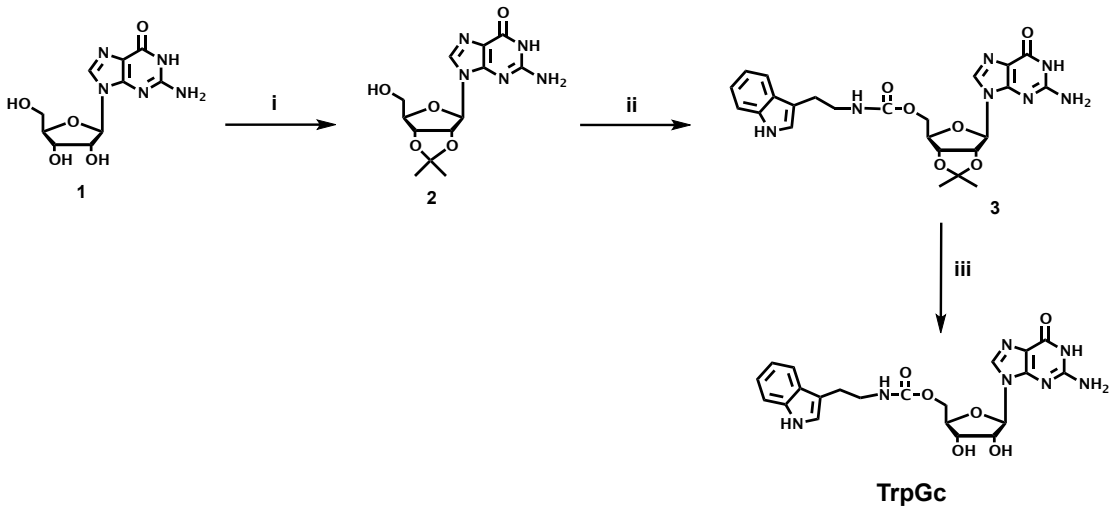

Reagents and conditions: i) cat perchloric acid, acetone, %; ii) p-chlorophenyl chloroformate, pyridine 2 h; tryptamine, 70%; iii) 80 % aq. TFA quant

Figure 2. Isothermal titration calorimetric curve of TrpGc. (Top) A typical binding isotherm created after plotting integrated heat peaks against the molar ratio of TrpGc (400 μM, 10 mM Tris, 150 mM NaCl, pH 7.5) titrated into the solution of hHint1 (30 μM). (Bottom) A dose response curve generated by the performing the titration of hHint1 activity in the presence of TrpGc in the presence of saturating concentration of the substrate (TpAd).

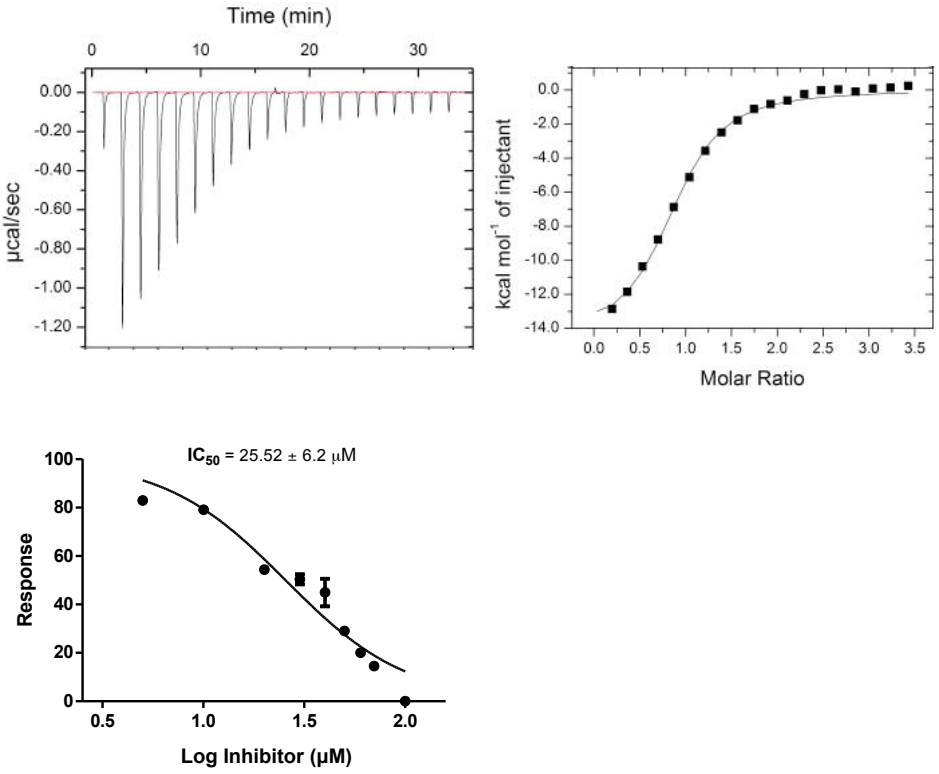

Table 1: Thermodynamic parameters of TrpGc binding to hHint1

Ligand	**K_d (uM)**	**ΔH (kcal/mol)**	**-TΔS (kcal/mol)**	**ΔG (kcal/mol)**	**n**
TrpGc	3.65 ± 1.00	-13.54 ± 1.00	9.54 ± 4.17	-4.1 ± 2.0	0.98 ± 0.5

analgesic response was observed following morphine (1 nmol, i.c.v, 20 minutes before) administration, when compared to the morphine treatment alone. This effect was clearly absent in Hint1$^{-/-}$ mice indicating that other Hint isoforms (Hint 2 and 3) cannot compensate for the loss of Hint1 activity in the opioid signaling pathway (**Figure 3A**). This result is also consistent with previously reported studies that demonstrated very little or no expression of Hint2 in brain tissues (**Chapter 1, Figure 9**). In addition, this effect was not only restricted to the morphine but also to the other opioids such as DAMGO (**Figure 3C**). To assess the blood-brain barrier (BBB) permeability, we performed subcutaneous injection of TrpGc in our studies. To our surprise, we observed an enhanced morphine antinociception effect (**Figure 3D**), indicating BBB permeability of TrpGc.

TrpGc prevents/rescues the development of morphine tolerance in mice

Administration of morphine at its ED_{80} values is known to decrease the antinociceptive response in mice to the successive test doses of the opioids. Tolerance becomes evident 24 h after the animals have received a single (priming) dose of morphine (1 nmol). Administration of TrpGc 20 min before the priming dose of morphine significantly reduced the development of tolerance in mice (**Figure 3B**). In mice that had received the priming dose of morphine, injection of TrpGc 20 min before the test dose restored the antinociceptive potency of the morphine. These results indicate that TrpGc can not only prevent but also rescue morphine tolerance in mice. In similar fashion, TrpGc given 50 min before the test dose produced an incomplete but still a significant amount of the opioid antinociception (**Figure 3B**).[17]

Figure 3. Tail flick assay for the analysis of opioids analgesia and tolerance in the presence or absence of TrpGc. A) Time-course: groups of ten CD1 mice were injected with 20 nmol of the Hint1 inhibitor TrpGc or vehicle 20 min before morphine (6 nmol), and antinociception was evaluated at the post-opioid intervals indicated. *Significantly different from the morphine control group that received vehicle instead of Hint1 inhibitors, $p < 0.05$. All drugs were icv injected. B) Morphine acute tolerance, prevention: CD1 mice were administered 20 nmol TrpGc or vehicle 20 or 50 min before a priming dose of 10 nmol morphine. After 24 h, all mice received a test dose of 10 nmol morphine, and anti-nociception was evaluated 30 min later. Morphine acute tolerance, rescue: the mice received the priming dose of 10 nmol morphine and 24 h later they were injected with 20 nmol TrpGc or vehicle 20 or 50 min before the test dose of 10 nmol morphine (Left). The bars represent the mean ± SEM of groups of eight mice. C) Effect of TrpGc on DAMGO-induced anti- nociception. CD1 mice received the vehicle, 20 nmol TrpGc 20 min before 100 pmol DAMGO. D) The effect of subcutaneous (sc) TrpGc (50 mg/kg) on the anti- nociception evoked by morphine (10 mg/kg, sc). Each point is the mean ± SEM of groups of eight mice. *Significantly different from the control group that received the opioid but vehicle instead of the Hint regulator, $p < 0.05$. Unless otherwise specified, all drugs were icv injected.

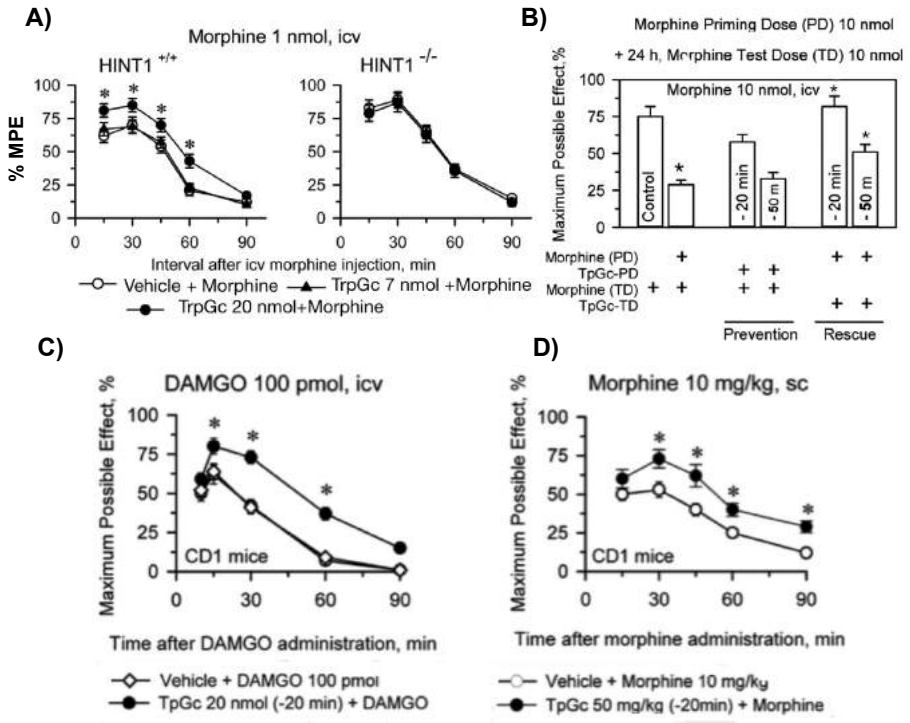
A)
Morphine 1 nmol, icv
HINT1 +/+
HINT1 -/-
% MPE
Interval after icv morphine injection, min
Vehicle + Morphine
TrpGc 7 nmol +Morphine
TrpGc 20 nmol+Morphine
B)
Morphine Priming Dose (PD) 10 nmol
+ 24 h, Morphine Test Dose (TD) 10 nmol
Morphine 10 nmol, icv
Maximum Possible Effect,%
Control
- 20 min
- 50 m
- 20 min
- 50 m
Morphine (PD)
TpGc-PD
Morphine (TD)
TpGc-TD
Prevention
Rescue
C)
DAMGO 100 pmol, icv
Maximum Possible Effect, %
CD1 mice
Time after DAMGO administration, min
Vehicle + DAMGO 100 pmol
TpGc 20 nmol (-20 min) + DAMGO
D)
Morphine 10 mg/kg, sc
Maximum Possible Effect, %
CD1 mice
Time after morphine administration, min
Vehicle + Morphine 10 mg/kg
TpGc 50 mg/kg (-20min) + Morphine

Figure 4. Evaluation of TrpGc on CCI mouse model of mechanical allodynia. Induction of mechanical allodynia in wild type (left) and HINT1$^{-/-}$ 129 mice (right): the effect of the Hint1 inhibitor, TrpGc. A) CCI neuropathic pain was induced in 129 mice, and paw withdrawal thresholds were measured in the contralateral and ipsilateral paw in both CCI operated and sham-operated mice (n= 10) before (0) and 3, 7, and 13 days after surgery. The force (in grams) at which the mice withdrew the paw in response to von Frey hair stimulation was determined as an index of mechanical allodynia. All data are presented as the mean ± SEM of eight mice. *Significantly different with respect to the ipsilateral paw; θ versus the corresponding paw in the wild-type mice, $p < 0.05$. B) Lower left and right panels: the effect of TrpGc on the mechanical allodynia displayed by wild type and Hint1 $^{-/-}$ mice. TrpGc (20 nmol) or vehicle were administered i.c.v to sham and CCI mice 7 days after surgery, and the nociceptive threshold was evaluated 30 min later. Each bar represents the mean ± SEM of eight mice. *Significantly different from the contralateral paw nociceptive threshold, $p < 0.05$.

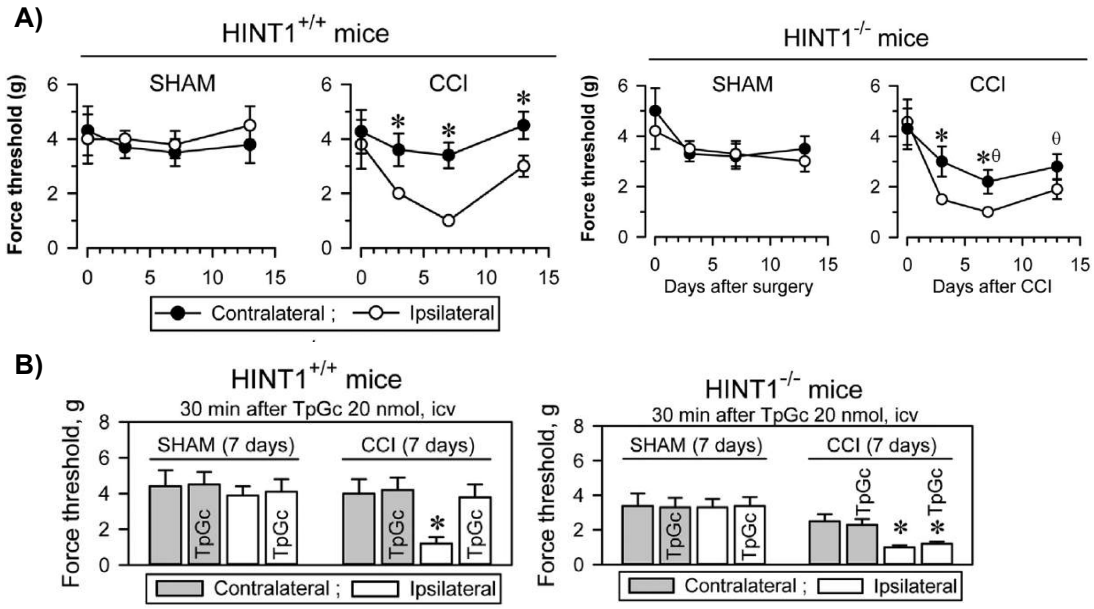
A)
HINT1+/+ mice
HINT1-/- mice
SHAM
CCI
Force threshold (g)
Days after surgery
Days after CCI
Contralateral ; Ipsilateral
B)
HINT1+/+ mice
HINT1-/- mice
30 min after TpGc 20 nmol, icv
SHAM (7 days)
CCI (7 days)
Force threshold, g
TpGc
Contralateral ; Ipsilateral

Figure 5. Time-course effect of a single dose of TrpGc injection (20 nmol, i.c.v) on CCI-induced mechanical allodynia. A group of ten CCI-operated 129 mice received the Hint1 inhibitor, and allodynia was determined at the post-TrpGc intervals indicated (days). The dashed line indicates the nociceptive threshold typical of sham- operated wild-type 129 mice. *Significantly different from the control nociceptive threshold of day 0 (7th after surgery), $p < 0.05$.

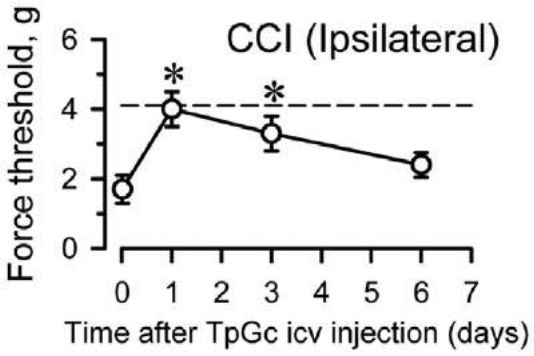

Inhibition of Hint1 reduces neuropathic pain in chronic constriction injury (CCI) model of mice

The output of the dorsal horn nociceptive network in the spinal cord is greatly enhanced during chronic pain, particularly via enhanced excitatory synaptic transmission of NMDA receptors.[7] Hence, we assessed the possible relevance of Hint1 in this disease using chronic constriction injury (CCI) model of neuropathic pain. In the CCI model, the mechanical sensitivity to pain threshold is evaluated by the ability of injured mice to withhold mechanical force of the von-Frey filament. Nerve-injured $Hint1^{+/+}$ and $Hint1^{-/-}$ mice maintained a healthy appearance and were well groomed. Although their body weight decreased after the surgery, it returned to the preoperative values within 2 to 4 days in all animals. Both $Hint1^{+/+}$ and $Hint1^{-/-}$ mice displayed increased sensitivity to mechanical allodynia on the contralateral side of the surgery (**Figure 4A,** left). Notably, $Hint1^{-/-}$ mice also displayed enhanced sensitivity on the ipsilateral side when compared to wild-type animals (**Figure 4A**, right). Administration of a single dose of TrpGc significantly reduced mechanical allodynia, an effect that was observed 30 min after the injection, which lasted for about 48-72 h (**Figure 5**). In contrast such effect was absent in $Hint1^{-/-}$ mice (**Figure 4B**).

Ex-vivo western blot analysis demonstrated that TrpGc reduces activation of NMDAR upon administration of morphine and in neuropathic pain

In the PAG matter of the brain, it has been proposed that the cross talk between MOR and NMDAR regulates the development of tolerance to opioids.[13, 15] Opioids are known to

modulate the association of MORs with NMDAR subunits (**Chapter1**, **Scheme 1**). This process engages NMDAR mediated negative feedback inhibition of the opioid signaling pathway. Morphine promotes the PKC-mediated phosphorylation of serine 890 in the NMDAR NR1 C1 segment, the Src-mediated phosphorylation of tyrosine 1325 of the NMDAR NR2A subunit, and enhanced CaMKII autophosphorylation, which requires NMDAR-activated PKA. TrpGc was administered to CD1 mice 30 min before administering the dose of 10 nmol morphine, and at various intervals, post-opioid, groups of mice were euthanized, and parameters reflecting NMDAR activity were determined in PAG synaptosomal membranes. TrpGc significantly reduced the capacity of morphine to promote these phosphorylation events (**Figure 6A**).

CCI is known to increase the phosphorylation of NMDAR and its downstream signaling proteins, both in the spinal cord as well as in the PAG synaptosomes. Hence, we also investigated the amount of NMDAR phosphorylation in the brain and spinal cord tissues of animals used in the CCI model of neuropathic pain. Sham and CCI operated mice studied 7 days following the surgery has been previously exhibited to display differences in the level of NMDAR phosphorylation. Notably, animals under neuropathic pain and treated with TrpGc, displayed a reduced amount of the phosphorylation events in a time-dependent manner, and 3 h later, the activity of CaMKII (based on P-Thr286), and NMDARs (based on P-Ser NR1 and P-Tyr NR2) was significantly reduced (**Figure 6B**). Hence, Hint1 inhibition reduces NMDAR mediated negative feedback regulation of the opioids.

Figure 6. Modulation of HINT enzymatic activity alters the regulatory connection between MOR and NMDAR. A) Ex vivo evaluation of NMDAR activity: CD1 mice were injected with 20 nmol TrpGc or vehicle, and 20 min later, all of the mice received 10 nmol morphine. All drugs were icv injected. Groups of mice were sacrificed at the post-opioid intervals indicated (m stands for min), and PAG synaptosomes were obtained to determine the levels of phosphorylation related to NMDAR activity in western blots. Actin was used as a loading control. Each bar is the mean ± SEM of groups of six mice. *Significantly different from the control group that received the opioid and the vehicle instead of TrpGc, $p < 0.05$. B) The effect of HINT enzymatic inhibitor on NMDAR-related molecular changes induced by CCI. TrpGc (20 nmol) was administered to CCI mice 7 days after surgery, and different groups of animals were killed at the post-TrpGc time intervals indicated. The effects of TrpGc on phosphorylated CaMKII and NMDAR NR subunits were determined by western blot analysis of spinal cord synaptosomal membranes. Each bar represents the mean ± SEM of six mice. *Significant difference with respect to the CCI control group, which received the vehicle instead of TrpGc, $p < 0.05$. All drugs were injected i.c.v.

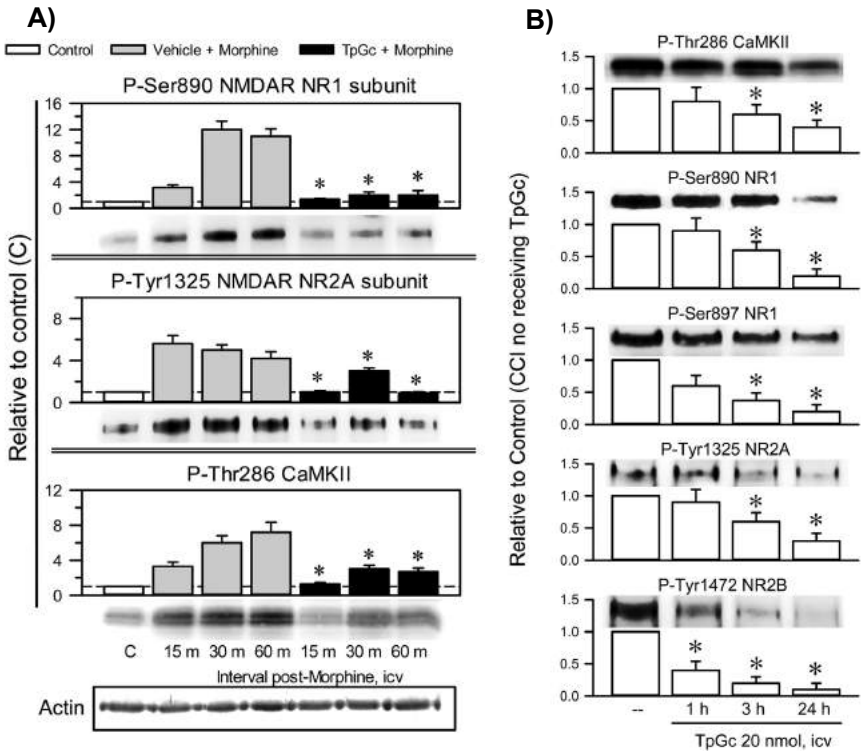
A)
Control
Vehicle + Morphine
TpGc + Morphine
P-Ser890 NMDAR NR1 subunit
P-Tyr1325 NMDAR NR2A subunit
P-Thr286 CaMKII
Relative to control (C)
C
15 m
30 m
60 m
15 m
30 m
60 m
Interval post-Morphine, icv
Actin
B)
P-Thr286 CaMKII
P-Ser890 NR1
P-Ser897 NR1
P-Tyr1325 NR2A
P-Tyr1472 NR2B
Relative to Control (CCI no receiving TpGc)
--
1 h
3 h
24 h
TpGc 20 nmol, icv

TrpGc prevents endomorphin-2 tolerance on the spinal cord

Encouraged by our promising results with TrpGc on morphine analgesic response, we next wanted to ask whether inhibition of Hint1 has any effect on endogenous opioids such as endomorphin-1 or 2. Both opioids previously have been shown to develop tolerance within few minutes of administration.[22] The model would provide us with an alternative for rapid pharmacological evaluation of Hint1 inhibitors *in vivo*. As seen in **Figure 7A,** administration of the endomorphin-2 (10 nmoles) elicits an analgesic response in mice on a hot plate assay. In control experiment administration of the second dose of endomorphin-2 elicits a lower analgesic response when compared to the priming dose. Animals treated with TrpGc (5 nmoles) before administration of the second dose elicited nearly an identical response to the first one, indicating rescue in the development of the tolerance. This result suggests that Hint1 active site plays an important role in the development of tolerance to opioids in the spinal cord pain circuit.

Inhibition of Hint1 antagonizes the effect of morphine on NMDA evoked behavior in mice

Spinal activation of NMDA receptors has been shown to play an important role in the nociceptive processes at the spinal level.[7, 8] Intrathecal administration of NMDA (0.3 nmoles i.t.), an agonist of NMDA receptor, induces hyperalgesic responses such as scratching, biting and licking behavior in mice (**Scheme 1**).[10] Administration of opioids inhibit these behavior in dose dependent manner. We wanted to investigate the effect of Hint1 inhibition on the cross talk between NMDA receptor and μ-opioid receptor on the

Figure 7. Effect of TrpGc on the development of Endomorphin-2 and morphine acute tolerance in mice. A) Endomorphin-2 acute tolerance, prevention: CD1 mice were administered 20 nmol TrpGc or vehicle 5 min before a priming dose of 10 nmol endomorphin-2. After 30 min, all mice received a test dose of the 10 nmol morphine, and anti-nociception was evaluated 2.5 min later. The bars represent the mean ± SEM of groups of four mice. B) % Inhibition of NMDA evoked behavior (upon administration of 0.3 nmoles of NMDA intrathecally) in a dose dependent manner by morphine (circle). TrpGc (black triangle) antagonized the effect of morphine and right shifted the dose response curve by at least 10 fold. Values represents standard deviation within n = 3 mice.

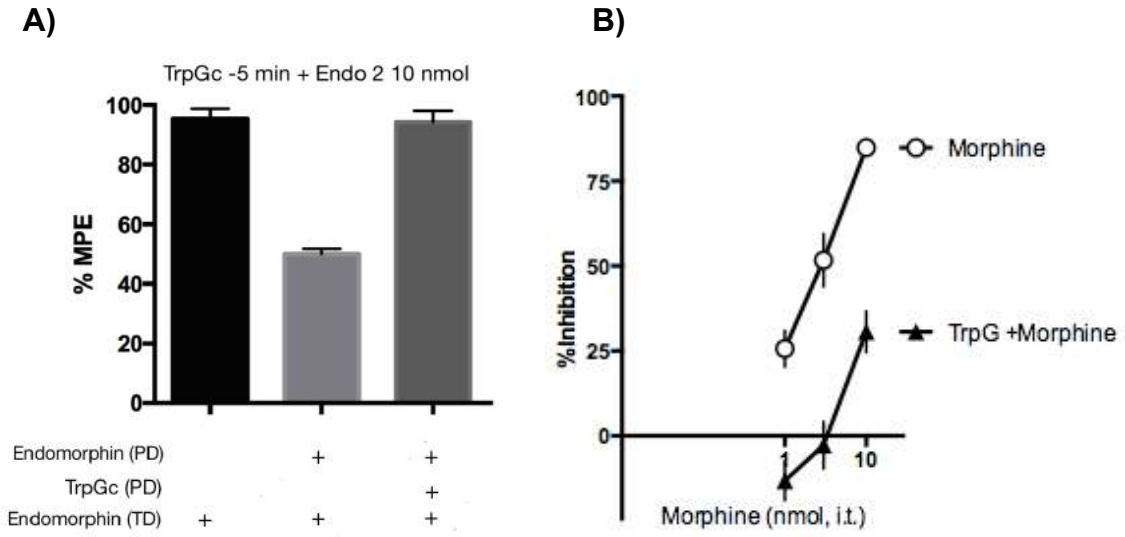

spinal nociceptive process. Co-administration of TrpGc along with NMDA and morphine antagonized the opioids analgesic effect in a dose dependent manner (**Figure 7B**). A ten-fold shift in the dose response curve to the right was observed upon Hint1 inhibitions (**Figure 7B**). Our results clearly indicate an important role of Hint1 active site in regulating bidirectional cross talk between MOR and NMDAR on the spinal cord.

Discussion

Results from our current study strongly suggest that Hint1 active site is important for the bidirectional cross talk between GPCRs and NMDARs. Inhibition of Hint1 not only increases the analgesic effect but also prevents/rescues the development of the opioid tolerance. One of the significant findings was that the pretreatment of animals with a single dose of TrpGc alone reduces neuropathic pain, an effect that lasted for 3-4 days in animals. Functional assembly of NMDAR requires both NR1 (GluN1) and NR2A (GluN2A) or NR2B (GluN2B) subunits. Both GluN2A and GluN2B play a very different role in synaptic plasticity and NMDA-induced neuropathic pain.[23-25] Moreover, recent results from ji and co-workers have clearly demonstrated that GluN2B, but not GluN2A is responsible for the development of neuropathic pain in the spinal cord.[8] Our results point to the fact that Hint1 may be involved in regulating the assembly or activation of different NMDAR subunits for differential functions. The fact that pretreatment with a single dose of a small molecule *Hint1* inhibitor reduces the neuropathic pain in animals for 4-5 days without morphine is very intriguing result. Are the observed effect of *Hint1* inhibition on neuropathic pain resulting from a decrease in the development of tolerance to endogenous opioids such as endomorphins or directly modulating NMDAR function?

Investigating the effect of a *Hint1* inhibitor on neuropathic pain in MOR knockout mice or in the presence of an MOR antagonist could be used to address such question.

From functional point of view, MOR is negatively regulated by NMDA receptor. Our molecular studies indicated that TrpGc reduces activation of NMDAR and hence prevents/rescues the development of opioid's tolerance. We also discovered that TrpGc antagonizes morphine's effect on NMDA evoked behavior in animals. These results indicate that Hint1 is a critical regulator of the bidirectional cross talk between MOR and NMDA receptors. However, correlation of the Hint1 active site in regulating NMDAR activity still remains largely unknown. In our study, we also found that $Hint1^{-/-}$ mice are more sensitized to pain on the ipsilateral side in CCI model, when compared to wild type (**Figure 4A**). The ratio of NMDA/AMPA receptor in the spinal lamina II neurons has been previously shown to be important in amplifying neuropathic pain.[8, 26] Future genetic studies with catalytically impaired or less active Hint1 mutants mice models and electrophysiological studies would help to correlate Hint1 activity to NMDAR function.[27]

NMDAR regulates a variety of physiological processes by regulating the flux of Ca^{2+} ions across the cellular membrane. Dysregulation of NMDAR has been associated with disorders such as chronic pain, Schizophrenia and Alzheimer's disease.[23, 25] It is also speculated that activity of NMDAR can be modulated by a variety of different GPCRs. For example, both cannabinoid 1 receptor (CB1) and dopaminergic receptors are known modulate the function of NMDA receptor.[28] [29] Clearly, such cross talks has been evolved to regulate complex functions of the brain. Consistent with this, Hint1 knock out animals exhibit less nicotine dependence and increased amphetamine sensitivity.[30, 31] An aberrant

expression of Hint1 is also observed in patients suffering from schizophrenia. Taken together, it is likely that Hint1 has an important role in the modulation of the NMDAR functions. Thus, Hint1 inhibitors could also serve as chemical probes to study function of Hint1 in regulating nicotine dependence and amphetamine sensitivity. In addition, our Hint1 inhibitors could be of potential therapeutic interest as adjuvants to reduce the development of tolerance to opioids as well as reduce the dosage requirement of the opioids clinically.

Materials and Methods

General Methods and Materials:

Guanosine was purchased from Acros Organics. p-Chlorophenyl Chloroformate (cat no: 363871) and Tryptamine (cat no: 246557 Sigma Aldrich) was purchased from Sigma-Aldrich. All solvents were purchased from Fischer Scientific and used as received unless otherwise noted. Pyridine was purchased in a sure seal bottle from Sigma-Aldrich. Thin-layer chromatography was performed using EMD pre-coated silica gel 60 F-254 plates. All preparative separations were performed using Teledyne Isco combiflash system and using RediSepRf high performance gold silica pre-packed columns. High-resolution mass spectrometry was performed LTQ Orbitrap Velos (Thermo ScientificTM). Samples and compounds during synthesis were freeze-dried with a lyophilizer available from Labonaco. All ^{1}H- and ^{13}C-NMR spectra were collected in d_6-DMSO (Cambridge Isotope Laboratories, Cambridge, MA) at 25 °C using AscendTM Bruker spectrometer 500 MHz at the Department of Medicinal Chemistry CCRB NMR facility at the University of Minnesota unless otherwise stated. All NMR chemical shifts were recorded in δ parts per

million using d_6-DMSO as internal reference. Thermodynamic measurements for protein-ligand association were performed in 96-well plates (Nunc 260251 U96 DeepWell 96-Well x 1.3 ml from Thermo Scientific) using MicroCal Auto-ITC200 system (GE Healthcare life sciences). Nickel nitrilotriacetic acid (Ni-NTA) was purchased from Qiagen and cobalt column agarose from Thermofishcer Scientific. Biological buffers were purchased from Sigma-Aldrich. Protease inhibitor tablets were obtained from Roche.

Male albino CD-1 mice (Charles River), and a mouse knock-out strain on a 96% 129 mice genetic background carrying a disrupted Hint1 allele and the corresponding wild type (a gift from I.B. Weinstein/J.B. Wang), were used in these studies. Genotypes were confirmed by PCR analysis of DNA extracted from tail biopsies, and the animals used in this study were 8- to 12-week-old adult male mice. The mice were maintained at 22 °C on a diurnal 12 h light/dark cycle. Procedures involving mice adhered strictly to the guidelines of the European Community for the Care and Use of Laboratory Animals (Council Directive 86/609/EEC) and Spanish Law (RD53/2013) regulating animal research. For the NMDA evoked behavior and endomorphin tolerance studies were performed at University of Minnesota animal care RAR facilities with guidelines strictly adhering to IACUC approved protocols. Morphine sulfate (Merck, Darmstadt, Germany) was dissolved in saline. The inhibitor of Hint enzymatic activity TrpGc was prepared in 1:1:18 (v/v/v) mixture of ethanol: Kolliphor EL (Sigma, C5135): physiological saline and injected icv into the lateral ventricles in a volume of 4 μl. The intrathecal administration of endomorphin-2 and TrpGc was prepared as above and injected in 5 μl. Studies with

subcutaneous evaluation of the morphine and TrpGc was performed at 10 mg/kg and 50 mg/kg doses.

Protein Expression and Purification:

The full-length sequence of hHint1 was expressed from the pMCSG7 vector (N-terminal, tobacco etch virus (TEV) protease cleavable His_6 tag) in Rosetta2 pLysS cells. The cells were grown in 2 x 1L LB (Fisher Scientific) media with ampicillin (100 mg/L, Sigma-Aldrich), chloramphenicol (34 mg/L, Sigma-Aldrich), and glucose (0.1% w/v, BD Difco) at 37 °C with shaking at 250 rpm. At OD_{600} = 0.7, cultures were induced to a final concentration of 1 mM IPTG (Denville Scientific Inc) and incubated at 25°C overnight. The cultures were harvested by centrifugation at 7,500 *g* at 4 °C for 10 min and the pellets were collected, then resuspended in buffer A (50 mM HEPES pH 7.0, 300 mM NaCl, 10% glycerol, 10 mM imidazole), which was then adjusted to 1 $mg \cdot mL^{-1}$ lysozyme and Benzonase nuclease (20 µl). The resuspended cells were lysed by sonication (eight cycles of 30 s on, 30 s off) at 4 °C. The cell debris was removed from the lysate by centrifugation at 16,000 *g* at 4 °C for 45 min. The supernatant was loaded onto a nickel affinity column, washed with buffer A, and then eluted with an imidazole gradient using buffer B (50 mM HEPES pH 7.0, 300 mM NaCl, 10% glycerol, 500 mm imidazole). Fractions containing desired protein was combined and to it was added N-terminally His-tagged TEV protease 2% (w/w). The resulting solutions was transferred to a dialysis tubing (molecular weight cut-off of 6000-7000 Da) and dialyzed against 2 L of TEV cleavage buffer (50 mM HEPES pH 7.0, 300 mM NaCl, 10% glycerol, 0.5 mM EDTA and 1 mM DTT) overnight at 4 °C. The dialyzed protein was then buffer exchanged into

buffer A and passed through cobalt affinity chromatography to remove TEV protease. The flow through obtained was concentrated to 5 mL and further purified using size exclusion chromatography (SEC buffer, 20 mM Tris pH 7.5, 150 mM NaCl, 10% glycerol). Pure fractions were collected and concentrated. The protein concentration was then determined using A_{280} absorbance in nanodrop using calculated extinction coefficient of 8480 M^{-1} cm^{-1} and molecular weight of 14000 Da. The final protein was stored at −80 °C until in use.

Isothermal Titration Calorimetry (ITC):

ITC experiments were conducted on a MicroCal Auto-ITC200 system (GE Healthcare life sciences). All titration experiments were performed at 20 °C in ITC buffer (10 mM Tris, 150 mM NaCl, pH 7.5). hHint1 was exchanged into ITC buffer using Micro biospin6 columns (BioRad, USA) and final protein concentrations were determined as described above. To determine the dissociation constant of stock concentration (400 μM) of TrpGc was titrated with 30 μM of hHint1. Twenty injections of ligand were injected (injection volume 2 μl) into the protein cell. The resulting change in enthalpy was measured and the background heat of dilution was subtracted by performing similar experiments in the absence of inhibitors. The background heat of dilution was subtracted from the resulting data and was fitted into one-site binding model using the ITC_{200} microcal software. The resulting association constant obtained by fitting the curve was converted into K_d using $K_a = 1/K_d$ relationship.

Evaluation of antinociception and production of acute tolerance of morphine

Antinociception was assessed at different time intervals after administration of the drugs using the corresponding vehicle as a control. The response of the animals to nociceptive stimuli was determined by the warm water (52 °C) tail-flick test and antinociception was expressed as a percentage of the maximum possible effect (MPE 1⁄4 100 [test latency baseline latency]/[cut-off time (10 s) baseline latency]). The baseline latencies ranged from 2 to 2.5 s and the vehicle did not affect them.

Animals received an icv priming dose of morphine that produces approximately 80% of the maximum antinociceptive effect. The experimental groups received, TpGc or the vehicle prior to the morphine-priming dose. Development of acute tolerance was ascertained by evaluating the antinociceptive response 24 h post-injection, when the antinociceptive effect of priming morphine dose had dissipated as witnessed by the restoration of baseline latencies in the tail-flick test. Pharmacological rescue of the acute tolerance induced via priming does of morphine was evaluated by administering TrpGc (20 nmol, icv) 20 and 50 min before administering the second dose of morphine (24 h post-priming dose).

Evaluation of the prevention of the acute tolerance to endomorphin-2 by TrpGc

Antinociception was assessed at different time intervals after administration of the drugs using the corresponding vehicle as a control as describe above. Animals received an i.t-priming dose of endomorphin-2 (10 nmol) that produces approximately 90% of the maximum antinociceptive effect. The experimental groups received TrpGc (20 nmol) or

the vehicle prior to the endomorphin-2 priming dose and antinociception was assessed from the first dose in the animals. All animal groups after 30 minutes received second dose of endomorphin-2 and evaluating the antinociceptive response after 2.5 min to assess the development of acute tolerance from the first dose.

Chronic constriction nerve injury pain model

After testing the basal mechanical sensitivity of the mice, neuropathic pain was induced by chronic constriction injury (CCI) under isoflurane/oxygen anesthesia,[32] using a modification of the procedure described by Bennett and Xie.[33] Briefly, a 0.5 cm incision was made in the right mid-thigh, the biceps femoris muscle was separated and the sciatic nerve was exposed proximal to its trifurcation. Two ligatures (5/0 braided silk suture; Lorca Marin, Murcia, Spain, 70014) were tied around this nerve, approximately 1 mm apart, until a short flick of the ipsilateral hind limb was observed. The incision was then closed with a 4-0 Ethicon silk suture in layers. The same procedure was used for sham surgeries except that the sciatic nerve was exposed but not ligated.

The tactile pain threshold was then assessed on days 0, 3, 7, and 13 post-surgery, both for the ipsilateral and contralateral hind paws, with the individual mice placed in a transparent plastic cage with a wire mesh bottom that allowed full access to the paws. After a habituation period of 20 min, a mechanical stimulus was delivered to the plantar surface from below the floor of the test chamber to measure allodynia using an automatic von Frey apparatus (Ugo Basile #37450, Comerio, Italy). A steel rod (0.5 mm diameter) was pushed against the hind paw over a 10 s period using increasing force, from 0 to 10

g. When the mouse withdrew its hind paw, the mechanical stimulus was automatically stopped and the force at which withdrawal occurred was recorded. At each time point, three separate threshold measurements were obtained from each hind paw and then averaged.

Western blot Analysis

Membranes from mesencephalic periaqueductal grey matter (PAG) were prepared as described previously,[15] and the separated proteins were then transferred onto 0.2 mm polyvinylidene difluoride (PVDF) membranes (BioRad #162-0176. Spain). The membranes were probed for 24 h at 6 C with the selected antibodies diluted in Tris-buffered saline (TBS) + 0.05% Tween 20 (TTBS) in DecaProbe chambers (PR 150, Hoefer-GE, Spain). All the antibodies used in the study have been shown to bind their target protein in vitro, and their labeling of nervous tissue was greatly reduced by pre-absorption with the recombinant protein or the antigenic peptide when available. The primary antibodies were detected using horseradish peroxidase conjugated secondary antibodies (1:10,000 in TTBS) and antibody binding was visualized with Immobilon Western Chemiluminescent HRP substrate (Millipore WBKLS0100). Chemiluminescence was recorded with a ChemiImager IS-5500 (Alpha Innotech, California, USA) equipped with a Peltier cooled CCD camera that provided a real-time readout of 30 frames per second (35 °C; high signal-to-noise ratio; dynamic range of up to 3.4 optical density units), and densitometry (average optical density of the pixels within the object area/mm^2) was performed using Quantity One Software (BioRad). The antibodies used were raised against: MOR1 2EL (second external loop) and MOR1 CT

(C-terminal, 387e398);[18, 34] HINT1 (Abnova H00003094-A01); NMDAR1 phospho S890 (Cell signaling 3381); NMDAR2A phospho Y1325 (Abcam ab16646); Phospho-Ca^{2+}/calmodulin-dependent protein kinase IIa (CaMKII Thr286, Cell Signaling 3361) and Actin (Cell signaling, 8456).

Studies on NMDA evoked behavior in mice:

NMDA induced behavior test compare the number of hindlimb-directed biting behaviors (nociception) elicited with in a mouse after i.t delivery of NMDA (0.3 nmoles). MOR agonist such as morphine antagonizes this behavior in the dose dependent manner (1, 3 and 10 nmol i.t). Pre-treatment with TrpGc (20 nmol) 5 min before the administration of morphine reduces its efficacy and shifted morphine dose response curve by at least ten fold in mice (n=3). In a control experiment co-treatment with NMDA and TrpGc does not inhibit the NMDA evoked behavior in mice. For these tests, percent antinociception was calculated as percent inhibition ± SEM by the formula [(Control – Experimental)/Control] × 100%.

Synthetic procedure for the preparation of TrpGc

2´, 3´-O-isopropylidene Guanosine (1):

To a cold stirred suspension of guanosine (5.01g, 17.7 mmol) in acetone (300 ml) was added catalytic amount of perchloric acid (1.25 ml) drop-wise. The suspension became gradually clear and the reaction was monitored using TLC (20:80:0.1 MeOH/$CHCl_3$/TEA solvent). At the end of 2 h, ammonium hydroxide (2 equivalent to perchloric acid, 2.75 ml) was added drop-wise to neutralize the reaction mixture under an ice bath. The

resulting product precipitated out from the solution upon neutralization. The reaction mixture was then evaporated under rotary evaporator to complete dryness. The crude reaction mixture was then triturated with ice-cold water (200 ml) overnight. The insoluble material was filtered and washed with cold diethyl ether to collect the desired product (3.99 g, 12.39 mmol) in 70 % yield. The ^{1}H NMR spectrum was (DMSO-d_6): 0.00 (s, TMS internal standard), 1.32 (s, 3H), 1.52 (s, 3H), 3.50-3.56 (m, 2H), 4.10-4.13 (t, 1H), 4.97 (d, 1H), 5.04 (t, 1H), 5.18 (d, 1H), 5.93 (d, 1H), 6.5 (s, 2H), 7.91 (s, 1H) and 10.66 (s, 1H). ^{13}C- DMSO-d_6: 157.16, 154.15, 151.20, 136.30, 117.21, 113.51, 88.87, 87.09, 84.04, 81.64, 62.07, 27.53 and 25.71 ppm. HRMS (ESI+) calcd for $C_{13}H_{18}N5O_5$ [(M+H)+] 324.1308 found 324.1304

Synthesis of 2′, 3′-Isopropylidine-5'-O-[(3-Indolyl)-1-Ethyl]Carbamoyl Guanosine (2):

A solution of p-Cl phenyl chloroformate (52 μl, 0.3708 mmoles) was added dropwise to a stirred solution of **(1)** (100mg, 0.309 mmoles in 5 ml anhydrous pyridine at 0 °C) over a period of 30 minutes. The solution was stirred at room temperature until TLC and ESI MS analysis showed complete consumption of the starting material (2.5 hours). To the solution of an activated carbonate ester of nucleoside was added a tryptamine (99 mg, 0.618 mmoles in pyridine) to form nucleoside carbamate in one-pot. At the end of 24 hours the reaction mixture was then evaporated to dryness under vacuum. The resulting crude mixture was dissolved in ethyl acetate and washed with $NaHCO_3$ (2 x 15 ml) and brine (1 x 10 ml). The organic layer was dried over Na_2SO_4 (anhydrous) and evaporated.

Combiflash was run to purify and isolate the product (236 mg) in 75% yield over two-step reactions performed in one-pot. The ^{1}H NMR spectrum was (DMSO-d6): 1.32 (s, 3H), 1.58 (s, 3H), 2.80 (t, 2H), 3.24 (q, 2H), 4.00- 4.30 (m, 3H), 5.10 (d, 1H), 5.24 (d, 1H), 6.00 (s, 1H), 6.58 (s, 2H), 6.96 (t, 1H), 7.12 (t, 1H), 7.18 (s, 1H), 7.36 (d, 1H), 7.40 (t, 1H), 7.50 (d, 1H), 7.84 (s, 1H), 10.72 (s, 1H), 10.82 (s, 1H) ppm. ^{13}C- DMSO-d_6: 173.42, 156.59, 152.79, 148.73, 140.08, 136.90, 127.12, 121.84, 121.16, 118.41, 117.93, 114.21, 113.35, 111.09, 90.83, 84.94, 84.32, 81.48, 63.76, 34.76, 26.22, 24.40, 26.22, 24.39, 20.66 ppm. Low resolution ESI-MS [M+H] 510.1

Synthesis of 5′-O-[(3-Indolyl)-1-Ethyl]Carbamoyl Guanosine (Guanosine-5′-Tryptamine Carbamate, TrpGc)

2 (50 mg, 0.098 mmoles) was dissolved in a solution of TFA/H_2O (4:1, 2.5 ml) at rt. The reaction was completed in 20 minutes as indicated by TLC. The reaction mixture was evaporated and combiflash was run to purify the product. A total of 35 mg (yield 76.1 %) of the final product was isolated. The ^{1}H NMR spectrum was (DMSO-d_6): 2.38 (t, 2H), 3.17 (q, 2H), 4.23- 4.33 (m, 2H), 4.56 (t, 1H) 5.14 (d, 1H), 5.39 (d, 1H), 6.10 (s, 1H), 6.38 (s, 2H), 6.96 (t, 1H), 7.15 (t, 1H), 7.21 (s, 1H), 7.32 (d, 1H), 7.40 (t, 1H), 7.48 (d, 1H), 7.80 (s, 1H), 10.65 (s, 1H), 10.78 (s, 1H) ppm**.** ^{13}C- DMSO-d_6: 172.48, 159.81, 150.01, 148.92, 140.74, 136.20, 126.84, 122.34, 120.97, 119.15, 118.27, 118.78, 11.95, 111.37, 87.89, 81.66, 73.14, 70.19, 63.82, 34.31, 20.16 ppm. Low resolution ESI-MS [M+H] 470.0 HRMS (ESI+) calcd for $C_{21}H_{23}N_7O_6$ [(M+H)+] 470.1788 found 470.1772

References:

1. Basbaum, A. I.; Bautista, D. M.; Scherrer, G.; Julius, D., Cellular and molecular mechanisms of pain. *Cell* **2009,** *139* (2), 267-84.
2. Hucho, T.; Levine, J. D., Signaling pathways in sensitization: toward a nociceptor cell biology. *Neuron* **2007,** *55* (3), 365-76.
3. Woolf, C. J.; Salter, M. W., Neuronal plasticity: increasing the gain in pain. *Science* **2000,** *288* (5472), 1765-9.
4. Kandel, E. R.; Dudai, Y.; Mayford, M. R., The molecular and systems biology of memory. *Cell* **2014,** *157* (1), 163-86.
5. Gordley, R. M.; Williams, R. E.; Bashor, C. J.; Toettcher, J. E.; Yan, S.; Lim, W. A., Engineering dynamical control of cell fate switching using synthetic phospho-regulons. *Proc Natl Acad Sci U S A* **2016,** *113* (47), 13528-13533.
6. Ji, R. R.; Kohno, T.; Moore, K. A.; Woolf, C. J., Central sensitization and LTP: do pain and memory share similar mechanisms? *Trends Neurosci* **2003,** *26* (12), 696-705.
7. Liu, X. J.; Salter, M. W., Glutamate receptor phosphorylation and trafficking in pain plasticity in spinal cord dorsal horn. *Eur J Neurosci* **2010,** *32* (2), 278-89.
8. Chen, G.; Xie, R. G.; Gao, Y. J.; Xu, Z. Z.; Zhao, L. X.; Bang, S.; Berta, T.; Park, C. K.; Lay, M.; Chen, W.; Ji, R. R., β-arrestin-2 regulates NMDA receptor function in spinal lamina II neurons and duration of persistent pain. *Nat Commun* **2016,** *7*, 12531.
9. Sakurada, T.; Manome, Y.; Tan-No, K.; Sakurada, S.; Kisara, K., The effects of substance P analogues on the scratching, biting and licking response induced by intrathecal injection of N-methyl-D-aspartate in mice. *Br J Pharmacol* **1990,** *101* (2), 307-10.
10. Aanonsen, L. M.; Wilcox, G. L., Phencyclidine selectively blocks a spinal action of N-methyl-D-aspartate in mice. *Neurosci Lett* **1986,** *67* (2), 191-7.
11. Masuyama, T.; Shimizu, T.; Iwashita, T.; Yoshimura, N.; Fukuda, T., Spinal antinociceptive effect of substance P on the responses induced by intrathecally injected NMDA in mice. *Brain Res* **1996,** *722* (1-2), 200-2.
12. Corder, G.; Doolen, S.; Donahue, R. R.; Winter, M. K.; Jutras, B. L.; He, Y.; Hu, X.; Wieskopf, J. S.; Mogil, J. S.; Storm, D. R.; Wang, Z. J.; McCarson, K. E.; Taylor, B. K., Constitutive μ-opioid receptor activity leads to long-term endogenous analgesia and dependence. *Science* **2013,** *341* (6152), 1394-9.
13. Garzón, J.; Rodríguez-Muñoz, M.; Sánchez-Blázquez, P., Direct association of Mu-opioid and NMDA glutamate receptors supports their cross-regulation: molecular implications for opioid tolerance. *Curr Drug Abuse Rev* **2012,** *5* (3), 199-226.
14. Guang, W.; Wang, H.; Su, T.; Weinstein, I. B.; Wang, J. B., Role of mPKCI, a novel mu-opioid receptor interactive protein, in receptor desensitization, phosphorylation, and morphine-induced analgesia. *Mol Pharmacol* **2004,** *66* (5), 1285-92.

15. Rodríguez-Muñoz, M.; Sánchez-Blázquez, P.; Vicente-Sánchez, A.; Berrocoso, E.; Garzón, J., The mu-opioid receptor and the NMDA receptor associate in PAG neurons: implications in pain control. *Neuropsychopharmacology* **2012,** *37* (2), 338-49.
16. Sánchez-Blázquez, P.; Rodríguez-Muñoz, M.; Berrocoso, E.; Garzón, J., The plasticity of the association between mu-opioid receptor and glutamate ionotropic receptor N in opioid analgesic tolerance and neuropathic pain. *Eur J Pharmacol* **2013,** *716* (1-3), 94-105.
17. Garzón, J.; Herrero-Labrador, R.; Rodríguez-Muñoz, M.; Shah, R.; Vicente-Sánchez, A.; Wagner, C. R.; Sánchez-Blázquez, P., HINT1 protein: a new therapeutic target to enhance opioid antinociception and block mechanical allodynia. *Neuropharmacology* **2015,** *89*, 412-23.
18. Rodríguez-Muñoz, M.; Sánchez-Blázquez, P.; Vicente-Sánchez, A.; Bailón, C.; Martín-Aznar, B.; Garzón, J., The histidine triad nucleotide-binding protein 1 supports mu-opioid receptor-glutamate NMDA receptor cross-regulation. *Cell Mol Life Sci* **2011,** *68* (17), 2933-49.
19. Kawasumi, M.; Nghiem, P., Chemical genetics: elucidating biological systems with small-molecule compounds. *J Invest Dermatol* **2007,** *127* (7), 1577-84.
20. Bardaweel, S. K.; Ghosh, B.; Wagner, C. R., Synthesis and evaluation of potential inhibitors of human and Escherichia coli histidine triad nucleotide binding proteins. *Bioorg Med Chem Lett* **2012,** *22* (1), 558-60.
21. Chou, T. F.; Baraniak, J.; Kaczmarek, R.; Zhou, X.; Cheng, J.; Ghosh, B.; Wagner, C. R., Phosphoramidate pronucleotides: a comparison of the phosphoramidase substrate specificity of human and Escherichia coli histidine triad nucleotide binding proteins. *Mol Pharm* **2007,** *4* (2), 208-17.
22. Wu, H. E.; Darpolor, M.; Nagase, H.; Tseng, L. F., Acute antinociceptive tolerance and partial cross-tolerance to endomorphin-1 and endomorphin-2 given intrathecally in the mouse. *Neurosci Lett* **2003,** *348* (3), 139-42.
23. Zhou, Q.; Sheng, M., NMDA receptors in nervous system diseases. *Neuropharmacology* **2013,** *74*, 69-75.
24. Lau, C. G.; Zukin, R. S., NMDA receptor trafficking in synaptic plasticity and neuropsychiatric disorders. *Nat Rev Neurosci* **2007,** *8* (6), 413-26.
25. Paoletti, P.; Bellone, C.; Zhou, Q., NMDA receptor subunit diversity: impact on receptor properties, synaptic plasticity and disease. *Nat Rev Neurosci* **2013,** *14* (6), 383-400.
26. Ren, W.; Centeno, M. V.; Berger, S.; Wu, Y.; Na, X.; Liu, X.; Kondapalli, J.; Apkarian, A. V.; Martina, M.; Surmeier, D. J., The indirect pathway of the nucleus accumbens shell amplifies neuropathic pain. *Nat Neurosci* **2016,** *19* (2), 220-2.
27. Wei, M.; Zhang, J.; Jia, M.; Yang, C.; Pan, Y.; Li, S.; Luo, Y.; Zheng, J.; Ji, J.; Chen, J.; Hu, X.; Xiong, J.; Shi, Y.; Zhang, C., α / β -Hydrolase domain-containing 6 (ABHD6) negatively regulates the surface delivery and synaptic function of AMPA receptors. *Proc Natl Acad Sci U S A* **2016,** *113* (19), E2695-704.

28. Sánchez-Blázquez, P.; Rodríguez-Muñoz, M.; Garzón, J., The cannabinoid receptor 1 associates with NMDA receptors to produce glutamatergic hypofunction: implications in psychosis and schizophrenia. *Front Pharmacol* **2014,** *4*, 169.
29. Hallett, P. J.; Spoelgen, R.; Hyman, B. T.; Standaert, D. G.; Dunah, A. W., Dopamine D1 activation potentiates striatal NMDA receptors by tyrosine phosphorylation-dependent subunit trafficking. *J Neurosci* **2006,** *26* (17), 4690-700.
30. Jackson, K. J.; Wang, J. B.; Barbier, E.; Damaj, M. I.; Chen, X., The histidine triad nucleotide binding 1 protein is involved in nicotine reward and physical nicotine withdrawal in mice. *Neurosci Lett* **2013,** *550*, 129-33.
31. Barbier, E.; Zapata, A.; Oh, E.; Liu, Q.; Zhu, F.; Undie, A.; Shippenberg, T.; Wang, J. B., Supersensitivity to amphetamine in protein kinase-C interacting protein/HINT1 knockout mice. *Neuropsychopharmacology* **2007,** *32* (8), 1774-82.
32. Sánchez-Blázquez, P.; Rodríguez-Muñoz, M.; Herrero-Labrador, R.; Burgueño, J.; Zamanillo, D.; Garzón, J., The calcium-sensitive Sigma-1 receptor prevents cannabinoids from provoking glutamate NMDA receptor hypofunction: implications in antinociception and psychotic diseases. *Int J Neuropsychopharmacol* **2014,** *17* (12), 1943-55.
33. Bennett, G. J.; Xie, Y. K., A peripheral mononeuropathy in rat that produces disorders of pain sensation like those seen in man. *Pain* **1988,** *33* (1), 87-107.
34. Garzón, J.; Rodríguez-Muñoz, M.; López-Fando, A.; Sánchez-Blázquez, P., Activation of mu-opioid receptors transfers control of Galpha subunits to the regulator of G-protein signaling RGS9-2: role in receptor desensitization. *J Biol Chem* **2005,** *280* (10), 8951-60.

Chapter 3

Design, synthesis and *in vivo* evaluation of nucleotidomimetic inhibitors of hHint1

INTRODUCTION:

Human histidine triad nucleotide binding protein 1 (hHint1) has emerged as a protein of interest due to its recently discovered potential as a new therapeutic target for the treatment of pain.[1, 2] Human Hint1 belongs to the histidine triad (HIT) superfamily, which are characterized by a conserved sequence motif, His-X-His-X-His-XX, where X is a hydrophobic residue. Human Hint1 exists as a homodimer and possesses nucleoside phosphoramidase and acyl-AMP hydrolase activity, with a substrate preference for purine over pyrimidine nucleosides.[3] Structural and kinetic studies have shown that hHint1 possess two identical and independent nucleotide-binding subunits.[4, 5] Each monomer consists of five anti-parallel β sheets and an alpha helix motif. A conserved string of hydrophobic residues in or adjacent to the β-sheets creates a binding pocket (S1) for the nucleobase, while the aspartate (D43) residue anchors the ribose sugar. The α-monophosphate group interacts with a conserved string of polar residues including the partially positive His114 and the nucleophilic His112 in the active site. The side chains of the nucleoside phosphoramidates or acyl-AMP can occupy a relative shallow and solvent accessible pocket containing the only tryptophan residue in hHint1. A nucleophilic histidine (His112) residue forms part of the active site triad, which is responsible for the catalysis by hHint1. A detailed investigation of the kinetic mechanism of hHint1 has revealed that the mechanism proceeds by rapid formation of the nucleotidylated-His intermediate, followed by partially rate limiting water mediated hydrolysis and subsequent release of the nucleoside monophosphate from the active site (**Scheme 4B**, Chapter 1).[4] The nucleoside phosphoramidase activity of hHint1 has been shown to be necessary for the activation of several preclinical and clinically approved antiviral and

anticancer phosphoramidate pronucleotides.[6-8] In addition, Chou et al demonstrated that lysyl t-RNA synthetase generated lysyl-AMP is also a substrate for hHint1 in vitro.[9]

Hint proteins are highly conserved across all the kingdoms of life, suggesting that they have an important biological function. Hint1 has been implicated in the regulation of MITF/USF2 transcriptional activation complex in mast cells,[10] t-RNA synthetase amino acid adenylation,[9] apoptosis[11] and tumorigenicity.[12] In addition Hint1 is widely expressed in the region of brain primarily responsible for the modulation of pain [periaquaductal grey area (PAG)], addiction properties (nucleus accumbens) and motor & sensory functions (cerebral cortex).[1] Moreover, Hint1$^{-/-}$ mice have been shown to exhibit increased sensitivity to amphetamine and decreased nicotine dependence.[13, 14] Hint1$^{-/-}$ mice also display an enhanced analgesic response to morphine.[15] Molecular mechanistic studies in this context have found that N-methyl-D-aspartate receptor (NMDAR) mediated feedback inhibition of opioid analgesia is critically dependent on Hint1.[16] Nevertheless, the role of Hint1 active site and potential endogenous substrate regulating this response has remained enigmatic.

Chemical genetics is a powerful approach to elucidate biological functions of genes or proteins of interest using screens of diverse and targeted small molecules.[17] Recently, our laboratory has designed and synthesized a non-hydrolyzable substrate analog for hHint1 (TrpGc, **see Fig. 1**). TrpGc inhibits hHint1 with a low micromolar binding affinity (K_d = 3.65 ± 1.0 μM).[2] Using reverse chemical genetics, we demonstrated that the TrpGc not only enhances morphine analgesia, but also rescues and prevents the development of NMDAR mediated morphine tolerance in mice.[2] In addition, a single dose of TrpGc was

able to reduce mechanical allodynia in animals for several days. Interestingly, inhibition of Hint1 also antagonizes morphine-mediated inhibition of NMDA evoked behavior as described in previous chapter. Nevertheless, the structure-activity relationship of TrpGc and the role of Hint1 on NMDAR functions have remained elusive. TrpGc suffers from poor solubility and low micromolar binding affinity for hHint1. Hence, the development of water-soluble analogs with a higher binding affinity would enhance the utility of the probes to serve as a pharmacological tool for elucidating the biological role of the Hint1 in NMDAR regulation. Herein, we present our medicinal chemistry efforts to optimize TrpGc, which resulted in the development of first submicromolar binding inhibitors for hHint1. The newly designed inhibitors were also shown to successfully modulate NMDA evoke behavior *in vivo*.

RESULTS

hHint1 prefers non-polar side chain in the molecular recognition of the nucleoside carbamates

To investigate the importance of the indole ring in the shallow pocket, we began by designing analogs of TrpGc in which the aromatic indole side chain is replace with other side chains. Structure of all the compounds and their binding affinity in this section is reported in Table 1. Compound **4** with an ethylamine side chain (**Table 1**) was synthesized in similar fashion described for the synthesis of TrpGc in chapter 2 (**Scheme 2**). The coupling of the nucleoside carbamates (Chapter 2, **Scheme 2**) typically proceeds over a 24 hours. We investigated and utilized microwave in the synthesis of the carbamates in this chapter. The coupling reaction proceeded very quickly and was completed within ten minutes. The yields of the coupling reactions for the different amine containing side chains are reported in **Table 1**. We investigated the binding affinity of **4** for Hint1 using isothermal titration calorimetry (ITC). Removal of the indole side chain did not significantly alter the binding affinity for hHint1, when compared to TrpGc. Next, we wanted to investigate if the ethylene linker between the carbamate backbone and the aromatic ring was of optimum length. Hence, we made two carbamate analogs with phenyl (**5**) and benzyl amine (**6**) side chains. Replacing the tryptamine with the phenyl did not change the binding affinity but incorporating a one-carbon-shortened linker with benzyl amine decreased the binding affinity of the compound by two fold over TrpGc. The decrease in the binding affinity reflects the negative impact of increased rigidity of the linker on the binding to hHint1. One of the key features of the shallow binding pocket S2 is the presence of the only tryptophan (W123) in hHint1

(**Figure 3 and 4**). We asked if we could gain an increase in binding affinity by incorporating polar and positive charged residues in the side chain of the analogs in order to create cation-pi interactions with W123. With this aim in mind we designed compounds with imidazole side chain (**7**) and a primary amine (**8**). The compound with an histamine side chain would be partially positive and the primary amine would have a full positive charge at a neutral pH. The synthesis of the carbamate compound with primary amine side chain was achieved with coupling of the mono protected boc of diethyl amine under similar fashion to TrpGc. Whereas the coupling of the imidazole compound was achieved in DMF instead of pyridine due to limited solubility of histamine. Deprotection of acetonide protected 2′ 3′-OH and the dimethyl formamide protected amine groups was achieved using aqueous triflouroacetic acid (TFA). ITC analysis revealed that modifications resulting in **7** were well tolerated without any impact on the binding affinity to hHint1 in comparison to TrpGc. In contrast, a full positive charge as in **8**, reduced the binding affinity to hHint1 by four fold. Together these results indicate hHint1 does not prefer substrate or analogs with positive and polar side chains.

Table 1: Dissociation constant and yields in the microwave-assisted synthesis of nucleoside carbamates

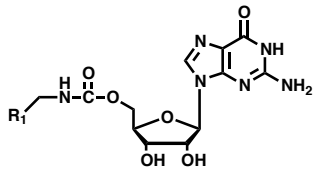

Compound	R_1	K_d (µM)	Yield (%)[a]	
			Normal	Microwave
TrpGc	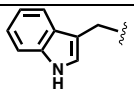	3.65 ± 1.00	75	72
4	CH_3	2.45 ± 0.59	67	75
5	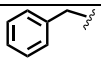	1.56 ± 0.01	83	60
6		8.09 ± 0.09	65	56
7	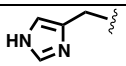	3.19 ± 0.41	34	-
8[b]		12.0 ± 3.10	62	58

[a] Yields reported for the coupling between 2′ 3′-OH acetonide protected nucleoside and amine to form carbamate

[b] Determined using fluorescent displacement assay described in chapter 5

Human Hint1 prefers acyl-sulfamate and sulfamide in comparison to carbamate backbone of the nucleotidomimetic inhibitors

Replacement of the acyl-phosphate linker of enzyme substrates with a bioisosteric acyl-sulfamate or acyl-sulfamide backbone has been shown to be a successful strategy for the generation of water-soluble and potent inhibitors. For example, 5´-amino-5´-N-(biotinyl)sulfamoyl-5'-deoxyadenosine (Bio-AMS, **Figure 1**) is a bisubstrate subnanomolar inhibitor of biotin protein ligase and contains a acyl-sulfamide backbone. Bio-AMS displays potent anti-tubercular activity against multidrug-resistant *Mycobacterium tuberculosis* strains.[18] Consequently, we chose to evaluate non-hydrolyzable nucleotide analogs for hHint1 that contain an acyl-sulfamate or acyl-sulfamide linker that mimics the corresponding phosphoramidate and acyl-phosphate moieties. We began by comparing the effect of a non-hydrolyzable nucleotide analog Bio-AMS with TrpGc on the activity of hHint1 using a fluorescence assay described previously.[3] At a fixed saturating substrate concentration, both TrpGc and Bio-AMS exhibited a dose dependent decrease in the activity of hHint1 with maximum half inhibitory concentration (IC_{50}) values of 1.0 ± 0.3 μM and 25.5 ± 6.0 μM respectively (**Figure 1**, bottom). We next employed isothermal titration calorimetry (ITC) to investigate the nature of non-covalent interactions on the inhibitory activity of Bio-AMS on hHint1. The ITC studies provided an experimental dissociation constant (K_d) of 0.32 ± 0.1 μM with an n value of 1.0 ± 0.1 indicating one binding site per hHint1 monomer. Bio-AMS was found to bind approximately 11 and 209 fold more tightly than TrpGc and guanosine monophosphate (GMP) respectively, and to be dominated by enthalpy and not entropy (**Table 2**).

Figure 1. Chemical structures and dose response curves of TrpGc and BioAMS. (Top) Chemical structures of TrpGc and BioAMS inhibitors of hHint1. (Bottom) Comparison of a dose response curve generated by the performing the titration of hHint1 activity in the presence of TrpGc (left, generated in Chapter 2) and Bio-AMS (right). The hHint1 activity was performed at a saturating concentration of the TrpAMP substrate (10 μM) using fluorescence activity described previously.[3] The resulting response vs concentration was fitted into one site model using a graph pad prism to determine inhibitory concentration that resulted into 50% of inhibition (IC_{50}).

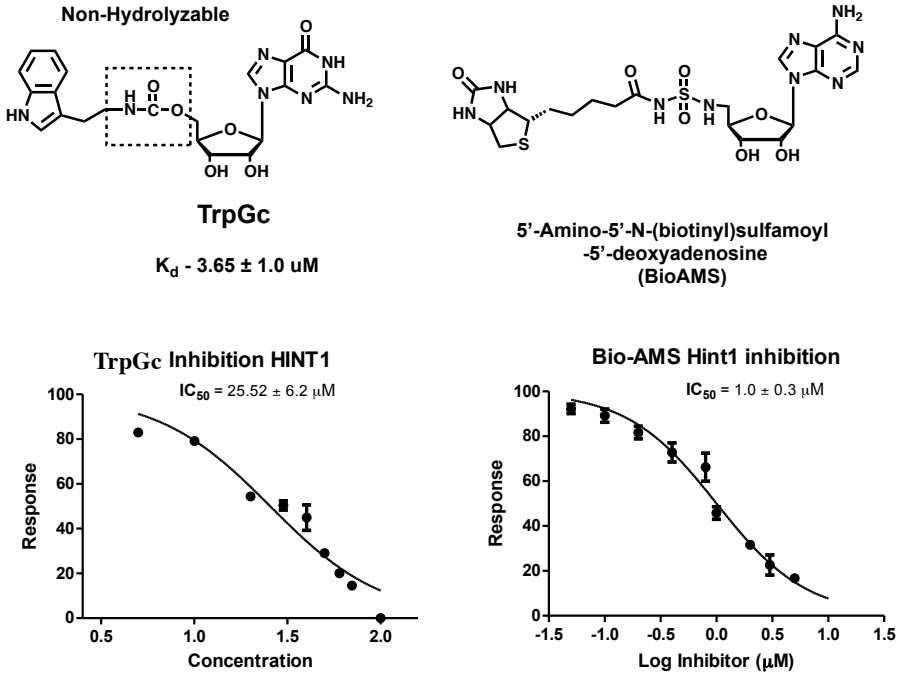

In order to avoid potential off target effects on enzymes utilizing adenosine and adenosine nucleotide based substrates, we sought to develop analogues of TrpGc containing an acyl-sulfamate or acyl-sulfamide backbone. The first inhibitor examined was based on the replacement of the carbamate backbone in TrpGc with a bioisosteric acyl-sulfamate backbone. The synthesis of compound **9** (**Scheme 1**) began with 5´-OH sulfamoylation of 2´,3´-*O*-isopropylidene guanosine (**14**) to provide intermediate **15**. Coupling of **15** with the N-hydroxysuccinic acid ester of 3-indole propionic acid (**22**) in the presence of DBU (1,8-Diazabicyclo[5.4.0] undec-7-ene) afforded **16**. Deprotection of the acetonide in compound **16** with aqueous TFA yielded the final compound **9**. In similar fashion compound **10** with a butyric acid side chain was synthesized (**Scheme 1** for structure). Replacement of the 5´-oxygen atom in the acyl-sulfamate with nitrogen affords an acyl-sulfamide backbone, which increases the pKa of the backbone NH by 2-3 units. The increased pKa has been shown to increase the stability and the binding affinity of Bio-AMS towards biotin protein ligase.[20] Hence, we designed compound **11** to investigate the impact of the enhanced negative charge of the backbone on the binding affinity of hHint1. The synthesis of compound **11** (**Scheme 2**) began with protection of the exocyclic nitrogen on compound **14** with N, N-dimethyl formamide dimethylacetal to yield N, N-dimethyl aminomethylene-2´-3´-*O*-isopropylidene guanosine (**17**). Iodination of the 5´-hydroxy group in **17** with methyltriphenoxyphosphonium iodide (MTPI) in a Moffat reaction afforded the iodination of the 5′-OH. Displacement of the iodide with sodium azide followed by reduction under the Staudinger reaction conditions yielded compound **19** with a 5´-amine on the ribose sugar. Next, the corresponding 5´-amino nucleoside was converted to the 5´-sulfamide by refluxing compound **19** with sulfamide

($NH_2SO_2NH_2$) in 1,4-dioxane for 2 h.[19] Surprisingly, this step also resulted in the removal of the N, N-dimethyl aminomethylene of the exocyclic amine along with the formation of the desired product (data not shown). The crude 5´-sulfamide nucleoside was then stirred in sodium hydroxide/methanol solution to completely deprotect the N, N-dimethyl aminomethylene group to afford **20** in an overall yield of 34 % over two steps. Coupling of **20** to the N-hydroxysuccinic acid ester of 3-indole propionic acid (**22)** in the presence of DBU followed by the deprotection of the acetonide with aqueous TFA (trifluoroacetic acid) yielded the final compound **11**. TrpGc exhibits very poor aqueous solubility with upto 30-40 uM of the solution can be prepared in the aqueous buffer (with 1-2% DMSO) from the stock solution (prepared in 100% DMSO). All the compounds prepared above displayed superior aqueous solubility compared to TrpGc. Stock solutions up to 5 mM for the guanosine analogues (compound **9**, **10** and **11**) were easily prepared in aqueous buffers without using DMSO.

Scheme 1: Synthetic scheme for the synthesis of guanosine acyl-sulfamates

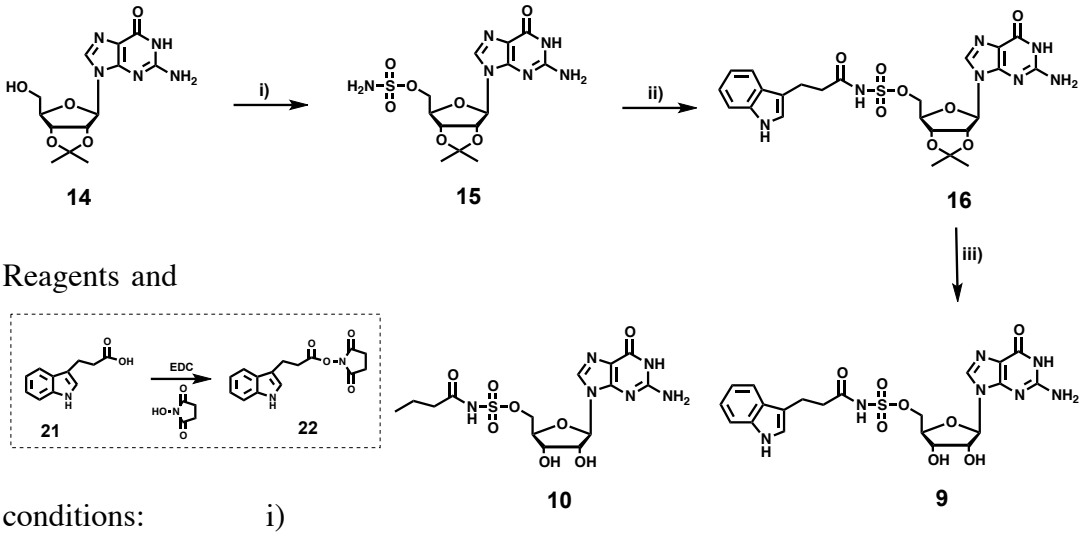

Reagents and conditions: i) NH_2SO_2Cl, DMA, 85%; ii) 22, DBU, DMF 55%; iii) 80 % aq. TFA quant.

Scheme 2: Synthetic scheme for the synthesis of guanosine acyl-sulfamides

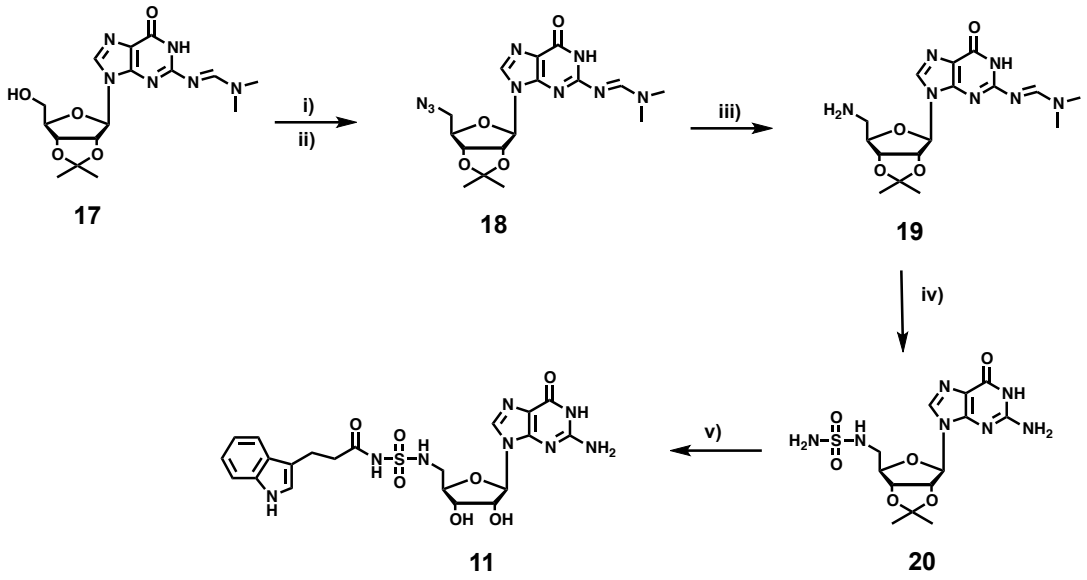

Reagents and conditions: i) MTPI, THF, -70 °C for 30 min and then RT for 4 h 92 %; ii) NaN_3, DMF, RT overnight, 55 %; iii) Triphenyl phosphine/aq dioxane, triethylamine, 50 °C, 3 h, 54 %; iv) $NH_2SO_2NH_2$, 1, 4-dioxane reflux for 2 h; and 4N NaOH/MeOH for 2 h, 33 %; v) 22, DBU in DMF, overnight, 55%; and 80 % aq. TFA, 1 h quant

Our next step was to evaluate the in vitro binding affinity of the new series of analogues for hHint1 using isothermal calorimetry (ITC) In comparison to TrpGc, compound **9** displayed a 4.5 fold increase in binding affinity with a measured dissociation constant of 0.81 ± 0.11 μM for hHint1 (**Table 2**). The increased binding affinity of **9** is likely due to electrostatic and/or hydrogen-bonding interactions of the acyl-sulfamate backbone, with polar side chains in the active site, as indicated by the increased gain in the enthalpic component over TrpGc. Increasing the pKa of the backbone with a sulfamide in compound **11** did not alter the binding affinity of compound **9** as indicated by their similar dissociation constants. Attachment of an indole side chain intramolecularly to a nucleoside has been shown to dynamically quench the fluorescence of the indole side chain due to stacking interactions of the indole ring on the nucleobase.[20] Therefore, one might predict that compounds **9** and **11** are likely to encounter a higher entropic penalty upon binding to hHint1. Consequently, one might propose that removal of the indole group in compound **10** would likely increase binding affinity by decreasing the entropic cost of binding to hHint1. Surprisingly, the dissociation constant for compound **10** for hHint1 was found to be 3-4 fold greater in comparison to **9** (**Table 2**). Comparing the thermodynamic parameters of **9** and **10** revealed no significant differences in the entropy of binding. However, compound **10** displayed a nearly 2 kcal mol^{-1} decrease in the enthalpy of binding. These results indicate that increasing interactions associated with the active site can improve the ligand binding affinity. Also, these results are in contrast to the observed characteristics binding in the carbamate series, where smaller side chains are tolerated. These indicate potentially the role of the free energy of ligand solvation and

Table 2: Thermodynamic parameters and dissociation constants of hHint1-ligand complexes determined using ITC

Compound	K_d (μM)	ΔH, kcal mol^{-1}	-TΔS, kcal mol^{-1}	ΔG, kcal mol^{-1}
TrpGc	3.65 ± 1.00	-13.54 ± 1.00	9.54 ± 4.17	-4.1 ± 2.0
BioAMS	0.32 ± 0.1	21.30 ± 2.40	12.68 ± 2.68	-8.7 ± 0.20
9	0.81 ± 0.11	-16.51 ± 0.17	8.05 ± 0.88	-8.46 ± 0.4
10	2.90 ± 0.25	-13.59 ± 1.12	7.71 ± 0.27	-5.81 ± 1.0
11	0.92 ± 0.07	-14.75 ± 0.12	6.57 ± 0.17	-8.24 ± 0.12
12	0.23 ± 0.01	-17.31 ± 0.05	8.19 ± 0.13	-9.13 ± 0.11
GMP[a]	67 ± 7.9	-	-	-

[a]Data shown from the NMR titrations previously reported by Shapiro and co-workers.

the fine balance of hydrophilicity/hydrophobicity that is required for the complexation with hHint1.

Impact of a hydrophobic nucleoside in the molecular recognition of ligands by hHint1

Structural studies performed using x-ray crystallography or NMR provide a very important insight into the molecular recognition driving the interaction between a protein and a ligand. Using 2D-NMR studies, Shapiro and co-workers investigated and identified key interactions between nucleoside monophosphates and mouse Hint1.[21] Their ^{1}H-^{15}N HSQC investigations revealed large chemical shift perturbations ($\Delta\delta > 0.2$ ppm) for the residues surrounding the canopy holding the nucleobase and sugar upon addition of the nucleoside monophosphate. Isoleucine 44 in the **S1** hydrophobic pocket exhibited the largest chemical shift difference of $\Delta\delta = 1.11$ ppm indicating that nucleobase recognition maybe a key event in driving the molecular recognition of nucleotide based ligands by Hint1. We chose to explore the impact of a hydrophobic nucleoside inhibitor with an acyl-sulfamate backbone by replacing the guanosine base in **9** with a tricyclic ethenoadenosine base. Compound **12** provides an additional advantage of stability towards cyclonucleoside formation when compared to an adenosine nucleobase due to the extensive delocalization of the N-3 nitrogen electrons into the tricyclic ring system. The synthesis of compound 12 (**Scheme 3**) began with the cyclization of exocyclic amine in **23** with chloroacetaldehyde in mildly acidic sodium acetate buffer at 40 °C to yield the

Scheme 3: Synthetic scheme for the synthesis of Ethenoadenosine acyl-sulfamates

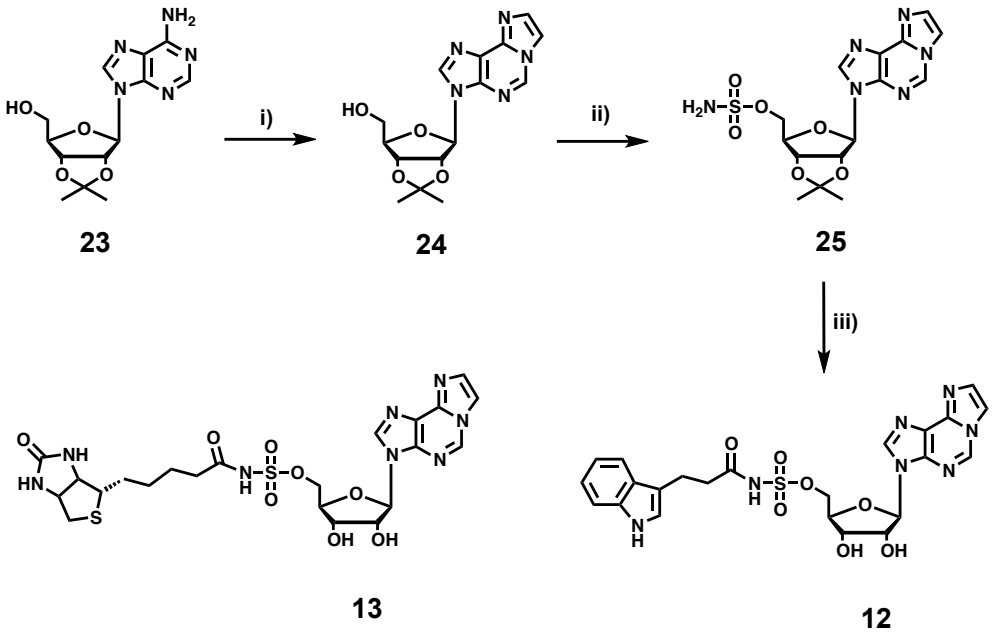

Reagents and conditions: i) chloroacetaldehyde, NaOAc 0.1M pH 6.5, 40 °C, 30%; ii) NH_2SO_2Cl, DMA, 85%; iii) 22 or biotin-NHS, DBU, overnight, 55%; and 80 % aq. TFA, 1 h quant

fluorescent compound **24**. The formation of **24** in the reaction mixture can be easily monitored on thin layer chromatography due to its fluorescent properties. Compound **24** was then treated with sulfamoyl chloride in the presence of triethylamine to yield compound **25**. Coupling of **25** with the N-hydroxysuccinic acid ester of 3-indole propionic acid in the presence of DBU followed by deprotection of the acetonide with aqueous TFA yielded compound **12** in an overall yield of 60 % over two steps. To avoid potential decomposition due to the intrinsically acidic free acyl-sulfamate group, all the acyl-sulfamate compounds (**9, 10** and **12**) were prepared and purified as a triethylammonium salt using reverse phase chromatography. Consistent with our hypothesis, compound **12** in which a tricyclic nucleobase has been incorporated, resulted in an increased binding affinity with a measured dissociation constant of 0.23 ± 0.01 μM (**Table 2**). Compound **12** displayed an increase in binding affinity of 16 and 291 fold over compound TrpGc and GMP, respectively. In comparison with **9**, a nearly 1 kcal mol^{-1} increase in the enthalpy of binding was observed for **12**, with no observable difference in the entropic component. Encouraged by this, we asked if replacing the tryptamine side chain in 12 with a biotin side chain would further increase the binding affinity. Compound **13** showed almost identical binding affinity to **12** (data no shown). These results indicate that, while ligand and active site desolvation is important, the interactions of the nucleobase with the active site dominate biomolecular recognition of the ligands by hHint1.

Figure 2: HPLC stability studies of Hint1 nucleoside acyl-sulfamate inhibitors. Compounds were monitored with UV absorbance of traces at 168-280 nm. Samples containing 50-100 μM of the resulting compounds, A) 9 B) 10 and C) 12 were incubated at 37 °C in PBS pH 7.4. At indicated time intervals 200 μl of the solution were injected on the HPLC and monitored for any appearance of degradation peaks.

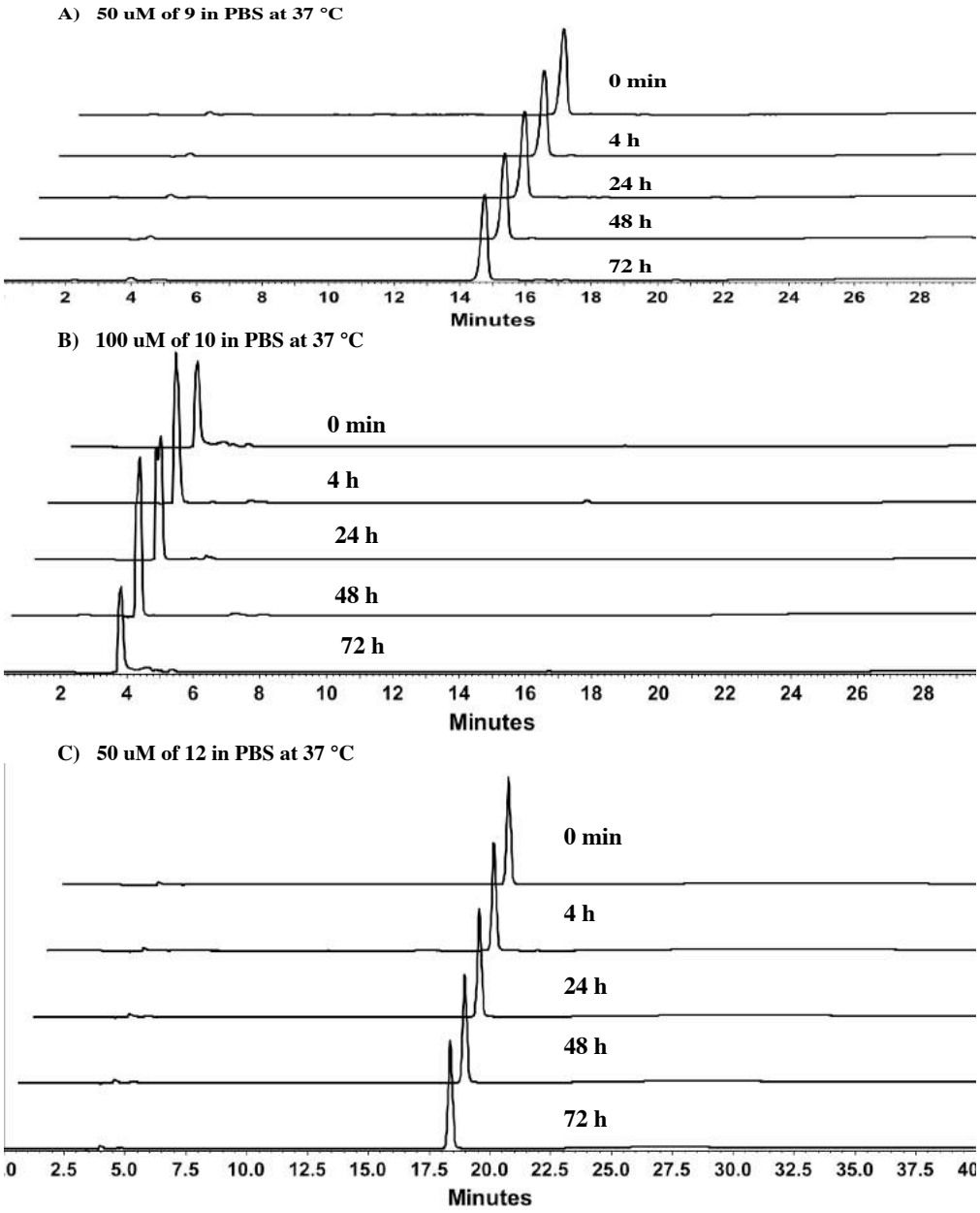
A) 50 uM of 9 in PBS at 37 °C
0 min
4 h
24 h
48 h
72 h
2 4 6 8 10 12 14 16 18 20 22 24 26 28
Minutes
B) 100 uM of 10 in PBS at 37 °C
0 min
4 h
24 h
48 h
72 h
2 4 6 8 10 12 14 16 18 20 22 24 26 28
Minutes
C) 50 uM of 12 in PBS at 37 °C
0 min
4 h
24 h
48 h
72 h
0 2.5 5.0 7.5 10.0 12.5 15.0 17.5 20.0 22.5 25.0 27.5 30.0 32.5 35.0 37.5 40
Minutes

HPLC studies to determine stability of nucleoside acyl-sulfamate inhibitors of hHint1 in an aqueous solution

Previously an acyl-sulfamate analogue of BioAMS was reported to be susceptible to undergo rapid decomposition via intramolecular displacement reaction to form inactive 3′-5′-cyclo-5′-deoxyadenosine and N-(biotinyl) sulfamic acid.[18] We wanted to investigate the stability of our inhibitors with acyl-sulfamate backbone before evaluating their effects in vivo. We evaluated stability of compounds **9**, **10** and **12** using high performance liquid chromatography (HPLC) at 37 °C in phosphate buffered saline (**Figure 2**). The peak of the starting material was monitored at 254 nm and 280 nm wavelength over a period of 48 hours. Determination of the area under the curve (AUC) for the compound peaks at interval of 0, 4, 24, 48 and 72 hours revealed little or no change. These results indicate that our compounds are stable for up to 72 hours in an aqueous buffer. This result is in striking contrast to the previously reported rapid decomposition of the acyl-sulfamate analog of Bio-AMS via cyclonucleoside formation.[18]

X-ray crystal structure analysis to investigate key interactions driving the molecular recognition of ligands by hHint1

To identify the key molecular interaction driving the molecular recognition of the inhibitors we obtained high-resolution x-ray crystal structures of **5**, **6** and **12** bound to hHint1. We first began by comparing the carbamate inhibitors **5** and **6** with AMP bound hHint1 structure (**Figure 3**).[22] In all the three structures the 2′ 3′-hydroxyl group on the ribose sugar was found to be in 2.5 Å away from the side chain oxygen atoms of the Asp

43 residue to form strong hydrogen bond interactions. This indicates that interaction of sugar is a key event in the driving the molecular recognition of nucleoside ligands by hHint1. An additional hydrogen bonding interaction between the carbonyl of carbamate inhibitors and the NH from the backbone of Ser107 over AMP was observed. It is likely this interaction is resulting in the gain of the binding affinity for hHint1 observed for carbamate nucleosides over AMP. The difference in the binding affinity observed between **5** and **6** was consistent with our hypothesis that the extra carbon in the side chain of **5** would provide more flexibility to accommodate this interaction.

Next, we wanted to investigate the interaction governing the molecular recognition of **12**. We obtained a 1.6 Å high-resolution structure of compound **12** in complex with hHint1 (**Figure 4**). Compared to the structure of **5** and **6**, an additional hydrogen bond between the carbonyl of the acyl-sulfamate of **12** and hydroxyl group in the side chain of Ser107 was observed. This observation is consistent with the gain in the binding affinity and the observed increase in the enthalpic contribution of binding (**Table 2**) with acyl-sulfamate inhibitors. They also are consistent with the preference of hHint1 for acyl-nucleoside monophosphate (NMP) substrates, suggesting a role for Ser107 in stabilizing negative charge development on the substrate carbonyl during catalysis. No additional interaction of acyl-sulfamate backbone was observed with the protein except the two oxygen atoms in resonance with sulfur can occupy both the conformation of the carbonyl in carbamate backbone. This observation is consistent with no difference observed between the sulfamate and sulfamide backbone inhibitors. With regard to the 5´ side-chain of compound **12**, stabilizing van der Waals interactions were observed between the linking methylenes and the indole ring of Trp123 (**Figure 4**). In addition, the planar tricyclic ring

Figure 3. High-resolution X-ray crystal structure analysis of AMP (yellow; pdb: 3TW2) and overlaid with the compound **5** (cyan) and **6** (pink) in interaction with hHint1 complex. A) H-bond interaction of the backbone **NH** of **S107** with the carbonyl of the backbone carbamate in compound **5** and **6**. B) H-bond interaction of the sugar and side chain are shown in dotted black lines.

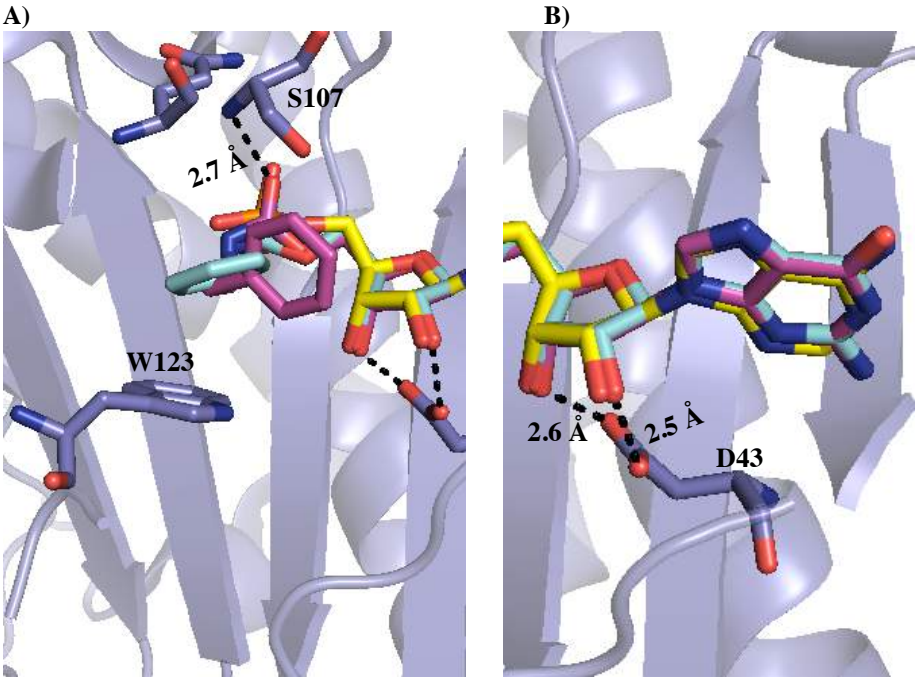

Figure 4. High-resolution x-ray crystal structure analysis of AMP (yellow; pdb: 3TW2) and overlaid with the compound **12** (cyan) in interaction with hHint1 (blue; pdb: 5I2E) complex. A) H-bond interaction of the sugar and side chain are shown in dotted black lines. B) Different orientations of isoleucine side chains observed in the hydrophobic nucleotide-binding pocket for AMP and compound **7** bound hHint1 structure is shown in yellow and blue respectively.

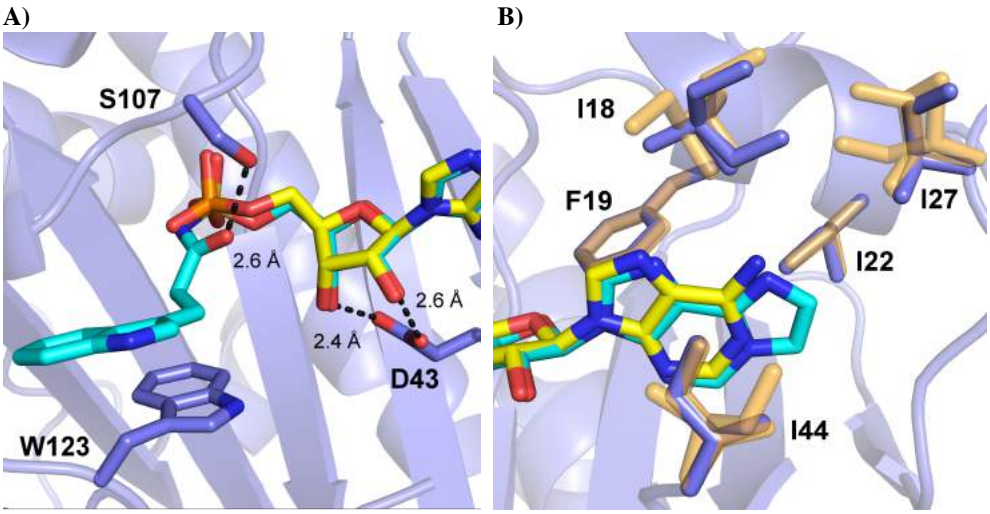

of the nucleobase is well accommodated by the hydrophobic S1 pocket (which is comprised largely of Ile18, Phe19, Ile22, Ile 27, and Ile44). When compared to the AMP bound structure, minor changes were observed in the side chain of the isoleucines in the **S1** pocket (**Figure 4**), with no significant variation in the protein backbone structure. Moreover, no significant changes in the overall conformation of the protein were observed when compared to the apo or nucleotide bound structures. (All the x-ray crystal structures reported here were acquired in association with alexander strom).

Compound 9 and 12 antagonizes the inhibition by morphine on the NMDA evoked biting and scratching behavior in mice

NMDA is an agonist of the NMDAR in the CNS. As described in the previous chapter that inhibition of Hint1 modulates the cross talk between the MOR and the NMDAR in the CNS. This modulation is bidirectional and ligand specific, meaning depending upon the first activation by either morphine or NMDA, Hint1 inhibition can either inhibit or synergize the activation of the NMDA receptor (Chapter 2, **Scheme 1 and 2**). Activation of the NMDAR via the agonist, such as NMDA, is known to induce biting and scratching behavior in mice (Chapter 2, **Scheme 2**). It is also known that upon administration of morphine intrathecally (i.t) this behavior can be inhibited. In collaboration with Wilcox lab, we have shown that TrpGc can antagonize the inhibitory effect of morphine on NMDA evoked behavior (Chapter 2 **Figure 7B**). We wanted to test the effect of our nucleoside acyl-sulfamates especially compound **9** and **12** on the NMDA evoked behavior in vivo. Animals were inthrathecally injected with 0.3 nmoles of NMDA and the biting and scratching response was recorded as maximum response. In another

Figure 5. % Inhibition of NMDA evoked behavior (upon administration of 0.3 nmoles of NMDA intrathecally) by morphine (open diamond). Compound **9** (green diamond), **12** (red inverted triangle) and TrpGc (black circle) antagonized the effect of morphine in a dose dependent manner. The ED_{50} values for **9**, **12** and **TrpGc** were calculated to be 1.2, 0.6 and 0.47 respectively. Table contains the values with standard deviation on n = 3 mice.

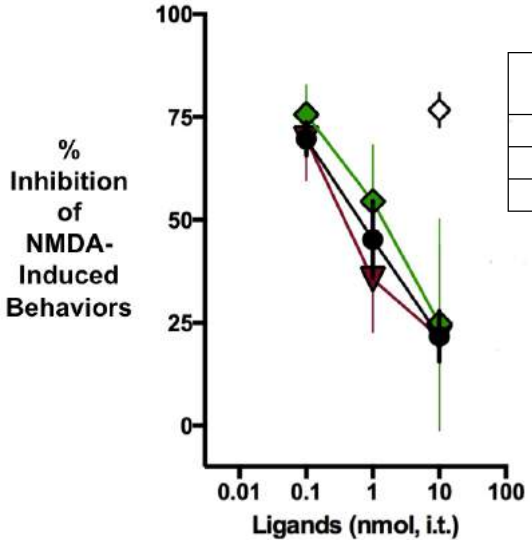

Compound	ED_{50} (μM)
TrpGc	0.61 ± 0.28
9	1.2 ± 0.49
12	0.47 ± 0.20

experiment, the behaviors of mice were recorded upon intrathecal administration of NMDA along with simultaneous administration of either morphine alone or in the presence of both morphine and an Hint1 inhibitor. A dose response of NMDA evoked behavior was plotted against the antagonistic effect of morphine in the presence of inhibitors. We showed that both compound **9** and **12** were equally or more effective in inhibiting the NMDA evoke behavior in mice when compare to compound TrpGc (**Figure 5**). (The in vivo biochemical evaluation studies reported here was performed in collaboration with Dr. George Wilcox lab).

Evaluation of cytotoxicity of Compound 9 and 12 on MiaPaca and U-87MG cell lines

Encouraged with the in vivo results, we next wanted to ask if compound **9** and **12** would show side effects associated with potentially targeting on tryptophan t-RNA synthetase. One could speculate that the primary amino group in the side chain of the amino acid would be critical for the recognition of the aminoacyl-AMP ligands by t-RNA synthetase. If the fundamental protein translation is affected, the compounds might exhibit a side effects associated with cellular toxicity. Our compounds lack the primary amino group and hence we reasoned that the potential for such side effects would be minimal. We tested the effects of our compounds on a neuronal (U-87 MG) and a pancreatic (MiaPaca) cancer cell line. The cells were treated with the respective compounds for 48 and 72 hours. We did not see any cytotoxicity at concentrations as high as 100 μM for TrpGc, **9** or **12** (**Figure 6**). Hence, it is unlikely that the compounds are inhibitors of protein translation.

Figure 6. Cell Cytotoxicity studies performed on the MiaPaca (left) and U87 MG (right) in the presence of the various concentration (0.5-100 μM) of the compound **3**, **9** and **12**. 5000 MiaPaca and 2500 U87-MG cells/per well treate with the inhibitors for 72 hours after which the cytotoxicity was measured using MTS assay.

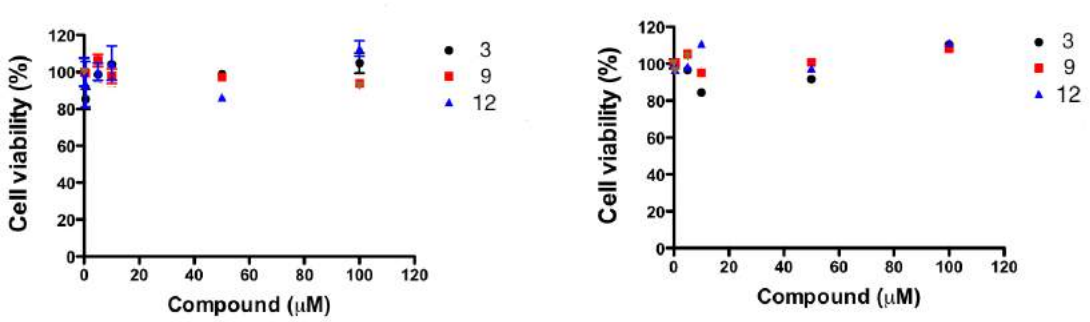

Discussion

We have designed and synthesized here first low micromolar binding nucleotidomimitic inhibitors of hHint1 with improved water solubility. We describe here also microwave-assisted synthesis of carbamates, which could be of potential utility in combinatorial synthesis for generating nucleoside carbamate libraries. Our systematic medicinal chemistry efforts in this study identified critical pharmacophores important in the molecular recognition of ligands by the hHint1. The current study also takes a step closer towards understanding the potential features of the enigmatic substrate of hHint1 in vivo. Aminoacyl-t-RNA synthetase generated amino acyl AMP has been speculated to be potential natural substrate for Hint1.[9] Previous x-ray crystallography studies indicated the potential role of cation-pi interactions between positively charged groups of the ligand and W123 for the molecular recognition. Our efforts to capitalize on this cation-pi interaction with primary amine in the side chain negatively impacted the binding to hHint1 for compounds **7** and **8**. This result indicates that rigidity provided within the stereochemistry of the amino acid is critical for governing that interaction. The same pocket also contains a positively charged arginine and it is possible that stereochemistry and rigidity avoids the repulsion between the two positive charges that was absent in our compounds **7** and **8**. Based on this observation one could potentially design a compound with a negatively charged carboxylate in the side chain to create a salt bridge interaction, which was not evaluated in the current study. Also, we did not chose to design and evaluate any amino acid side chains in our inhibitors due to their potential off target effects on t-RNA synthetases. Next, our studies focused on the optimization of the backbone chemistry. Replacing the carbamate backbone with a more polar and negatively

charged acyl-sulfamate resulted in the gain in the binding affinity over TrpGc. X-ray crystal structure analysis of hHint1-**12** complex identified an additional interaction between a carbonyl group in acyl-sulfamate and Ser107, which was absent in carbamate inhibitors. Removal of the indole side chain in compound **9** with a butyl group resulted in the loss in the binding affinity. This result was unexpected as the indole moiety was found to be not necessary for the binding of compound **4** of the carbamate series. One explanation may rest on the fine role of balancing hydrophilicity/hydrophobicity in the molecular recognition. Finally, incorporation of an hydrophobic nucleobase ethenoadenosine in place of guanosine in **9**, resulted in the identification of the acyl-sulfamate **12**, which exhibited approximately 16- and 300-fold higher binding affinity towards hHint1 than TrpGc and GMP, respectively. This result was consistent with a gain in the increase in interaction with Ile44 that has been previously reported to be crucial for the binding of the ligand to Hint1. All the ligand evaluated in the current study maintained the key interaction of 2′ 3′-OH ribose sugar with the oxygen atoms in the aspartate residue (Asp 43). In all the hHint1-ligand complexes the ribose sugar adopted in an envelope conformation for its interaction with Asp 43. Hence, the role of sugar pucker and its impact on binding of ligands and inhibitors needs to be evaluated and addressed in future studies. Our studies with ITC indicate that a favorable enthalpic contribution and a fine balance between hydrophilicity/hydrophobicity of the ligand are likely necessary for maintaining the binding affinity of ligands towards hHint1. In classical terms the hydrophobic effect has been known for producing thermodynamic signature with favorable gain in entropy due to the displacement of non-ordered water molecules in the apolar surface on the protein. Diederich and co-workers have proposed that solvents with

high cohesive interactions such as water prefer to interact with bulk solvent molecules rather than to solvate the complementary apolar surfaces of host and guest molecules. It has been proposed, "water molecules around apolar surfaces participate in fewer strong hydrogen bonds than bulk solvent molecules". Therefore, enthalpy is gained upon release of surface-solvating molecules to the bulk during the complexation step.[23] Hence, in many cases the extension of the ligands with hydrophobic side chains manifest with gain in enthalpic energy. Such effects are labeled as non-classical hydrophobic effects.[24, 25] It is possible that a part of these enthalpic contributions originate from multiple hydrophobic effects as seen with the complexation of arenes and aromatic substrates with biological receptors in water.[24-26] Future studies on the free energy of solvation of the ligands, as well as water map calculations on the protein-ligand complex, may assist in defining the role of multiple hydrophobic effects on ligand molecular recognition by the hHint1 active site.[25, 26] Finally, we also show that our most potent inhibitors **9** and **12** were cell permeable, non-toxic and successful in modulating the function of NMDAR in vivo. In conclusion, we have not only successfully developed the first low micromolar and water-soluble inhibitors of Hint1 but also effective pharmacological probes for the in vivo modulation of NMDAR function by Hint1.

Materials and Methods

General Methods and Materials:

Guanosine was purchased from Acros Organics. Chloroacetaldehyde solution (50% wt in water), Triphenylphosphine (cat no: T84409-1004), Methyl triphenoxy phosphonium iodide (MTPI, cat no: 226432-10), Chlorosulfonyl Isocynate (cat no: 142662-254), Sulfamide (cat no: 277310), Ethylamine (gas, cat no: 301264), Phenethylamine (cat no: 128945) and Histamine (cat no: H7125) was purchased from Sigma-Aldrich. All solvents were purchased from Fischer Scientific and used as received unless otherwise noted. Anhydrous solvents such as DMF, Acetonitrile were used directly from solvent dispensing system (J. C. Meyer) packed with two columns of neutral alumina and dispensed under argon. DMA and Pyridine was purchased in a sure seal bottle from Sigma-Aldrich. Thin-layer chromatography was performed using EMD pre-coated silica gel 60 F-254 plates. All preparative separations were performed using Teledyne Isco combiflash system and using RediSepRf high performance gold silica pre-packed columns. Microwave synthesis was performed on Discover SP from CEM corporation with an automated handling arm. Analytical HPLC for the stability studies were performed on Agilent C18 zorbax SB-Aq column (3.5 μm, 4.6 x 150 mm) using water (solvent A) and acetonitrile (solvent B) with 0.1% TEA as additive. High-resolution mass spectrometry was performed LTQ Orbitrap Velos (Thermo ScientificTM). Samples and compounds during synthesis were freeze-dried with a lyophilizer available from Labonaco. All ^{1}H- and 13C-NMR spectra were collected in d6-DMSO (Cambridge Isotope Laboratories, Cambridge, MA) at 25 °C using AscendTM Bruker spectrometer 500 MHz at the Department of Medicinal Chemistry CCRB NMR facility at the University of Minnesota unless otherwise stated. All NMR chemical shifts were recorded in δ parts per million using d6-DMSO as internal reference. Thermodynamic measurements for protein-ligand association were performed in 96-well plates (Nunc 260251 U96 DeepWell 96-Well x 1.3 ml from Thermo Scientific) using MicroCal Auto-ITC200 system (GE Healthcare life sciences). Nickel nitrilotriacetic acid (Ni-NTA) was purchased from Qiagen and cobalt column agarose from Thermofishcer Scientific.

Biological buffers were purchased from Sigma-Aldrich. Protease inhibitor tablets were obtained from Roche.

Protein Expression and Purification:

The procedure was similar to one described in the chapter 2.

Protein Crystallography:

Crystals were grown via hanging drop vapor diffusion, with drops comprised of 2 μL of protein (A280 = 6-10, in 50mM HEPES, 250 mM NaCl, 10% glycerol v/v, pH 7.5 buffer) and 2 μL of well solution. Well solutions contained 25-35% PEG 8K, and 100 mM MES at pH 6.1-6.5. Crystals formed after 3 days of incubation at 20 °C. Co-crystals with inhibitors were prepared by soaking pre-formed crystals in mother liquor containing 2.5 mM **9** or 25 mM for **5** and **6** for 15-60 minutes. After soaking, crystals were cryoprotected using 20% PEG 400 and flash vitrified with liquid nitrogen. Diffraction data were collected at 100K at beamline 17-ID (IMCA-CAT) using a Dectris Pilatus 6M Pixel Array Dectector at the Advanced Photon Source of Argonne National Laboratories in Argonne, IL. Molecular replacement was conducted with hHint1 coordinates (PDB ID 3TW2) using Phaser[27] within PHENIX.[28] Modeling and molecular visualization were performed in Coot.[29] Ligand restraints were calculated using JLigand,[30] and refinement was performed using PHENIX.

Isothermal Titration Calorimetry (ITC):

The procedure was similar to one described in the chapter 2.

Analytical HPLC studies to determine the stability of the Inhibitors:

Analytical studies were performed on a Beckman coulter system gold operated by Karat software, with an Agilent C18 Zorbax SBAq column (4.6 x 150 mm, 3.5 μm). Stock solutions (10 mM) of the inhibitors were prepared in a Tris buffer (10 mM Tris, 200 mM NaCl, pH 7.4). For stability studies, the stock solutions were diluted to a concentration of 50-100 uM using Phosphate Buffer Saline buffer (PBS) and incubated at 37 °C. At indicated time points 200 μl aliquots of the sample volume were withdrawn and injected into the HPLC system for monitoring the stability and degradation of the compounds. The samples were eluted using the gradient of solvent A (Water) and B (CH_3CN) with a 0.1% triethylamine additive (0-4 min: gradient 0% B, 4-14 min: gradient 20% B, 14-29 min: gradient 80% B, flow rate 0.5 ml/min) with detection at 168-400 nm.

MTS Cell Cytotoxicity studies:

The cell viability was carried out using standard MTS assay reagent kit from Promega (cell titre 96® aqueous one solution cell proliferation assay). Briefly the corresponding cell lines MiaPaca-2 and U-87 MG were seeded at density of 5 x 10^3 and 2.5 x 10^3 cells/well in a 96 well plate day before incubation with the treatment. Next day, the media was changed and treated with the inhibitor concentration ranging from 0.5-100 μM. The treatment was incubated for 72 h after which the media was replenished with 100 μl of fresh media plus 20 μl of the MTS reagent. The plates were then incubated at 37 °C for 4 h in an incubator. The data were recorded by measuring absorbance at a 490 nm wavelength by Synergy HT microplate reader.

Studies on NMDA evoked behavior in mice:

NMDA induced behavior test compare the number of hindlimb-directed biting behaviors elicited with in a mouse after i.t delivery of NMDA (0.3 nmoles). NMDAR antagonist and MOR agonist such as MK-801 and morphine antagonize this behavior in the dose dependent manner. Morphine (10 nmol) was injected i.t after 5 min of administration with NMDA. Inhibition of Hint1 with TrpGc has been previously shown to antagonize the effect of morphine. Both compounds **9** and **12** were administered 5 min after with 0.1, 1 and 10 nmol of doses to evaluate the efficacy in mice (n=3). For these tests, percent antinociception was calculated as percent inhibition ± SEM by the formula [(Control – Experimental)/Control] × 100%. The ED_{50} values were calculated by the method of Tallarida and Murray described previously.

General procedure for the synthesis of carbamates:

A solution of p-Cl phenyl chloroformate (1.2 eqvi 0.3708 mmoles) was added dropwise to a stirred solution of acetonide guanosine (1.0 eqvi, 0.309 mmoles in 5 ml anhydrous pyridine at 0 °C) over a period of 30 minutes. The solution was stirred at room temperature until TLC and ESI MS analysis showed complete consumption of the starting material (2.5 hours). To the solution of an activated carbonate ester of nucleoside was added a respective amine (2 eqvi, 0.618 mmoles in pyridine) to form nucleoside carbamate in one-pot. At the end of 24 hours the reaction mixture was then evaporated to dryness under vacuum. The resulting crude mixture was dissolved in ethyl acetate and washed with $NaHCO_3$ (2 x 15 ml) and brine (1 x 10 ml). The organic layer was dried over Na_2SO_4 (anhydrous) and evaporated. Combiflash was run to purify and isolate the product in yield reported over two-steps. The isolated product from the above step was

deprotected using a solution of TFA/H_2O (4:1, 2.5 ml) at rt. The reaction was completed in 20 minutes as indicated by TLC. The reaction mixture was evaporated and combiflash was run to purify the product.

General procedure for the synthesis of using microwave:

A solution of p-Cl phenyl chloroformate (1.2 eqvi 0.3708 mmoles) was added dropwise to a stirred solution of acetonide guanosine (1.0 eqvi, 0.309 mmoles in 5 ml anhydrous pyridine at 0 °C) over a period of 30 minutes. To the solution of an activated carbonate ester of nucleoside was added a respective amine (2 eqvi, 0.618 mmoles in pyridine) to form nucleoside carbamate. The reaction vessel was sealed and prestirred for 30 sec. Next with high stirring; the vessel was heated at temperature of 50 °C, with power of 200 watt for 10 min in the microwave synthesizer. The resulting crude mixture was dissolved in ethyl acetate and washed with $NaHCO_3$ (2 x 15 ml) and brine (1 x 10 ml). The organic layer was dried over Na_2SO_4 (anhydrous) and evaporated. Combiflash was run to purify and isolate the product in yield reported over two-steps. The yields for each carbamate inhibitor are reported in Table 1.

Synthesis of 5′-O-[1-Ethyl]Carbamoyl Guanosine (4)

Here ethylamine was commercially available in the gaseous form and was transferred in three neck flask under anhydrous condition and cooled under -78 C to form liquid. The ^{1}H NMR spectrum was (DMSO-d_6): 1.01 (t, 3H), 2.99 (q, 2H), 3.99-4.05 (m, 3H), 4.17 (m, 1H), 4.46 (m, 1H), 5.27 (t, 1H), 5.45 (t, 1H), 5.69 (t, 1H), 6.47 (s, 2H), 7.28 (m, 1H), 7.91 (s, 1H) and 10.63 (s, 1H). ^{13}C- DMSO-d_6: 157.21, 156.26, 154.20, 152.04, 135.93,

117.12, 86.43, 82.80, 73.46, 71.07, 64.37, 35.52 and 15.52 ppm. Low resolution ESI-MS [M+H] 355.1, HRMS (ESI+) calcd for $C_{13}H_{18}N5O_5$ [(M+H)+] 355.1366 found 355.1367

Synthesis of 5′-O-[3-Phenyl-1-Ethyl]Carbamoyl Guanosine (5)

The ^{1}H NMR spectrum was (DMSO-d_6): 2.69 (t, 2H), 3.19 (q, 2H), 4.00 (s, 1H), 4.01 (m, 2H), 4.01 (m, 2H), 4.17 (m, 1H), 4.48 (m, 1H), 5.28 (d, 1H), 5.44 (d, 1H), 5.70 (d, 1H), 6.47 (s, 2H), 7.20 (d, 3H), 7.26-7.28 (m, 2H), 7.41 (t, 1H), 7.91 (s, 1H) and 10.62 (s, 1H). ^{13}C- DMSO-d_6: 157.19, 156.38, 154.19, 152.03, 139.75, 135.95, 129.11, 128.81, 126.56, 117.15, 86.43, 82.77, 73.45, 71.05, 64.47, 42.5 and 36.0 ppm. Low resolution ESI-MS [M+H] 431.1, HRMS (ESI+) calcd for $C_{13}H_{18}N5O_5$ [(M+H)+] 431.1679 found 431.1675

Synthesis of 5′-O-[3-Benzyl-1-Ethyl]Carbamoyl Guanosine (6)

The ^{1}H NMR spectrum was (DMSO-d_6): 4.08 (m, 3H), 4.20 (m, 3H), 4.48 (m, 1H), 5.28 (d, 1H), 5.45 (d, 1H), 5.70 (d, 1H), 6.47 (s, 2H), 7.24-7.26 (m, 3H), 7.31-7.33 (m, 3H), 7.88 (t, 1H) and 7.91 (s, 1H). ^{13}C- DMSO-d_6: 157.20, 156.72, 154.19, 152.04, 140.09, 135.95, 128.77, 127.49, 127.28, 117.12, 86.42, 82.74, 73.45, 71.04, 64.69 and 40.26. Low resolution ESI-MS [M+H] 416.9 HRMS (ESI+) calcd for $C_{13}H_{18}N5O_5$ [(M+H)+] 417.1523 found 417.1519

Synthesis of 5′-O-[3-Imidazolyl-1-Ethyl]Carbamoyl Guanosine (7)

The ^{1}H NMR spectrum was (DMSO-d_6): 2.75 (t, 3H), 3.99 (m, 1H), 4.05 (m, 2H), 4.18-4.21 (m, 1H), 4.46 (m, 1H), 5.30 (m, 1H), 5.48 (m, 1H), 5.71 (d, 1H), 6.5 (s, 2H), 7.41 (s, 1H), 7.47 (t, 1H), 7.86 (s, 1H), 8.90 (s, 1H), 10.66 (s, 1H) and 14.06. ^{13}C- DMSO-d_6:

157.20, 156.46, 154.22, 135.84, 134.38, 131.52, 129.14, 117.12, 116.71, 86.52, 82.64, 73.51, 71.02, 64.26, 60.92 and 25.40 ppm. Low resolution ESI-MS [M+H] 421.2 HRMS (ESI+) calcd for $C_{13}H_{18}N5O_5$ [(M+H)+] 421.1584 found 421.1519

Synthesis of 5′-O-[3-amino-1-Ethyl]Carbamoyl Guanosine (8)

The ^{1}H NMR spectrum was (DMSO-d_6): 2.86 (t, 2H), 3.30 (q, 2H), 4.02 (m, 1H), 4.09-4.13 (m, 2H), 4.25 (d, 1H), 4.45 (q, 1H), 5.31 (d, 1H), 5.51 (d, 1H), 5.70 (d, 1H), 6.50 (s, 2H), 7.46 (t, 1H), 7.74 (s, 2H), 7.88 (s, 1H) and 10.66 (s, 1H). ^{13}C- DMSO-d_6: 157.20, 156.46, 154.23, 151.98, 135.86, 117.10, 86.62, 82.49, 73.53, 70.98, 64.95, 39.22 and 38.51 ppm. Low resolution ESI-MS [M+H] 370.2 HRMS (ESI+) calcd for $C_{13}H_{18}N5O_5$ [(M+H)+] 370.1475 found 370.1472

General procedure for Acid-NHS ester preparations:

N-Hydroxysuccinimide (0.62 g, 0.0053 mol, 1.0 equiv.) followed by EDC (0.00795 mmol, 1.5 equiv.) was added to a stirred solution of the respective acid (0.0053 mol, 1.0 equiv) in anhydrous THF (13 mL). The solution was stirred for 21 h at room temperature and evaporated under vacuum to dryness. The resulting crude residue was dissolved in ethylacetate (80 mL). The organic phase was washed with saturated $NaHCO_3$ (2x20 mL) and NaCl solution (2x20 mL), dried with Na_2SO_4, and filtered. The organic solvent was removed under vacuum to give crude NHS ester. The crude product was recrystallized with ethylacetate/petroleum ether to obtain the desired NHS ester. The esters were used for coupling without any further purification. ^{1}H and ^{13}C NMR indicated relatively clean esters (see below).

Synthesis of 2,5-dioxopyrrolidin-1-yl-3-(1H-indol-3-yl) propanoate (22):

Above NHS ester was prepared using general procedure above. The resulting compound was obtained in 46% yield. ^{1}H NMR spectrum was (DMSO-d_6): 2.82 (s, 4H), 3.05 (t, 4 H), 6.99 (s, 1H), 7.09 (t, 1H), 7.22 (s, 1H), 7.36 (d, 1H), 7.56 (d, 1H) and 10.88 (s, 1H). ^{13}C- DMSO-d_6: 170.31, 168.68, 136.27, 126.68, 122.82, 121.07, 118.38, 118.37, 112.06, 111.48, 31.35, 25.62 and 19.89. Low resolution ESI-MS [M+H] 287.0

Synthesis of 2,5-dioxopyrrolidin-1-yl-pentanoate (23):

Above NHS ester was prepared using general procedure above. The resulting compound was obtained in 47% yield. ^{1}H NMR spectrum was (DMSO-d_6): 1.06 (t, 3H), 1.79 (q, 2H), 2.63 (s, 2H) and 2.82 (s, 4 H). ^{13}C- DMSO-d_6: 172.00, 170.22, 33.47, 26.57, 19.24 and 13.68.

Synthesis of Sulfamoyl Chloride:

To a 20 mL round-bottom flask charged with chlorosulfonyl isocyanate (600 μL, 6.85 mmol) under N_2 on ice bath, was added formic acid (285.5 μL, 6.85 mmol) dropwise over 5 mins under vigorous stirring. After 10 min, the reaction was brought to the room temperature. A generation of white fog was detected in the flask during room temperature. After stirring for an additional hour, the reaction mixture slowly turned into a white solid, which was used directly in the next step without any purification.

Synthetic Procedure for the Preparation of Inhibitor 9

2´, 3´-O-isopropylidene Guanosine (14):

To a cold stirred suspension of guanosine (5.01g, 17.7 mmol) in acetone (300 ml) was added catalytic amount of perchloric acid (1.25 ml) drop-wise. The suspension became gradually clear and the reaction was monitored using TLC (20:80:0.1 MeOH/$CHCl_3$/TEA solvent). At the end of 2 h, ammonium hydroxide (2 equivalent to perchloric acid, 2.75 ml) was added drop-wise to neutralize the reaction mixture under an ice bath. The resulting product precipitated out from the solution upon neutralization. The reaction mixture was then evaporated under rotary evaporator to complete dryness. The crude reaction mixture was then triturated with ice-cold water (200 ml) overnight. The insoluble material was filtered and washed with cold diethyl ether to collect the desired product (3.99 g, 12.39 mmol) in 70 % yield. The ^{1}H NMR spectrum was (DMSO-d_6): 0.00 (s, TMS internal standard), 1.32 (s, 3H), 1.52 (s, 3H), 3.50-3.56 (m, 2H), 4.10-4.13 (t, 1H), 4.97 (d, 1H), 5.04 (t, 1H), 5.18 (d, 1H), 5.93 (d, 1H), 6.5 (s, 2H), 7.91 (s, 1H) and 10.66 (s, 1H). ^{13}C- DMSO-d_6: 157.16, 154.15, 151.20, 136.30, 117.21, 113.51, 88.87, 87.09, 84.04, 81.64, 62.07, 27.53 and 25.71 ppm. HRMS (ESI+) calcd for $C_{13}H_{18}N5O_5$ [(M+H)+] 324.1308 found 324.1304

2´,3´-O-isopropylidene-5'-O-(sulfamoyl)guanosine (15):

A solution of 8 (0.5 g, 1.54 mmol) in dimethyl acetamide (5 mL) was stirred for 30 min at 0 °C. Next, sulfamoyl chloride (1.69 mmol, 194.2 mg) was added to the reaction mixture after which reaction was brought to the room temperature and stirred for an additional one hour. An excess of TEA (1.5 mL, excess) was added and stirring was continued for an additional 10 min. The reaction mixture was finally quenched with

MeOH (5 ml) under ice bath. The reaction mixture was evaporated to dryness and the crude reaction mixture was dissolved in ethyl acetate and washed with saturated $NaHCO_3$ and Brine. The organic layer was collected dried over Na_2SO_4, filtered and evaporated to dryness. Purification by flash chromatography (20:80:1 MeOH/CH_2Cl_2/TEA) afforded the title compound (600 mg, 1.49 mmol) in 97% yield (with 1.5 equivalent of TEA). ^1H NMR spectrum was (DMSO-d_6): 1.18 (t, 13.45 H), 1.33 (s, 3H), 1.54 (s, 3H), 3.03 (m, 8.86 H), 4.13-4.24 (m, 2H), 4.33 (m, 1H), 5.16 (dd, 1H), 5.25 (d, 1H), 5.33 (s, 1H), 6.05 (d, 1H), 6.66 (s, 2H), 7.61 (s, 2H), 7.86 (s, 1H) and 10.84 (s, 1H). ^{13}C- DMSO-d_6: 156.68, 153.74, 150.47, 136.17, 113.26, 88.49, 84.02, 83.47, 81.07, 54.77, 51.94, 45.21, 26.84, 25.21, 8.62 and 7.20 ppm. Low resolution ESI-MS [M+H] 403.1 HRMS (ESI+) calcd for $C_{13}H_{19}N_6O_7S$ [(M+H)+] 403.1036 found 403.10262

5´-O-(N-(3-Indole propionic acid) sulfamoyl-2´, 3´-O-isopropylidene guanosine triethylammonium salt (16):

To an ice cold stirred solution of 9 (200 mg, 0.5 mmol) and 22 (214 mg, 0.75 mmol) in DMF (2 mL) was added DBU (1.1 equiv, 82 μl, 0.55 mmol). After stirring for an additional 10 min the reaction mixture was brought to room temperature and stirred overnight. Next, the volatiles were evaporated under reduced pressure and the mixture was directly loaded onto the C18 column. The purification was achieved using a gradient reverse chromatography (A-ACN, B-1% TEA in water, washed with 2% B and eluted with a gradient of 2-90 % of solvent A). Fractions containing the product were pooled and concentrated. The concentrate was freezed and lyophilized to obtain 150 mg (0.26 mmol, 51 % yield) of the title product as TEA salt (1.0 equivalent of TEA as determined

by NMR). ^{1}H NMR spectrum was (DMSO-d_6): 1.16 (t, 8.61 H), 1.30 (s, 3H), 1.51 (s, 3H), 2.37 (t, 2H), 2.85 (t, 2H), 3.07 (m, 5.00), 3.17 (m, 2 H), 3.93 (m, 1H), 4.09 (m, 1H), 4.27-431 (m, 2H), 5.10 (d, 1H), 5.21 (d, 1H), 5.76 (s, 1H), 5.96 (d, 1H), 6.61 (s, 2H), 6.93 (t, 1H), 7.03 (t, 2H), 7.07 (s, 1H), 7.30 (d, 1H), 7.46 (d, 1H), 7.93 (s, 1H), 10.64 (s, 1H) and 10.68 (s, 1H). ^{13}C- DMSO-d6: 157.18, 154.19, 151.07, 136.67, 127.64, 122.36, 121.17, 118.68, 118.46, 117.25, 113.40, 111.68, 89.51, 84.43, 83.95, 82.05, 79.65, 55.38, 49.06, 46.23, 27.52, 25.65 and 9.20 ppm. Low resolution ESI-MS [M+H] 574.0, [M-H] 572.0 HRMS (ESI+) calcd for $C_{24}H_{28}N_7O_8S$ [(M+H)+] 574.1720 found 574.1716

5´-O-[N-(3-Indole propionic acid)sulfamoyl] guanosine triethylammonium salt (9):

A solution of 10 (25 mg, 0.044 mmol) in 80% aqueous TFA (2 ml) was stirred for 30 min after which the reaction mixture was evaporated to dryness (co-evaporated 1% TEA/ethanol for removing TFA). The reaction mixture was loaded onto a celite packed cartridge and purified by using reverse phase chromatography (A-ACN, B-Water + 0.1% TEA). The peak eluted at 20% of ACN contained the final product. Fractions containing the product were combined, concentrated and lyophilized to obtain the desired final product in quantitative yields (with 1 equivalent of TEA). ^{1}H NMR spectrum was (DMSO-d_6): 1.14 (t, 10 H), 2.35 (t, 2H), 2.84 (t, 2H), 3.00 (m, 6 H), 3.98 (m, 2H), 4.13 (s, 2H), 4.55 (m, 1H), 5.20 (s, 1H), 5.38 (s, 1H), 5.70 (d, 1H), 6.50 (s, 2H), 6.94 (t, 1H), 7.02 (t, 1H), 7.06 (s, 1H), 7.28 (d, 1H), 7.46 (d, 1H), 7.96 (s, 1H), 10.60 (s, 1H) and 10.68 (s, 1H). ^{13}C-DMSO-d_6: 157.22, 154.09, 151.95, 136.66, 136.22, 127.68, 122.39, 121.14, 118.75, 118.47, 117.09, 115.28, 111.66, 86.75, 83.27, 73.79, 71.47, 67.66, 21.94 and 9.47 ppm. Low resolution ESI-MS [M-H] 532.1 HRMS (ESI+) calcd for $C_{21}H_{24}N_7O_8S$

[(M+H)+] 534.1407 found 534.1400. The final purity of the compound was ≥99 % as indicated by HPLC.

Synthetic Procedure for the Preparation of Inhibitor 10

5´-O-(N-(3-butyric acid) sulfamoyl-2´, 3´-O-isopropylidene guanosine triethylammonium salt:

The procedure is similar as described for 4 above using NHS ester (23). The resulting compound was obtained in 60% yield as TEA salt (1.2 equivalent of TEA as determined by NMR). ^{1}H NMR spectrum was (DMSO-d_6): 0.83 (t, 3H), 1.18 (t, 13 H, TEA), 1.30 (s, 3H), 1.46 (m, 2H), 1.51 (s, 3H), 2.0 (t, 2H), 2.8 (broad, 7H), 3.89 (m, 1H), 4.19 (m, 1H), 4.29 (m, 1H), 5.07 (dd, 1H), 5.19 (dd, 1H), 5.95 (d, 1H), 6.58 (s, 2H), 7.91 (s, 1H) and 10.63 (s, 1H). ^{13}C- DMSO-d_6: 177.93, 156.64, 153.84, 150.78, 136.251, 116.88, 118.49, 113.05, 89.09, 84.12, 83.61, 81.70, 66.78, 45.88, 41.30, 27.15, 25.27, 19.37 and 14.15 ppm. Low resolution ESI-MS [M+H] 473.1 HRMS (ESI+) calcd for $C_{17}H_{25}N_6O_8S$ [(M+H)+] 473.1455 found 473.1450.

5´-O-[N-(3-Butyric acid)sulfamoyl] guanosine triethylammonium salt (10):

The procedure is similar as described for 4 above. The resulting compound was obtained in 71% yield as TEA salt (1.3 equivalent of TEA as determined by NMR). The final product is highly hygroscopic in nature. ^{1}H NMR spectrum was (DMSO-d_6): 0.83 (t, 3H), 1.18 (t, 12 H), 1.46 (m, 2H), 2.0 (t, 2H), 3.0 (q, 8H), 3.58 (m, 2H), 4.03 (s, 2H), 4.10-4.15 (m, 2H), 4.48 (m, 1H), 5.24 (dd, 1H), 5.41 (dd, 1H), 5.70 (d, 1H), 6.48 (s, 2H), 7.91 (s, 1H) and 10.61 (s, 1H). ^{13}C- DMSO-d_6: 177.93, 156.64, 153.84, 150.78, 136.251, 116.88,

113.05, 89.09, 84.12, 83.61, 81.70, 66.78, 45.88, 41.30, 19.37 and 14.15 ppm. HRMS (ESI+) calcd for $C_{14}H_{21}N_6O_8S$ [(M+H)+] 433.1142 found 433.1134.

Synthetic Procedure for the Preparation of Inhibitor 12

2´, 3´-O-isopropylidene Adenosine (23):

To a cold stirred solution of adenosine (2.02g, 7.56 mmol) in acetone (150 ml) was added catalytic amount of perchloric acid (0.91 ml) in a drop-wise manner. The milky white suspension turned clear after 2 h of stirring. The solution was then neutralized using ammonium hydroxide (2 equivalents to perchloric acid) under ice-bath. The reaction mixture was then evaporated to complete dryness and purified using flash silica gel chromatography (gradient: 0% for 4 min, 0-15% for 4-10 min and eluted at 15% MeOH:CH_2Cl_2). Fractions containing the product were evaporated to obtained the desired product (2.3 g, 3.58 mmol) in 99 % yield. The ^{1}H NMR spectrum was (DMSO-d_6): 1.29 (s, 1H), 1.33 (s, 3H), 1.55 (s, 3H), 3.54-3.56 (m, 2H), 4.22 (m, 1H), 4.97 (dd, 1H), 5.23 (t, 1H), 5.35 (d, 1H), 6.12 (d, 1H), 7.34 (s, 2H), 8.17 (s, 1H) and 8.35 (s, 1H). ^{13}C-DMSO-d_6: 156.60, 153.09, 149.28, 140.16, 119.57, 113.51, 90.07, 86.82, 83.68, 81.82, 62.05, 27.55 and 25.66 ppm. HRMS (ESI+) calcd for $C_{13}H_{18}N_5O_4$ [(M+H)+] 308.1359 found 308.1351.

2´, 3´-O-isopropylidene EthenoAdenosine (24):

To a stirred solution of 11 (1.1 g, 3.58 mmol) in sodium acetate buffer (100 ml, 0.1 M pH 6.5) was added 25 ml of chlorocetaldehyde solution (50% wt), heated to 40 °C and stirred overnight. Next day, the reaction mixture was brought to the room temperature and

extracted with EtOAc (2 x 100 ml). The organic layer was then washed with saturated $NaHCO_3$ and Brine. The organic layer was dried over Na_2SO_4 and evaporated to dryness under reduced pressure. Purification by flash silica gel chromatography (gradient: 0% for 4 min, 0-15% for 4-10 min and eluted at 15:75 MeOH/CH_2Cl_2) afforded the title compound in 33% (400 mg) yield. The ^{1}H NMR spectrum was (DMSO-d_6): 1.35 (s, 3H), 1.57 (s, 3H), 3.55-3.56 (m, 2H), 4.12-4.16 (m, 1H), 4.99 (d, 1H), 5.09 (t, 1H), 5.37 (d, 1H), 6.27 (d, 1H), 7.58 (s, 1H), 8.10 (s, 1H), 8.53 (s, 1H) and 9.31 (s, 1H). ^{13}C- DMSO-d_6: 140.90, 140.41, 138.39, 137.65, 133.31, 123.66, 113.61, 112.74, 90.37, 87.27, 84.35, 81.81, 61.92, 27.51, and 25.66 ppm. Low resolution ESI-MS [M+H] 332.1 HRMS (ESI+) calcd for $C_{15}H_{18}N_5O_4$ [(M+H)+] 332.1359 found 332.1350.

2´, 3´-O-isopropylidene-5´-O-(sulfamoyl)EthenoAdenosine (25):

In a 10 ml round-bottom flask containing 12 (100 mg, 0.30 mmol, 1 eq.) was dissolved in anhydrous DMF (1 mL). To the cold stirred solution was added sulfamoyl chloride (103.4 mg, 0.90 mmol, 3 eq.) followed by the slow addition of triethylamine (40.4 µL, 0.30 mmol, 1.0 eq.). The reaction solution was stirred for an additional 1 h at room temperature. DMF was evaporated under vacuum and the crude mixture was then purified using reverse phase chromatography to obtain (0.27 mmoles, 110 mg) desired product in 90% yield. The ^{1}H NMR spectrum was (DMSO-d_6): 1.37 (s, 3H), 1.59 (s, 3H), 4.16-4.23 (m, 2H), 4.47 (m, 1H), 5.15 (d, 1H), 5.48 (d, 1H), 6.39 (d, 1H), 7.60 (s, 3H, broad peak overlaid with 1H), 8.13 (s, 1H), 8.50 (s, 1H) and 9.31 (s, 1H). ^{13}C- DMSO-d_6: 140.91, 140.70, 138.18, 137.82, 133.32, 123.90, 114.15, 112.82, 90.08, 84.15, 81.53,

68.44, 46.18, 27.36, and 25.78 ppm. Low resolution ESI-MS [M+H] 411.1 HRMS (ESI+) calcd for $C_{15}H_{19}N_6O_6S$ [(M+H)+] 411.1087 found 411.1076.

2´,3´-O-isopropylidene-5´-O-[N-(3-Indolepropionicacid)sulfamoyl]EthenoAdenosine Triethylammonium salt (12a):

The procedure is similar as described for **4** above using NHS ester (**22**). The resulting compound was obtained in 55% yield as TEA salt (1.1 equivalent of TEA as determined by NMR). ^{1}H NMR spectrum was (DMSO-d_6): 1.15 (t, 9 H), 1.33 (s, 3H), 1.57 (s, 3H), 2.35 (t, 2H), 2.84 (t, 2H), 3.06 (broad, 6H), 4.04 (d, 2H), 4.45 (m, 1H), 5.07 (m, 1H), 5.39 (m, 1H), 6.30 (d, 1H), 6.95 (m, 1H), 7.02 (m, 1H), 7.06 (s, 1H), 7.29 (d, 1H), 7.46 (d, 1H), 7.56 (d, 1H), 8.08 (s, 1H), 8.59 (s, 1H), 9.30 (s, 1H) and 10.67 (s, 1H). ^{13}C- DMSO-d_6: 140.93, 140.44, 138.47, 137.67, 136.66, 133.29, 127.66, 123.47, 122.36, 121.15, 118.71, 118.45, 113.63, 112.71, 111.67, 90.37, 84.57, 84.34, 82.10, 46.23, 27.52, 25.62, 21.93 and 9.28 ppm. Low resolution ESI-MS [M+H] 582.2 HRMS (ESI+) calcd for $C_{26}H_{28}N_7O_7S$ [(M+H)+] 582.1771 found 582.1764.

5´-O-[N-(3-Indole propionic acid)sulfamoyl]EthenoAdenosine Triethylammonium salt (12):

The procedure is similar as described for 4 above. The resulting compound was obtained in 74% yield as TEA salt (1.3 equivalent of TEA as determined by NMR). The final product is highly hygroscopic in nature. ^{1}H NMR spectrum was (DMSO-d_6): 1.10 (t, 13 H), 2.37 (t, 2H), 2.87 (t, 2H), 2.91 (broad, 6H), 4.06-4.22 (d, 5H), 4.67 (m, 1H), 5.37 (m, 1H), 5.53 (m, 1H), 6.07 (d, 1H), 6.94 (m, 1H), 7.03 (m, 1H), 7.08 (s, 1H), 7.29 (d, 1H),

7.48 (d, 1H), 7.56 (d, 1H), 8.07 (s, 1H), 8.62 (s, 1H), 9.29 (s, 1H) and 10.67 (s, 1H). ^{13}C-DMSO-d_6: 141.01, 140.37, 139.11, 137.51, 136.66, 133.21, 127.68, 122.39, 121.14, 118.75, 118.46, 115.30, 112.62, 111.65, 87.86, 83.66, 74.61, 71.48, 46.22 and 21.99 ppm. HRMS (ESI+) calcd for $C_{23}H_{24}N_7O_7S$ [(M+H)+] 542.1458 found 542.1457. The final purity of the compound was ≥99 % as indicated by HPLC.

5´-O-[N-(3-biotinyl-butanoic)sulfamoyl]EthenoAdenosine Triethylammonium salt (13) (Synthesized and purified by Andrew Zhou)**:**

The procedure is similar as described for 4 above. The resulting compound was obtained in 74% yield as TEA salt (1.0 equivalent of TEA as determined by NMR). The final product is highly hygroscopic in nature. ^{1}H NMR spectrum was (DMSO-d_6): 1.15 (s, 9 H), 1.29 (m, 3H), 1.46 (m, 4H), 1.60 (m, 2H), 1.98 (s,, 2H), 2.77 (m, 1H), 3.06 (s, 7 H), 4.11-4.25 (m, 6H), 4.25 (s, 1H), 4.64 (s, 1H), 5.35 (s 1H), 5.51 (m, 1H), 6.01 (m, 1H), 6.31 (m, 1H), 6.40 (s, 1H), 7.55 (s, 1H), 8.08 (s, 1H), 8.56 (s, 1H) and 9.29 (s, 1H). ^{13}C-DMSO-d_6: 163.25, 141.23, 140.27, 139.32, 137.40, 132.93, 123.20, 112.51, 87.77, 83.62, 74.37, 71.33, 67.66, 61.43, 59.52, 56.17, 46.20, 28.73, 28.58, 26.49 and 9.27 ppm. Low resolution ESI-MS [M+H] 597.1 HRMS (ESI+) calcd for $C_{22}H_{29}N_8O_8S_2$ [(M+H)+] 597.1550 found 597.1525

Synthetic Procedure for the Preparation of Inhibitor 11

N,N-Dimethylaminomethylene-2´,3´-O-isopropylideneguanosine (17):

To a suspension of 8 (0.575 g, 1.78 mmol) in DMF (6 mL), N,N-dimethylformamide dimethyl acetal (0.891 mL, 6.7 mmol) was added under argon to yield an orange-brown

solution. The reaction mixture was stirred at 50 °C for 4 h. The solvent was removed under reduced pressure and at elevated temperatures; the white residue was then removed by filtration. The filtrate was dried under reduced pressure, dissolved in MeOH (2.5 mL) and precipitated with 5 mL of EtOAc. After storage overnight at 4 °C, the precipitate was removed by filtration and washed thoroughly with EtOAc. The precipitate was dried overnight under reduced pressure and the product was obtained as a white powder in 80% yield (0.538 g, 1.42 mmol). The ^{1}H NMR spectrum was (DMSO-d_6): 1.33 (s, 3H), 1.55 (s, 3H), 3.04 (s, 3H), 3.16 (s, 3H), 3.51-3.55 (m, 2H), 4.12-4.15 (m, 1H), 4.97 (dd, 1H), 5.05 (t, 1H), 5.28 (d, 1H), 6.04 (d, 1H), 8.02 (s, 1H), 8.57 (s, 1H) and 11.37 (s, 1H). ^{13}C-DMSO-d_6: 158.7, 158.03,157.86, 149.92, 137.64, 120.24, 113.58, 88.97, 86.74, 83.93, 81.57, 61.87, 41.22, 35.12, 27.54 and 25.71 ppm. Low resolution ESI-MS [M+H] 379.0 HRMS (ESI+) calcd for $C_{16}H_{23}N_6O_5$ [(M+H)+] 379.1730 found 379.1738.

N,N-Dimethylaminomethylene-2´,3´-O,O-isopropylidene-5´-deoxy-5´-azido (18):

(Preparation of N,N-Dimethylaminomethylene-2´,3´-O-isopropylidene-5´-deoxy-5´-Iodo (14a) as described previously) A stirred suspension of 14 (0.440g, 1.162 mmol) in anhyd THF (22 mL) under argon was cooled to –70 °C. To this solution was added Methyltriphenoxyphosphonium iodide (0.788 g, 1.742 mmol; 1.5 equiv). Due to the light sensitivity of the reactant and the product all subsequent steps were carried out under the exclusion of light. After 30 min of stirring the reaction mixture was brought to the room temperature and stirred for another 4 h. The reaction was stopped by the addition of MeOH (10 mL) and evaporated to dryness under reduced pressure to obtain an oily dark residue. The residue was dissolved in MeOH/$CHCl_3$ (1:4; 2.5 mL) and subjected to silica

gel normal chromatography (Combiflash: $CHCl_2$/MeOH, 9:1). After purification the desired product was obtained as an yellow-orange solid in 92% yield (0.522 g, 1.15 mmol). The ^1H NMR spectrum was (DMSO-d_6): 1.18 (t, 1H), 1.36 (s, 3H), 1.56 (s, 3H), 1.99 (s, 1H), 3.06 (s, 3H), 3.19 (s, 3H), 3.48-3.52 (m, 2H), 4.02 (q, 1H), 4.29 (m, 1H), 5.00 (dd, 1H), 5.44 (dd, 1H), 6.16 (d, 1H), 8.04 (s, 1H), 8.60 (s, 1H) and 11.43 (s, 1H). ^{13}C- DMSO-d_6: 170.82, 157.98, 158.55, 157.78, 149.53, 138.21, 120.42, 113.81, 89.70, 86.67, 84.30, 84.22, 60.23, 41.68, 35.21, 27.31, 26.22, 25.64, 21.25, 14.57 and 7.04 ppm. Low resolution ESI-MS [M+H] 489.0 HRMS (ESI+) calcd for $C_{16}H_{22}IN_6O_4$ [(M+H)+] 489.0747 found 489.0736. To a stirred solution of (14a) (400 mg, 0.8 mmol) in dry DMF (5ml) was added sodium azide (260 mg, 8 mmol). The reaction mixture was stirred under argon at RT overnight. Next day, the precipitate in the reaction mixture was filtered and washed with cold methanol. The filtrate was evaporated to dryness and the crude product was purified using flash chromatography. The desired peak was eluted at 10 % MeOH/$CHCl_3$ mixture, which was combined and evaporated to obtain 166 mg of the final product in 55% yield. The ^1H NMR spectrum was (DMSO-d_6): 1.35 (s, 3H), 1.56 (s, 3H), 3.06 (s, 3H), 3.19 (s, 3H), 3.54-3.59 (m, 2H), 4.26 (m, 1H), 5.00 (dd, 1H), 5.43 (d, 1H), 6.11 (d, 1H), 8.04 (s, 1H), 8.61 (s, 1H) and 11.41 (s, 1H). ^{13}C- DMSO-d_6: 158.59, 158.02, 157.85, 149.85, 137.82, 120.41, 114.04, 88.78, 84.78, 83.67, 81.71, 51.95, 41.68, 35.15, 27.43, and 25.70 ppm. Low resolution ESI-MS [M+H] 404.0 HRMS (ESI+) calcd for $C_{16}H_{23}N_6O_5$ [(M+H)+] 404.1795 found 404.1786

N,N-Dimethylaminomethylene-2´,3´-O,O-isopropylidene-5´-deoxy-5´-amino (19):

To a stirred solution of 15 (160 mg, 0.392 mmol) in dioxane (12 mL) was added H_2O (1.6 mL), TEA (65.6 uL, 0.464 mmol) and triphenylphosphine (0.312 g, 1.18 mmol). The reaction was then stirred for 3 h at 50 ℃. The reaction was brought to the room temperature, concentrated, and the residue was purified using flash silica column chromatography. Then product was eluted using a gradient of 20% $CH_3OH/CHCl_3$ (containing 0.5% TEA) over a period of 20 mins. The product eluted in a broad peak, which was concentrated to get the desired product (80 mg, 0.212 mmol) in 54% yield. The ^1H NMR spectrum was (DMSO-d_6): 0.95 (s, 1H), 1.33 (s, 3H), 1.54 (s, 3H), 2.74-2.77 (m, 2H), 3.04 (s, 3H), 3.19 (s, 3H), 4.08 (m, 1H), 4.98 (dd, 1H), 5.34 (d, 1H), 5.99 (d, 1H), 8.03 (s, 1H) and 8.56 (s, 1H). ^{13}C- DMSO-d_6: 158.63, 158.04, 157.81, 149.95, 137.98, 120.46, 113.66, 89.94, 86.68, 83.38, 81.85, 46.18, 43.82, 35.14, 27.56 and 25.78 ppm. Low resolution ESI-MS [M+H] 378.1 HRMS (ESI+) calcd for $C_{16}H_{24}N_7O_4$ [(M+H)+] 378.1890 found 378.1885.

N,N-Dimethylaminomethylene-2´,3´-O,O-isopropylidene-5´-deoxy-5´-N-sulfamoyl (20):

To a stirred solution of 16 (0.150 g, 0.31 mmol) in 1,4-dioxane (8 ml) was added sulfamide (0.090 g, 0.93 mmol) and the reaction mixture was refluxed for 2 h. The reaction mixture was then evaporated and redissolved in CH_2Cl_2 (15 ml) and water (15 ml). The organic layer was washed with brine, dried over Na_2SO_4 and evaporated to dryness under reduced pressure. The crude product (17) was dissolved in MeOH/4N NaOH (5 ml, 1:1) solution and heated at 60 °C for 2 h and 20 mins. At the end of the reaction, 1N HCl was added under ice the reaction mixture. Methanol from the reaction

mixture was evaporated and the aqueous solution was then lyophilized to obtain crude white product. The crude product was then purified using reverse phase chromatography to obtain desired product (0.030 g, 0.074 mmol) in 24 % yield. ^{1}H NMR spectrum was (DMSO-d_6): 0.941 (t, 1H), 1.34 (s, 3H), 1.54 (s, 3H), 2.43 (m, 1H), 3.12-3.22 (m, 2 H), 4.28 (m, 1H), 5.02 (dd, 1H), 5.22 (dd, 1H), 5.93 (d, 1H), 6.60 (s, 2H), 6.72 (s, 2H), 6.97 (s, 1H), 7.87 (s, 1H) and 10.76 (s, 1H). ^{13}C- DMSO-d_6: 157.40, 154.41, 150.71, 137.09, 117.90, 113.70, 89.65, 84.38, 83.05, 82.19, 43.82, 27.56 and 25.77 ppm. HRMS (ESI+) calcd for $C_{13}H_{20}N_7O_6S$ [(M+H)+] 402.1196 found 402.1193.

5´-N-[N-(3-Indole propionic acid)sulfamoyl] guanosine triethylammonium salt (11):

To a cold stirred solution of 17 (20 mg, 0.05 mmol) and 22 (1.5 equiv, 21.4 mg, 0.075 mmol) in DMF (0.4 mL) was added DBU (1.1 equiv, 8.2 μl, 0.055 mmol). After 10 min the reaction mixture was brought to the room temperature and stirred overnight. Next, the volatiles were evaporated under reduced pressure and the crude reaction mixture was used for the final step without any purification. To the crude reaction mixture was added 80% aq TFA (1 ml) and stirred for 30 mins. After which the reaction mixture was evaporated to dryness (co-evaporated 1% TEA/ethanol for removing TFA) under reduce pressure. The reaction mixture was loaded onto the combiflash and purified using reverse phase chromatography (A-ACN, B-Water + 0.1% TEA). The peak eluted at 20% of ACN contained the desired product. Fractions containing the product were pooled, concentrated and lyophilized to obtain the desired final product in quantitative yields (with 1 equivalent of TEA). ^{1}H NMR spectrum was 700 MHz (DMSO-d_6): 0.95 (t, 9 H), 2.43 (m, 2H), 2.73 (m, 6 H), 2.87-2.97 (m, 4H), 3.87-3.92 (m, 2H), 4.11 (m, 1H), 4.41-

4.50 (m, 3H), 5.51 (d, 1H), 5.57 (d, 1H), 6.85-6.95 (m, 4H), 7.39-7.41 (m, 2H), 7.69-7.74 (m, 2H), and 10.71 (d, 1H). ^{13}C-DMSO-d_6: 157.58, 156.42, 154.12, 151.15, 136.83, 128.76, 128.10, 127.44, 123.16, 121.19, 118.39, 111.64, 91.22, 88.26, 80.68, 78.38, 72.61, 71.79, 66.19, 53.68, 52.36, 46.27 and 10.21 ppm. HRMS (ESI+) calcd for $C_{21}H_{25}N_8O_7S$ [(M+H)] 533.1567 found 533.1567. The final purity of the compound was ≥99 % as indicated by HPLC.

References:

1. Liu, Q.; Puche, A. C.; Wang, J. B., Distribution and expression of protein kinase C interactive protein (PKCI/HINT1) in mouse central nervous system (CNS). *Neurochem Res* **2008,** *33* (7), 1263-76.
2. Garzón, J.; Herrero-Labrador, R.; Rodríguez-Muñoz, M.; Shah, R.; Vicente-Sánchez, A.; Wagner, C. R.; Sánchez-Blázquez, P., HINT1 protein: a new therapeutic target to enhance opioid antinociception and block mechanical allodynia. *Neuropharmacology* **2015,** *89*, 412-23.
3. Chou, T. F.; Baraniak, J.; Kaczmarek, R.; Zhou, X.; Cheng, J.; Ghosh, B.; Wagner, C. R., Phosphoramidate pronucleotides: a comparison of the phosphoramidase substrate specificity of human and Escherichia coli histidine triad nucleotide binding proteins. *Mol Pharm* **2007,** *4* (2), 208-17.
4. Zhou, X.; Chou, T. F.; Aubol, B. E.; Park, C. J.; Wolfenden, R.; Adams, J.; Wagner, C. R., Kinetic mechanism of human histidine triad nucleotide binding protein 1. *Biochemistry* **2013,** *52* (20), 3588-600.
5. Lima, C. D.; Klein, M. G.; Hendrickson, W. A., Structure-based analysis of catalysis and substrate definition in the HIT protein family. *Science* **1997,** *278* (5336), 286-90.
6. Murakami, E.; Tolstykh, T.; Bao, H.; Niu, C.; Steuer, H. M.; Bao, D.; Chang, W.; Espiritu, C.; Bansal, S.; Lam, A. M.; Otto, M. J.; Sofia, M. J.; Furman, P. A., Mechanism of activation of PSI-7851 and its diastereoisomer PSI-7977. *J Biol Chem* **2010,** *285* (45), 34337-47.
7. Drontle, D. P.; Wagner, C. R., Designing a pronucleotide stratagem: lessons from amino acid phosphoramidates of anticancer and antiviral pyrimidines. *Mini Rev Med Chem* **2004,** *4* (4), 409-19.
8. Li, S.; Jia, Y.; Jacobson, B.; McCauley, J.; Kratzke, R.; Bitterman, P. B.; Wagner, C. R., Treatment of breast and lung cancer cells with a N-7 benzyl guanosine monophosphate tryptamine phosphoramidate pronucleotide (4Ei-1) results in chemosensitization to gemcitabine and induced eIF4E proteasomal degradation. *Mol Pharm* **2013,** *10* (2), 523-31.
9. Chou, T. F.; Wagner, C. R., Lysyl-tRNA synthetase-generated lysyl-adenylate is a substrate for histidine triad nucleotide binding proteins. *J Biol Chem* **2007,** *282* (7), 4719-27.
10. Lee, Y. N.; Nechushtan, H.; Figov, N.; Razin, E., The function of lysyl-tRNA synthetase and Ap4A as signaling regulators of MITF activity in FcepsilonRI-activated mast cells. *Immunity* **2004,** *20* (2), 145-51.
11. Li, H.; Zhang, Y.; Su, T.; Santella, R. M.; Weinstein, I. B., Hint1 is a haplo-insufficient tumor suppressor in mice. *Oncogene* **2006,** *25* (5), 713-21.
12. Wang, L.; Zhang, Y.; Li, H.; Xu, Z.; Santella, R. M.; Weinstein, I. B., Hint1 inhibits growth and activator protein-1 activity in human colon cancer cells. *Cancer Res* **2007,** *67* (10), 4700-8.

13. Barbier, E.; Zapata, A.; Oh, E.; Liu, Q.; Zhu, F.; Undie, A.; Shippenberg, T.; Wang, J. B., Supersensitivity to amphetamine in protein kinase-C interacting protein/HINT1 knockout mice. *Neuropsychopharmacology* **2007,** *32* (8), 1774-82.
14. Jackson, K. J.; Wang, J. B.; Barbier, E.; Damaj, M. I.; Chen, X., The histidine triad nucleotide binding 1 protein is involved in nicotine reward and physical nicotine withdrawal in mice. *Neurosci Lett* **2013,** *550*, 129-33.
15. Guang, W.; Wang, H.; Su, T.; Weinstein, I. B.; Wang, J. B., Role of mPKCI, a novel mu-opioid receptor interactive protein, in receptor desensitization, phosphorylation, and morphine-induced analgesia. *Mol Pharmacol* **2004,** *66* (5), 1285-92.
16. Rodríguez-Muñoz, M.; Sánchez-Blázquez, P.; Vicente-Sánchez, A.; Bailón, C.; Martín-Aznar, B.; Garzón, J., The histidine triad nucleotide-binding protein 1 supports mu-opioid receptor-glutamate NMDA receptor cross-regulation. *Cell Mol Life Sci* **2011,** *68* (17), 2933-49.
17. Kawasumi, M.; Nghiem, P., Chemical genetics: elucidating biological systems with small-molecule compounds. *J Invest Dermatol* **2007,** *127* (7), 1577-84.
18. Duckworth, B. P.; Geders, T. W.; Tiwari, D.; Boshoff, H. I.; Sibbald, P. A.; Barry, C. E.; Schnappinger, D.; Finzel, B. C.; Aldrich, C. C., Bisubstrate adenylation inhibitors of biotin protein ligase from Mycobacterium tuberculosis. *Chem Biol* **2011,** *18* (11), 1432-41.
19. Dawadi, S.; Viswanathan, K.; Boshoff, H. I.; Barry, C. E.; Aldrich, C. C., Investigation and conformational analysis of fluorinated nucleoside antibiotics targeting siderophore biosynthesis. *J Org Chem* **2015,** *80* (10), 4835-50.
20. Gruber, B. A.; Leonard, N. J., Dynamic and static quenching of 1,N6-ethenoadenine fluorescence in nicotinamide 1,N6-ethenoadenine dinucleotide and in 1,N6-etheno-9-(3-(indol-3-yl) propyl) adenine. *Proc Natl Acad Sci U S A* **1975,** *72* (10), 3966-9.
21. Bai, G.; Feng, B.; Wang, J. B.; Pozharski, E.; Shapiro, M., Studies on ligand binding to histidine triad nucleotide binding protein 1. *Bioorg Med Chem* **2010,** *18* (18), 6756-62.
22. Dolot, R.; Ozga, M.; Włodarczyk, A.; Krakowiak, A.; Nawrot, B., A new crystal form of human histidine triad nucleotide-binding protein 1 (hHINT1) in complex with adenosine 5'-monophosphate at 1.38 Å resolution. *Acta Crystallogr Sect F Struct Biol Cryst Commun* **2012,** *68* (Pt 8), 883-8.
23. Meyer, E. A.; Castellano, R. K.; Diederich, F., Interactions with aromatic rings in chemical and biological recognition. *Angew Chem Int Ed Engl* **2003,** *42* (11), 1210-50.
24. Persch, E.; Dumele, O.; Diederich, F., Molecular recognition in chemical and biological systems. *Angew Chem Int Ed Engl* **2015,** *54* (11), 3290-327.
25. Snyder, P. W.; Mecinovic, J.; Moustakas, D. T.; Thomas, S. W.; Harder, M.; Mack, E. T.; Lockett, M. R.; Héroux, A.; Sherman, W.; Whitesides, G. M., Mechanism of the hydrophobic effect in the biomolecular recognition of arylsulfonamides by carbonic anhydrase. *Proc Natl Acad Sci U S A* **2011,** *108* (44), 17889-94.

26. Breiten, B.; Lockett, M. R.; Sherman, W.; Fujita, S.; Al-Sayah, M.; Lange, H.; Bowers, C. M.; Heroux, A.; Krilov, G.; Whitesides, G. M., Water networks contribute to enthalpy/entropy compensation in protein-ligand binding. *J Am Chem Soc* **2013,** *135* (41), 15579-84.
27. McCoy, A. J.; Grosse-Kunstleve, R. W.; Adams, P. D.; Winn, M. D.; Storoni, L. C.; Read, R. J., Phaser crystallographic software. *J Appl Crystallogr* **2007,** *40* (Pt 4), 658-674.
28. Adams, P. D.; Afonine, P. V.; Bunkóczi, G.; Chen, V. B.; Davis, I. W.; Echols, N.; Headd, J. J.; Hung, L. W.; Kapral, G. J.; Grosse-Kunstleve, R. W.; McCoy, A. J.; Moriarty, N. W.; Oeffner, R.; Read, R. J.; Richardson, D. C.; Richardson, J. S.; Terwilliger, T. C.; Zwart, P. H., PHENIX: a comprehensive Python-based system for macromolecular structure solution. *Acta Crystallogr D Biol Crystallogr* **2010,** *66* (Pt 2), 213-21.
29. Emsley, P.; Cowtan, K., Coot: model-building tools for molecular graphics. *Acta Crystallogr D Biol Crystallogr* **2004,** *60* (Pt 12 Pt 1), 2126-32.
30. Lebedev, A. A.; Young, P.; Isupov, M. N.; Moroz, O. V.; Vagin, A. A.; Murshudov, G. N., JLigand: a graphical tool for the CCP4 template-restraint library. *Acta Crystallogr D Biol Crystallogr* **2012,** *68* (Pt 4), 431-40.

Chapter 4

Caught Before Release: An Alternate Slow Substrate for Sofosbuvir Activating Enzyme, Human Histidine Triad Nucleotide Binding Protein 1 (hHint1)

INTRODUCTION:

The human histidine triad nucleotide binding proteins (or "hHints") are members of the larger superfamily of histidine triad proteins (the HITs). These enzymes possess a broad range of catalytic capabilities that share a common conserved nucleotide-binding domain with a characteristic sequence motif (H-*X*-H-*X*-H-*X*-*X*, where *X* are hydrophobic residues).[1, 2] Hints are distinctive members of the superfamily and are known for their ability to efficiently catalyze acyl-AMP and nucleoside phosphoramidate hydrolysis.[3, 4] They are the oldest and most widely distributed members of the HIT superfamily and are conserved across all the kingdoms of life, from archaea to eukaryotes, with humans expressing three family members (hHint1, hHint2, and hHint3).[2] Although Hints have been associated with a variety of biological processes, including the hydrolysis of aminoacyl adenylates,[5, 6] tumor suppression,[7, 8] and multiple central nervous system functions,[9, 10] the biological role of Hint catalysis and its endogenous substrate in cells remains enigmatic.

Over the past decade, the nucleoside phosphoramidase activity of human Hint enzymes has been exploited to activate nucleotide prodrugs (i.e. proTides). Potential nucleotide-based anti-cancer and antiviral agents that are negatively charged and suffer from poor oral bioavailability, rapid degradation in the blood, and an inability to penetrate cellular membranes, limiting their therapeutic utility.[11] Moreover, downregulation of the kinases responsible for nucleoside phosphorylation *in vivo* can lead to the rapid development of resistance and limits the use of nucleosides as an

Figure 1. A) Position of catalytic residues in the hHint1 active site as exemplified by high resolution complex with AMP (gray, PDB ID 3TW2). Apo structures, such as 1KPA, nearly identical. Only backbone atoms of Pro46 and Glu47 are shown. B) The kinetic mechanism of hHint1, shown with kinetic parameters for the substrate **1**.[23]

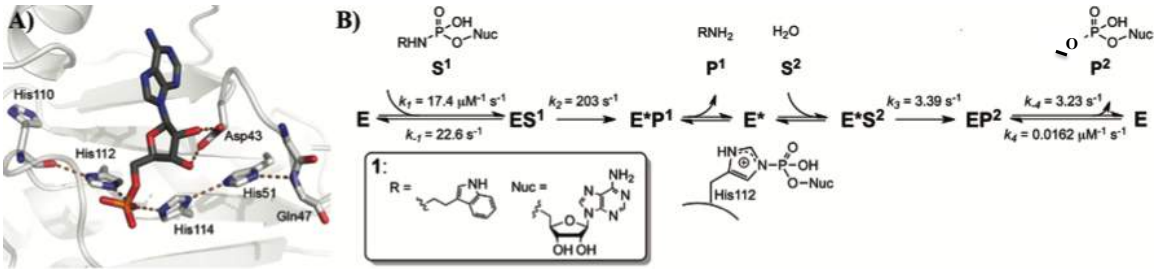

alternative approach.[12] ProTides offer an attractive opportunity to deliver antiviral and anticancer nucleotide-based therapies to circumvent these limitations.[13] The curative hepatitis C drug, sofosbuvir (Sovaldi® and a component of Harvoni®), is a pyrimidine nucleotide prodrug that undergoes multiple steps of activation culminating in the intracellular release of the poorly bioavailable 2´-deoxy2´-α-fluoro-β-C-methyluridine-5´-monophosphate (dFMU-MP) by hHint1 through P-N bond hydrolysis. dFMU-MP is subsequently converted by nucleotide kinases to the active metabolite, dFMU-TP.[14, 15] A comprehensive steady-state kinetic analysis has shown that hHint1 has a modest preference for purine over pyrimidine based nucleotide phosphoramidate substrates.[3] An in-depth structural understanding of the catalytic mechanism would be beneficial to fully exploit hHint enzymes for the pronucleotide activation. Human Hint1 has been the subject of a number of structural studies with[16, 17] and without[18, 19] bound nucleotides, nucleotidyl inhibitors[20] and substrate mimetics.[6, 16] These studies have revealed a network of specific hydrogen bonds involving the conserved triad of histidines (His110, His112, and His114), as well as His51 that are configured to promote stabilization of a cationic residue and binding of an anionic nucleoside monophosphates (**Figure 1A**). The carbonyl of His110 accepts a hydrogen bond from His112 (ND1H tautomer), which then enhances the nucleophilicity His112. (**Figure 1A**).

A detailed investigation on the kinetics of hHint1 catalysis has demonstrated a double-displacement or "ping-pong" mechanism for this enzyme, which results in the overall retention of stereochemistry (**Figure 1B**).[23] In the first half of the mechanism, a nucleotide phosphoramidate substrate (**S**^{1}) binds to and reacts with Histidine in the active site to release an alkyl amine (**P**^{1}) forming a nucleotidylated enzyme intermediate (**E***).

Pre-steady-state kinetic analysis has revealed that the rate of nucleotidylated enzyme formation is very rapid and nearly diffusion-limited. During the second half of the reaction, the nucleotidylated histidine in the active site (His112) undergoes hydrolysis ($\mathbf{S^2}$), resulting in the eventual release of a nucleotide monophosphate product ($\mathbf{P^2}$) from the active site. Based on a series of solvent viscosity studies, it has been suggested that the rate governing the product ($\mathbf{P^2}$) release maybe coupled to a kinetically silent conformational change in the protein structure.[21]

One of the major challenges associated with the structural isolation of the intermediates along this reaction trajectory is that one of the partially rate-limiting steps – the hydrolysis of the nucleotidylated enzyme – is facilitated by ubiquitous water. In order to alter the kinetics so that the intermediate might be trapped using cryo-crystallography, we thought to employ nucleoside thiophosphoramidates as the substrates. Thiophosphorylhistidines have been found to be more water stable to hydrolysis than phosphohistidines.[22] By using a more slowly hydrolyzed substrate, we have been able to capture the first nucleotiylated-Histidine intermediate during hHint1 catalysis (**E***), and the product-bound complex ($\mathbf{EP^2}$). This information should facilitate mechanistic and theoretical studies of nucleotidylated histidine formation, as well as the design of new ProTides.

Results

Design of the slow substrate and synthesis.

Previous work in our laboratory has shown that fluorogenic purine nucleoside tryptamine phosphoramidates such as **1** and **2** (**Figure 2A**, **Table 1**) are excellent substrates for hHint1-mediated hydrolysis.[3] Therefore making it difficult to trap the covalent histidine phosphate intermediate. In order to reduce the chemical reactivity of these substrates and thus potentially trap the nucleotidylated-His intermediate (**E***), we envisioned an analog in which the 5' oxygen atom is replaced with a less electronegative sulfur atom (**3**; TrpGMPS; **Figure 2A**). We expected this substitution would reduce the acid-liability of the bond between the nitrogen of His112 and the nucleotide phosphorus. Thus providing a longer lifetime for the **E*** complex.

To install the 5'-sulfur onto guanosine, we adopted the strategy previously reported by Hodgson and co-workers for the one-step aqueous preparation of N,S-dialkylthiophosphoramidates[23] (**Scheme 1**). We investigated the stability of **3** at pH 2.0, 4.0 and 7.0 and found it to be stable at pH 7, but showed decomposition at pH 2 and 4 (**Figure 3**). We investigated the steady state hydrolysis of **2** and **3** (**Table 1**) using a continuous fluorescence assay described previously.[3] (**Figure 2B**) Steady-state kinetics with hHint1 revealed that the turnover rate (k_{cat}) for **3** is 120-fold slower than that for **2**, resulting in a 177-fold decrease in the substrate specificity (k_{cat}/K_m) over **2** (**Table 1** and **Figure 2B**). As predicted, incorporation of a sulfur atom resulted in a significantly slower rate of hydrolysis by Hint1.

We performed NMR titration experiments to monitor hydrolysis of **3** in the presence of hHint1. Upon incubation at a protein to ligand ratio of 1:100, the half-life of **3** was found to be 88 min (**Figure 2C**). The observed half-life can be converted to velocity using the initial substrate concentration ($v=[S]x0.693/t_{1/2}$). Accordingly, the calculated velocity was found to be 39 μM/min and turnover rate to be 0.013 s^{-1}(enzyme concentration 50 μM), which is consistent with the k_{cat} value obtained using fluorescence assay. Therefore, the rate of hydrolysis of the thionucleotidylhistidine has been significantly reduced, when compared to the nucleotidylhistidine intermediate. Thus we believed that we can trap the intermediate using time-lapse cryo-crystallography.

Scheme 1: Synthesis of TrpGMPS

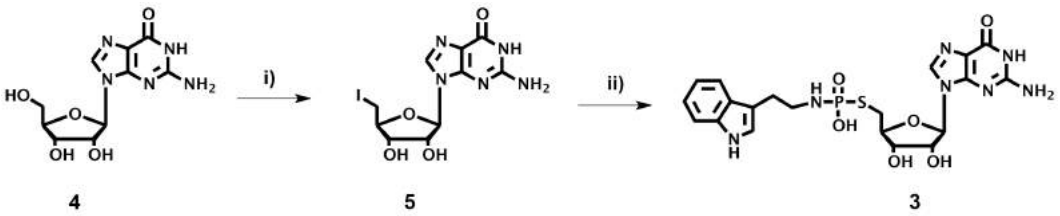

[a]Reagents and conditions**:** i) PPh_3, Imidazole, I_2, RT,61%; ii) a) Tryptamine, $PSCl_3$, 1M NaOH, water, b) **5**, 30%;

Table 1. Steady State Kinetic parameters comparison of substrate hydrolysis by hHint1**.** Values are reported from triplicate measurements as mean ± S.D.

Compound	K_m (μM)	k_{cat} (s^{-1})	k_{cat}/K_m (x 10^7, s^{-1} M^{-1})	k_{cat}/K_m / k_{cat}/K_m [3]
1	0.13 ± 0.02	2.1 ± 0.1	1.5 ± 0.3	242
2	0.21 ± 0.02	2.3 ± 0.1	1.1 ± 0.1	177
3	0.305 ± 0.04	0.019 ± 0.001	0.0062 ± 0.002	1

Figure 2. A) Chemical structures of hHint1 substrates (**1** and **2**) and the designed slow substrate of hHint1 (**3**). B) Steady state kinetics and Michaelis-Menten analysis of the hydrolysis of **3** by hHint1. C) Time-dependent analysis of **3** hydrolysis by hHint1 (1:100 ratio protein:ligand) as monitored under non-steady state via ^{31}P NMR.

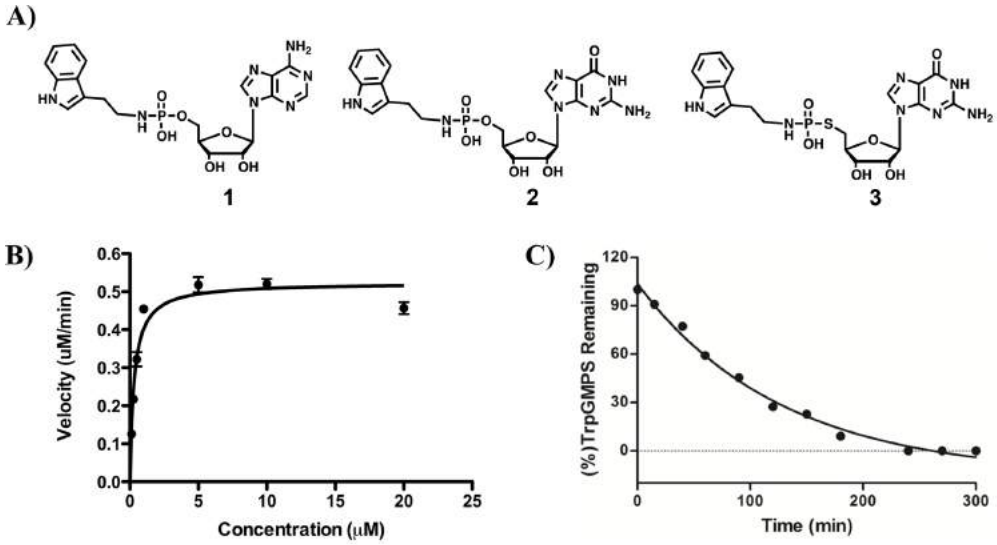

Figure 3: HPLC stability studies performed by monitoring the UV trace at absorbance 168-254 nm for the nucleoside. Samples containing 50 μM of **3** at pH A) 7.0 B) 4.0 and C) 2.0 were incubated at 37 °C in PBS. At indicated time intervals 200 μl of the solution were injected on the HPLC and monitored for any appearance of degradation peaks. Area under the curve was obtained from the traces and plotted against the time and fitted with an exponential decay curve equation using graph pad prism.

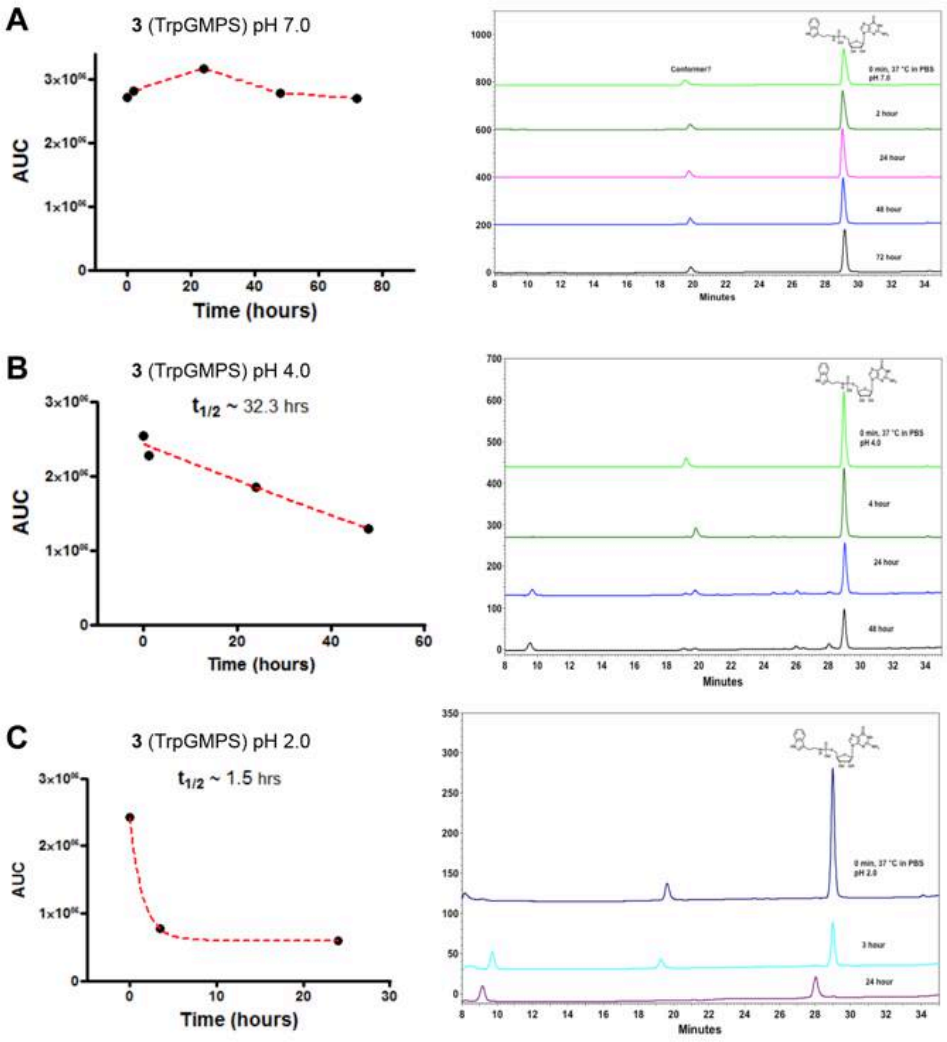

Figure 4. A) X-ray crystal structure complex of **E*** (brown, 5IPD). Inversion of the phosphorus center and standard 2'-*endo* pucker is observed in the E* complex. B) Comparison of product complexes. The catalytic product GMPS (5IPE, purple) is overlaid with AMP (3TW2).

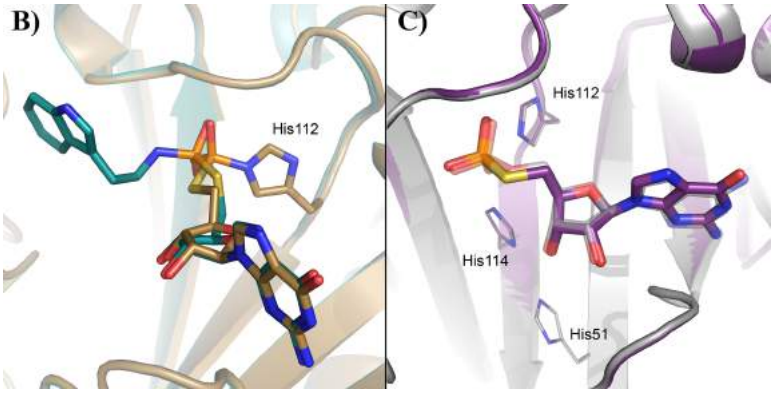

Capture of Nucleotidylated-Histidine Complex (E*).

In order to potentially capture the nucleotidylated histidine intermediate along the reaction trajectory, **3** was soaked into *apo* wild-type protein crystals, which were then flash-frozen in time-course experiments. A 15-minute soak of an *apo* crystal using 5.5 mM **3** at 4 °C yields a complex with 1.75 Å resolution. The complex appears to show the full conversion of the enzyme to the guanylated intermediate **E*** with no remaining density for the tryptamine portion of the substrate (**Figure 5**).

The nucleotide portion of the molecule shows reasonable overlap with previously determined product complexes through the 5' carbon, with an RMSD of 0.6 Å for those atoms. A small shift likely result from the longer bonds required to accommodate the sulfur atom that replaces the 5' oxygen. This shift does not alter hydrogen bonding and puckering of the ribose sugar, (standard 2'-*endo* pucker). (**Figure 4B**)

In the covalent **E*** complex, one phosphoryl oxygen is hydrogen bonded to the backbone NH atoms of Ser107 and Val108, as well as the side chain of Ser107, while the other is hydrogen bonded to the side chains of Asn99 and His114.

Figure 5. Omit map (mF_o-DF_c) stereo views of ligand density, contoured at 3σ. (B) The **E*** complex, 5IPD. (C) The **EP^2** complex, 5IPE.

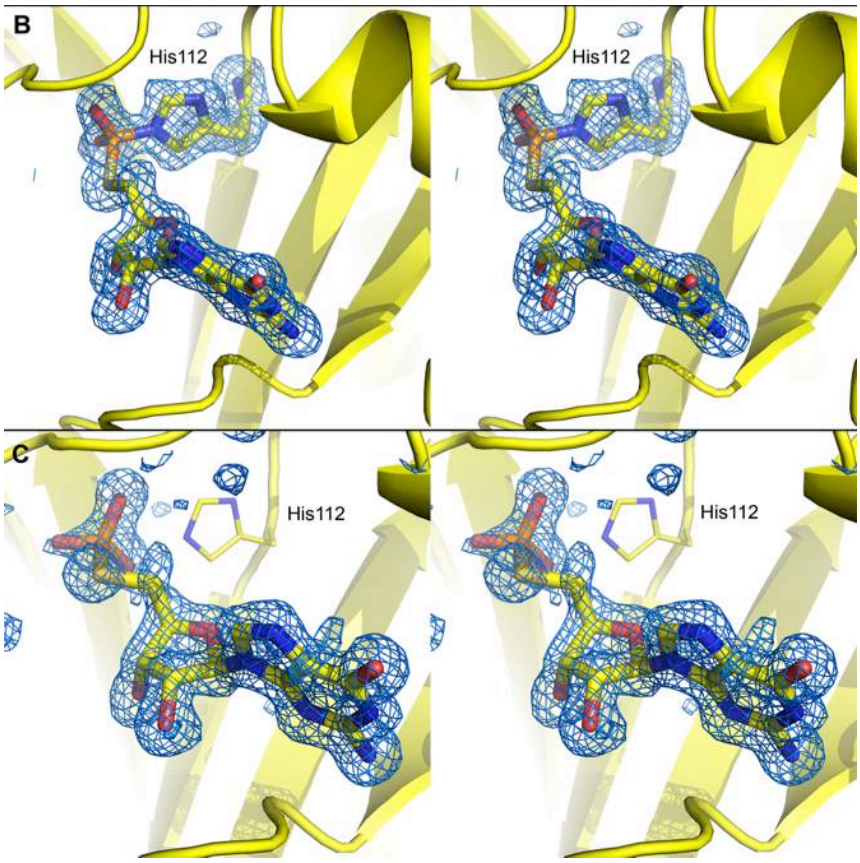

Enzymes that perform similar hydrolytic reactions involving a covalently modified histidine have significantly different active site compositions. Comparing these enzymes to hHint1 reveals a number of differentiating factors that may impact details of catalysis. In the phospholipase D and histidine phosphatase families, the positively charged covalent histidine-intermediate is usually stabilized by ion pairing to a nearby acidic residue.[24, 25] Maintenance of the protonated state of the nucleophilic histidine is necessary to facilitate the hydrolytic step of the reaction. In other family members, such as *E. coli* phosphoglycerate mutase, the covalently modified and positively charged histidine is only stabilized by hydrogen bonding to a carbonyl; consequently lower stability may explain the low crystallographic occupancy of the covalent intermediate in reported crystal structures.[25, 26] In hHint1, this stabilization is achieved by hydrogen bonding to the carbonyl of His110.

For the hydrolytic step in related enzymes, water is often activated for attack by a nearby histidine with assistance from an aspartic acid (PLD and Tpd1), or by an acidic residue alone (PAP and fructose-2,6-biphosphatase).[27, 28] However, there are no nearby acidic residues in hHint1 to perform this function. Therefore, we propose that water serves as the nucleophile and is deprotonated by a phosphoryl oxygen. The step is partially rate-limiting, likely due to the poor nucleophilicity of water. There are no crystallographic waters that are positioned to perform a nucleophilic attack in the **E*** structure. The electrophilicity of the phosphorus center may be enhanced by strong interactions between the phosphoryl oxygens and nearby hydrogen bond donors: Asn 99 ND2 (2.8 Å), Gly105 N (2.5 Å) Ser107 sidechain (3.4 Å), Val108 N (3.1 Å), and His114 NE2 (3.0 Å) (**Figure 7**, left). Collapse of the second pentacoordinate transition state

would thus yield a neutral His112 and neutral AMP molecule. Of the HIT family members that have been structurally characterized, only Galactose-1-phosphate uridyltransferase (GalT) has been previously captured in the **E*** state. In GalT, the usual HIT family motif (H-*X*-H-*X*-H-*X*-*X*) has been replaced with (H-*X*-H-*X*-**Q**-*X*-*X*).[29] The function of this enzyme is to transfer a UMP molecule from UDP-glucose to galactose-1-phosphate. Since it acts as a transferase rather than a hydrolase, the **E*** state must be significantly more stable than in hHint1, to ensure that the uridylated histidine is available during substrate exchange. Indeed, a similar **E*** complex of the *E. coli* GalT enzyme was prepared and described in 1996 by Wedekind *et al*., by soaking crystals in 5 mM UDP-glucose, the native substrate, for two or more hours at 4 °C (PDB ID 1HXQ).[29] The **E*** complex formed but did not undergo hydrolysis during this extended incubation time. Given our proposed mechanism, the GalT intermediate could be hydrolyzed by the same water nucleophile. However, hydrogen bonding surrounding the phosphate in the GalT **E*** intermediate complex is significantly poorer than that observed in hHint1 (**Figure 7**, right). Consequently, the electrophilicity and reactivity of the intermediate phosphorous is significantly reduced, thus allowing direct observation of the E* state in GalT; the comparable state in hHint1 catalysis could only be trapped using a substrate engineered for slow turnover.

Figure 6: The small structural change necessary to accommodate ligand binding. In apo structures such as 1KPA (white), the sidechain of Ser107 is in the phosphate pocket. When any type of ligand is observed to bind, such as AMP in 3TW2 (gray), Ser107 and the surrounding backbone moves to allow it.

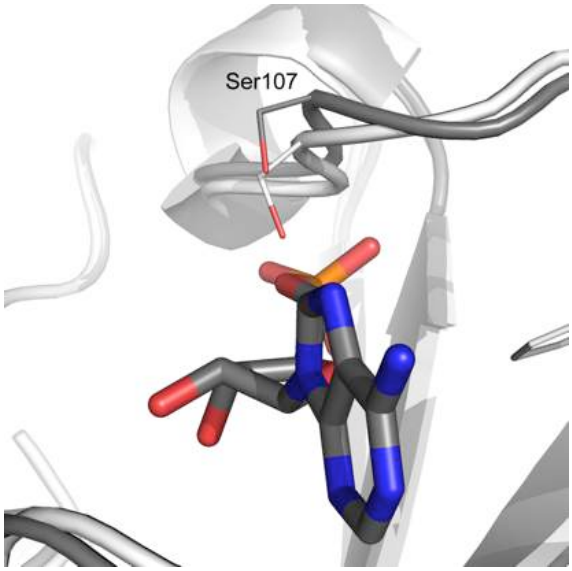

Figure 7. Comparison of hHint1 and GalT **E*** active site configurations. The hHint1 active site (5IPD) has a hydrogen bonding sphere that increases the electrophilicity of the phosphorus (left). In the GalT active site (1HXP), the analogous interactions are longer, and only one significant hydrogen bond to the intermediate is made (right).

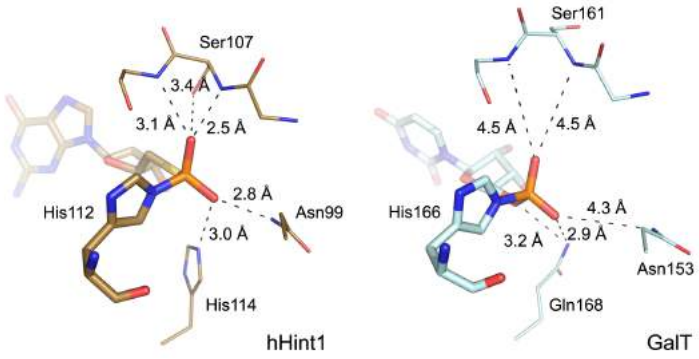

Hint1-Product Complex (EP^2).

Structure 5IPE, the 1.45 Å resolution product $\mathbf{EP^2}$ complex, was achieved by soaking the substrate **3** (5.5 mM) into a crystal at room temperature for 45 minutes (**Figure 5C**). There is no density in this structure to indicate a phosphorus-nitrogen bond, either to the tryptamine nitrogen or His112. Therefore, this structure represents a fully hydrolyzed $\mathbf{EP^2}$ complex.

This structure is largely indistinguishable from other product complexes in the literature, with an RMSD of 0.3 Å to the AMP in 3TW2 (**Figure 4C**). Minor differences are attributable to the sulfur substitution which must accommodate a more acute P-S-C5' angle (107°) compared to the same angle in AMP (120°). The hydrogen bond network is largely preserved from the covalent **E*** complex, though the phosphorus-His112 covalent bond in the **E*** complex is replaced by a phosphoryl oxygen-His112 hydrogen bond in the $\mathbf{EP^2}$ complex.

Catalytic turnover of **3** is not observed during our time-dependent crystallographic experiments with the wild-type enzyme. This is consistent with the understanding of catalysis reached from detailed analysis of enzyme kinetics, where final product release is shown to be partially rate limiting, and a partially rate-limiting conformational change has been proposed to accompany nucleotide ($\mathbf{P^2}$) release.[21] In our crystallographic experiment, evidence for turnover would be the presence of overlapping species in the $\mathbf{EP^2}$ complex density, as new $\mathbf{S^1}$ substrate would diffuse into the recycled active site. However, density for only the $\mathbf{P^2}$ product is observed. We speculate that the observed conformational change to recycle the active site may be inhibited by crystal packing. There is only one small structural change that consistently distinguishes **E** state structures

such as 1KPA[18] from ligand-bound structures; the backbone surrounding Ser107, which overlies the phosphate binding area, shifts by about 1 Å to accommodate any bound nucleotide-type ligand (**Figure 6**). Nevertheless, the nature of any structural change required for product release will require further investigation. Complementary techniques to investigate protein dynamics such as NMR spectroscopy may provide an insight into the nature of the conformational change accompanied during the product release step.

Solvent Kinetic Isotope Studies

Phosphoramidate hydrolysis formally requires the transfer of a proton to the leaving primary amine group and hydrolysis of the intermediate via water in the catalytic cycle of hHint1 (**Figure 1B**). To probe the role of proton transfer in hHint1 catalysis, we carried out solvent kinetic isotope effect studies. The Solvent Kinetic Isotope Effect (SKIE), expressed as the ratio of rate constants when protons from H_2O are replaced with deuterium from D_2O, will be pronounced when the rate limiting reaction step involves proton transfer. We evaluated solvent kinetic isotope effects on the overall rate of Hint1 reaction (k_{cat}) over the accessible pH (or pD) range of 6-9 using steady-state kinetics.

For rate studies, **1** was used as the substrate (**Figure 2**); $^{H/D}k_{cat}$ values of 4.0 and 2.7 were obtained at pD 6.6 and pD 8, respectively (**Table 2**). The pD dependence on k_{cat} showed an intrinsic SKIE of 2.1 (**Figure 8**). To determine whether the SKIE of 2.1 could result from a higher relative viscosity of D_2O (η^{rel} = 1.24) compared to H_2O (η^{rel} = 1), control assays were conducted in HEPES buffer containing varying amounts of sucrose (0, 14, 24, or 32%) (data not shown). Since the k_{cat} decreases by 1.13 fold in buffer with a viscosity of equal to 100% D_2O correction.

Table 2. Proton inventory experiments of pre-steady state WT hint1 and H114A adenylation rate measured using **1** at pL 6.6 and 8.0.

Protein	H_2O	D_2O	Solvent isotope effect
	k_2 (s^{-1})	k_2 (s^{-1})	$^{H/D}k_2$
wild type (pL 6.6)	470 ± 20	226 ± 3	2.1± 0.1
H114A (pL 6.6)	479 ± 30	480 ± 20	1.0 ± 0.1
wild type (pL 8.0)	587 ± 10	519 ± 18	1.0 ± 0.1
H114A (pL 8.0)	183 ± 4	190 ± 3	1.0 ± 0.03

Figure 8. Solvent kinetic isotope effect studies and comparison of pH (▲, **1**) dependence and pD (Δ, **1**) dependence of steady state kinetic parameters (k_{cat}). The pH profile data were fit by eq 5 yielding pK_1= 6.68 ± 0.09, pK_2= 8.03 ± 0.16, r = 0.72 ± 0.11, $(k_2)_{lim}$ = 673 ± 50 s^{-1}, while the pD profile data yield pK_1 = 7.53 ± 0.18, pK_2 = 8.15 ± 0.10, r = 7.35 ± 2.05, q = 1.68 ± 0.16, $(k_2)_{lim}$= 416 ± 14 s^{-1}, thus the intrinsic solvent isotope effect is $^{H/D}(k_2)_{lim}$ = 1.85.

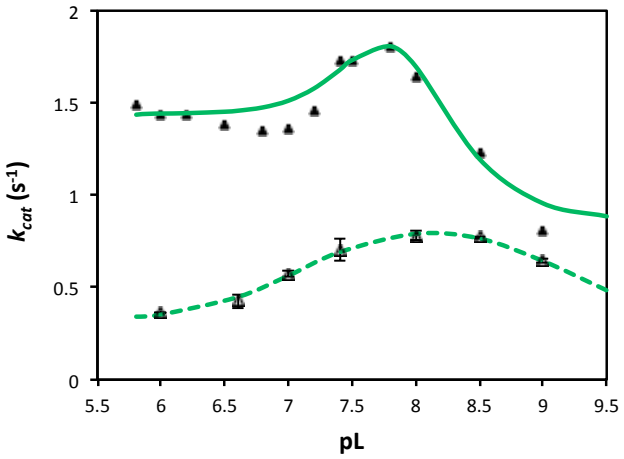

of the SKIE for the viscosity effect gave a corrected SKIE of 1.85 (calculated by 2.1/1.13=1.85). These SKIE results indicate that proton transfer occurs during the catalysis by hHint1.

Proton Inventory Studies

The solvent kinetic isotope effect may originate from proton transfer involved in the rate-limiting step. To elucidate how many protons are "in flight" at each of the step, proton inventory experiments were conducted by determining rates of reaction in buffers with different mole fractions of D_2O and H_2O. A linear change in reaction rate with the mole fraction of D_2O indicates a single proton transfer event. We began by investigating the role of proton transfer during the first step in the catalysis by examining the rate of adenylation (k_2) using stop flow experiments. Adenylation in the wild-type enzyme was found to be linearly dependent on the atom fraction of D_2O (n) (**Figure 9A and B**). The plots were fit into a simplified Gross-Butler equation, with the isotopic fractionation factor for the transition state proton being 0.42 for **1** ($SKIE_{app}$ = 2.1) at pL 6.6 and 0.88 for **1** ($SKIE_{app}$ = 1.1) at pL 8.0 (**Table 2**). Thus, one proton is apparently transferred during the adenylation step.

Based on the crystallographic evidence in this study, His114 forms a hydrogen bond (distance 2.8 Å) with one of the phosphate oxygens in both the hHint1 H112N-substrate and nucleotidylated intermediate complexes. Protonation of His114 at ND1 might allow a protonated NE2 to transfer a proton to the primary amine leaving group as the ND1H tautomer of the histidine is adopted. To test this hypothesis, we performed

comparable the proton inventory studies with a hHint1 enzyme with His114 mutated to alanine (H114A).[21] The adenylation rate, k_2, for the H114A mutant remained unchanged with deuterium fraction at both pL values (**Figure 9A and B**, **Table 2**). This data suggests that His114 is not involved in proton transfer during the adenylation step.

Next, we performed proton inventory studies under steady state kinetic conditions with wild type hHint1. We observed that the k_{cat} decreased proportionally relative to the atom fraction of deuterium water (n). The fractionation factor for the transition state proton was 0.21 and 0.34 for compound **1** ($SKIE_{app}$ = 4.0) (**Figure 9C and D** and **Table 3**). This indicates that there is a transfer of a single proton that is involved in the rate-limiting steps, which includes including the chemical hydrolysis and possible

Figure 9. Proton inventory experiments of pre-steady state enzyme adenylation at pL 6.6. (A) and pL 8.0 (B). The enzyme adenylation rate constants (k_2) were obtained by fitting the data to eq **1 and 2**. ${}^{0}k_2$ represents the k_2 in 0 mole fraction D_2O, and ${}^{n}k_2$ represents the k_2 in n mole fraction D_2O. According to eq **4,** the normal solvent isotope effect for WT hH1 catalyzed **1** hydrolysis (Δ) hydrolysis fit best to a line with a slope of -0.58 (R^2= 0.97, **1**) at pL 6.6 (A), -0.12 (R^2= 0.99, **1**) at pL 8.0 (B). Assays were also conducted on H114A catalyzed **1** hydrolysis reactions at both pLs (×). No SKIE on the rates of H114A adenylation was observed**.** Proton inventory experiments on steady state enzyme kinetics at pL 6.6 (C) and pL 8.0 (D). Under saturated concentration of substrates, the rate constants (k_{cat}) were obtained by fitting the data to eq 3. ${}^{0}k_{cat}$ represents the k_{cat} in 0 mole fraction D_2O, and nkcat represents the kcat in n mole fraction D_2O. According to eq 4, the normal solvent isotope effect for WT hH1 catalyzed **1**

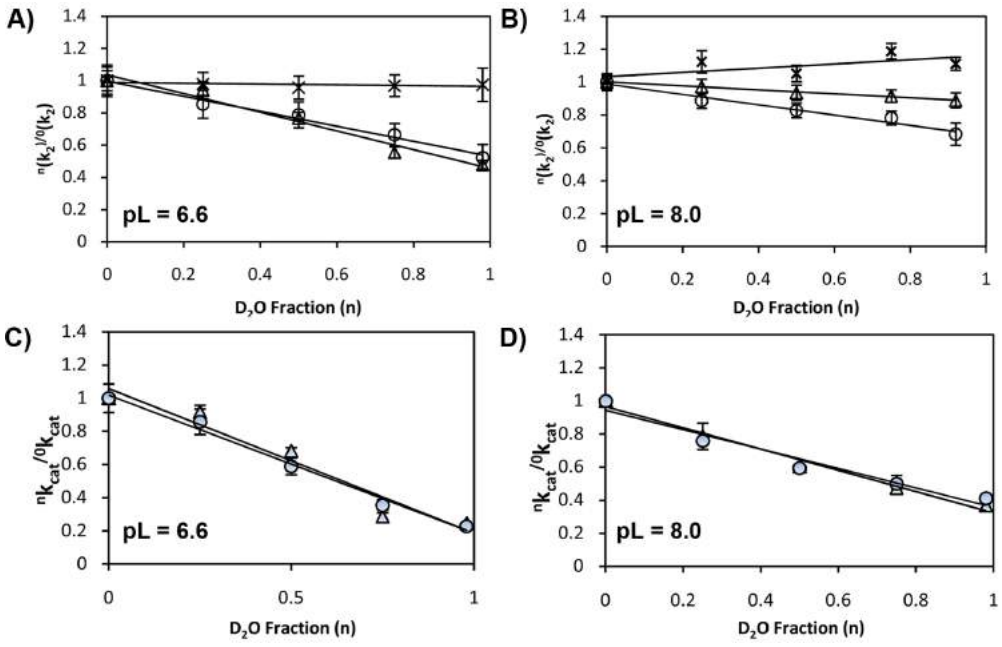

Table 3. Proton inventory experiments of steady state wild-type hHint1 turn over rate measured using **1** at pL 6.6 and 8.0**.** Values are reported from triplicate measurements as mean ± S.D.

Protein	H_2O	D_2O	Solvent isotope effect
	k_{cat} (s^{-1})	k_{cat} (s^{-1})	$^{H/D}k_{cat}$
wild-type (pL 6.6)	1.7 ± 0.04	0.42 ± 0.002	4.4 ± 0.57
wild-type (pL 8.0)	1.7 ± 0.02	0.64 ± 0.02	2.7 ± 0.07

Figure 10. Water binding in the hHint1 active site. (Left) Three water molecules, **W1**, **W2**, and **W3**, are bound behind the phosphoramidate (5IPC, teal) or sulfamate (5I2E, magenta) portion of the ligand. They also appear in the apo structure (1KPA, white) (Center) The same three water molecules are bound identically in the E* state (5IPD, tan), overlaid with the apo structure (white). (Right) An additional water molecule, **W4**, is found in product complexes 5IPE (purple) and 3TW2 (gray) changing the hydrogen bonding patterns, overlaid with the apo structure (white).

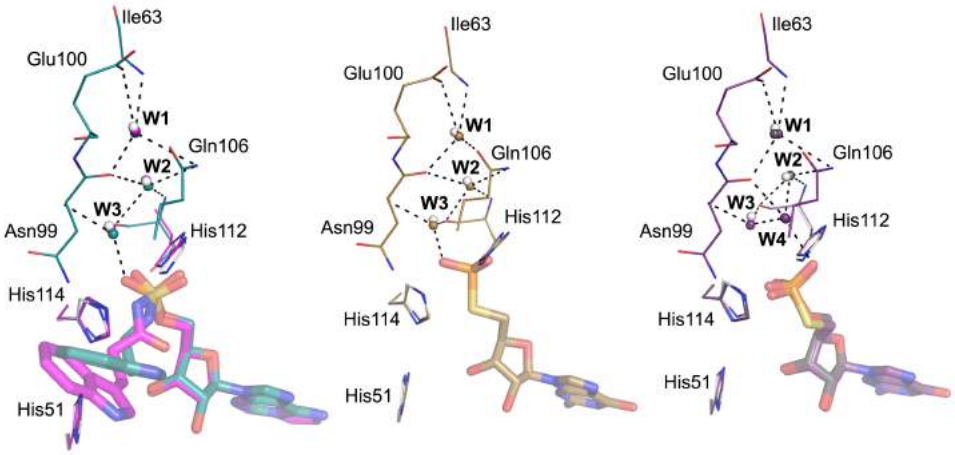

conformational changes associated with product release.

Role of structural waters

Our biochemical results above clearly indicate the transfer of two protons during the catalytic mechanism of hHint1. In addition, the transfer is not dependent on H114 protonation, consistent with the observed protonation state of NE1 and its hydrogen bonding to the phosphoryl oxygen atom in the X-ray crystal structures. This raises an alternative possibility of the transfer of the proton via a Grothuss mechanism, whereby protons move rapidly in an aqueous environment. Such a mechanism is easily facilitated in cases where an acceptor and a donor site are connected via ordered water molecules.[30] Conventional diffusion would be extremely slow because of reliance on a concentration gradient and the aqueous neutral solution contains a low concentration of protons ($\sim 10^{-7}$ M).

Upon close inspection of the x-ray crystal structure of hHint1, we identified a string of three structural waters that are well ordered and strongly hydrogen bonded (**Figure 10**, left). These water molecules are highly coordinated and are buried within the core of the protein, forming a chain of hydrogen bonds between the active site and residues on the opposite side of the protein. Water **W1** participates in four strong hydrogen bonds to the backbone amine of Ile63 (2.9 Å), the Gln106 sidechain amine (2.8 Å), Water **W2** (3.0 Å) and the backbone carbonyl of Asn99 (3.2 Å). Water **W2** participates in three strong hydrogen bonds to the backbone amine of His112 (3.1 Å), Water **W1** (3.0 Å) and Water **W3** (2.9 Å). Water **W3** participates in four hydrogen bonds

to the backbone amine of Asn99 (2.8 Å), Water **2** (2.9 Å), the backbone carbonyl of His112 (2.7 Å) and the phosphoryl oxygen (2.9 Å) of the substrate, intermediate and product. In addition, other weaker hydrogen bonds (3.4-3.9 Å) can be found to each of the channel waters. Thus, regardless of substrate or product occupancy or the presence of the intermediate, each of the conserved waters in the water channel participates in multiple hydrogen bonds. (**Figure 10**, left and center panels).

In the hHint1 product complexes (3TW2, 5IPE), an additional water (**W4**) is present in the active site, presumably to help disperse the charge of the nucleoside monophosphate. When present, both water **W2** and water **W3** donate a hydrogen bond to water **W4** (3.0 and 2.8 Å, respectively), and water **W4** donates hydrogen bonds to His112 CO (2.8 Å) and a phosphoryl oxygen (2.9 Å) (**Figure 10**, right). The appearance of water **W4** in the product complexes has led us to speculate that the conformational change required for product release may correspond to the reorganization of this ordered solvent structure.

Such a chain of waters could potentially serve as a 'proton wire' to transfer a proton through the enzyme, as has been proposed for proteins such as bacteriorhodopsin[31], carbonic anhydrase[32], and green fluorescent protein[33]. There are a small number of evolutionary differences among human HIT family members, which may have had an impact on the proton wire mechanism. In human Fhit, (5FIT), the three water molecules are conserved, while in human DcpS (3BL9)[34], there does not appear to be a solvent-connected end of the wire opposite the active site. However in human aprataxin (4NDH)[35] and human GalT (5IN3), the channel is completely solvent-exposed, which may facilitate its function. It is also possible that the water channel in hHint1

might act as a lubricant, easing rearrangements of the peptide amide-carbonyl hydrogen bonding network that participate in conformational dynamics and ligand molecular recognition. Such dynamic changes might not be easily captured by x-crystallography.

Discussion

The thiophosphroamidate GMP (**3**) has the optimal geometry and resistance to hydrolysis required to make it an effective surrogate for investigating the hHint1 catalyzed hydrolysis of nucleotide phosphoramidates. The three snapshots of the hHint1 catalytic cycle achieved using **3** provide valuable insight into this pharmaceutically relevant enzyme. In order to capture different intermediates along the reaction trajectory, the compounds were soaked into *apo* protein crystals, which were then flash-frozen and characterized using x-ray crystallography.

The crystal structures that capture states in the catalytic cycle of hHint1 are consistent with the kinetic mechanism proposed by Zhou et al.[21] The mechanism employed by hHint1, and by extension, other Hint enzymes, is unique among phospho-histidine enzymes given the paucity of charged residues in the active site. In enzymes of similar nature in the PLD and histidine phosphatase families, charged residues perform critical roles: binding to poly-charged substrates (i.e. DNA, IP_6, fructose-2,6-bisphosphate), stabilizing the covalent adduct, serving as a proton donor, and activating water.[24, 25, 28, 36-39] In hHint1, the only potentially charged residue, His114, does not appear to be charged during the catalytic cycle. In addition, little or no evidence of immediate water availability for the hydrolysis of the nucleotidylated intermediate was observed by x-ray crystallographic analysis. Our structural studies, SKIE and proton inventory

experiments suggest that transfer of one proton is associated with each the adenylation of hHint1 and the rate-limiting intermediate hydrolysis step. Despite the presence of a potential proton-donating residue, His114, in the active site, proton transfer during the catalytic steps appears to be mediated by a highly conserved water channel. How this channel facilitates proton transfers during attack of the His112 nucleophile to form the intermediate or during water attack during intermediate hydrolysis is not clear.

The application of NMR structural experiments coupled with biochemical mutagenesis and computational studies could shed light on the driving forces governing formation and hydrolysis of the nucleotidylated hHint1 intermediate, as well as the impact of the structure of nucleoside phosphoramidates on hHint1 substrate specificity.

Materials and Methods

Synthesis

Installation of a 5'-sulfur onto guanosine first involves *in situ* thiophosphorylation of tryptamine using thiophosphoryl chloride ($SPCl_3$) under basic aqueous conditions to generate tryptamine thiophosphoramidate.[23] This step is relatively fast and the reaction can be easily monitored using phosphorus NMR. Addition of the 5'-iodo guanosine to the reaction mixture then resulted in nucleophilic displacement by the sulfur with the final desired compound obtained in 30% yield. The details on the synthetic procedures are available in the supplemental information. (**Scheme 1**)

Synthetic Procedure for the Preparation of 3

Synthesis of 5'-Deoxy-5'-Iodo-Guanosine (5):

To a stirred solution of guanosine hydrate (**4**, 0.75 g, 2.5 mmol), triphenyl phosphine (2.16 g, 8.25 mmol), and imidazole (1.13, 16.5 mmol) in N-methyl-2-pyrrolidinone (10 ml), iodine was added (2.01 g, 7.9 mmol) over a period of 5 minutes. The reaction mixture warmed up during the addition and was stirred for 3 hours at room temperature. After 3 hours, the solution was diluted with dichloromethane (100 ml) and water (30 ml). A white solid precipitated from the solution and was collected by filtration to obtain 0.6 g (61 %) of the desired product. The ^{1}H NMR spectrum was (DMSO-d_6): 3.47 (m, 1H), 3.56 (m, 1H), 3.95 (m, 1H), 4.07 (m, 1H), 4.64 (m, 1H), 5.40 (d, 1H), 5.53 (d, 1H), 5.72 (d, 1H), 6.49 (s, 2H), 7.93 (s, 1H) and 10.66 (s, 1H). ^{13}C- DMSO-d_6: 156.73, 153.69, 151.43, 135.85, 116.74, 86.56, 83.75, 73.10, 72.68 and 8.03 ppm. Low resolution ESI-

MS [M+H] 393.9, HRMS (ESI+) calcd for $C_{10}H_{13}IN_5O_4$ [$(M+H)^+$] 394.0012 found 394.0016

General Synthesis of nucleoside thiophosphoramidate:

Alkyl or aryl amine (1eq, 0.68 mmol) was added to a solution of 1M NaOH (5 eq, 3.4 mmol) and water (0.45 ml) in a round bottom flask and stirred for 20 minutes. A solution of thiophosphoryl chloride (1 eq, 0.68 mmol) dissolved in dry THF (2ml) was added dropwise to the reaction mixture over the period of 10 minutes. Aliquots of the reaction mixture were withdrawn to monitor the formation of thiophosphoramidate using ^{32}P-NMR. The reaction was completed within 20-40 minutes, after which a portion of 5'-Iodo nucleoside was added (1.5 eqiv, 1.02 mmol) to the reaction mixture and heated at 50°C overnight. After 3 hours, another half eqiv of the 5'-Iodo nucleoside was added and the reaction mixture was monitored using ^{32}P-NMR. The next day, the reaction mixture was neutralized using 1N HCl and lyophilized. The crude reaction mixture was passed through cation exchange resin to remove of excess tryptamine, salts and sodium ions. The eluent from the cation ion exchange column was again lyophilized and purified using reverse phase chromatography. All the nucleoside thiophosphoramidates were finally purified using reverse phase chromatography.

Synthesis of 5'-Deoxy-5'-S-Guanosine Tryptamine thiophosphoramidate (3):

The compound was prepared using the general procedure described above.

The final product was obtained in 30 % yield. The ^{1}H NMR spectrum was (DMSO-d_6): 2.82 (m, 4H), 3.02 (m, 3H), 3.62 (m, 1H), 3.99 (m, 1H), 4.41 (m, 1.0), 4.48 (m, 1H), 5.15 (d, 1H), 5.65 (d, 1H), 6.96 (t, 1H), 7.03 (t, 1H), 7.13 (s, 1H), 7.31 (d, 1H), 7.53 (m, 1H),

7.87 (s, 1H) 10.64 (s, 1H) and 10.76 (s, 1H). ^{32}P- DMSO-d_6: 17.24, ^{13}C- DMSO-d_6: 157.31, 154.35, 136.41, 127.84, 122.87, 121.20, 118.89, 118.50, 117.37, 113.18, 111.71, 88.31, 84.53, 74.73, 72.15, 45.90, 43.27, 32.40, 28.04 and 27.98 ppm. Low resolution LC_ESI-MS [M+H] 522.2, [M-H] 520.1 HRMS calcd for $C_{20}H_{23}N_7O_6PS$ [(M-H)] 520.1174 found 520.1145

General Kinetic Methods.

Human Hint1 kinetics were monitored using phosphorus NMR and was performed in buffer (20 mM Tris, 200 mM NaCl and 1mM $MgCl_2$ at pH 7.4). All the buffer reagents were purchased from Sigma Aldrich unless otherwise stated. All NMR chemical shifts were recorded in δ parts per million using d_6-DMSO (Sigma- cat no: 570672) as internal reference. Fluorescence measurement studies were performed using Varian Cary Eclipse fluorescence spectrophotometer.

Protein purification.

The H114A mutant was prepared and purified from the plasmid as described previously.[23] The wild type hHint1 protein was expressed in the similar fashion. The constructs in a pMCSG7[25] vector (N-terminal, TEV-cleavable His_6-tag) were grown Rosetta2 pLysS cells in TB media using ampicillin (100 μg/mL, GoldBio) and chloramphenicol (30 μg/mL, Fisher Scientific) at 37 °C and shaking at 270 rpm until OD_{600} = 1.0, when they where induced to an IPTG (TekNOVA) concentration of 1 mM. The cultures were incubated at 18 °C overnight with shaking at 270 rpm. The cultures were harvested by centrifugation at 5,000 x *g*, and the cell pellets were resuspended in

Buffer A (50 mM HEPES (Sigma), 300 mM NaCl (Macron Fine Chemicals), 10% glycerol (Fisher Scientific), 0.5 mM TCEP (Thermo Scientific), 10 mM imidazole (Sigma), pH 7.0), adjusted to 1 mM $MgCl_2$ (EMD) and 1 mg/mL lysozyme (bioPLUS). Benzonase nuclease (1.5-2 μL, Sigma) was added. The cells were lysed by sonication (8-16 x (30 s on, 30 s off)), and cell debris was removed by centrifugation at 40,000 x *g* for 45 minutes. The lysate was clarified by syringe filtration (0.45 μm, Merk Millipore Ltd.) and applied to 2 x 5 mL GE HisTrapFF columns. The protein was eluted with an imidazole gradient to Buffer B (50 mM HEPES, 300 mM NaCl, 10% glycerol, 0.5 mM TCEP, pH 7.0).

The His_6 tag was cleaved with TEV protease, used at 2% (m/m) during an overnight dialysis step at 4 °C against TEV cleavage buffer (50 mM HEPES, 300 mM NaCl, 5% glycerol, 0.5 mM TCEP, pH 7.0). The cleaved protein mixture was reapplied to the nickel column, and the flow-through portion was collected. The flow-through fractions were concentrated to approximately 5 mL and applied to a HiPrep 16/60 Sephacryl S-100 HR column using SEC buffer (20 mM Tris (Fluka), 300 mM NaCl, 5% glycerol, pH 7.0). The pure fractions were pooled. In the wild type preparation, these fractions were concentrated to A_{280} = 10, aliquoted and frozen without further treatment.

Structural Biology.

Crystals of wild-type hHint1 was prepared using hanging-drop vapor diffusion at 20 °C. For wild-type crystals, drops were set up consisting of 2 uL of protein (A_{280} = 5) and 2 uL of well solution (1 M MES (Sigma) pH 6.1-6.4, PEG 8K (Acros Organics) 34-39%). For H112N crystals, drops consisted of 2 uL of protein (A_{280} = 3) and 2 uL of well

solution (1 M MES pH 6.5, 37% PEG 8K). The details on the soaking and crystallization conditions of each structure are described in detail in the supplemental information.

Data for structures 5IPB, 5IPC, and 5IPD, were collected at APS beamline 17-ID-B (IMCA-CAT) of Argonne National Labs equipped with a Dectris Pilatus 6M Pixel Array Detector. The data were processed using AutoPROC.[40] Data for structure 5IPE were collected at ALS Beamline 4.2.2 of Lawrence Livermore National Labs and were processed using XDS.[41]

The structures were solved using Phaser[42] and the coordinates from structure 3TW2.[17] The structures were refined using REFMAC5[43] in the CCP4 suite[44] and Phenix[45], and they were visualized and modified using coot.[46] Ligand restraints were calculated using JLigand or elbow.[47, 48] Data processing and refinement statistics are available in **Supplemental Table 2**.

Crystal packing does noticeably impact substrate binding in these crystals; we observe substrate binding and catalysis in only one of the two, seemingly equivalent monomers of the hHint1 homodimer, a fact attributed to crystal packing. In this monoclinic (C2) crystal form, the active site of the B chain is partially occupied by the β1-β2 loop of the B chain of a symmetry mate, thus precluding binding in that site.

Structures that are compared have been overlaid using the "HIT-NBD" (Histidine Triad protein-Nucleotide Binding Domain) core substructure overlay method available at https://drugsite.msi.umn.edu/.[49]

Solvent Kinetic Isotope Effect

The solvent isotope effect experiments were conducted in phosphate buffers (100 mM) made of 98% deuterium water at pD 6.6 and 8, where the pD values = pH meter reading + 0.4. The solvent isotope effect was expressed as the ratio of the kinetic parameter in water and in deuterium water (H/D). For solvent isotope effect in pre-steady-state kinetics, the reaction rates of the adenylation of Hint1 were monitored at 25°C using a fluorescence stopped flow apparatus with **1** (5-40 μM) in one syringe and hHint1 (wild-type, 69 μg/ml, 5 μM) in the other syringe, as described previously.[23] The time-course curves were fit by a single exponential equation with a steady-state term (Eq. 1) using JMP IN 7 software, where A is the amplitude of the burst, k_{lin} is the linear rate of increase of fluorescence, and k_b is the burst rate, or the observed pseudo-first-order rate constant.[23] The results represent the average of six experiments. The kinetic parameters $k_2, K_m^{\text{adenylyl}}, k_2/K_m^{\text{adenylyl}}$ for **1** turnover were obtained by non-linear fitting to the data by Eq. 1 and Eq. 2, and [S] is the substrate concentration.

$$P(t) = Ae^{-k_b * t} + k_{lin} \cdot t + C \qquad \text{Eq. 1}$$

$$k_b = \frac{k_2 \times [S]}{K_m^{adenyl} + [S]} \qquad \text{Eq. 2}$$

For solvent isotope effect in steady state kinetics, the steady state fluorescence assay was performed at 25°C using Varian/Cary Eclipse Fluorimeter as described previously.[23] The initial velocity of hydrolysis was measured with hHint1 or H114A mutant (6 nM - 50 nM) and varied concentrations of **1** (0-10 μM). The curves were fit to Eq. 3 to yield the first order rate constant k_{cat} and apparent Michaelis-Menten constant K_m

using JMP7 software, where v is the initial velocity, $[E]_t$ is the total enzyme concentration, and [S] is the substrate concentration.

$$v = \frac{k_{cat}[E]_t[S]}{K_m + [S]} \qquad \text{Eq. 3}$$

The pH dependence of the pre-steady state parameters were calculated using equation,

$$k_{cat} = \frac{(k_{cat})_{\lim}\left(10^{pKa_1 - pH} + r + q \times 10^{pH - pKa_2}\right)}{10^{pKa_1 - pH} + 1 + 10^{pH - pKa_2}} \qquad \text{Eq. 5}$$

Proton Inventory Studies

Proton inventory studies were performed for both pre-steady state and steady state kinetic studies. Phosphate buffers for the proton inventory studies with different deuterium atom fractions n were prepared gravimetrically by mixing appropriate quantities of buffers made up in H_2O and D_2O. The pD was adjusted according to pD = pH meter reading + 0.4. For pre-steady state kinetics using a stopped-flow instrument, the final concentration of enzyme was 2.5 μM and final concentrations of **1** (5-60 μM). The results represent the average of six experiments. In each H_2O-D_2O system, k_2, $K_m^{adenylyl}$, and $k_2/K_m^{adenylyl}$ were calculated. The plot of ${}^nk_2/{}^0k_2$ vs. n was made at pL 8.0, where ${}^nk_2$ represents k_2 rate constant in the n mole fraction of D_2O, ${}^0k_2$ represents k_2 rate constant in H_2O, and n is the solvent mole fraction of D_2O. For steady state experiments, ${}^nk_{cat}/{}^0k_{cat}$ was plotted at pL 6.6 against n, where k_{cat} is the observed first-order rate constant. Proton-inventory data were fit to the simplified Gross-Butler equation for a one-proton-transfer

model (Eq. 7), where j is the fractionation factors of the transition state proton, and it can be calculated from the slope (j-1) of the PI plot.

$${}^{n}k/{}^{0}k = \left(1 - n + \mathrm{n} \times \mathrm{j}\right) \qquad \text{Eq. 4}$$

REFERENCES

1. Brenner, C., Hint, Fhit, and GalT: function, structure, evolution, and mechanism of three branches of the histidine triad superfamily of nucleotide hydrolases and transferases. *Biochemistry* **2002,** *41* (29), 9003-14.
2. Martin, J.; St-Pierre, M. V.; Dufour, J. F., Hit proteins, mitochondria and cancer. *Biochim Biophys Acta* **2011,** *1807* (6), 626-32.
3. Chou, T. F.; Baraniak, J.; Kaczmarek, R.; Zhou, X.; Cheng, J.; Ghosh, B.; Wagner, C. R., Phosphoramidate pronucleotides: a comparison of the phosphoramidase substrate specificity of human and Escherichia coli histidine triad nucleotide binding proteins. *Mol Pharm* **2007,** *4* (2), 208-17.
4. Chou, T. F.; Tikh, I. B.; Horta, B. A.; Ghosh, B.; De Alencastro, R. B.; Wagner, C. R., Engineered monomeric human histidine triad nucleotide-binding protein 1 hydrolyzes fluorogenic acyl-adenylate and lysyl-tRNA synthetase-generated lysyl-adenylate. *J Biol Chem* **2007,** *282* (20), 15137-47.
5. Chou, T. F.; Wagner, C. R., Lysyl-tRNA synthetase-generated lysyl-adenylate is a substrate for histidine triad nucleotide binding proteins. *J Biol Chem* **2007,** *282* (7), 4719-27.
6. Wang, J.; Fang, P.; Schimmel, P.; Guo, M., Side chain independent recognition of aminoacyl adenylates by the Hint1 transcription suppressor. *J Phys Chem B* **2012,** *116* (23), 6798-805.
7. Li, H.; Zhang, Y.; Su, T.; Santella, R. M.; Weinstein, I. B., Hint1 is a haplo-insufficient tumor suppressor in mice. *Oncogene* **2006,** *25* (5), 713-21.
8. Zhang, Y. J.; Li, H.; Wu, H. C.; Shen, J.; Wang, L.; Yu, M. W.; Lee, P. H.; Bernard Weinstein, I.; Santella, R. M., Silencing of Hint1, a novel tumor suppressor gene, by promoter hypermethylation in hepatocellular carcinoma. *Cancer Lett* **2009,** *275* (2), 277-84.
9. Rodríguez-Muñoz, M.; Sánchez-Blázquez, P.; Vicente-Sánchez, A.; Bailón, C.; Martín-Aznar, B.; Garzón, J., The histidine triad nucleotide-binding protein 1 supports mu-opioid receptor-glutamate NMDA receptor cross-regulation. *Cell Mol Life Sci* **2011,** *68* (17), 2933-49.
10. Garzón, J.; Herrero-Labrador, R.; Rodríguez-Muñoz, M.; Shah, R.; Vicente-Sánchez, A.; Wagner, C. R.; Sánchez-Blázquez, P., HINT1 protein: a new therapeutic target to enhance opioid antinociception and block mechanical allodynia. *Neuropharmacology* **2015,** *89*, 412-23.
11. Wagner, C. R.; Iyer, V. V.; McIntee, E. J., Pronucleotides: toward the in vivo delivery of antiviral and anticancer nucleotides. *Med Res Rev* **2000,** *20* (6), 417-51.
12. Galmarini, C. M.; Mackey, J. R.; Dumontet, C., Nucleoside analogues: mechanisms of drug resistance and reversal strategies. *Leukemia* **2001,** *15* (6), 875-90.
13. Wiemer, A. J.; Wiemer, D. F., Prodrugs of phosphonates and phosphates: crossing the membrane barrier. *Top Curr Chem* **2015,** *360*, 115-60.
14. Murakami, E.; Tolstykh, T.; Bao, H.; Niu, C.; Steuer, H. M.; Bao, D.; Chang, W.; Espiritu, C.; Bansal, S.; Lam, A. M.; Otto, M. J.; Sofia, M. J.; Furman, P. A., Mechanism of

activation of PSI-7851 and its diastereoisomer PSI-7977. *J Biol Chem* **2010,** *285* (45), 34337-47.
15. Sofia, M. J.; Bao, D.; Chang, W.; Du, J.; Nagarathnam, D.; Rachakonda, S.; Reddy, P. G.; Ross, B. S.; Wang, P.; Zhang, H. R.; Bansal, S.; Espiritu, C.; Keilman, M.; Lam, A. M.; Steuer, H. M.; Niu, C.; Otto, M. J.; Furman, P. A., Discovery of a β-d-2'-deoxy-2'-α-fluoro-2'-β-C-methyluridine nucleotide prodrug (PSI-7977) for the treatment of hepatitis C virus. *J Med Chem* **2010,** *53* (19), 7202-18.
16. Lima, C. D.; Klein, M. G.; Hendrickson, W. A., Structure-based analysis of catalysis and substrate definition in the HIT protein family. *Science* **1997,** *278* (5336), 286-90.
17. Dolot, R.; Ozga, M.; Włodarczyk, A.; Krakowiak, A.; Nawrot, B., A new crystal form of human histidine triad nucleotide-binding protein 1 (hHINT1) in complex with adenosine 5'-monophosphate at 1.38 Å resolution. *Acta Crystallogr Sect F Struct Biol Cryst Commun* **2012,** *68* (Pt 8), 883-8.
18. Lima, C. D.; Klein, M. G.; Weinstein, I. B.; Hendrickson, W. A., Three-dimensional structure of human protein kinase C interacting protein 1, a member of the HIT family of proteins. *Proc Natl Acad Sci U S A* **1996,** *93* (11), 5357-62.
19. Dolot, R.; Kaczmarek, R.; Sęda, A.; Krakowiak, A.; Baraniak, J.; Nawrot, B., Crystallographic studies of the complex of human HINT1 protein with a non-hydrolyzable analog of Ap4A. *Int J Biol Macromol* **2016,** *87*, 62-9.
20. Shah, R.; Strom, A.; Zhou, A.; Maize, K. M.; Finzel, B. C.; Wagner, C. R., Design, Synthesis, and Characterization of Sulfamide and Sulfamate Nucleotidomimetic Inhibitors of hHint1. *ACS Med Chem Lett* **2016,** *7* (8), 780-4.
21. Zhou, X.; Chou, T. F.; Aubol, B. E.; Park, C. J.; Wolfenden, R.; Adams, J.; Wagner, C. R., Kinetic mechanism of human histidine triad nucleotide binding protein 1. *Biochemistry* **2013,** *52* (20), 3588-600.
22. Attwood, P. V.; Piggott, M. J.; Zu, X. L.; Besant, P. G., Focus on phosphohistidine. *Amino Acids* **2007,** *32* (1), 145-56.
23. Trmčić, M.; Hodgson, D. R., Synthesis of thiophosphoramidates in water: click chemistry for phosphates. *Chem Commun (Camb)* **2011,** *47* (21), 6156-8.
24. Leiros, I.; McSweeney, S.; Hough, E., The reaction mechanism of phospholipase D from Streptomyces sp. strain PMF. Snapshots along the reaction pathway reveal a pentacoordinate reaction intermediate and an unexpected final product. *J Mol Biol* **2004,** *339* (4), 805-20.
25. Davies, D. R.; Interthal, H.; Champoux, J. J.; Hol, W. G., Crystal structure of a transition state mimic for Tdp1 assembled from vanadate, DNA, and a topoisomerase I-derived peptide. *Chem Biol* **2003,** *10* (2), 139-47.
26. Bond, C. S.; White, M. F.; Hunter, W. N., High resolution structure of the phosphohistidine-activated form of Escherichia coli cofactor-dependent phosphoglycerate mutase. *J Biol Chem* **2001,** *276* (5), 3247-53.
27. Sharma, S.; Juffer, A. H., Hydrolysis of phosphohistidine in water and in prostatic acid phosphatase. *Chem Commun (Camb)* **2009,** (42), 6385-7.
28. Yuen, M. H.; Mizuguchi, H.; Lee, Y. H.; Cook, P. F.; Uyeda, K.; Hasemann, C. A., Crystal structure of the H256A mutant of rat testis fructose-6-phosphate,2-

kinase/fructose-2,6-bisphosphatase. Fructose 6-phosphate in the active site leads to mechanisms for both mutant and wild type bisphosphatase activities. *J Biol Chem* **1999,** *274* (4), 2176-84.
29. Wedekind, J. E.; Frey, P. A.; Rayment, I., The structure of nucleotidylated histidine-166 of galactose-1-phosphate uridylyltransferase provides insight into phosphoryl group transfer. *Biochemistry* **1996,** *35* (36), 11560-9.
30. Chaplin, M., Do we underestimate the importance of water in cell biology? *Nat Rev Mol Cell Biol* **2006,** *7* (11), 861-6.
31. Bondar, A. N.; Elstner, M.; Suhai, S.; Smith, J. C.; Fischer, S., Mechanism of primary proton transfer in bacteriorhodopsin. *Structure* **2004,** *12* (7), 1281-8.
32. Riccardi, D.; König, P.; Guo, H.; Cui, Q., Proton transfer in carbonic anhydrase is controlled by electrostatics rather than the orientation of the acceptor. *Biochemistry* **2008,** *47* (8), 2369-78.
33. Agmon, N., Kinetics of switchable proton escape from a proton-wire within green fluorescence protein. *J Phys Chem B* **2007,** *111* (27), 7870-8.
34. Singh, J.; Salcius, M.; Liu, S. W.; Staker, B. L.; Mishra, R.; Thurmond, J.; Michaud, G.; Mattoon, D. R.; Printen, J.; Christensen, J.; Bjornsson, J. M.; Pollok, B. A.; Kiledjian, M.; Stewart, L.; Jarecki, J.; Gurney, M. E., DcpS as a therapeutic target for spinal muscular atrophy. *ACS Chem Biol* **2008,** *3* (11), 711-22.
35. Tumbale, P.; Williams, J. S.; Schellenberg, M. J.; Kunkel, T. A.; Williams, R. S., Aprataxin resolves adenylated RNA-DNA junctions to maintain genome integrity. *Nature* **2014,** *506* (7486), 111-5.
36. DeYonker, N. J.; Webster, C. E., Phosphoryl transfers of the phospholipase D superfamily: a quantum mechanical theoretical study. *J Am Chem Soc* **2013,** *135* (37), 13764-74.
37. DeYonker, N. J.; Webster, C. E., A Theoretical Study of Phosphoryl Transfers of Tyrosyl-DNA Phosphodiesterase I (Tdp1) and the Possibility of a "Dead-End" Phosphohistidine Intermediate. *Biochemistry* **2015,** *54* (27), 4236-47.
38. Sharma, S.; Rauk, A.; Juffer, A. H., A DFT study on the formation of a phosphohistidine intermediate in prostatic acid phosphatase. *J Am Chem Soc* **2008,** *130* (30), 9708-16.
39. Stentz, R.; Osborne, S.; Horn, N.; Li, A. W.; Hautefort, I.; Bongaerts, R.; Rouyer, M.; Bailey, P.; Shears, S. B.; Hemmings, A. M.; Brearley, C. A.; Carding, S. R., A bacterial homolog of a eukaryotic inositol phosphate signaling enzyme mediates cross-kingdom dialog in the mammalian gut. *Cell Rep* **2014,** *6* (4), 646-56.
40. Vonrhein, C.; Flensburg, C.; Keller, P.; Sharff, A.; Smart, O.; Paciorek, W.; Womack, T.; Bricogne, G., Data processing and analysis with the autoPROC toolbox. *Acta Crystallogr D Biol Crystallogr* **2011,** *67* (Pt 4), 293-302.
41. Kabsch, W., XDS. *Acta Crystallogr D Biol Crystallogr* **2010,** *66* (Pt 2), 125-32.
42. McCoy, A. J.; Grosse-Kunstleve, R. W.; Adams, P. D.; Winn, M. D.; Storoni, L. C.; Read, R. J., Phaser crystallographic software. *J Appl Crystallogr* **2007,** *40* (Pt 4), 658-674.
43. Murshudov, G. N.; Skubák, P.; Lebedev, A. A.; Pannu, N. S.; Steiner, R. A.; Nicholls, R. A.; Winn, M. D.; Long, F.; Vagin, A. A., REFMAC5 for the refinement of

macromolecular crystal structures. *Acta Crystallogr D Biol Crystallogr* **2011,** *67* (Pt 4), 355-67.
44. Winn, M. D.; Ballard, C. C.; Cowtan, K. D.; Dodson, E. J.; Emsley, P.; Evans, P. R.; Keegan, R. M.; Krissinel, E. B.; Leslie, A. G.; McCoy, A.; McNicholas, S. J.; Murshudov, G. N.; Pannu, N. S.; Potterton, E. A.; Powell, H. R.; Read, R. J.; Vagin, A.; Wilson, K. S., Overview of the CCP4 suite and current developments. *Acta Crystallogr D Biol Crystallogr* **2011,** *67* (Pt 4), 235-42.
45. Adams, P. D.; Afonine, P. V.; Bunkóczi, G.; Chen, V. B.; Davis, I. W.; Echols, N.; Headd, J. J.; Hung, L. W.; Kapral, G. J.; Grosse-Kunstleve, R. W.; McCoy, A. J.; Moriarty, N. W.; Oeffner, R.; Read, R. J.; Richardson, D. C.; Richardson, J. S.; Terwilliger, T. C.; Zwart, P. H., PHENIX: a comprehensive Python-based system for macromolecular structure solution. *Acta Crystallogr D Biol Crystallogr* **2010,** *66* (Pt 2), 213-21.
46. Emsley, P.; Cowtan, K., Coot: model-building tools for molecular graphics. *Acta Crystallogr D Biol Crystallogr* **2004,** *60* (Pt 12 Pt 1), 2126-32.
47. Lebedev, A. A.; Young, P.; Isupov, M. N.; Moroz, O. V.; Vagin, A. A.; Murshudov, G. N., JLigand: a graphical tool for the CCP4 template-restraint library. *Acta Crystallogr D Biol Crystallogr* **2012,** *68* (Pt 4), 431-40.
48. Moriarty, N. W.; Grosse-Kunstleve, R. W.; Adams, P. D., electronic Ligand Builder and Optimization Workbench (eLBOW): a tool for ligand coordinate and restraint generation. *Acta Crystallogr D Biol Crystallogr* **2009,** *65* (Pt 10), 1074-80.
49. Finzel, B. C.; Akavaram, R.; Ragipindi, A.; Van Voorst, J. R.; Cahn, M.; Davis, M. E.; Pokross, M. E.; Sheriff, S.; Baldwin, E. T., Conserved core substructures in the overlay of protein-ligand complexes. *J Chem Inf Model* **2011,** *51* (8), 1931-41.

Chapter 5

Extended Conformer Driven Small Molecule Switch-on Fluorescent Probes to Study Human Histidine Triad Nucleotide Binding Protein 1 (hHint1)

INTRODUCTION:

Histidine triad nucleotide binding protein 1 (Hint1) has emerged as a key regulator of pain, opioid tolerance and addiction properties in the central nervous system (CNS).[1-3] Hint1 belongs to the histidine triad (HIT) superfamily which are characterized by their conserved nucleotide binding motif, His-X-His-X-His-XX, where X is a hydrophobic residue. hHint1 exists as a homodimer and possesses nucleoside phosphoramidase and acyl-AMP hydrolase activity, with a preference for substrates with purine over pyrimidine nucleosides.[4] The nucleoside phosphoramidase activity of hHint1 has been shown to be necessary for the activation of several preclinical and clinically approved antiviral and anticancer phosphoramidate pronucleotides.[5-8] In addition, Chou and Wagner et al. have demonstrated that lysyl t-RNA synthetase generated lysyl-AMP is a substrate for hHint1 *in vitro*.[9]

Hint1 has been shown to paly a role in modulating in N-methyl-D-aspartate (NMDA) receptors activation.[10] The interaction between Hint1 and NMDA receptor has been proposed to mediate the co-association of NMDAR with several G-protein coupled receptors (GPCRs) *in vivo*, including the μ-opioid receptor (MOR).[11, 12] Consistent with this observation, Hint1$^{-/-}$ mice exhibit an increased morphine analgesic response and sensitivity to amphetamine, while reduced nicotine dependence has been observed in self-administration studies.[1-3] In addition, mutations or aberrant expression of hHint1 is been associated with inherited peripheral neuropathy, schizophrenia and bipolar disorders.[13, 14] Nevertheless, the identity of the endogenous substrate that presumably is participating in these signaling events has yet to be determined.

Based on the results of our substrate specificity analysis of Hint1,[4] we have designed several competitive inhibitors.[15] Neuropharmacological studies with one of these inhibitors, **3** (TrpGc, see Chapter 2), revealed that it enhanced morphine analgesia, blocked the development of tolerance and relieved neuropathic pain in mice.[16] Thus these demonstrate that Hint1 regulates the function of MOR via its interaction with the NMDA receptor.[16] To facilitate interrogation of the molecular mechanisms governing the cellular function of Hint1, a fluorescent probe that switches on when bound to the protein would be a valuable mechanistic tool. In addition, a fluorescent switch on probe of the Hint1 active site would aid in the development of high throughput assays for the screening of potential Hint1 inhibitors.

Currently, there are two classes of small molecule based switch-on fluorescent probes: enzymatic activity-dependent probes and enzymatic activity independent probes.[17] In the later case, generally, a solvatochromic fluorophore is attached to the ligand specific to a target protein of interest. Upon binding to the target of interest, the change in the polarity of the environment results in an increase in the fluorescence intensity of the probe.[18] Unfortunately, these probes exhibit high background fluorescence and hence a low ratio of signal to background fluorescence is observed. Herein we report the first fluorescent reporter ligands for hHint1 with switchable properties guided by the principle used in the design of DNA or aptamer-based molecular beacons.[19] Upon binding to hHint1, these switchable probes undergo a conformational change resulting in the quencher becoming less hybridized with the fluorophore and thus exhibiting and increased fluorescence intensity. In the current work, we demonstrate the

utility of such probes in performing hHint1-ligand dissociation studies and the selective detection of hHint1 *in vitro*.

RESULTS

Design and synthesis of intramolecularly quenched fluorescent nucleotidomimetic probes for hHint1

We envisioned two important criteria for the successful development of fluorescent switch-on probes for hHint1: a) the probe should exhibit selectivity for hHint1 and b) a substantial difference in the fluorescence property of the free and the bound probe. One of the characteristic features of hHint1 is its nucleoside-binding motif, which exhibits a preference for binding purine over pyrimidine nucleoside monophosphates. Hence, we selected the fluorescent non-natural nucleosides, 1, N^6-ethenoadenosine (EtAd, $ex_{\lambda max}$ 278, $em_{\lambda max}$ 410 nm) (**7**) and thG ($ex_{\lambda max}$ 331, $em_{\lambda max}$ 450 nm), (**8**) to incorporate into the design of our fluorescent probes (**Figure 1A**).[20, 21] The selection of EtAd and thG was based on their high quantum yields (Ø = 0.56 for EtAd and Ø = 0.34 for thG) and long fluorescent lifetimes (τ ~ 20-25 ns) in aqueous buffers. The guanosine mimic, thG, has an additional advantage since it's excitation and emission maxima are at higher wavelengths compared to EtAd (**Figure 1B**) To address the second criteria, we decided to incorporate an indolyl group as a fluorescent quencher. A wide variety of chemical moieties can act as a quencher of fluorescence, For example tryptophan is known to induce quenching of certain dyes and fluorophores over relatively short distances via photon-induced electron transfer (PET).[22] Attachment of an indole side chain using a water-soluble acyl-sulfamate linker to the fluorophore nucleoside nearby resulting in quenching of the fluorescence

Figure 1. Non-natural fluorescent nucleosides A) Chemical structures of the fluorescent nucleosides thG (left) and EtAd (right) and B) Absorption (dashed lines) and Emission (solid lines) spectra of the respective nucleosides recorded in an aqueous buffer (20mM Tris, 150 mM NaCl, pH 7.4) at room temperature.

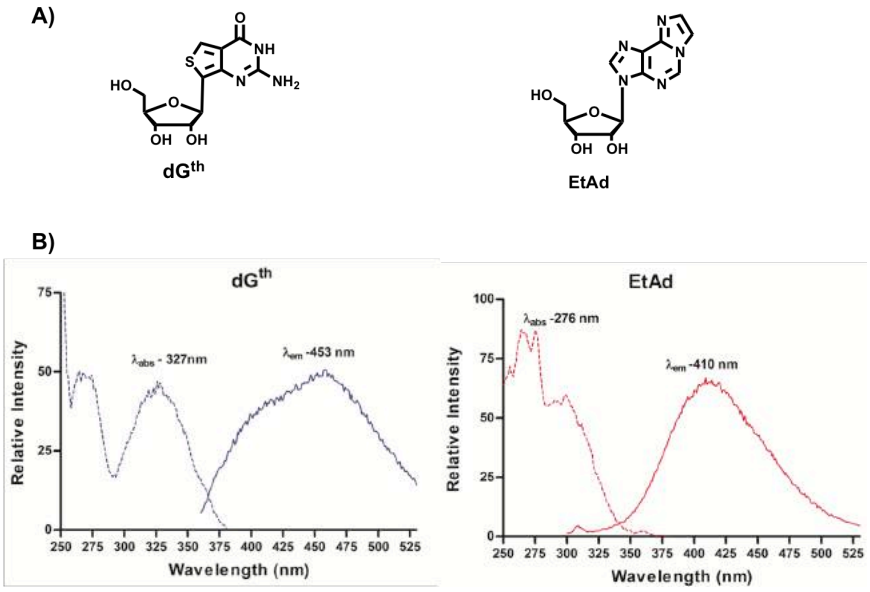

Figure 2. Extended conformer driven switch-on probes A) Concept of the designed intramolecularly quenched probes for hHint1 B) Upon incubation with hHint1, the probe hybridizes with the complementary active site, resulting in the extended conformer and hence regain in the fluorescence C) Chemical structures of the designed intramolecular quenched probes 7 and 8. Circled in red is a quencher (indole ring) and blue is the fluorescent nucleobase.

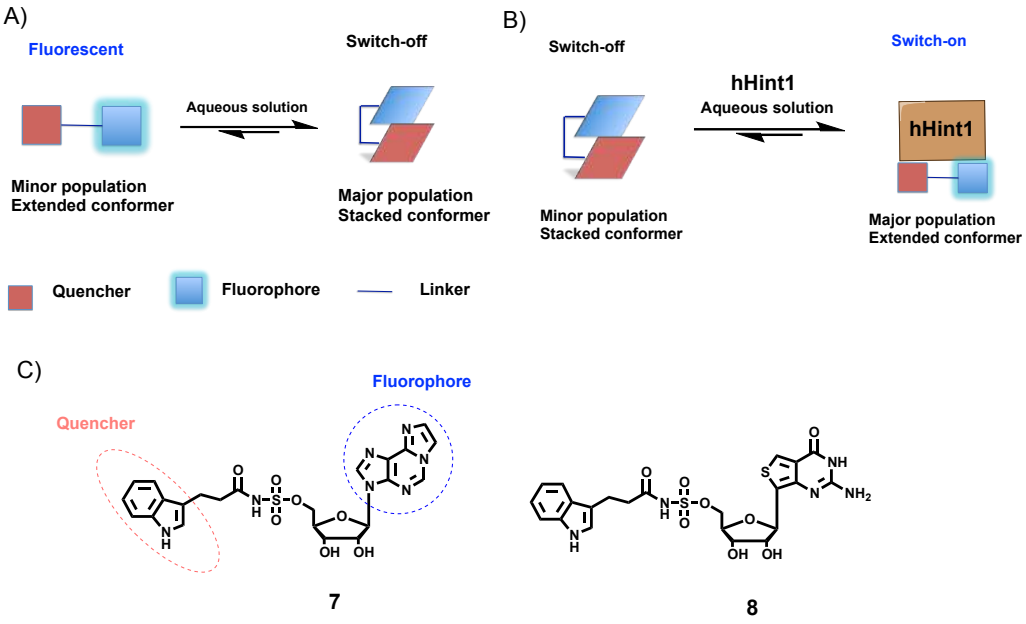

(**Figure 2A**). We therefore chose to prepare and investigate the fluorescence properties of 5'-indole-3-propionic acid ribose 1, N^6-Ethenoadenosine sulfamate (**7**) and 5'-indole-3-propionic acid ribose-2-aminothieno[3,4-d]pyrimidin-4(3H)-one sulfamate **(8**) (**Figure 2C**). Compound **7** has been recently reported as a sub-micromolar (K_d = 0.23 μM) inhibitor of hHint1 and was prepared as previously described.[15] The synthesis of compound **8** began with the preparation of 2-Aminothieno[3,4-d]pyrimidine G mimic nucleoside (thG) as reported by Shin et. al[20] with minor modifications (Method and materials for details). Next, we carried out the acetonide protection of the 2´, 3´- hydroxyl of the ribose sugar of thG, followed by sulfomyla-tion of the 5'-hydroxyl with sulfamoyl chloride to yield **6** (**Scheme 1**). Coupling of **6** with the activated NHS-ester of an indole-3-propionic acid (**22**) in the presence of DBU and subsequent removal of the acetonide group with aqueous TFA generated **8** in 60 % overall yield. When compared to the parent nucleosides, EtAd and thG, the quantum yields of compounds **7** and **8** exhibited a 49- and 19- fold decrease, respectively (**Table 1**).

Both probes exhibit intramolecular static and dynamic quenching of fluorescence in an aqueous solution

The quantum yield of a fluorophore depends on the ratio of the number of photons emitted via a radiative process to the number of photons absorbed upon excitation of an electron. The average time the electron spends in the excited state determines the lifetime of fluorescence. Typically, quenchers act by either reducing the quantum yield or the lifetime of a fluorophore. The mechanism of quenching of fluorescence can by either static or dynamic process. In static quenching, the quencher forms a dark ground-state

Scheme 1: Synthesis of compound 8

Scheme 1[a]

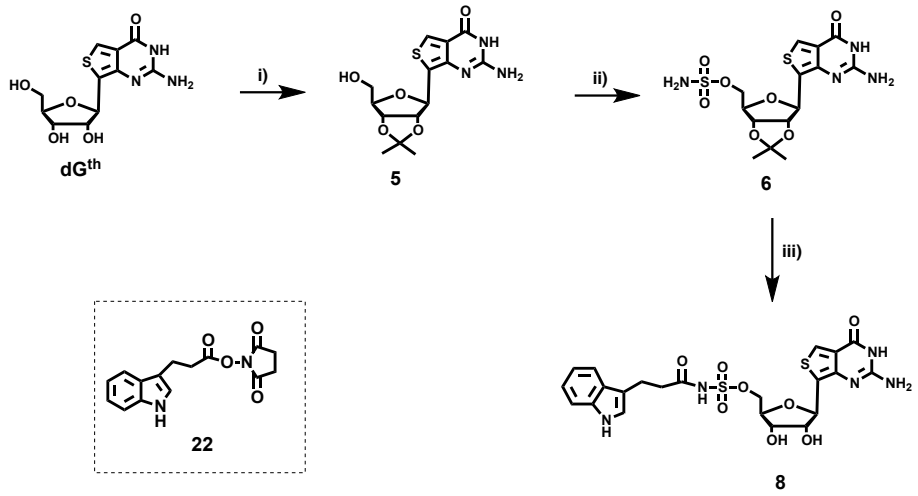

[a]Reagents and conditions: i) perchloric acid and acetone 2 h, ii) NH_2SO_2Cl, DMA, 85%; iii) 22, DBU, DMF 55%; iv) 80 % aq. TFA quant

Table 1: Photophysical properties for the fluorescent nucleoside analogues used in the current study

Compound	**Quantum yield (Ø)**	**Lifetime τ (ns)**	**Extended conformer γ (%)**	**Stacked conformer 1- γ (%)**	**k_q (1/s)**
EtAd	0.56	25	-	-	-
dGth	0.34	20	-	-	-
7	0.011	4.7	10.8	89.2	1.7×10^8
8	0.018	4.5	23.0	77	1.7×10^8

Figure 3. Time-resolved fluorescence studies on ethenoadenosine (black, fluorophore) and compound **7** (red, fluorophore + quencher). The decrease in the lifetime of fluorescence of **7** in comparison to parent nucleoside indicates dynamic quenching of the fluorophore.

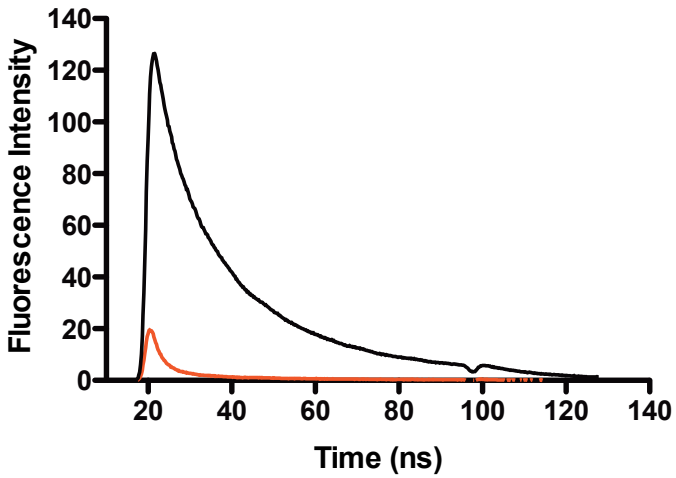

Figure 4. A) Fluorescent spectra changes of compound **7** and **8** (3 μM) upon addition of hHint1 (0.5-6 μM) (λ_{ex}= 278 nm for 7 and 330 nm for 8) in an aqueous assay buffer with slit width of 5 nm for both excitation and emission. B) Specific binding of probes to hHint1 (0.25 or 1 μM) observed with increasing concentration of ligands. The total increase in the fluorescence (λ_{ex}= 278 nm for 7, λ_{em}= 410 slit 10 and 330 nm for 8, λ_{em}= 453 slit 5) was subtracted from the background intensity and plotted against the concentration of the respective compounds. Data points represent three measurements including the standard deviations.

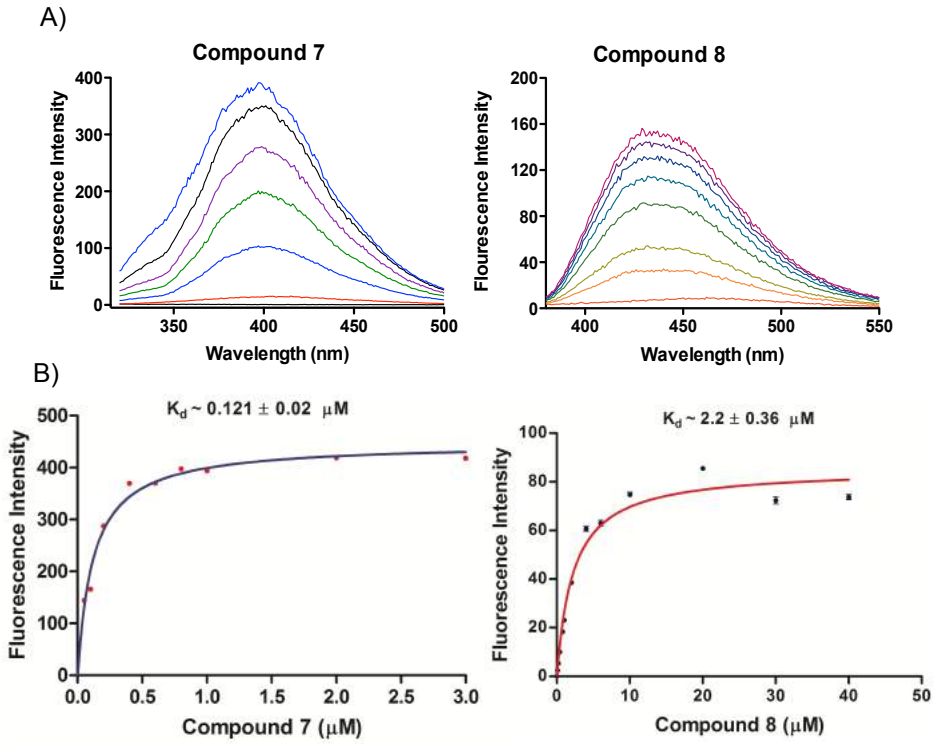

complex with the fluorophore and hence it reduces the quantum yield. In contrast, the collisional quenching reduces the average lifetime of an electron spent in the electronically excited state and hence reduces the lifetime of a fluorophore. The observed decrease in the quantum yields clearly indicates intramolecular static quenching in compound **7** and **8** likely via proximity pairing between the nucleobase and the indole ring. In addition, our studies on the measurement of an average fluorescence lifetime reflected a 4 to 5 fold reduction in the lifetime of our probes when compared to the parent nucleosides (**Table 1** and **Figure 3**). Based on the decrease in the fluorescence intensity and lifetime of the fluorophore, we estimate that in an aqueous solution, 89 % of the population of **7** and 77 % of probe **8** exists in the stacked conformation (**Table 1**). The decrease in the average lifetime also indicates that both our probes continuously undergo end-to-end dynamic collisional quenching. The unimolecular rate constant (k_q) for this process was calculated to be 1.7 x 10^8 per second. In conclusion, both compounds **7** and **8** undergo static and dynamic quenching.

Both probes exhibit switch-on fluorescence properties upon incubation with hHINT1 in an aqueous solution

Our rationale in the design of the quenched probes was that upon binding in the active site of hHint1, both the quencher and the fluorophore would become separated by sufficient distance (extended conformation) to result in unquenching and hence an increase in the fluorescence intensity (**Figure 2B**). Such phenomenon of fluorescence/FRET behavior has been previously observed upon binding of the cofactor

NADH to human 17-B-dehydrogenase complex, but has not been exploited in the design of an inhibitor for a target protein.[23] As expected, we observed an increase in the fluorescence intensity upon incubation of these probes in the presence of hHint1 (**Figure 4A**). Titration of these probes with an increasing amount of hHint1 yielded a fluorescence intensity curve, indicative of active site binding dependent phenomenon (**Figure 4B**). As a control, each probe by itself showed a linear increase in the emission signal intensity resulting from the auto or background fluorescence of the fluorophore (**Figure 5**). Fitting the observed data with a one site-binding model provided the dissociation constant of **7** to be 0.121 ± 0.02 μM and **8** to be 2.2 ± 0.36 μM. The binding affinity of the **7** is well in agreement with the previously reported dissociation constant obtained via ITC measurement. The dissociation constant of **8** was observed to be four fold lower than the recently reported guanosine analog of **8** by Shah and Wagner et al. This result indicates that the replacement of nitrogen's in the purine ring and the incorporation of a sulfur atom at C8 led to a decrease in the binding affinity.

X-ray crystal structure analysis of compound 7 bound with hHint1

To validate our hypothesis, that the extended conformation of the probe is driving the increase in fluorescence upon binding to hHint1, we obtained a high-resolution (1.6-Å) X-ray crystal structure of hHint1 bound with compound **7** (**Figure 6**). Comparing with the structure of AMP (pdb: 3TW2), additional hydrogen bonding between the carbonyl of the acyl-sulfamate of **7** and active site Ser 107 was observed. When compared with the hHint1-AMP structure, a rotation around the 5' O-S bond is observed for **7** compared to

Figure 5. Standard curves: Measure fluorescence intensity of compound **7** and **8** in the absence of hHint1. The total increase in the fluorescence (λ_{ex}= 278 nm for 7, λ_{em}= 410 slit 10 and 330 nm for **8**, λ_{em}= 453 slit 5) in the absence of hHint1 was plotted against the concentration of the respective compounds. Data points represent three measurements including the standard deviations.

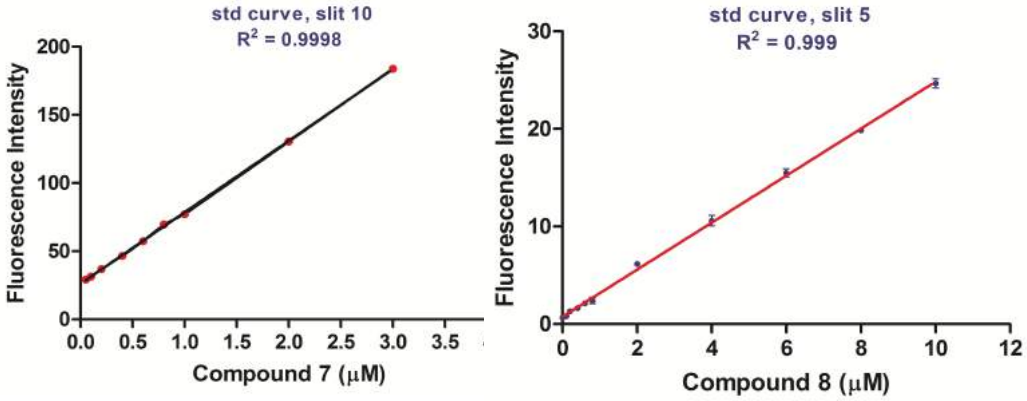

Figure 6. (Left) High-resolution x-ray crystal structure of compound **7** bound to hHint1. Extended conformer of the compound **7** is observed. (Right) X-ray crystal structure analysis of AMP (yellow; pdb: 3TW2) overlaid with the compound **7** (cyan) in interaction with hHint1 (blue; pdb: 5I2E) complex. H-bond interactions between the sugar and side chain are shown in dotted black lines. Different orientations of isoleucine side chains observed in the hydrophobic nucleotide-binding pocket for AMP and compound **7** bound hHint1 structures are shown in yellow and blue respectively.

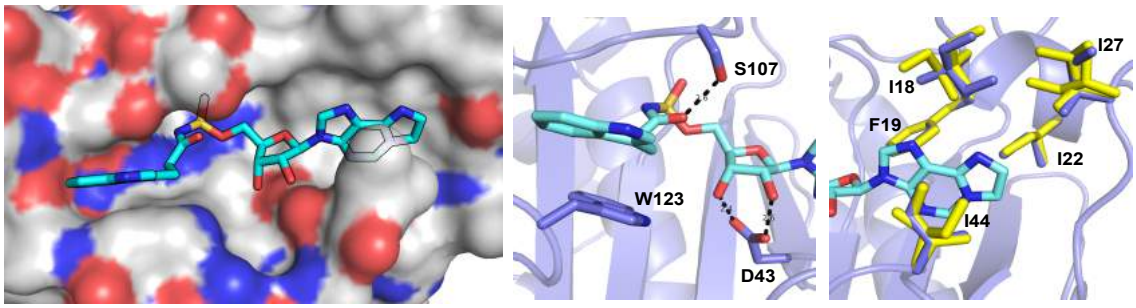

the 5' O-P for AMP binding, thus positioning the Ser 107 further away and 2.6-Å from the carbonyl. These results are consistent with the gain in the binding affinity and observed increase in the enthalpic contribution reported in the previous chapter. Several additional sets of molecular interactions were observed in both the enzyme-inhibitor structure. Examination of the ribose ring, revealed that as observed for all Hint-nucleotide structures, active site binding of the ribose sugar 2′ 3′- hydroxyl is driven by hydrogen bond interactions with the side chain oxygen atoms of Asp 43 (2.6-Å and 2.4-Å). With regard to the inhibitor side-chain, stabilizing van der Waals interactions were observed between the linking methylene's and the indole ring of Trp 123 (3.5-Å) in compound **7**. In addition, the planar tricyclic ring of the nucleobase is well accommodated by the hydrophobic S1 pocket (which is comprised largely of Ile 18, Phe 19, Ile 22, Ile 27, and Ile 44). When compared to the AMP bound structure, minor changes were observed in the side chain of the isoleucines in the S1 pocket and no significant variation in the backbone structure. As expected compound **7** is observed in fully extended conformation when bound in the active site of hHint1 (**Figure 6**). The bound structure shows that the surface area of **7** complements with the active site of hHint1. Moreover, no significant changes in the overall conformation of the protein were observed when compared to the apo or nucleotide bound structures.

Utility of switch-on probes in hHint1-ligand displacement studies

Since probes **7** and **8** occupy the active site of hHint1, monitoring their displacement by non-fluorescent ligands would allow us to determine the dissociation constants of the ligands. As can be seen in **Figure 7**, titration of the hHint1-**7** or **8** complex with the

inhibitors Bio-AMS or TpGc yielded a dose-dependent decrease in fluorescence. IC_{50} values obtained from the plot of the % decrease in fluorescence intensity vs. log dose

Figure 7. A) Competitive displacement studies (Left) Titration of Bio-AMS (0.025-12 μM) with hHint1 (0.25 μM) incubated with 0.4 μM of compound 7. (Right) Titration of compound 3 (TrpGc, 1-40 μM) with hHint1 (1.0 μM) incubated with 12 μM M of compound 8. B) (Left) Specific binding of compound 8 to hHint1_H112A (0.5) observed with increasing concentration of the ligand. The total increase in the fluorescence (λ_{ex}= 330 nm and λ_{em}= 453 nm, slit 5) was plotted against the concentration of the compound 8. Data points represent three measurements including the standard deviations. (Right) Titration of Hint1 substrate (TrpAMP, 0.025-12 μM) with hHint1_H112A (0.25 μM) incubated with 2.0 μM of compound 8. One site-binding model was used to fit the displacement curves. Data points represent three measurements, including the standard deviations.

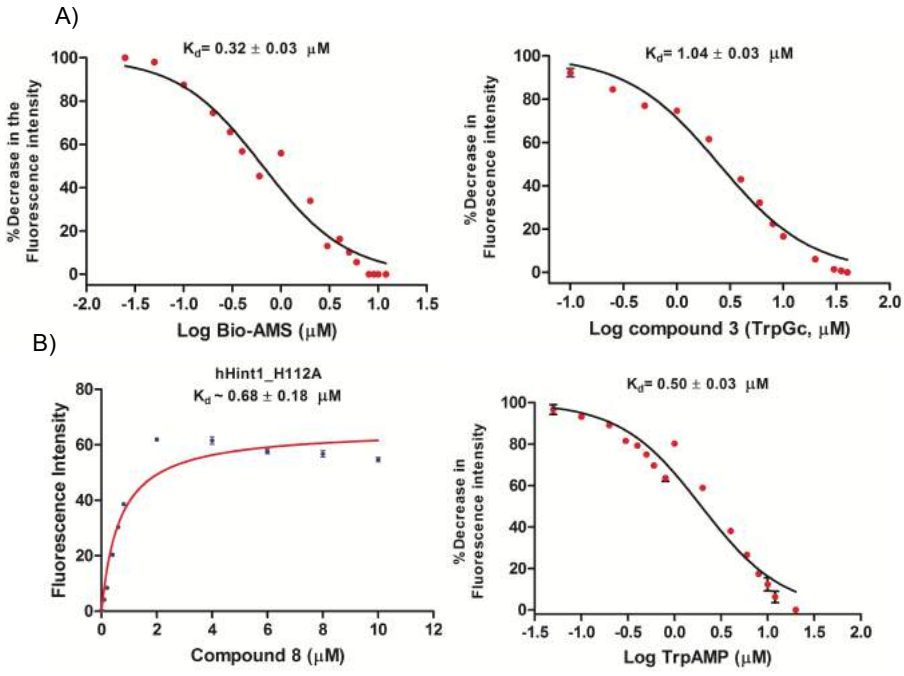

Figure 8. (Left) X-ray crystal structure analysis of AMP bound to hHint1 (pdb: 3TW2) to measure the distance between W123 and the nucleobase for FRET pairing (dotted line 13Å). (Right) FRET signal measurement upon incubating 8 μM of hHint1 alone (red) or in the presence of 8 (2 μM) (blue, λ_{ex}= 280 nm for 8, slit 5) in an aqueous assay buffer. The decrease in the emission intensity (λ_{em}= 360 nm for tryptophan, slit 5) of the protein was observed upon incubation with compound 8.

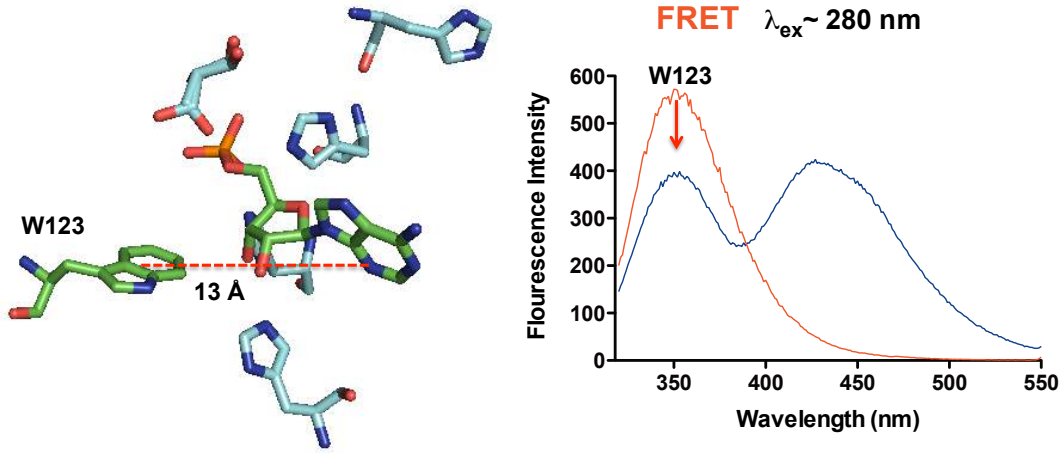

response curve were then converted using the Cheng-Prusoff equation to provide the inhibition constant (K_i) values. The values for both the inhibitors were found to be very similar to the previously reported dissociation constant values of 0.32 and 3.65 μM for Bio-AMS and TrpGc via ITC.[15] In similar fashion, the values of the inhibition constants for the nucleoside monophosphates (NMPs) to hHint1 ranged from 20-40 μM with a rank order of GMP≈AMP>CMP>UMP (**Table 2**). The inhibition constant value for GMP (24 μM) is nearly identical to the previously reported value of the dissociation constant value (67 μM) measured by NMR ^{15}N-^{1}H HSQC titration experiment.[24]

We next sought to evaluate whether the probes could be used to determine the binding affinity of nucleoside phosphoramidate substrates of hHint1. Instead of the catalytically active enzyme, we employed the catalytically inactive mutant of hHint1, H112A, in which the nucleophilic imidazole was replaced with an alanine residue.[9] As observed for the wild-type enzyme, incubation of hHint1_H112A mutant with **8** resulted in an increase in fluorescence intensity. Interestingly, the hHint1_H112A mutant exhibited a moderate gain (~4 fold) in the binding affinity for **8** compared to the wild-type enzyme (**Figure 7B, Table 2**). When the hHint1-**8** complex was then titrated with variable concentrations of the hHint1 substrate, TpAd, a dose-dependent decrease in fluorescence was observed corresponding to a dissociation constant of 0.5 ± 0.01 μM (**Figure 7B, Table 2**), which is in agreement with the calculated value of 1.33 μM based on the association and dissociation rates observed in the kinetic mechanism.[25]

Table 2: hHint1-ligand binding constants calculated using fluorescence displacement studies with switch-on probes.

Ligand	Wild type hHint1		hHint1_H112A	
	IC_{50} (μM)	K_i (μM)	IC_{50} (μM)	K_i (μM)
Bio-AMS[a]	1.77 ± 0.05	0.32 ± 0.01	-	-
3 (TrpGc)[b]	6.71 ± 0.04	1.04 ± 0.03	-	-
AMP[b]	141.9 ± 1.8	22.1 ± 2.1	-	-
GMP[b]	153.99 ± 2.0	23.9 ± 1.9	-	-
UMP[b]	246.82 ± 2.8	38.3 ± 2.3	-	-
CMP[b]	219.95 ± 2.4	34.1 ± 2.4	-	-
2 (TrpAMP)[b]	-	-	1.94 ± 0.05	0.50 ± 0.01

A fluorescent switch-on FRET probe: compound 8 as a FRET acceptor for tryptophan in the structure of hHint1

One of the key motivations in the development of **8** was the realization that the maximum excitation wavelength of ^{th}G (ex_{max} = 330-360 nm) overlaps with the fluorescence emission maxima wavelength for tryptophan (em_{max} = 340 nm). The critical Föster resonance distance (R_0) between tryptophan and the fluorescent nucleoside (^{th}G) has been reported to be 22 Å.[26] Inspection of the x-ray crystal structure revealed the presence of a single tryptophan residue (W123) located in the active site that is 13 Å away from the nucleobase-binding pocket (S1) (**Figure 8A**). Such proximity provides an opportunity for the development of a fluorescence resonance energy transfer (FRET) based switch-on probe for hHint1. FRET was verified by measuring the fluorescence emission spectra of hHint1 alone and in the presence of compound **8** (**Figure 8A**). Upon incubation with an excess amount of hHint1 and excitation at 280 nm; the emission at 360 nm was decreased with an increase in emission signal intensity at 450 nm. This observation is in agreement with those typically seen with FRET pairing molecules. Since the structure of **8** also incorporates an indole moiety, one might expect FRET from intramolecular indole side chain. Since the structure of **8** incorporates an indole moiety, one might expect FRET from not only W123 but also from the intramolecular indole side chain. Distinguishing between the two overlaps would be difficult. Our attempts to abolish FRET with a W123A mutation led to the loss of dimerization of hHint1 (data not shown). Mutations associated with a loss in dimerization of hHint1 have been reported to decrease its substrate specificity and Michaelis-Menten constant for the substrates.[27] Hence, we did

not observed fluorescence unquenching of compound **8** in the presence of hHint1_W123A mutant (data not shown).

Selectivity of Switch-on fluorescence probes

The human genome encodes for three different isoforms of Hint proteins: hHint1, 2 and 3, while prokaryotes such as Escherichia coli encodes only a single protein with phosphoramidase activity (ecHint). Our kinetic and substrate specificity studies with Hint enzymes have clearly shown differences among these isoforms. Incubation of compound **8** with each hHint1 isoforms resulted in differential amounts of fluorescence unquenching. Among them, hHint1 showed the highest, while both hHint3 and echinT exhibited the lowest amount of fluorescence intensity upon incubation with compound **8** (**Figure 9A**). The difference in the amount of unquenching also manifests the ability of the Hint isoforms to differentially bind acyl-NMP and their potential as in vivo regulators. These results are in agreement with the decrease in the Michaels-Menten constant observed for both hHint3 and echinT when the substrate specificity studies of the isoforms and the hHint1 are compared. Interestingly, among these isoforms, only hHint1 and 2 contains a tryptophan, in the active site but not the others. Consequently, we observed the FRET signal only in the presence of hHint1 and 2 (**Figure 10**).

Next, we wanted to ask if compound **8** would display similar switch-on properties in the presence of other adenylating or nucleoside binding proteins. We chose an aminoacyl t-RNA synthetase (lysRs) as a representative example and dihydrofolate reductase (DHFR) for its ability to bind a nucleotide-based cofactor NADPH. We also

Figure 9. Selectivity test of compound **8** with other proteins: Compound **8** (12 μM) was tested with A) 1 μM of Hint isoforms and three other nucleoside/nucleotide binding proteins or B) *E.coli* lysate (1 mg/ml) without/with hHint1. Student t-test perform on the values indicate, **** p-values < 0.0001, *** p-values ≥ 0.0001

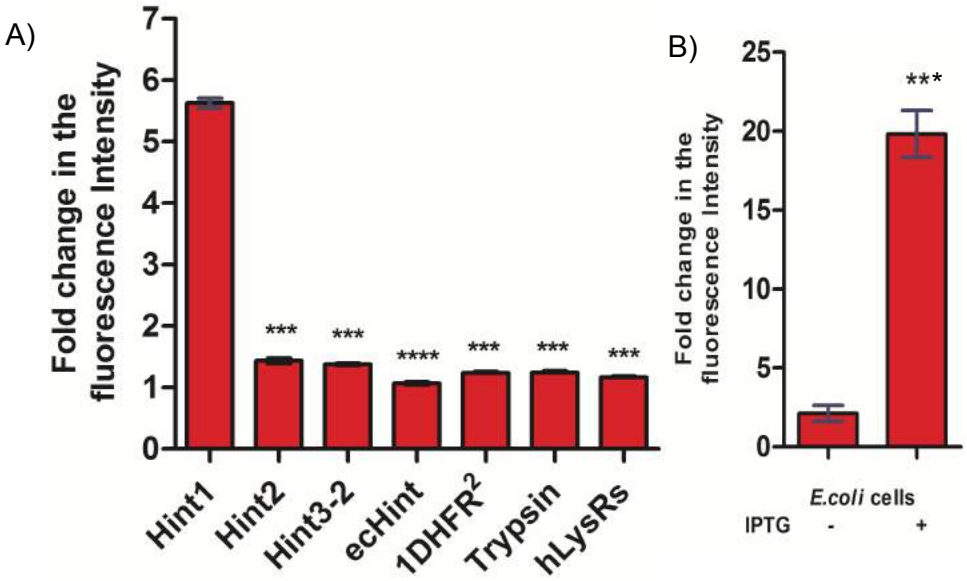

Figure 10. Comparison of signal from FRET pairing of compound 8 with tryptophan in the active site of Hint1 or 2 to other Hint proteins that lacks such tryptophan: Compound 8 (12 μM) was tested with 1 μM of Hint isoform proteins. The observed signal in Hint3-2 and echinT is resulting from the background fluorescence of the unbound probe and hasn't been normalized to that. Student t-test perform on the values indicate, *** p-values ≥ 0.0001.

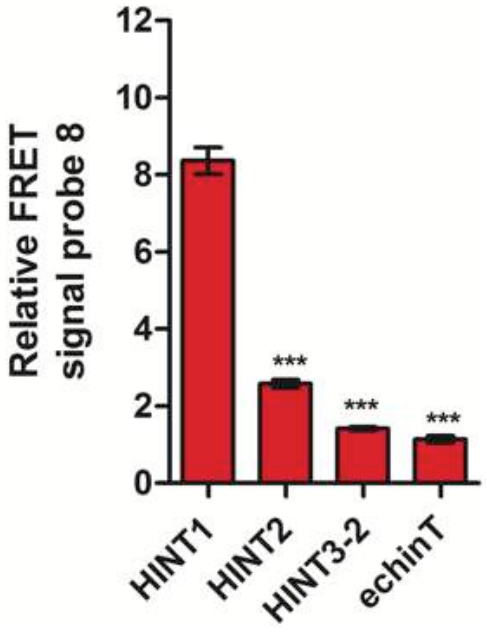

used an aminopeptidase protein trypsin in the study. We monitored the increase in the fluorescence intensity of Compound **8** (λ_{ex} = 330 nm, λ_{em} = 450 nm) in the presence of both proteins. Incubation of these proteins with Compound **8** yielded little or no increase in the fluorescence intensity (**Figure 9A**). Furthermore, incubation of **8** with the lysate of Escherichia coli (total protein 1 mg) yielded little or no increase in the fluorescence intensity. However, incubation of **8** with *E.coli* lysate (total protein concentration 1 mg/ml) obtained from cells transfected with hHint1 plasmid and induced to express hHint1 (1.5 h) resulted in a significant increase in the fluorescence intensity (**Figure 9B**). Together, these results demonstrate the ability of hHint1 to bind selectively and switch-on the fluorescence of **8**.

Utility of 8 in monitoring hHint1-substrate complex (ES) under steady state conditions

One of the key characteristics of a competitive inhibitor is its reversibility in binding and inhibiting an enzyme. In addition, any given amount of a competitive inhibitor can be displaced and maximum reaction velocity (V_{max}) of an enzyme can be reached under saturating substrate concentrations. Accordingly, a competitive inhibitor only changes the Michaels-Menten constant (K_m, becomes K_{mapp}) and not the V_{max} value. It is also interesting to conceive that **8** is not only a competitive inhibitor, but can also serve as a reporter in monitoring active site occupancy of hHint1 in real time. Hence, we envisioned that under saturating concentrations of our reporter/inhibitor incubate with hHint1, we expect the fluorescence intensity will correspond to nearly complete occupancy (> 90%) of the hHint1 active site. Under such conditions, upon the addition of an excess amount

Figure 11. Monitoring hHint1-substrate complex using compound **8** as a displacement probe. A) Schematic representation of the concept. Incubation of hHint1 (E) with excess of compound **8** (I) results in a certain amount of fluorescence intensity arising from the EI complex. Addition of the excess amount of the substrate ($S >> K_m$) results in the displacement of the inhibitor and formation of the ES complex. B) Displacement of compound 8 (12 μM) bound to hHint1 (1 μM) via the addition of excess substrate (compound 2, $S >> K_m$). The formation of ES complex is seen over a period of a few seconds after which the gain in the fluorescence intensity is due to the decreased substrate concentration ($S << K_m$). The excitation wavelength was 330 nm and slit width of 5 nm for both excitation and emission. C) Increasing the substrate concentration (compound 2) leads to increased inflection time (X_0) or mean residence transit time (MRTT). D) The plot of MRTT vs concentration of 2 yields a linear response. The catalytic turnover rate is calculated using the $1/slope = V_{max}/[E]*60$ (s^{-1}). The intercept of the line on the x-axis represents the minimum concentration of the substrate required to observe ES complex at a steady state. Data points represent three measurements including the standard deviations

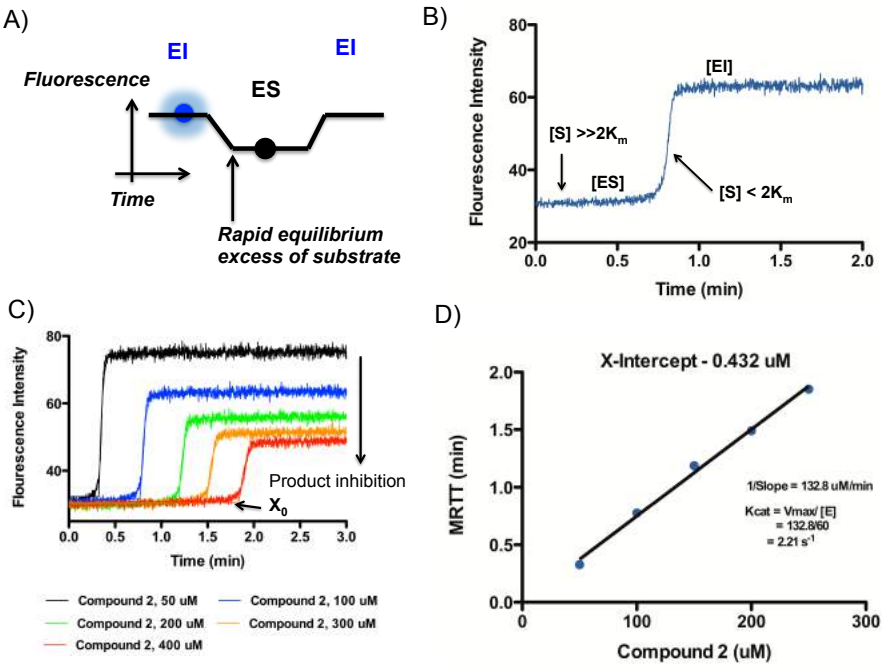

Table 3: Kinetic parameters for hHint1 substrates obtained using transit assay

Compound	Regular assay	Transit assay
	K_{cat} (s^{-1})	K_{cat} (s^{-1})
TrpAMP	2.1 ± 0.1	2.20
TrpGMPS	0.019 ± 0.001	0.017
L-ala AMP	-	1.38
D-ala AMP	-	2.0

Figure 12. A) Monitoring and comparison of the ES complex formation between **2** (left) or **11** (right) incubated with hHint1 (1 or 2 μM) and **8** (12 μM). 50 μM of the concentration of **2** or **11** was used in the comparison above. The decrease in the turn over rate of **11** is seen with increased duration of the ES complex break down. B) Label free detection of the D-alanine (**12**, left) and L-alanine (**13**, right) side chains containing adenosine phosphoramidate substrates of hHint1. The colors of the traces correspond to the concentration of the substrate added in the presence of hHint1 (1 μM) and **8** (12 μM). The preference is clearly seen in the steepness of the slope of **12** in comparison to the slope of **13**.

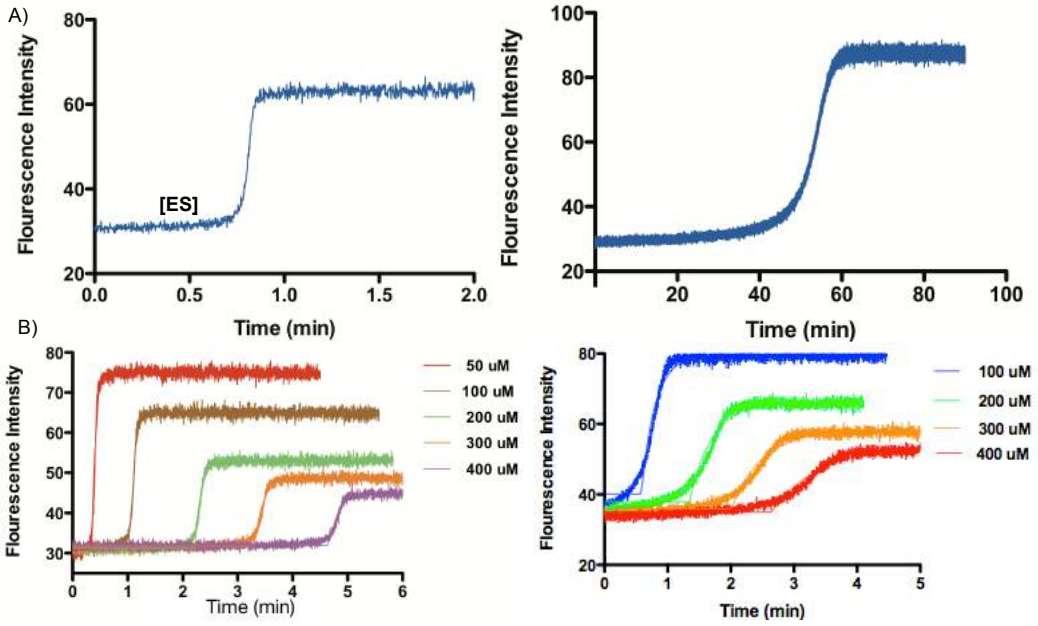

of the substrate (above saturating concentrations), one would expect a rapid dissociation of hHint1-**8** complex and hence a drop/decrease in the fluorescence intensity of the reporter. Such a drop in the fluorescence intensity would be expected until the substrate level reaches below $2K_{mapp}$ values, and a sigmoidal response curve would be expected (**Figure 11A**). An analogy to explain this model involves the transit method used by NASA's Kepler telescope to detect exoplanets revolving around a star in the galaxy. Upon transit of an exoplanet through the region between the star and the observer, it forecasts a shadow on the star disc, resulting in the decrease of the observed brightness of the star. The brightness of the star returns to its original intensity after completion of the transit.

To test this hypothesis, we incubated hHint1 (1 μM) in the presence of excess amounts of **8** (12 μM), which resulted in a stable fluorescence intensity monitored over a period of time. Upon quick addition of the Hint1 substrate (TrpAMP, 100 μM) to this reaction mixture, we observed a drop in the fluorescence intensity of the bound compound **8**. The intensity was reduced to the background level indicating the complete displacement of the probe from the active site of hHint1 and formation of the ES complex. This ES complex remained steady for a few seconds, after which a steady recovery in the fluorescence intensity was observed, likely due to decreased concentration of the substrate after enzymatic hydrolysis (**Figure 11B**). The amount of steady time observed for the ES complex was directly proportional to the amount of substrate added (**Figure 11C**). Interestingly, upon increasing the concentration of the

substrate, the amount of recovery in the final fluorescence intensity at the end of the enzymatic reaction was also decreased (**Figure 11C**). The decreased final observed intensity indicates product inhibition (AMP or NMP) that is consistent with the reported kinetic mechanism of hHint1.

Label free detection of hHint1-substrate complex via monitoring transit turnover time

We next asked if we could extrapolate turn over rates of TrpAMP from the dose dependent sigmoidal curves above. In theory, if we define the influx point X_0 (**Figure 11B**) at each concentration of substrate as the mean transit time (MRTT) required for the substrate concentration to fall below twice the K_m value, plotting MRTT values against the substrate concentration should yield a linear response curve and the slope should provide the velocity of the enzymatic reaction. We used the model plateau followed by one phase association equation to define X_0 into the sigmoidal curves. Fitting of the model at each concentration of the substrate provided us with the inflection points (X_0). Next, we plotted those values again each substrate concentration to provide a linear curve (**Figure 11D**). Upon dividing the slope of the linear curve by the enzyme concentration used in the reaction, we derived a rate of 2.1 ± 0.1 s^{-1}. The observed rate is in perfect agreement with the K_{cat} value obtained with our regular florescence assay (**Table 3**). Next, we asked if we could use this assay to define kinetic parameters for a substrate of hHint1 with a slower turnover rate such as TrpGMPS. The incorporation of a sulfur atom should make the adenylated intermediate less hydrolytically labile and hence should exhibit a poor turnover rate by hHint1. Steady state kinetics analysis with our regular

assay revealed a 120-fold decrease in the turnover rate (k_{cat}) and a 170-fold decrease in the substrate specificity (k_{cat}/K_m) of TrpGMPS (**Table 3**). Consistent with this result, our transit assay displayed a slower breakdown of an ES complex as seen by an increased transit turnover time (**Figure 12A**). Finally, we display the utility of this approach in performing label free detection of hHint1 specificity with substrates containing non-tryptamine side chains. We chose alanine side chains due to their wide utility in the design of preclinical/clinical antiviral and anticancer phosphoramidate pronucleotides. We made adenosine phosphoramidate analogs containing either L or D alanine side chains. The preference for D-alanine over L-alanine side chain was clearly visible by looking at the sigmoidal curves (**Figure 12B**). The turn over rates obtained with transit assay confirmed a preference for D over L-alanine side chains by hHint1 (**Table 3**).

Discussion

We report here the design, synthesis, and evaluation of the first switch-on fluorescence probes for hHint1. We utilized the principle of molecular beacons to create the small molecule switch-on probes. The design consists of an intramolecular quencher connected via a linker to a fluorophore such that the proximity of the quencher in a solution results in the intramolecular quenching of the fluorescence in solution. Calculation of the quantum yield showed a significant decreased by 30 to 50 fold when compared to the fluorophore in the absence of a quencher. The decrease in the fluorescence was primarily due to stacked conformations of the probes in an aqueous buffer. Such minimal background is rarely observed in the design of solvatochromic fluorescent probes. Upon incubation with hHint1, an increase in the fluorescence intensity was observed due to the extended conformation of **7** bound to hHint1. These dependencies resulted in the observed selectivity of our probes to switch on only in the presence of hHint1. Minimal background interference and a significant increase in the fluorescence intensity upon incubation allowed for the detection of hHint1 with high signal-to-noise ratio (5-20 fold). One could exploit such strategy using the appropriate linker, fluorophore and quencher pairs in the design of fluorescent reporters for other non-enzymatic or enzymatic proteins.

Opioid tolerance, addiction, and hyperalgesia are dependent on the molecular changes associated with events at both the pre and postsynaptic levels of the central nervous system. Hint1 is a postsynaptic protein proposed to be involved in the regulation of the NMDAR receptor upon exposure of opioids in animals.[12] We have recently shown that blocking of the hHint1 active site with an inhibitor (**3**) results in increased morphine

analgesia and reduced tolerance in animal studies. Hence, the development and identification of new inhibitors is of potential therapeutic value. Our fluorescent probes allow for a rapid mix and measurement of fluorescence for a displacement assay for hHint1. The assay circumvents the high protein concentration required for the recently reported ITC studies with hHint1 inhibitors.

Compound **8** and its cognate fluorescent nucleoside displays properties that make them suitable for the development of a high-throughput-screening (HTS) assay for the identification of new nucleoside or non-nucleoside inhibitors of hHint1. One of the significant limitations that commonly arise in fluorescent-based high throughput assays is the interference from the library compounds that are fluorescent, resulting in false negative or positive hits.[28] Typically, fluorescent compounds in the screening library have a fluorescence lifetime of less than 5 ns. Hence, the use of fluorescence lifetime as the readout parameters for HTS has been shown to increase the robustness against associated artifacts and compound related interferences.[29, 30] Both our probes exhibit a remarkable change in their fluorescence lifetime (4-5 fold) when unquenched or bound to hHint1. This exceptionally long lifetime (20-25 ns) would offer a robust assay with high quality primary screening data.

To fully understand the correlation between the hHint1 conformational changes in the regulation of the function in CNS, it is essential to comprehend the principle governing the molecular recognition of ligands by Hint1. The structure of hHint1 consists of a nucleoside-binding fold, and it is likely that the binding of an endogenous nucleoside

acyl-NMP or NMP in the active site could potentially modulate its interaction with other proteins. The ability of our probes to light up upon binding to hHint1 provides a simple and easy means to evaluate the impact of the perturbations on the protein structure on the acyl-NMP binding. Notably, an increase in the binding affinity was clearly evident with the catalytically inactive H112A mutation in hHint1. The relative increase in the fluorescence intensity of **8** upon binding to hHint1 provides an insight into the first step in the formation of the ES complex. The ability of **8** to differentiate between hHint1 and Hint2 despite their high sequence and structural similarity indicates the underlying differences in their ability to form an ES complex. Recently, numerous point mutations in hHint1 were identified from clinical patients and were hypothesized to contribute to the cause of peripheral neuropathy associated with neuromyotonia.[13, 31] In such a scenario, our probes could serve as valuable tools in evaluating the impact of these mutations on the binding of nucleosides or acyl-NMPs for hHint1. Using a catalytically inactive mutant in the displacement studies, we report the first binding affinities for a nucleoside phosphoramidate (**2**) for hHint1. Compound **8** could also serve as a non-covalent label for hHint1 or hHint1_H112A to probe interactions between hHint1 and neuronal proteins, which are still largely unknown. In addition, the probe could be used as a FRET pairing probe with green fluorescent protein (GFP) or dye-labeled protein of interest to monitor hHint1-protein interactions in vitro.

Protein-protein and protein-ligand interactions are fundamental molecular process governing cellular signaling processes. Such interactions could be easily monitored using a simple FRET or fluorescence lifetime experiment. For e.g. Rizo and Sudhöf co-workers

used a FRET experiment to confirm the calcium dependent binding of a phospholipid to synataxin.[32] In the study, FRET measurement was performed between a dansyl labeled phospholipid and the tryptophan in the binding pocket of the target protein. In similar fashion, compound **8** could serve as a non-covalent label for hHint1 or hHint1_H112A to probe for interactions between hHint1 and neuronal proteins involved in NMDAR signaling regulation, which are still largely unknown. The probe could be used as a FRET pairing probe with green fluorescent protein (GFP) or dye-labeled protein of interest to monitor hHint1-protein interactions *in vitro*.

Apart from the role of hHint1 in the CNS, the nucleoside phosphoramidase activity of hHint1 is of interest to many pharmaceutical companies. Several anticancer nucleosides prodrugs rely on the catalytic activity of hHint1 in the metabolic activation of the drug. One such example is the blockbuster Hepatitis C drug, sofosbuvir (Sovaldi® and a component of Harvoni®), which undergoes multiple steps of activation to overcome the poor bioavailibity of the parent nucleoside. The bioactivation is mediated by the hHint1-catalyzed hydrolysis of the phosphoramidate backbone in the pyrimidine-based nucleoside prodrug. Sovaldi contains an L-alanine side chain, which contributes the amine to form the phosphoramidate backbone. Determination of side chain preference with regard to hHint1 substrate specificity has hitherto been limited by the dependence of our existing assay on the spectroscopically active indole side chain. In the current study, we show the utility of compound **8** in label free monitoring of the hHint1-susbtrate complex. The indirect assay is independent of the spectroscopic properties of the substrate. Using a catalytically inactive mutant in the displacement studies, we report the

first binding affinity value obtained for a nucleoside phosphoramidate (**2**) for hHint1. These displacement studies and assay with **8** provides a valuable tool to measure the binding affinity and evaluate the substrate specificity of hHint1, which could help enable the design of future nucleoside based prodrugs.

In conclusion, we have developed a novel fluorescent/FRET probes with switch on properties for selective detection of hHint1. The probes would serve as a valuable tool for the future discovery of hHint1 inhibitors and towards gaining insights into the role of conformational dynamics in the molecular recognition of ligands by hHint1.

Materials and Methods

Fluorescence Spectroscopy: hHint1-Ligand binding and displacement studies

All fluorescence measurements were performed in an aqueous assay buffer (20 mM Tris, 150 mM NaCl pH 7.4). All fluorescence measurements were performed in a 1 cm four sided, 2 ml quartz cuvette. The total sample of 600-µl solution including the protein and ligand was used in the cuvettes to perform fluorescence measurements. All the readings were recorded at room temperature. The excitation and emission wavelengths and the slit width are described in the legends of the respective figures. The excitation wavelength for thG and **8** was 330 nm and the emission spectral scan was recorded from 360-530 nm. The excitation wavelength for EtAd and **7** was 280 nm, and the emission spectral scan was recorded from 320-530 nm. In the case of FRET measurement, the excitation wavelength for **8** was done at 280 nm, and emission spectra were recorded from 320-520 nm.

For hHint1-ligand binding studies hHint1 was incubated with successive increase in the concentration of **7** (0.05 -3 µM) or **8** (0.25-40 µM). The mixture was incubated for 30 s before the excitation and following with emission spectral intensity recording at 410 nm and 450 nm. The increase in the fluorescence intensity upon successive increase of the ligand concentration was subtracted from the blank measurement. A blank was recorded in the presence of just the ligand and no protein to yield a linear curve. The resulting sigmoidal dose response curve was plotted in the graph pad prism and fitted using one site-binding model to yield the dissociation constant (K_d) values.

For hHint1-ligand displacement studies hHint1 was incubated with either **7** or **8** at saturating concentrations. The mixture was incubated for 60 s before the addition of the desired ligand for the displacement of the fluorescence. The excitation and emission intensity was recorded. The decrease in the fluorescence intensity upon successive addition of the ligand was normalized to the blank and the resulting dose response curve was plotted in the graph pad prism. The dose response curve was fitted with one site-binding model to yield the IC_{50} values. The values were then converted to the inhibitory constant (K_i) values using Cheng-Prusoff equation.

Fluorescence Spectroscopy: Quantum yield, Fluorescence lifetime and Quenching studies

All the fluorescence and absorbance measurement was performed in the assay buffer. All the readings were recorded at the room temperature. The UV visible measurements were performed in the cary eclipse UV spectrophotometer. 5 nm slit width was used for all the measurements.

Quantum yields ($Ø_F$) for the thG, nucleoside analogs **7** and **8** were calculated using the following equation.

$$Ø_{F(x)} = (A_s/A_x)(F_x/F_s)(n_x/n_s)^2 Ø_{F(s)}$$

Where s is the standard, x is the nucleoside, A is the absorbance at the excitation wavelength, F is the area under the emission curve, n is the refractive index of the solvent and ØF is the quantum yield. The standard compound used in the study was EtAd and its reported quantum yield (0.56). The excitation wavelength of 280 nm for 7 and 330 nm for dGth and 8 was used in the calculation of the quantum yields.

Time resolved fluorescence spectroscopy or fluorescence decay curve measurements were recorded using time correlated single photon count (TCSPC). Samples (1 μM ligands) were excited with tunable dye laser range of 280-305 nm (instrument MatrixUV scientific) with excitation wavelength set at 305 nm for EtAd and 7. A subnanosecond pulse diode laser 355 ± 5 nm was used for thG and **8**. Emission was selected using a band pass filter (405 ± 5 nm and 430 ± 5 nm). To avoid anisotropy effects, emission polarizer was set at the magic angle (54.7°) during lifetime measurements. The instruments response function was acquired on the sample containing assay buffer using scattered excitation light detected with emission light polarizer set to vertical (0°) but without an emission filter. The PMT voltage for the emission detection was set to 600 V. The details on the instrument set up is described elsewhere. Fluorescent lifetime decay curves were analyzed using multi exponential decay simulation and nonlinear least square minimization. The observed waveform was fit by the decay simulation which had been iteratively convolved with the measured instrument response function (IRF) using fargo fit analysis software.[32, 33]

Based on the quantum yields and fluorescence lifetime studies, the fraction of population of 7 and 8 in stacked conformation resulting in the static quenching was calculated using equation,

$$\gamma = (F/F_0)\ (\boldsymbol{\tau}/\ \boldsymbol{\tau}_0)$$

Where γ is the fraction of population in open conformer, 1- γ gives population in closed conformer. F and F_0 is the fluorescence in the presence and absence of the quencher. Parent nucleoside served as control for the absence of an intermolecular quencher. $\boldsymbol{\tau}$ and $\boldsymbol{\tau}_0$ is the fluorescence lifetime in the presence and absence of the quencher. The ratio of $\boldsymbol{\tau}$/

$\boldsymbol{\tau}_0$ gave the fraction of the population under dynamic quenching. The unimolecular rate constant (kq) for the dynamic intramolecular quenching was calculated using equation,

$(\boldsymbol{\tau}/\ \boldsymbol{\tau}_0) = 1\ + kq\ (\boldsymbol{\tau}_0)$

$kq = 1/\ \boldsymbol{\tau}\ -\ 1/\ \boldsymbol{\tau}_0$

hHint1 substrate kinetics using mean residence transit turnover assay (MRTT):

To a solution containing hHint1 (1 μM) in an assay buffer was incubated with a saturating concentration of **8** (12 μM). The fluorescence of the solution (600 ul) in a quartz cuvette was measured at excitation wavelength of 330 nm and emission 450 nm. The intensity was measured over a minute and was stable. To this fluorescent solution, 50 -500 μM of the desired nucleoside phosphoramidate was added and rapidly mixed. The displacement of the fluorescence in real time was monitored at steady state kinetics over a period of 1-150 minutes. The resulting data was exported into the excel file and replotted using graph pad prism. The real time fluorescence vs intensity sigmoidal plot was fitted using plateau followed by one phase association equation as shown below. The inflection time (X_0), described as mean residence transit time (MRTT), measured was then plotted against the substrate concentration to obtain a linear curve. The MRTT plot was fitted with a linear curve. The inverse of the slope divided by the hHint1 concentration provided the turn over rate of the substrate by hHint1. The x-axis intercept provides the measurement of the binding affinity and hence the apparent K_{mapp} values. The original Km value was obtained by using Cheng-Prusoff like equation shown below.

$Y = Y_0 + (Plateau - Y_0) * (1 - \exp(-K * (X-X_0))$

If $X<X_0$

X_0 is the time where association begins

Y_0 is the average Y value up to time X_0

Plateau is the Y value at infinite times

K is the rate constant, expressed in the reciprocal of the X-axis time units

Synthesis and characterization of compound 8

2-Aminothieno[3,4-d]pyrimidin-4(3H)-one (S2)

Same as described previously in reference.[20] Yield obtained 73.6%. The ^{1}H NMR spectrum was (DMSO-d_6): 6.07 (s, 2H), 6.96 (s, 1H) and 8.23 (s, 1H). ^{13}C- DMSO-d_6: 159.01, 151.01, 150.74, 127.55, 124.18 and 109.22 ppm. Low resolution ESI-MS [M+H] 168.0

N^2-DMF 2-aminothieno[3,4-d]pyrimidin-4(3H)-one (S3)

Same as described previously in reference.[20] Obtained in 95.9% yield. The ^{1}H NMR spectrum was (DMSO-d_6): 2.74 (s, 1H), 2.90 (s, 1H), 3.03 (s, 3H), 3.15 (s, 3H), 7.23 (d, 1H), 8.27 (d, 1H) and 8.61 (s, 1H). ^{13}C- DMSO-d_6: 127.96, 127.13, 126.08, 112.14, 41.18, 36.25, 35.03 and 31.24 ppm. Low resolution ESI-MS [M+H] 223.0

N^2-DMF 2-aminothieno[3,4-d]pyrimidine G mimic 2,3,5-tri-O-benzoylnucleoside (S4)

Same as described previously in reference.[20] Obtained in 20% yield. The crude product from this step was used without purification towards the next step. Low resolution ESI-MS [M+H] 667.2

2-Aminothieno[3,4-d]pyrimidine G mimic nucleoside (S5)

Same as described previously in reference with minor modification in this step.[20] Treatment with saturated methanolic ammonia was found to result in the partial deprotection after overnight heating at 65 °C. Hence, the reaction was evaporated to dryness next day and stirred in 4N NaOH/MeOH (1:1, 5ml each) for 2 h. The reaction was then neutralized and organic was evaporated. The aqueous solvent was frozen and lyophilized to obtain the crude material. The material was loaded onto the reverse phase chromatography to purify and yield final product in 58.4% yield. The ^{1}H NMR spectrum was (DMSO-d_6): 3.52 (m, 2H), 3.78 (m, 1H), 3.94 (m, 1H), 4.02 (t, 1H), 4.85 (s, 1H), 5.12 (d, 1H), 6.21 (s 2H) and 8.131 (s, 1H). ^{13}C- DMSO-d_6: 161.06, 153.22, 147.71, 124.88, 124.81, 85.54, 77.42, 77.05, 72.29, 62.85 and 40.91 ppm. Low resolution ESI-MS [M+H] 300.0

2′, 3′-O-O-isopropylidene-2-Aminothieno[3,4-d]pyrimidine G mimic nucleoside (5)

To a cold stirred suspension of **S5** (50.0 mg, 0.177 mmol) in acetone (3 ml) was added catalytic amount of perchloric acid (12.5 μl). The reaction was monitored using TLC (20:80:0.1 MeOH/$CHCl_3$/TEA solvent). After 2 h ammonium hydroxide (2 equivalent to perchloric acid, 27.5 μl) was added to neutralize the reaction mixture under an ice bath.

The reaction mixture was then evaporated under rotary evaporator to complete dryness. The crude material was purified using reverse phase chromatography to isolate desired product (39.9 mg, 0.124 mmol) in 70 % yield. The ^{1}H NMR spectrum was (DMSO-d_6): 1.31 (s, 3H), 1.50 (s, 3H), 3.53 (m, 2H), 3.90 (m, 1H), 4.71 (m, 1H), 4.81 (m, 1H), 4.97 (t, 1H), 5.33 (d, 1H), 6.20 (s, 2H) and 8.25 (s, 1H). ^{13}C- DMSO-d_6: 158.77, 151.25, 148.17, 126.79, 124.31, 123.90, 114.20, 86.10, 85.08, 82.21, 79.65, 62.16, 27.82, and 27.79 ppm. Low resolution ESI-MS [M+H] 340.1 HRMS (ESI+) calcd for $C_{14}H_{18}N_3O_5S$ [(M+H)+] 340.0967 found 340.09524

2′, 3′-O-O-isopropylidene-5'-O-(sulfamoyl)-2-Aminothieno[3,4-d]pyrimidine G mimic nucleoside (6)

A solution of **4** (30 mg, 0.088 mmol) in dimethyl formamide (5 mL) was stirred for 30 min at 0 °C. Next, sulfamoyl chloride (0.26 mmol, 30.6 mg) was added to the reaction mixture after which the reaction was brought to the room temperature and stirred for an additional one hour. An excess of TEA (12 µl, excess) was added and stirring was continued for an additional 10 min. The reaction mixture was finally quenched with MeOH (5 ml) under ice bath. The reaction mixture was evaporated to dryness and the crude reaction mixture was then purified by reverse phase chromatography to afford the title compound (33 mg, 0.079 mmol) in 89.6 % yield. ^{1}H NMR spectrum was (DMSO-d_6): 1.32 (s, 3H), 1.53 (s, 3H), 4.15 (m, 3H), 4.83-4.90 (m, 2H), 5.37 (m, 1H), 6.24 (s, broad 2H), 7.81 (s, 2H), 8.28 (s, 1H) and 10.58 (s, 1H). ^{13}C- DMSO-d_6: 158.76, 151.37, 148.31, 127.13, 124.36, 123.1, 114.55, 85.94, 81.88, 81.75, 79.30, 68.76, 46.24, 27.72

and 25.81 ppm. Low resolution ESI-MS [M+H] 419.1 HRMS (ESI+) calcd for $C_{14}H_{19}N_4O_7S_2$ [(M+H)+] 419.0695 found 419.0679

5´-O-[N-(3-Indole propionic acid)sulfamoyl]-2-Aminothieno[3,4-d]pyrimidine G mimic nucleoside (8)

To an ice cold stirred solution of **6** (20 mg, 0.072 mmol) and 22 (30.8 mg, 0.108 mmol) in DMF (0.2 mL) was added DBU (1.1 equiv, 11.8 μl, 0.079 mmol). After stirring for 10 min the reaction mixture was brought to room temperature and stirred overnight. Next, the volatiles were evaporated under reduced pressure and the mixture was used further for next step without any purification. In the next step, the crude mixture was dissolved in 80% aqueous TFA (0.2 ml) and stirred for 30 min. The reaction mixture was evaporated to dryness (co-evaporated 1% TEA/ethanol for removing TFA) and purified using reverse phase chromatography (A-ACN, B-Water + 0.1% TEA). The eluted peak was concentrated and lyophilized to obtain the desired final product in 60% yields (16.5 mg with 1.0 equivalent of TEA). ^{1}H NMR spectrum was (DMSO-d_6): 1.10 (s, 12.0 H), 2.34 (m, 2.0 H), 2.85 (m, 9H), 3.88-3.96 (m, 4H), 5.12-5.18 (m, 2H), 6.18 (s, broad 2H), 6.94 (m, 1H), 7.07 (m, 2H), 7.29 (d, 1H), 7.48 (d, 1H), 8.16 (s, 1H), 10.48 (s, 1H) and 10.68 (s, 1H). ^{13}C-D_2O: 183.35, 135.98, 126.74, 122.48, 121.54, 118.82, 118.50, 113.93, 111.34, 82.25, 76.24, 71.01, 68.81, 46.64, 38.78, 21.15 and 8.19 ppm. Low resolution ESI-MS 550.1 HRMS (ESI+) calcd for $C_{22}H_{24}N_5O_8S_2$ [(M+H)+] 550.1066 found 550.1045

General synthesis of nucleoside phosphoramidate:

1-Ethyl-3-[3-(dimethylamino)propyl]carbodiimide hydrochloride (4.5 equiv) was added to a solution of nucleoside 5'monophosphate and L-or D-alanine methylester (5 equiv) in water (pH adjusted to 6.5 with 1N NaOH) at room temperature for 3 hour and lyophilized. The resulting solid was then purified using flash chromatography (CH_3Cl_3/MeOH/H_2O 5:3:0.5 with 0.5% NH_4OH). The desired product peak was isolated and purified using cation exchange column to exchange sodium as the counter ion. The eluent from the cation ion exchange column was again lyophilized and purified using reverse phase to get the desired final product.

2(*R*)-[Adenosyl-5′-(phosphorylamino)]-Alanine Methyl Ester (12)

Synthesized as described above. Obtained in 50% yield. The ^{1}H NMR spectrum was (DMSO-d_6): 1.15 (d, 3H), 3.72 (s, 3H), 3.99 (m, 1H), 4.22 (m, 1H), 4.57 (m, 1H), 5.75 (m, 1H), 5.90 (d, 1H), 7.25 (s, 2H), 8.15 (s, 1H) and 8.44 (s, 1H). ^{32}P-DMSO-d_6: 3.84 ^{13}C-DMSO-d_6: 176.47, 156.43, 153.05, 150.17, 139.85, 119.24, 87.25, 84.82, 84.77, 74.73, 71.84, 64.14, 51.82, 50.69, and 21.50 ppm. Low resolution ESI-MS [M-H] 431.3 HRMS (ESI+) calcd for $C_{14}H_{21}N_6O_8P$ [(M+H)+] 433.1237 found 433.1220

2(*S*)-[Adenosyl-5′-(phosphorylamino)]-Alanine) Methyl Ester (13)

Synthesized as described above. Obtained in 30% yield. The ^{1}H NMR spectrum was (DMSO-d_6): 1.17 (d, 3H), 3.52 (s, 3H), 3.72 (m, 3H), 3.99 (S, 1H), 4.21 (s, 1H), 4.57 (m, 1H), 5.67 (d, 1H), 5.89 (d, 1H), 7.25 (s, 2H), 8.16 (s, 1H) and 8.44 (s, 1H). ^{32}P-DMSO-d_6:

3.85 ^{13}C- DMSO-d_6: 176.49, 156.43, 153.02, 150.13, 139.84, 119.24, 87.33, 84.73, 74.80, 71.77, 64.03, 51.76, 50.68, and 21.57 ppm. Low resolution ESI-MS [M-H] 431.3 HRMS (ESI+) calcd for $C_{14}H_{21}N_6O_8P$ [(M+H)+] 433.1237 found 433.1220

References:

1. Guang, W.; Wang, H.; Su, T.; Weinstein, I. B.; Wang, J. B., Role of mPKCI, a novel mu-opioid receptor interactive protein, in receptor desensitization, phosphorylation, and morphine-induced analgesia. *Mol Pharmacol* **2004,** *66* (5), 1285-92.
2. Barbier, E.; Zapata, A.; Oh, E.; Liu, Q.; Zhu, F.; Undie, A.; Shippenberg, T.; Wang, J. B., Supersensitivity to amphetamine in protein kinase-C interacting protein/HINT1 knockout mice. *Neuropsychopharmacology* **2007,** *32* (8), 1774-82.
3. Jackson, K. J.; Wang, J. B.; Barbier, E.; Damaj, M. I.; Chen, X., The histidine triad nucleotide binding 1 protein is involved in nicotine reward and physical nicotine withdrawal in mice. *Neurosci Lett* **2013,** *550*, 129-33.
4. Chou, T. F.; Baraniak, J.; Kaczmarek, R.; Zhou, X.; Cheng, J.; Ghosh, B.; Wagner, C. R., Phosphoramidate pronucleotides: a comparison of the phosphoramidase substrate specificity of human and Escherichia coli histidine triad nucleotide binding proteins. *Mol Pharm* **2007,** *4* (2), 208-17.
5. Murakami, E.; Tolstykh, T.; Bao, H.; Niu, C.; Steuer, H. M.; Bao, D.; Chang, W.; Espiritu, C.; Bansal, S.; Lam, A. M.; Otto, M. J.; Sofia, M. J.; Furman, P. A., Mechanism of activation of PSI-7851 and its diastereoisomer PSI-7977. *J Biol Chem* **2010,** *285* (45), 34337-47.
6. Drontle, D. P.; Wagner, C. R., Designing a pronucleotide stratagem: lessons from amino acid phosphoramidates of anticancer and antiviral pyrimidines. *Mini Rev Med Chem* **2004,** *4* (4), 409-19.
7. Li, S.; Jia, Y.; Jacobson, B.; McCauley, J.; Kratzke, R.; Bitterman, P. B.; Wagner, C. R., Treatment of breast and lung cancer cells with a N-7 benzyl guanosine monophosphate tryptamine phosphoramidate pronucleotide (4Ei-1) results in chemosensitization to gemcitabine and induced eIF4E proteasomal degradation. *Mol Pharm* **2013,** *10* (2), 523-31.
8. Abraham, T. W.; Kalman, T. I.; McIntee, E. J.; Wagner, C. R., Synthesis and biological activity of aromatic amino acid phosphoramidates of 5-fluoro-2'-deoxyuridine and 1-beta-arabinofuranosylcytosine: evidence of phosphoramidase activity. *J Med Chem* **1996,** *39* (23), 4569-75.
9. Chou, T. F.; Wagner, C. R., Lysyl-tRNA synthetase-generated lysyl-adenylate is a substrate for histidine triad nucleotide binding proteins. *J Biol Chem* **2007,** *282* (7), 4719-27.
10. Rodríguez-Muñoz, M.; Sánchez-Blázquez, P.; Vicente-Sánchez, A.; Berrocoso, E.; Garzón, J., The mu-opioid receptor and the NMDA receptor associate in PAG neurons: implications in pain control. *Neuropsychopharmacology* **2012,** *37* (2), 338-49.
11. Rodríguez-Muñoz, M.; Sánchez-Blázquez, P.; Vicente-Sánchez, A.; Bailón, C.; Martín-Aznar, B.; Garzón, J., The histidine triad nucleotide-binding protein 1 supports mu-opioid receptor-glutamate NMDA receptor cross-regulation. *Cell Mol Life Sci* **2011,** *68* (17), 2933-49.

12. Garzón, J.; Rodríguez-Muñoz, M.; Sánchez-Blázquez, P., Direct association of Mu-opioid and NMDA glutamate receptors supports their cross-regulation: molecular implications for opioid tolerance. *Curr Drug Abuse Rev* **2012,** *5* (3), 199-226.
13. Zimoń, M.; Baets, J.; Almeida-Souza, L.; De Vriendt, E.; Nikodinovic, J.; Parman, Y.; Battaloğlu, E.; Matur, Z.; Guergueltcheva, V.; Tournev, I.; Auer-Grumbach, M.; De Rijk, P.; Petersen, B. S.; Müller, T.; Fransen, E.; Van Damme, P.; Löscher, W. N.; Barišić, N.; Mitrovic, Z.; Previtali, S. C.; Topaloğlu, H.; Bernert, G.; Beleza-Meireles, A.; Todorovic, S.; Savic-Pavicevic, D.; Ishpekova, B.; Lechner, S.; Peeters, K.; Ooms, T.; Hahn, A. F.; Züchner, S.; Timmerman, V.; Van Dijck, P.; Rasic, V. M.; Janecke, A. R.; De Jonghe, P.; Jordanova, A., Loss-of-function mutations in HINT1 cause axonal neuropathy with neuromyotonia. *Nat Genet* **2012,** *44* (10), 1080-3.
14. Varadarajulu, J.; Schmitt, A.; Falkai, P.; Alsaif, M.; Turck, C. W.; Martins-de-Souza, D., Differential expression of HINT1 in schizophrenia brain tissue. *Eur Arch Psychiatry Clin Neurosci* **2012,** *262* (2), 167-72.
15. Shah, R.; Strom, A.; Zhou, A.; Maize, K. M.; Finzel, B. C.; Wagner, C. R., Design, Synthesis, and Characterization of Sulfamide and Sulfamate Nucleotidomimetic Inhibitors of hHint1. *ACS Med Chem Lett* **2016,** *7* (8), 780-4.
16. Garzón, J.; Herrero-Labrador, R.; Rodríguez-Muñoz, M.; Shah, R.; Vicente-Sánchez, A.; Wagner, C. R.; Sánchez-Blázquez, P., HINT1 protein: a new therapeutic target to enhance opioid antinociception and block mechanical allodynia. *Neuropharmacology* **2015,** *89*, 412-23.
17. Kobayashi, H.; Ogawa, M.; Alford, R.; Choyke, P. L.; Urano, Y., New strategies for fluorescent probe design in medical diagnostic imaging. *Chem Rev* **2010,** *110* (5), 2620-40.
18. Zhuang, Y. D.; Chiang, P. Y.; Wang, C. W.; Tan, K. T., Environment-sensitive fluorescent turn-on probes targeting hydrophobic ligand-binding domains for selective protein detection. *Angew Chem Int Ed Engl* **2013,** *52* (31), 8124-8.
19. Wang, K.; Tang, Z.; Yang, C. J.; Kim, Y.; Fang, X.; Li, W.; Wu, Y.; Medley, C. D.; Cao, Z.; Li, J.; Colon, P.; Lin, H.; Tan, W., Molecular engineering of DNA: molecular beacons. *Angew Chem Int Ed Engl* **2009,** *48* (5), 856-70.
20. Shin, D.; Sinkeldam, R. W.; Tor, Y., Emissive RNA alphabet. *J Am Chem Soc* **2011,** *133* (38), 14912-5.
21. Spencer, R. D.; Weber, G.; Tolman, G. L.; Barrio, J. R.; Leonard, N. J., Species responsible for the fluorescence of 1:N6-ethenoadenosine. *Eur J Biochem* **1974,** *45* (2), 425-9.
22. Mansoor, S. E.; Dewitt, M. A.; Farrens, D. L., Distance mapping in proteins using fluorescence spectroscopy: the tryptophan-induced quenching (TrIQ) method. *Biochemistry* **2010,** *49* (45), 9722-31.
23. Li, B.; Lin, S. X., Fluorescence-energy transfer in human estradiol 17 beta-dehydrogenase-NADPH complex and studies on the coenzyme binding,. *Eur J Biochem* **1996,** *235* (1-2), 180-6.

24. Bai, G.; Feng, B.; Wang, J. B.; Pozharski, E.; Shapiro, M., Studies on ligand binding to histidine triad nucleotide binding protein 1. *Bioorg Med Chem* **2010,** *18* (18), 6756-62.
25. Zhou, X.; Chou, T. F.; Aubol, B. E.; Park, C. J.; Wolfenden, R.; Adams, J.; Wagner, C. R., Kinetic mechanism of human histidine triad nucleotide binding protein 1. *Biochemistry* **2013,** *52* (20), 3588-600.
26. Xie, Y.; Maxson, T.; Tor, Y., Fluorescent ribonucleoside as a FRET acceptor for tryptophan in native proteins. *J Am Chem Soc* **2010,** *132* (34), 11896-7.
27. Chou, T. F.; Tikh, I. B.; Horta, B. A.; Ghosh, B.; De Alencastro, R. B.; Wagner, C. R., Engineered monomeric human histidine triad nucleotide-binding protein 1 hydrolyzes fluorogenic acyl-adenylate and lysyl-tRNA synthetase-generated lysyl-adenylate. *J Biol Chem* **2007,** *282* (20), 15137-47.
28. Simeonov, A.; Jadhav, A.; Thomas, C. J.; Wang, Y.; Huang, R.; Southall, N. T.; Shinn, P.; Smith, J.; Austin, C. P.; Auld, D. S.; Inglese, J., Fluorescence spectroscopic profiling of compound libraries. *J Med Chem* **2008,** *51* (8), 2363-71.
29. Pritz, S.; Doering, K.; Woelcke, J.; Hassiepen, U., Fluorescence lifetime assays: current advances and applications in drug discovery. *Expert Opin Drug Discov* **2011,** *6* (6), 663-70.
30. Petersen, K. J.; Peterson, K. C.; Muretta, J. M.; Higgins, S. E.; Gillispie, G. D.; Thomas, D. D., Fluorescence lifetime plate reader: resolution and precision meet high-throughput. *Rev Sci Instrum* **2014,** *85* (11), 113101.
31. Laššuthová, P.; Brožková, D.; Krůtová, M.; Neupauerová, J.; Haberlová, J.; Mazanec, R.; Dvořáčková, N.; Goldenberg, Z.; Seeman, P., Mutations in HINT1 are one of the most frequent causes of hereditary neuropathy among Czech patients and neuromyotonia is rather an underdiagnosed symptom. *Neurogenetics* **2015,** *16* (1), 43-54.
32. Fernandez, I.; Araç, D.; Ubach, J.; Gerber, S. H.; Shin, O.; Gao, Y.; Anderson, R. G.; Südhof, T. C.; Rizo, J., Three-dimensional structure of the synaptotagmin 1 C2B-domain: synaptotagmin 1 as a phospholipid binding machine. *Neuron* **2001,** *32* (6), 1057-69.

Chapter 6

Structure and Functional Characterization of Human Histidine Triad Nucleotide Binding Protein 1 mutations associated with Inherited Axonal Neuropathy with Neuromyotonia

INTRODUCTION:

Inherited peripheral neuropathies (IPNs) are a group of neurodegenerative disorders that primarily develop due to the damage of the peripheral nervous system (PNS). IPNs are classified based on their pathology (axonal or demyelinating), neurophysiology (including motor or sensory functions), and mode of inheritance.[1, 2] Most of the genetic mutations linked to peripheral neuropathies are associated with the maintenance of Schwann cells and components of the axons in the peripheral nervous system.[3] Defects in such components result in the alteration of nerve conduction velocity in the PNS. Although sensory nerves are mainly affected, the more prominent symptoms of IPNs are associated with motor difficulties such as steppage gait, pes cavus, sensory loss in feet and lower calves and atrophy in hands. Because of these prominent features, the diagnosis of IPNs mainly includes electromyography and nerve conduction velocities.[4]

Currently, more than fifty different genes associated with the various forms of hereditary motor and sensory neuropathies have been identified. The most common types are autosomal dominant inherited demyelinating (Charcot Marie Tooth 1 [CMT1], 40% to 50% of all IPNs) and autosomal dominant axonal (CMT2, 10% to 50%) neuropathies. One rare form is autosomal recessive axonal neuropathy with neuromyotonia. Patients diagnosed with neuromyotonia mainly exhibit persistent muscle contraction after voluntary movement, resulting from the hyperexcitability of the peripheral nervous system and not the muscle itself. Genetic mutations in KCNA1, which encodes a voltage-gated potassium channel, have been diagnosed and associated with the peripheral nerve excitability disorders. [5, 6]

Recently, genetic mutations in human Histidine triad nucleotide-binding protein 1 (hHint1) have been identified in clinical patients suffering from axonal peripheral neuropathy with neuromyotonia.[7-10] Human Hint1 belongs to the histidine triad (HIT) superfamily characterized by their conserved sequence motif, His-X-His-X-His-XX, where X is a hydrophobic residue. Human Hint1 exists as a homodimer and possesses nucleoside phosphoramidase and acyl-AMP hydrolase activity.[11] In total, eight mutations including both homo and heterozygous hHint1 variants were identified from a group of 33 families. These mutations are recessive in nature meaning mutant copies from each parent are necessary to develop the pathophysiology. **Table 1** includes the list of the mutations and the number of families affected. Most of these patients exhibited symptoms associated with motor difficulties such as gait impairment and myotonia in the hands and feet.

The studies also demonstrated that single copies of each mutant protein were unable to rescue the growth of a yeast strain devoid of Hint1 ortholog under restrictive conditions[7]. The authors of this work concluded that loss of the function was primarily responsible for the observed phenotype. Surprisingly, a recent study failed to produce the pathophysiology of axonal degeneration or motor deficit in Hint1 KO mice.[12] This clearly indicates that the loss of Hint1 function alone could not only account for the observed pathophysiology in clinical patients. One possible explanation might be that these mutations exhibit dual gain-of and loss-of-function properties. Hence, a detailed biochemical characterization of these mutations will help in developing better mice models to understand the pathophysiology of neuropathy with neuromyotonia. In this

Table 1: hHint1 mutations identified from patients suffering from autosomal recessive peripheral neuropathy with neuromyotonia and their symptoms

Alterations		Number of families	Symptoms
Amino acid change	**Nucleotide change**		
p.[Arg37pro] + p.[Arg37pro]	c.[110G>C] + c.[110G>C]	23	GI, myotonia hands, foot deformities
p.[Arg37pro] + p.[Cys84R]	c.[110G>C] + c.[250T>C]	1	GI, stiffness legs
p.[Arg37pro] + p.[Gly89V]	c.[110G>C] + c.[266G>T]	2	GI, stiffness legs, GI, stiffness legs
p.[Arg37pro] + p.[His112Asn]	c.[110G>C] + c.[334C>A]	1	GI
p.[His51Arg] + p.[C84R]	c.[152A>G] + c.[250T>C]	1	Cramp, weakness, thumbs
p.[Gln62*] + p.[Gly93Asp]	c.[182C>T] + c.[278G>A]	1	GI, muscle stiffness
p.[His112Asn] + p.[His112Asn]	c.[334C>A] + c.[334C>A]	3	GI, falling
p.[Trp123*] + p.[Trp123*]	c.[368G>A] + c.[368G>A]	1	GI
Total 8 mutations		33	

study, we report *in vitro* biochemical characterization of the hHint1 mutations associated with axonal neuropathy with neuromyotonia.

RESULTS

Expression and purification of hHint1 mutations associated with peripheral neuropathy

Six mutations of hHint1 associated with peripheral neuropathy were studied (Figure 1). Site-directed mutagenesis was used to insert point mutations (C84R, G89V, R37P, W123*, H112N, and G93D) and most of the constructs were expressed in the soluble fractions with the molecular weight of 55 kDa as per the SDS page analysis (**Figure 1**). Mutant H51R showed reduced expression and stability and could not be purified in a non-aggregated form (data not shown). The Q62* truncation mutation would lack a well-formed hHint1 active site (**Figure 2**); therefore we chose not to express and perform characterization on the Q62* mutant. Previously, we developed a purification protocol using affinity chromatography by taking advantage of Hint proteins' ability to bind nucleoside monophosphates such as adenosine monophosphate (AMP). However, mutations in hHint1 could alter the ability of the mutants to bind AMP. Hence, we designed a maltose binding protein (MBP) fusion construct encoding an N-terminal His_6 tag to purify hHint1 mutants using Ni-NTA affinity column (**Figure 2**). The MBP fusion may aid in folding and solubility of the mutant proteins. The fusion plasmid encodes a TEV protease cleavage site that can be exploited to separate hHint1 from MBP. Next, the fusion proteins were purified on the Ni-NTA resin, dialyzed and stored in -80 °C before further purification on the size exclusion chromatography (SEC). The fusion protein was

treated with TEV protease under dialysis, and the MBP was separated using Ni-NTA resin before characterization. The final yields of all the constructs ranged from 5-10 mg per liter of *E.coli* culture.

Size Exclusion Chromatography analysis of hHint1 mutants

Based on the known structure of WT hHint1, the mutations associated with peripheral neuropathy are scattered throughout the hHint1 fold. Many are in proximity to the dimeric interface or active site, though some are simply surface residues (**Figure 3**). Because some of the known mutations affect resides at the dimeric interface, we investigated the impact of hHint1 mutations on homodimer stability. We used a Superdex-200 (SEC) column in line with the UV-absorption detector to monitor the apparent elution time and molecular weight of the purified proteins. The resolution limit of the column precludes separation dimeric (28 kDa) and monomeric (14 kDa) species. We chose instead to investigate the MBP fusion proteins with SEC to determine the molecular weight of the mutant proteins (55 kDa (monomer MBP-hHint1) or 110 kDa (dimer)) in order to circumvent the resolution limit of the column. As shown in **Figure 3**, a fusion of Dihydrofolate Reductase (DHFR-DHFR) with a molecular weight of 36 kDa elutes at approximately 34 minutes and the wild-type dimeric MBP-hHint1 fusion protein at 28 minutes. Both proteins were used as controls for the molecular weight determination of the mutant proteins. The retention time of the mutants H112N, C84R, and G89V was identical to the wild-type protein indicating they exist as dimers in solution (**Figure 4**), while the mutations R37P, G93D and W123* elute at approximately

Figure 1. SDS-PAGE gel analysis of the expression and purity of hHint1G93D_MBP. Lane 1 is the standard protein ladder with black arrow indicating the molecular weight standard of 50 kDa. Lanes 2 and 3 are the *E.coli* cell lysate and the flow through of the lysate loaded onto the Ni-NTA column, respectively. Lanes 3-12 illustrate the wash and the fractions collected after elution of the protein from the column using an elution buffer containing high imidazole (250 mM).

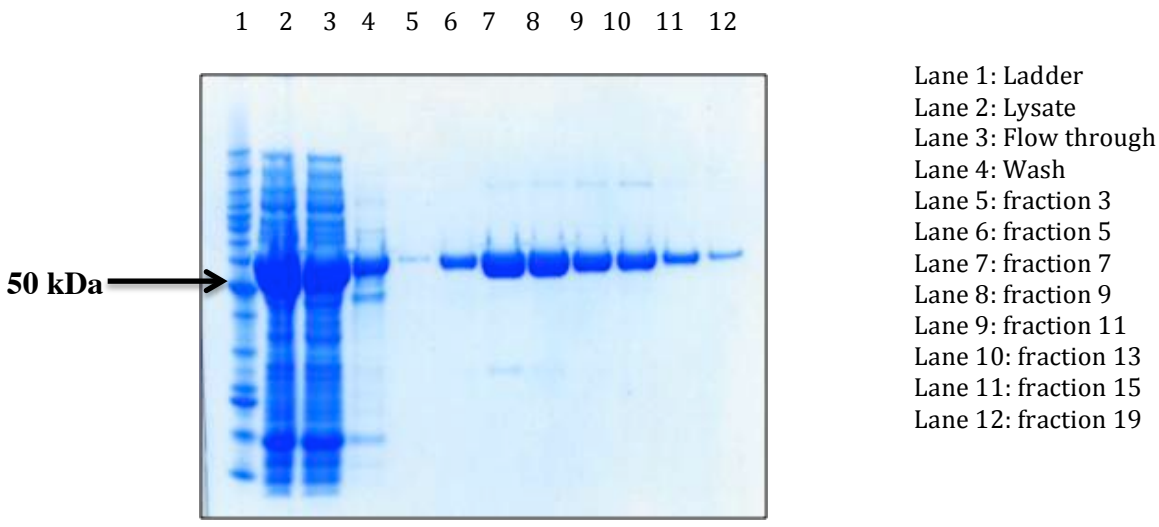

Figure 2: (Top) Primary amino acid sequence of Human Hint1. Highlighted in blue are the residues associated with peripheral neuropathy in clinical patients. Residues in the red are the Histidines in the active site involved in the catalysis of hHint1. (Bottom) Construction of the plasmid encoding Hexa Histidine tag along with maltose binding protein at the N-terminus of the fusion hHint1 protein. The fusion protein contains a TEV linker sequence to cleave and separate hHint1 protein from the MBP protein.

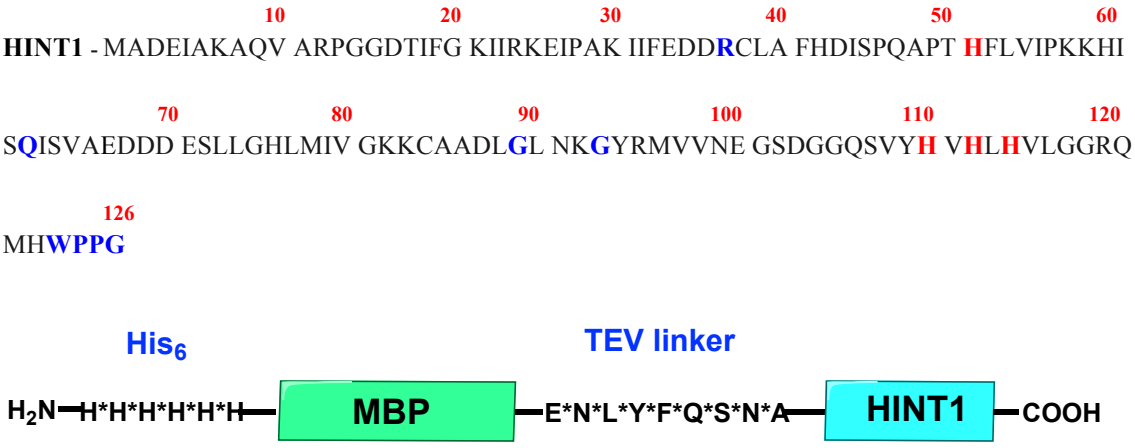

Figure 3: Structure mapping of the location of the hHint1 mutations associated with peripheral neuropathy onto one monomer (green) of the wild-type protein. The dimeric interface is stabilized by a long alpha helix connected with a loop to a β-strand of each monomer subunit. The G93D mutation resides in this loop, while the C84R and G89V mutations are located on the long alpha helix. The H51R, H112N and W123* mutations are located in the active site of hHint1. C-terminal residues including residues 123-126 form a dimer-stabilizing crossover, but residues 124-126 are absent in the W123* mutation.

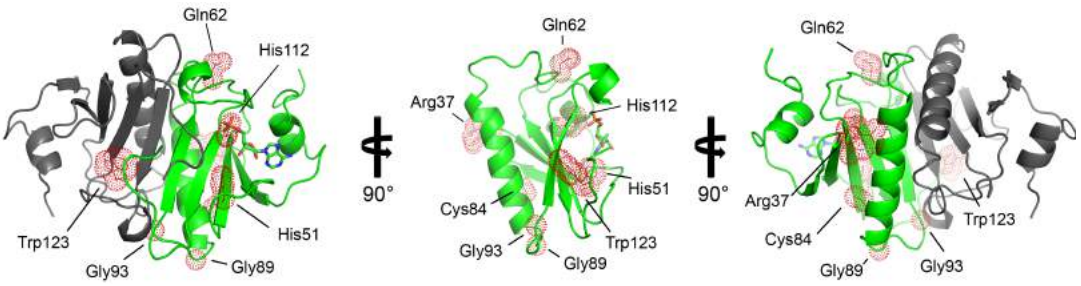

Figure 4: Dimeric hHint1 mutants: Size exclusion chromatography analysis of the hydrodynamic radius of mutant hHint1 proteins expressed as a maltose binding protein (MBP) fusion. Red trace and elution at 33 minutes is the fusion of dihydrofolate reductase with the molecular weight of 34 kDa. Black trace and elution at 28 minutes is the fusion of wild type MBP-hHint1 fusion protein with the molecular weight of 110 kDa as dimer. The mutant proteins H112N, G89V and C84R in green, pink and blue traces eluted around 28 minutes aligned with the molecular weight of the wild type protein as a dimer.

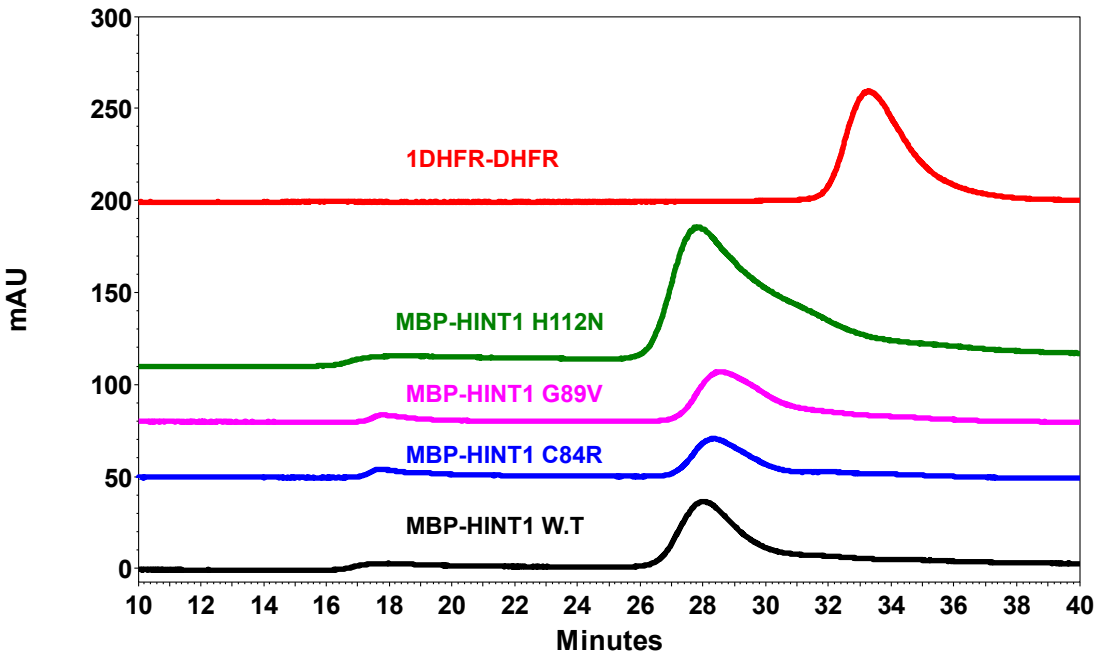

Figure 5: Monomeric hHint1 mutants: Size exclusion chromatography analysis of the hydrodynamic radius of mutant hHint1 proteins expressed as a maltose binding protein (MBP) fusion. Red trace and elution at 33 minutes is the fusion of dihydrofolate reductase with the molecular weight of 34 kDa. Black trace and elution at 28 minutes is the fusion of wild type MBP-hHint1 fusion protein with the molecular weight of 110 kDa as dimer. The mutant proteins R37P, G93D and W123* in blue, brown and violet traces eluted around 33 minutes aligned with the molecular weight of a monomer hHint1.

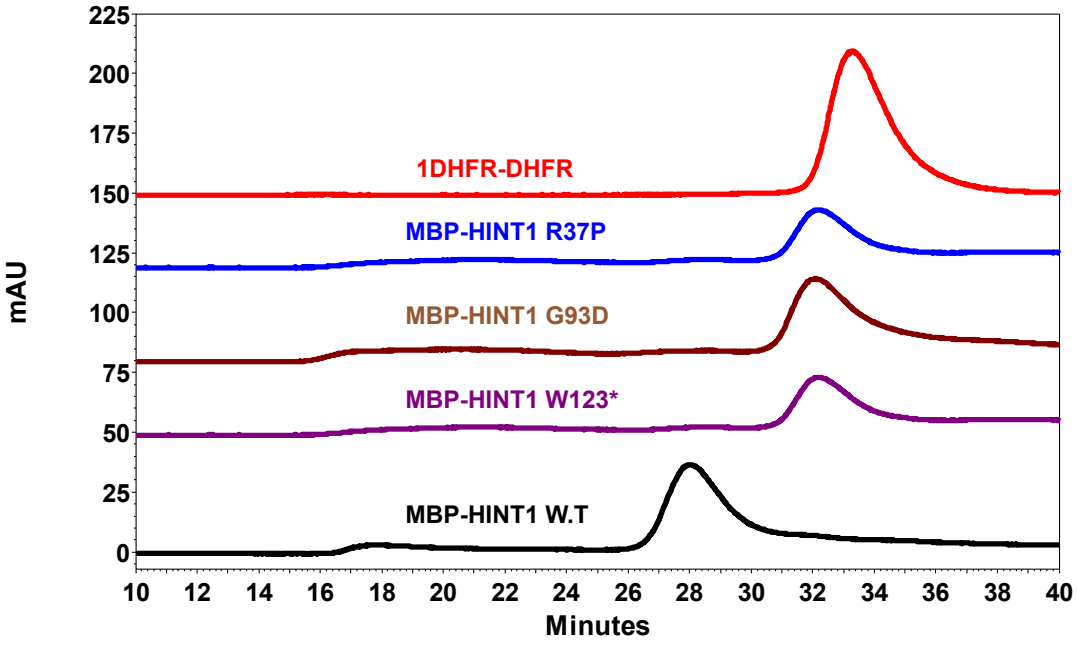

Figure 6. Size exclusion chromatography analysis of the hydrodynamic radius of mutant hHint1 proteins expressed as maltose binding protein (MBP) fusions. Blue trace and elution at 28 minutes is the fusion of wild type MBP-hHint1 fusion protein with the molecular weight of 110 kDa as dimer. The mutant proteins (A) W123A (B) P124A, (C) P125A and (D) P126A in purple, pink, dark green and light green traces eluted around 33 minutes aligned with the molecular weight of a monomer hHint1.

A) hHint1_W123A

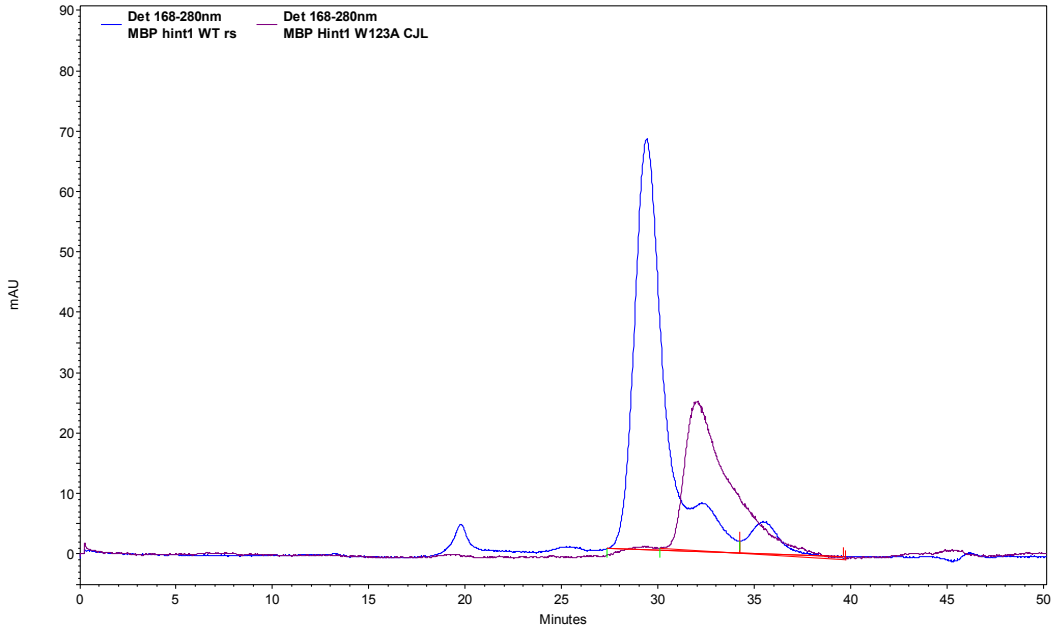

B) hHint1_P124A

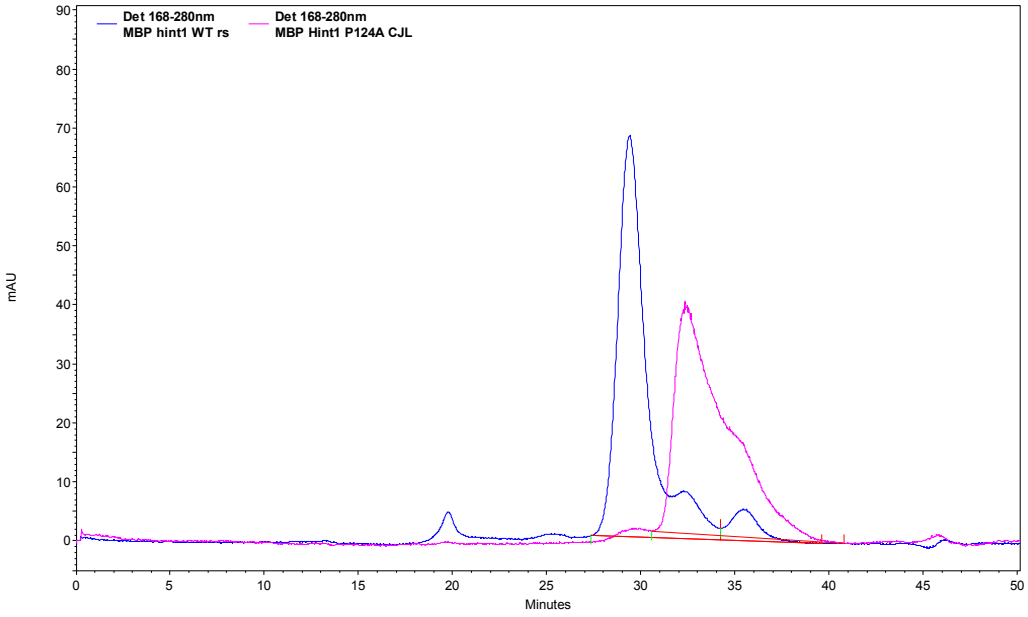

C) hHint1_P125A

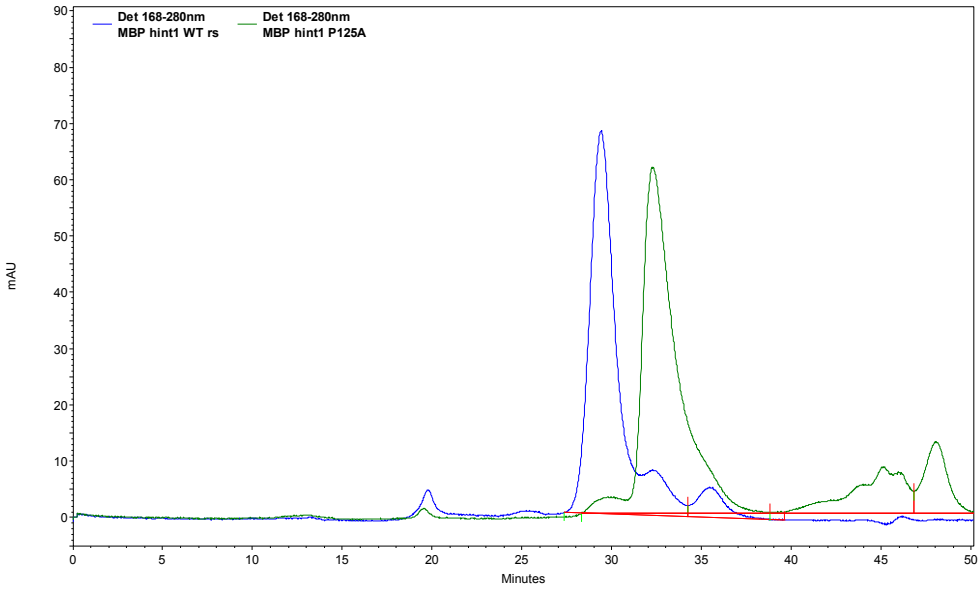

D) hHint1_G126A

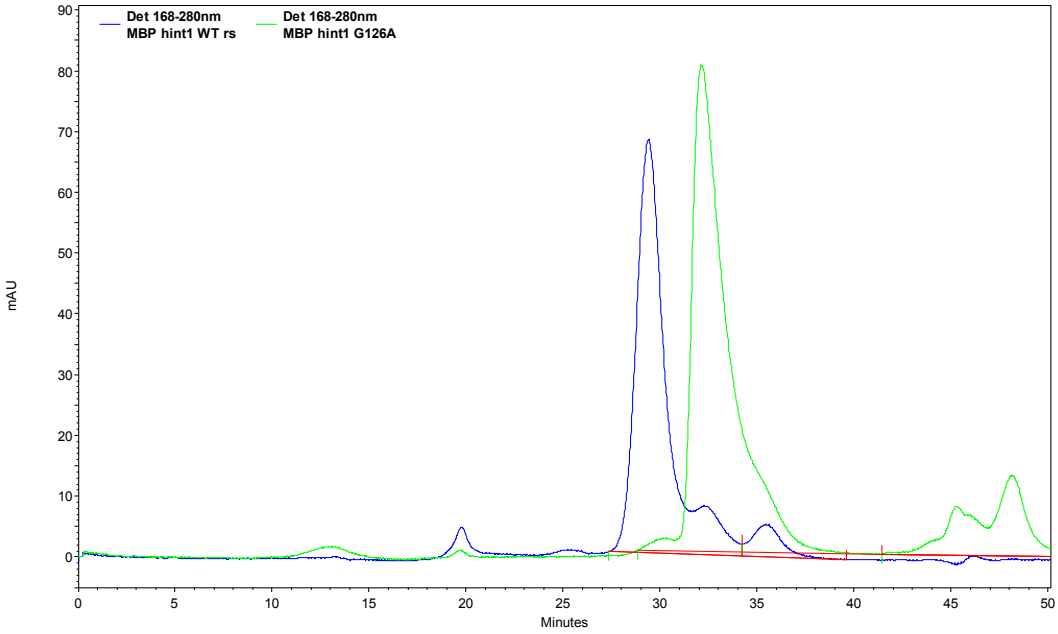

33 minutes indicating they exist as monomers in solution (**Figure 5**). Our result with W123* mutant was intriguing; deletion of the four C-terminal amino acids prevents dimer formation. Interestingly, a brief alanine scan performed on these four residues resulted in consistently monomeric hHint1 proteins (**Figure 6A-D**).

Secondary structure analysis

Circular dichroism (CD) spectra of the wild-type and mutant proteins were collected in the far-UV region (190-260 nm) to assess the potential impact of mutations on secondary structure. As seen in **Figure 7A**, mean residual ellipticity (MRE) traces of the dimeric mutant proteins (C84R, H112N, and G89V) superimpose well on the wild-type protein suggesting identical composition in alpha-helical and beta secondary structure elements. In contrast, the monomeric R37P (blue trace, **Figure 7B**) showed a partial loss of secondary structure compare to wild type (red trace). The near UV-absorption was reduced in the R37P mutant indicating incorrect or improper folding. Interestingly, the other monomeric mutants G93D and W123* were nearly identical to each other with only minimal differences in the 200-210 nm region, suggesting minor changes in their conformations.

Characterization of a catalytically inactive hHint1 H112N mutant.

A mutated enzyme was prepared wherein the active site nucleophile, His112, was replaced with isosteric but catalytically inactive asparagine (hHint1 H112N).[36] The H112N mutant enzyme was expressed in *E. coli* and purified using procedures similar to

Figure 7: CD spectroscopy. CD spectra of the wild type and mutants of hHint1 were collected in the far-UV region from 190 to 260 nm at 23 °C with protein concentration of 10-15 μM. The results are expressed as the mean residue ellipticities. A) hHint1 (red trace), G89V (black trace), C84R (yellow) and H112N (green) were found to nearly identical to wild type hHint1. These mutants were found to be dimeric in structure. B) hHint1 (red trace), G93D (yellow) and W123* (brown) were found to be slightly different in the region compared to the 190- to 210-nm region. In contrast, R37P mutant (purple) was found to have lost secondary structure.

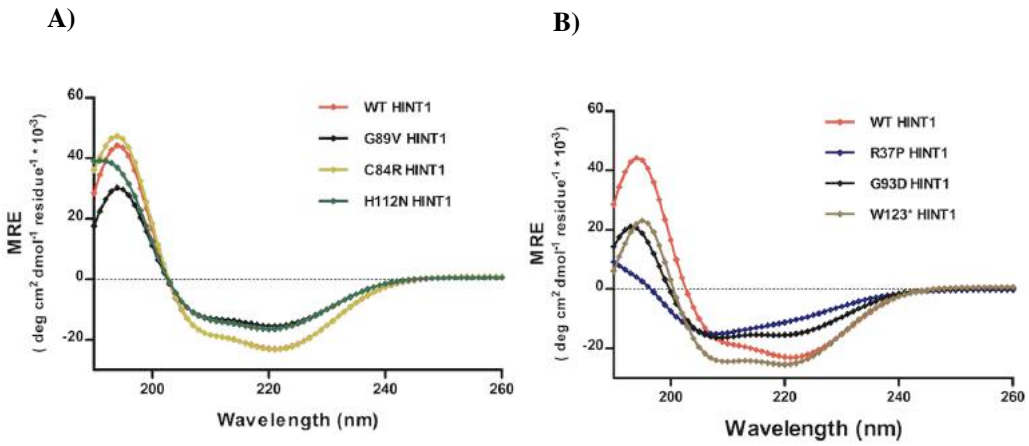

those applicable to the wild-type protein. However, crystallization and crystallography revealed that the mutant enzyme co-purified with bound cellular AMP, which extensive dialysis could not remove (data not shown). Thus, to remove the contaminating nucleotide, it was necessary to denature and refold the protein. The need for a different purification protocol suggested that the affinity of H112N for nucleotides might be increased, so isothermal titration calorimetry (ITC) was used to determine the binding affinity of AMP in both the wild-type and H112N mutant enzymes. The K_D of the mutant enzyme for AMP was determined to be 385 ± 5 nM, 150-fold tighter binding than that determined for the wild-type enzyme (59 ± 7 μM). In addition, the K_D of TrpAMP was measured using ITC in H112N; the affinity for TrpAMP was found to be (78 ± 7 nM)(**Table 2**).

Following refolding, *apo* H112N could be crystallized under conditions similar to the wild-type hHint1. The substitution of the nucleophilic histidine for asparagine does not significantly change the active site architecture, and only a slight difference in the position of residue 112 is observed, possibly to make a hydrogen bond with His114, when compared to the wild-type protein.

Steady-state kinetic characterization of hHint1 mutations

To evaluate the impact of the mutations on hHint1 catalytic activity, we performed steady-state enzyme kinetics using tryptamine adenosine phosphoramidate substrate (TpAd) in a previously described fluorogenic assay.[11] Both the dimeric mutants C84R and G89V exhibited the same specificity and activity compared to wild-type enzyme (**Table 3**). Interestingly, the Michaelis-Menten kinetic constant (K_m) increased 10-40 fold

Table 2: Isothermal titration calorimetry results. Values are reported from triplicate (AMP and TrpAMP) measurements as mean ± S.D.

Compound	Protein	K_D (μM)
AMP	Wild-type	59 ± 7
AMP	H112N	0.385 ± 0.005
TrpAMP	H112N	0.078 ± 0.007

Table 3: Comparison of steady-state kinetic parameters of hydrolysis of a fluorogenic phosphoramidate substrate by Hint1 mutants

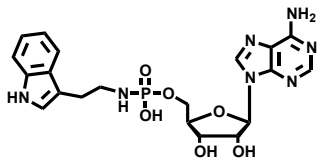

TpAd

Mutation	K_m (μM)	K_{cat} (s^{-1})	K_{cat}/K_m x 10^6 ($M^{-1}s^{-1}$)	Ratio K_{cat}/K_m
W.T	0.106 ± 0.01	2.36 ± 0.27	22.26 ± 3.78	1.0
C84R	0.157 ± 0.01	2.84 ± 0.10	18.23 ± 1.63	0.82
G89V	0.137 ± 0.03	2.87 ± 0.08	22.02 ± 4.89	0.99
W123*	1.0 ± 0.35	0.038 ± 0.01	0.038 ± 0.068	0.0017
G93D	4.06 ± 0.26	0.017 ± 0.01	0.004 ± 0.001	0.00018
R37P	ND	ND	ND	ND
I44F	1.14 ± 0.13	0.82 ± 0.12	0.64 ± 0.086	0.029
D43N	5.14 ± 0.21	5.70 ± 0.08	1.11 ± 0.01	0.050

for the monomeric mutants indicating the significant negative impact of breaking the dimeric interface on the ability of mutants to bind the substrate and possibly to bind nucleoside monophosphate products. We also observed a 50-150 fold decrease in the catalytic turnover rate (K_{cat}) for hydrolysis in the monomeric mutants. Moreover, the overall specificity for TpAd was reduced up to 5000 fold in the monomeric mutants when compared to the wild type enzyme. The homodimeric structure is critical to the stability of the protein, for binding to the ligand as well as for the hHint1 catalytic mechanism.

Ability of hHint1 mutations to switch-on fluorescent probes

Recently, we have designed novel fluorogenic non-natural nucleoside-based switch-on fluorescent probes to study the ability of hHint1 to bind nucleotides. The probes are non-hydrolyzable mimics of the substrate, and a conformational change required upon binding to hHint1 results in an increase of fluorescence (**Figure 8**). A separation of a quencher from the fluorophore that accompanies the conformational change results in an increase in fluorescence like that exploited in molecular beacons. These tools provide a facile means to non-covalently label and monitor the impact of mutations on the formation of enzyme-substrate (ES) complex or transition state during catalysis. The increase in the amount of fluorescence upon incubation of the probe with the monomeric mutants proteins differed from that observed with the wild-type protein, at the similar protein and probe concentrations. Consistent with the kinetic studies, both dimeric mutants (C84R and G89V) showed a similar amount of fluorescence unquenching to WT. (**Figure 8**). Meanwhile, the H112N mutant showed approximately double the

Figure 8: (**Top**) Design of the switch-on fluorescent probe that is quenched in the solution and upon binding to hHint1 leads to an increase in the fluorescence intensity. The nucleoside acyl-sulfamate chemical structure of the probe is shown on right. (**Bottom**) The impact of the mutations on the ability of hHint1 mutations associated with peripheral neuropathy to bind the nucleotidomimetic analog of the substrate as manifested in the amount of fluorescence unquenching relative to wild type.

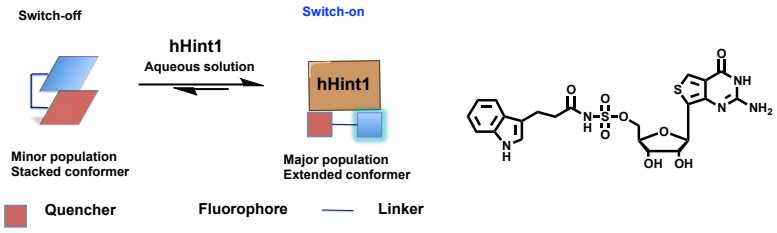

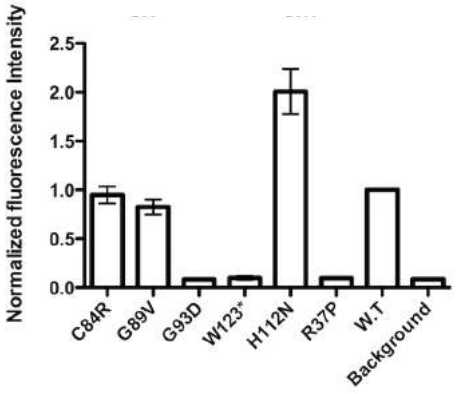

Figure 9: Structures are colored according to residue rmsd values from the corresponding residues in structure 3TW2. Lighter colors indicate smaller rmsd values, darker colors indicate larger rmsd values. (**Left**) Comparison of the overall structure of the H112N mutant (5IPB, blue shades) to the wild-type 3TW2. There is no significant difference in the overall structure due to the mutations. In this image, the N-terminus of one chain is colored red, as the rmsd value is outside of the tolerance for the color scale. The overall comparison of the C84R mutant is very similar. In both chains, the mutation sites are indicated with red dots around the alpha carbon. (**Right**) Comparison of active site residues between wild-type (3TW2, white), C84R mutant (red shades), and H112N mutant (5IPB, blue shades), all in apo form. The AMP molecule is included for reference only. There is no significant difference in the active site residues due to the mutations, though some residues, such as Ser107 and Ile44, are mobile.

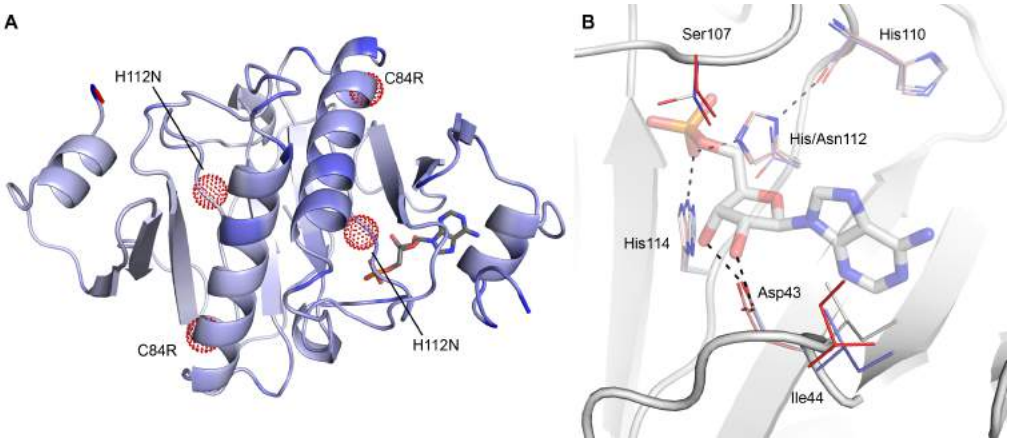

Figure 10: Mutants incapable of forming homodimers. (A) Glycine 93 of one chain is packed tightly against Glu100 of the complementary chain. Mutation of this residue to aspartic acid results in a steric clash and potential charge-charge repulsion. (B) The C-terminus of one chain participates in a significant protein-protein interaction with the complementary chain. Both Pro124 and Pro125 (chain B) participate in significant non-bonded interactions with chain A (e.g., residues Gln47, Val97, Leu116, and Met121) and their rigidity results in superior shape complementarity to the pocket in chain A. The C-terminal carboxylate (chain B) also forms a salt bridge with Arg119 (chain A), and it can hydrogen bond with His112 N (chain A). Pro125 O (chain B) may hydrogen bond with Arg95 (chain A). Hydrogen bonds are shown as dashed black lines.

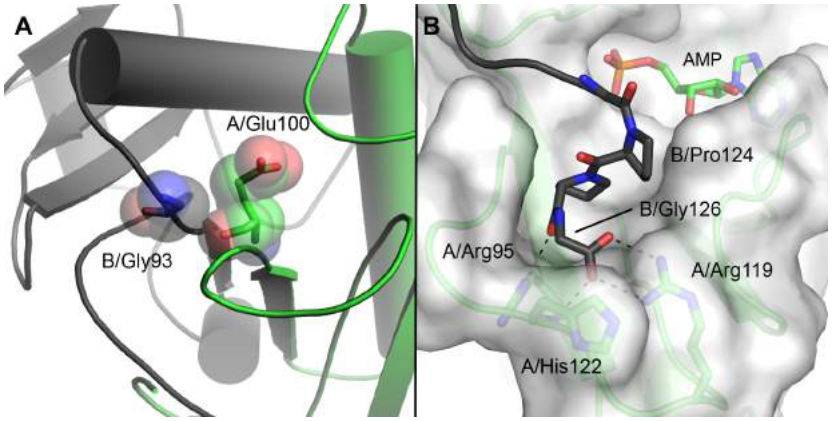

fluorescence of the wild type. This is consistent with the previously observed increase in affinity of this mutant for nucleoside monophosphates. The monomeric mutants did not exhibit any increase in fluorescence when compared to the background fluorescence of the probe in the absence of protein. These results further support our observations that monomeric mutants lose their ability to bind nucleoside monophosphate (NMPs) and substrates.

X-ray crystal structure analysis of the hHint1 mutations

The results from our study clearly indicated that not all mutations result in the loss of the catalytic activity. Both C84R and G89V were found to be catalytically similar to the wild type protein in our biochemical studies. It is possible the mutations might alter the conformation in the structure of the protein without significantly altering the catalytic activity, which might be account for neuropathy in ways unrelated to catalysis. Hence, we obtained a high-resolution (1.1 Å) x-ray crystal structure of the C84R mutant for analysis and compared it with the previously reported hHint1_H112N (5IPB) and wild-type [ref 3tw2]. We have demonstrated that H112N binds NMPs with high affinity when compared to the wild-type structure. In both H112N and C84R mutants, the overall structure is identical to the wild-type protein (**Figure 9A**). The active sites of H112N and C84R, too, are essentially the same as the wild-type protein, with the active site histidines having very low rmsds to the corresponding residues in the wild-type structure. Some residues that participate in ligand recognition are flexible in the absence of a ligand. (**Figure 9B**).

Mapping structural features that are critical for the molecular recognition of ligands by hHint1

The active site of hHint1 consists of a nucleoside-binding motif and previous ^{1}H-^{15}N HSQC ligand titration experiment indicated that Ile44 in the foreground of the active site is critical for a stacking interaction and for molecular recognition of the nucleobase.[13] Another key residue is Asp43, which plays a significant role in the molecular recognition of the 2′- and 3′-OH groups of the ribose sugar with hydrogen-bonding interactions (**Figure 9**). We wanted to investigate the impact of point mutations on these residues on the catalytic activity of hHint1, as we believe that Ile44 acts as a thumb to clamp the binding of the nucleobase in the hydrophobic pocket (**Figure 9**). To accomplish this, we substituted a bulkier amino acid such as phenylalanine or tryptophan at position 44. Upon mutating the residue to phenylalanine (I44F), we observed that it decreased the K_m approximately tenfold and K_{cat} by 2 to 3 fold. A 24-fold decrease in the overall specificity was found for the mutants compared to the wild-type. Next, we made a mutant where the negatively charged aspartate residue (Asp43) was mutated to a neutral asparagine (D43N). We observed that this mutation resulted in a 50-fold decrease in K_m and a 2 to 3-fold increase in the catalytic turnover rates.

Discussion

Human Hint1 is a homodimeric protein, and the enzymatic active site couples the cross talk of the GPCRs and NMDARs [14]. Neuropharmacological inhibition of hHint1 has been recently shown to increase opioid analgesia and prevents as well as rescues the development of tolerance in mice. The same study also showed that inhibition of hHint1

reduces neuropathic pain in animals in the absence of the opioids.[15] These results demonstrate an important role of the hHint1 active site in regulating the perception of pain. Recently, several genetic point mutations in hHint1 have been identified in patients suffering from peripheral neuropathy. One characteristic symptom associated with peripheral neuropathies is severe pain and tingling in the outer extremities such as fingers and feet.[7] In contrast, the peripheral neuropathy patients identified with hHint1 mutations mainly exhibited motor symptoms such as stiffness, gait movements, or involuntary peripheral nerve excitation. In support of this difference, a recent genetic KO studies in mice also failed to develop symptoms associated with neuromyotonia. Clearly, there is a gap in our biochemical understanding and the observed phenotype. Hence, we wanted to investigate the structural and functional consequences of neuropathy-associated hHint1 mutants.

We began by examining the impact of these mutations on the homodimeric structure of hHint1 that might be vital in the crosstalk between GPCR and NMDA receptors. Three of the six mutants (R37P, G93D, W123*) were found to correlate with the size of the 14-kDa monomer *in vitro*, while the other mutants (C84R, G89V, H112N) retained their dimeric state. The first monomeric mutation, R37P, lies in a loop connecting the first and second antiparallel β-strands that form part of the nucleoside-binding motif near the N-terminus. While the impact of the mutation is not immediately clear from the structure, our secondary structure analysis shows that this mutant is partially unfolded. The other two monomeric mutants retain their secondary structure with only minor perturbations.

The G93D mutation lies in a loop connecting an alpha helix with a beta strand at the

monomer:monomer interface in the native hHint1 dimer. If packed as in the dimer, both steric and electrostatic repulsion would result between Asp93 and the negatively charged Glu100 from the complementary chain (**Figure 10A**). This two-fold incompatability is likely prevents formation of a stable homodimer by this mutant. Another interesting observation was the inability of the mutant W123* to form a homodimer. In the wild-type structure, prolines 124 and 125 in the C-terminal loop provide both excellent shape complementarity and necessary rigidity for stabilization via a crossover interaction that results in the terminus being squarely packed against the opposite monomer (**Figure 10B**). In addition, the free carboxylate of Glycine 126 (Chain A) can form an electrostatic interaction with R119 (Chain B), and the backbone amide nitrogen of Histidine 122 (Chain A) can also interact with one of the oxygen atoms in the free carboxylate of G126 (Chain B). Attempts to alter any of the three residues in the loop with alanine resulted in the destabilization of the dimer. (**Figure 10B**).

We also assessed the nucleoside phosphoramidase activity of the monomeric mutants G93D and W123* using steady-state kinetic analysis. The catalytic turnover rate (K_{cat}) was decreased by 130-fold for G93D and 60-fold for W123* mutant, while the Michaelis-Menten constants (K_m) were increased by 10- to 40-fold in these mutants compared to wild type. The mutants are clearly less effective phosphoramidases, as indicated by their overall decrease in kinetic specificity (K_{cat}/K_m). These results suggest that the dimeric structure is critical for the molecular recognition of the nucleoside monophosphate. Consistent with this result, we saw little or no increase from baseline upon incubation of our switch-on fluorescence probe upon incubation with the

monomeric mutants.

The hHint1 mutations H112N, G89V, and C84R were all found to be dimeric. Mutant H112N has been previously reported to exhibit increased affinity for the nucleoside monophosphates and has a nearly identical x-ray crystal structure as with the wild-type hHint1. Glycine 89 resides in the loop connecting the long alpha helix to the last β-strand. Mutation of this glycine with a bulkier hydrophobic and bulkier residue was tolerated without impact on the dimerization of hHint1. The C84R mutation resides in the long alpha helix at the dimeric interface, and it was found to retain the dimeric structure. Our kinetic analysis demonstrated equivalent enzymatic activity of the C84R and G89V mutants compared to the wild-type hHint1. Nevertheless, we observe decreased thermal stability of all the mutants compared to wild-type hHint1. A high-resolution X-ray crystal structure of the C84R mutant reveals no significant changes due to the mutation, consistent with kinetic studies. Only a minor change was observed due to the cysteine to arginine mutation.

The lack of neuropathy symptoms in HINT1$^{-/-}$ mice indicates that mice can compensate the loss of Hint1 better than humans. However, such compensation may be difficult to detect, as the site of action is restricted to neuronal cells in this application and because the identity of the biochemical substrate of hHint1 is unknown. There has been speculation about the possible endogenous substrates, such as AP_4A, in regulating hHint1 interaction with transcription factors in tumor cells [16]. The role of cyclic-AMP in the downstream regulation of GPCR signaling pathway and levels of AMP upon phosphodiesterase is well known [17]. It is also possible that the levels of endogenous

nucleoside monophosphate could regulate hHint1 interactions and function in CNS. From the x-ray crystal structure, it is quite evident that nucleoside-binding motif could govern its *in vivo* function.

In the current study, we chose to evaluate the role of the key residues involved in the molecular recognition of the nucleoside monophosphate. Results from the previous ^{1}H-^{15}N HSQC experiments clearly indicate a significant shift in the Ile44 indicating the potential role of this residue in stacking with the nucleobase. We mutated residue 44 to larger hydrophobic rings such as phenylalanine and tryptophan. The results indicate a significant change in the catalytic specificity with increasing the size of the ring. One explanation is that incorporating the bulkier group hinders the binding of an incoming nucleobase. The molecular recognition of both the substrate and product by hHint1 relies heavily on the interaction of residue 44 with the nucleobase. It is possible that the decrease in the K_{cat} for both the mutants is due to increase in the hydrophobic stacking interaction that impacts the release of the product in the final step.

We next investigated the important interaction of the 2′- and 3′-hydroxyl groups in the ribose sugar with Asp43. This interaction is clearly important since it is conserved in all the x-ray crystal structures published of hHint1 to date. We mutated the negative charged aspartate to a neutral asparagine (D43N) to alter the electrostatics of the interaction. The mutation had significantly impacted the recognition of the nucleobase as indicated by a 50-fold decrease in K_m value and an increase in K_{cat} values by 2- to 3-fold in our kinetic assay. These results are consistent with our previous observation that decreases in NMP affinity for the active site can lead to the faster release of the product in the rate-limiting

step of hHint1 catalysis. It is clear that molecular recognition and occupancy of nucleoside drives the kinetics of hHint1 and potentially its endogenous function via nucleoside-containing ligands or substrates.

While the endogenous function and substrate(s) of hHint1 remain unknown, we have recently shown that pharmacological inhibition of hHint1 could block the activation of the NMDAR function [15]. How the catalytic activity of hHint1 is involved in the regulation of CNS functions and disorders including peripheral neuropathy have remained a mystery. We have performed a detailed structural and *in vitro* functional characterization of hHint1 in the current work. The knowledge gained from the study of these mutations could be applied to develop genetic mutant mouse models to understand the pathophysiology of peripheral neuropathy as well as the role of hHint1 in neuropathic pain. Of certain interest are two mutants, C84R and G89V, which retain both quaternary structure and catalytic activity; these mutants may be essential in understanding the role of hHint1 in the pathophysiology of peripheral neuropathy. Future work includes electrophysiological and genetic experiments to link activity and dimeric structure of hHint1 to the *in vivo* function unrelated to catalysis.

Materials and Methods

General Methods and Materials:

Nickel nitrilotriacetic acid (Ni-NTA) was purchased from Qiagen and maltose binding amylose agarose from New England Bio labs. Biological buffers were purchased from Sigma-Aldrich. Protease inhibitor tablets were obtained from Roche.

Cloning and construction of the MBP-hHint1 plasmid:

The full-length gene for human histidine triad nucleotide binding protein 1 (*HINT1*) was obtained in a pGSA02 vector, and it was amplified by the polymerase chain reaction (PCR) using Pfu Turbo (Agilent Technologies) and the primer pairs hHint1_WT_F and hHint1_WT_R (Integrated DNA Technologies). The PCR products were separated by gel electrophoresis, and then the product of interest was purified from the agarose gel (Zymoclean™ Gel DNA Recovery Kit, Zymo Research). The hHint1_MBP construct was prepared for insertion into ligation-independent cloning (LIC) site of the pMCSG9 vector[18, 19] by treatment with T4 polymerase (Promega), then introduced into a pMCSG9 vector (N-terminal, Tobacco Etch Virus (TEV) cleavable Maltose Binding Protein fusion; ampicillin resistance) that had been opened with *SspI* and also prepared with T4 polymerase.

The hHint1_MBP-containing vectors were transformed into *E. coli* XL1 Blue supercompetent cells (prepared with Z-Competent™ *E. coli* Transformation Kit, Zymo Research) according to the manufacturer's instructions. Clones positive for the vector were selected on ampicillin agar and confirmed by colony PCR with PCR Supermix (Invitrogen), the TEV_forward primer, and the T7_reverse primer (Integrated DNA

Technologies), and a positive, confirmed clone was grown 5 mL LB broth with 100μg/mL ampicillin; the plasmids were then harvested (Zyppy™ Plasmid Miniprep Kit, Zymo Research). The gene sequences were verified by DNA sequencing (Biomedical Genomics Center, University of Minnesota). The plasmid was transformed into *Escherichia coli* BL21 (DE3) Rosetta2 pLysS (chloramphenicol resistant) supercompetent cells (prepared with Z-Competent™ *E. coli* Transformation Kit, Zymo Research) according to the manufacturer's instructions. Positive clones were selected on ampicillin plus chloramphenicol agar.

Primers:

hHint1_WT_F: 5' ACTTCCAATCCAATGCCATGGCAGATG

hHint1_WT_R: 5' TTATCCACTTCCAATGCTATTAACCAG

T7_forward: 5' GGTACCGAGAACCTGTACTTCCAATCCAAT

T7_reverse: 5' GCTAGTTATTGCTCAGCGG

Protein Expression and Purification:

The full-length sequence of hHint1 was expressed from the pMCSG9 vector (N-terminal His_6 tag, Maltose binding protein followed a tobacco etch virus (TEV) protease cleavable linker followed by hHint1) in BL21 (DE3) pLysS cells. The cells were grown in 2 x 1L LB (Fisher Scientific) media with ampicillin (100 mg/L, Sigma-Aldrich) at 37 °C with shaking at 250 rpm. At OD_{600} = 0.7, cultures were induced to a final concentration of 1 mM IPTG (Denville Scientific Inc) and incubated at 30°C overnight. The cultures were harvested by centrifugation at 7,500 *g* at 4 °C for 10 min and the pellets were collected, then resuspended in buffer A (50 mM HEPES pH 7.0, 300 mM NaCl, 10% glycerol,

10 mM imidazole), which was then adjusted to 1 $mg \cdot mL^{-1}$ lysozyme and 1X protease inhibitor from the 100X cocktail stock. The resuspended cells were lysed by sonication (eight cycles of 30 s on, 30 s off) at 4 °C. The cell debris was removed from the lysate by centrifugation at 16,000 *g* at 4 °C for 45 min. The supernatant was loaded onto a nickel affinity column, washed with buffer A, and then eluted with an imidazole gradient using buffer B (50 mM HEPES pH 7.0, 300 mM NaCl, 10% glycerol, 250 mm imidazole). Fractions containing desired protein were combined, buffer exchanged (20 mM Tris, 150 mM NaCl, 1 mM DTT, 1mM $MgCl_2$ at pH 7.4) and a portion was reserved to perform size exclusion chromatography. To the other portion was added N-terminally His-tagged TEV protease 2% (w/w) to cleave the MBP from the fusion protein. The resulting solution was transferred to a dialysis tubing (molecular weight cut-off of 6000-7000 Da) and dialyzed against 2 L of TEV cleavage buffer (50 mM HEPES pH 7.0, 300 mM NaCl, 10% glycerol, 0.5 mM EDTA and 1 mM DTT) overnight at 4 °C. The dialyzed protein was then buffer exchanged into buffer A and passed through Ni-NTA affinity chromatography to remove TEV protease and maltose binding protein. The fractions containing protein were collected and concentrated. The protein concentration was then determined using A_{280} absorbance using calculated extinction coefficient of 8480 M^{-1} cm^{-1} and molecular weight of 14000 Da. The purity of the protein was determined using SDS page analysis. The final protein was stored at −80 °C until in use.

In the H112N preparation, the protein was refolded to remove a co-purified nucleotide contaminant. To refold the protein, the pooled fractions were first dialyzed (NMWCO = 10000 Da, Thermo dialysis cassette) against SEC buffer with the addition of 8 M urea (J.T. Baker) overnight at room temperature. This procedure was repeated at 4

°C with decreasing concentrations of urea: 4 M, 2 M, and 0 M to fully refold the protein and remove the urea. The folding of the protein was confirmed using differential scanning fluorimetry. The protein was concentrated to A_{280} = 10, aliquotted, and frozen.

X-ray crystallography:

Crystals of hHint1 C84R were prepared using hanging-drop vapor diffusion at 20 °C. For crystallization, drops were set up consisting of 2 uL of protein (A_{280} = 5) and 2 uL of well solution (1 M HEPES (Sigma) pH 7.0, PEG 8K (Acros Organics) 35%). The crystal was then transferred to a solution containing the mother liquor supplemented with 20% PEG 400, followed by flash vitrification in liquid nitrogen.

Data for structure were collected at ALS Beamline 4.2.2. The data were processed using AutoPROC.[20] The data were processed using hkl2000.[21][ref] The structures were solved using Phaser[22] and the coordinates from structure 3TW2.[23] The structures were refined using REFMAC5[24] in the CCP4 suite[25] and Phenix,[26] and they were visualized and modified using coot.[27] Ligand restraints were calculated using JLigand[28] or elbow.

Steady state kinetic measurement with the fluorescence assay:

Steady-state kinetic studies were carried out with fluorogenic adenylate and phosphoramidate substrates as previously described.[11] The excitation wavelength was set at 280 nm, fluorescence emission was measured at 360 nm, and excitation and emission slits were set at 10 nm for concentration of the adenylate substrate ranging from 0.5 to 2 μM in HEPES buffer (20 mM, pH 7.2) or 5 nm for concentration ranging from 10 to 50 μM in HEPES buffer containing 1 mM $MgCl_2$. The fluorescence intensity was monitored

for 2 min to obtain the baseline and to allow the temperature to stabilize at 25 °C, and then enzyme (2 or 50 pmol) was added to initiate reactions. The Michaelis–Menten constants, K_{cat} (s^{-1}) and K_m (μM), were deter- mined by JumpIN nonlinear regression. Variants represented standard deviations of the fit.

Circular dichroism spectroscopy:

CD spectra of proteins were obtained at 23 °C with a J710 spectropolarimeter (Jasco). Proteins at concentrations of 10-15 μM in sodium phosphate buffer (10 mM, 150 mM NaCl, pH 7.2) were analyzed in a quartz cuvette with path length of 1 mm, and spectra were accumulated and averaged over nine scans. Using Excel program performed subtraction of buffer background from the protein spectrum.

Size Exclusion Chromatography:

The apparent molecular weight of recombinant purified proteins was analyzed by analytical gel filtration chromatography on Superdex 200 size exclusion columns (GE Healthcare). The proteins were eluted with P500 buffer (0.5 M NaCl, 50 mM potassium phosphate, 1 mM EDTA, pH 7.0, filtered through a 0.02 μm filter) as described. Retention times were monitored by protein absorbance (absorbance 280 nm).

Fluorescence Spectroscopy: hHint1 mutants-ligand binding studies with switch-on probes

All fluorescence measurements were performed in an aqueous assay buffer (20 mM Tris, 150 mM NaCl pH 7.4). All fluorescence measurements were performed in a 1 cm four sided, 2 ml quartz cuvette. 600 μl of the total sample solution including the protein and

ligand was used in the cuvettes to perform fluorescence measurements. All the readings were recorded at room temperature. The excitation and emission wavelengths and the slit width are described in the legends of the respective figures. The excitation wavelength for the switch-on probe was 330 nm and the emission spectral scan was recorded from 360-530 nm as described previously. A 12 μM of the probe was incubated with 1 μM of the mutant protein and the fluorescence increase in the intensity was recorded. The control measurement is performed in the absence of the protein. The increase in the fluorescence intensity in the presence of the mutant protein was compared to the wild type protein and the relative fold increase was plotted as the bar graph measurement. The concentration of the protein was determined using both using a NanoDrop 1000 instrument (Thermo Scientific) and a BCA assay.

References:

1. Saporta, M. A.; Shy, M. E., Inherited peripheral neuropathies. *Neurol Clin* **2013,** *31* (2), 597-619.
2. Ouvrier, R.; Geevasingha, N.; Ryan, M. M., Autosomal-recessive and X-linked forms of hereditary motor and sensory neuropathy in childhood. *Muscle Nerve* **2007,** *36* (2), 131-43.
3. Suter, U.; Scherer, S. S., Disease mechanisms in inherited neuropathies. *Nat Rev Neurosci* **2003,** *4* (9), 714-26.
4. Saporta, A. S.; Sottile, S. L.; Miller, L. J.; Feely, S. M.; Siskind, C. E.; Shy, M. E., Charcot-Marie-Tooth disease subtypes and genetic testing strategies. *Ann Neurol* **2011,** *69* (1), 22-33.
5. Wuttke, T. V.; Jurkat-Rott, K.; Paulus, W.; Garncarek, M.; Lehmann-Horn, F.; Lerche, H., Peripheral nerve hyperexcitability due to dominant-negative KCNQ2 mutations. *Neurology* **2007,** *69* (22), 2045-53.
6. Dedek, K.; Kunath, B.; Kananura, C.; Reuner, U.; Jentsch, T. J.; Steinlein, O. K., Myokymia and neonatal epilepsy caused by a mutation in the voltage sensor of the KCNQ2 K+ channel. *Proc Natl Acad Sci U S A* **2001,** *98* (21), 12272-7.
7. Zimoń, M.; Baets, J.; Almeida-Souza, L.; De Vriendt, E.; Nikodinovic, J.; Parman, Y.; Battaloğlu, E.; Matur, Z.; Guergueltcheva, V.; Tournev, I.; Auer-Grumbach, M.; De Rijk, P.; Petersen, B. S.; Müller, T.; Fransen, E.; Van Damme, P.; Löscher, W. N.; Barišić, N.; Mitrovic, Z.; Previtali, S. C.; Topaloğlu, H.; Bernert, G.; Beleza-Meireles, A.; Todorovic, S.; Savic-Pavicevic, D.; Ishpekova, B.; Lechner, S.; Peeters, K.; Ooms, T.; Hahn, A. F.; Züchner, S.; Timmerman, V.; Van Dijck, P.; Rasic, V. M.; Janecke, A. R.; De Jonghe, P.; Jordanova, A., Loss-of-function mutations in HINT1 cause axonal neuropathy with neuromyotonia. *Nat Genet* **2012,** *44* (10), 1080-3.
8. Zhao, H.; Race, V.; Matthijs, G.; De Jonghe, P.; Robberecht, W.; Lambrechts, D.; Van Damme, P., Exome sequencing reveals HINT1 mutations as a cause of distal hereditary motor neuropathy. *Eur J Hum Genet* **2014,** *22* (6), 847-50.
9. Laššuthová, P.; Brožková, D.; Krůtová, M.; Neupauerová, J.; Haberlová, J.; Mazanec, R.; Dvořáčková, N.; Goldenberg, Z.; Seeman, P., Mutations in HINT1 are one of the most frequent causes of hereditary neuropathy among Czech patients and neuromyotonia is rather an underdiagnosed symptom. *Neurogenetics* **2015,** *16* (1), 43-54.
10. Boaretto, F.; Cacciavillani, M.; Mostacciuolo, M. L.; Spalletta, A.; Piscosquito, G.; Pareyson, D.; Vazza, G.; Briani, C., Novel loss-of-function mutation of the HINT1 gene in a patient with distal motor axonal neuropathy without neuromyotonia. *Muscle Nerve* **2015,** *52* (4), 688-9.
11. Chou, T. F.; Baraniak, J.; Kaczmarek, R.; Zhou, X.; Cheng, J.; Ghosh, B.; Wagner, C. R., Phosphoramidate pronucleotides: a comparison of the phosphoramidase substrate specificity of human and Escherichia coli histidine triad nucleotide binding proteins. *Mol Pharm* **2007,** *4* (2), 208-17.

12. Seburn, K. L.; Morelli, K. H.; Jordanova, A.; Burgess, R. W., Lack of neuropathy-related phenotypes in hint1 knockout mice. *J Neuropathol Exp Neurol* **2014,** *73* (7), 693-701.
13. Bai, G.; Feng, B.; Wang, J. B.; Pozharski, E.; Shapiro, M., Studies on ligand binding to histidine triad nucleotide binding protein 1. *Bioorg Med Chem* **2010,** *18* (18), 6756-62.
14. Rodríguez-Muñoz, M.; Sánchez-Blázquez, P.; Vicente-Sánchez, A.; Bailón, C.; Martín-Aznar, B.; Garzón, J., The histidine triad nucleotide-binding protein 1 supports mu-opioid receptor-glutamate NMDA receptor cross-regulation. *Cell Mol Life Sci* **2011,** *68* (17), 2933-49.
15. Garzón, J.; Herrero-Labrador, R.; Rodríguez-Muñoz, M.; Shah, R.; Vicente-Sánchez, A.; Wagner, C. R.; Sánchez-Blázquez, P., HINT1 protein: a new therapeutic target to enhance opioid antinociception and block mechanical allodynia. *Neuropharmacology* **2015,** *89*, 412-23.
16. Yannay-Cohen, N.; Razin, E., Translation and transcription: the dual functionality of LysRS in mast cells. *Mol Cells* **2006,** *22* (2), 127-32.
17. Lodish H; Berk A; SL, Z., *Molecular Cell Biology.* 4th edition. ed.; New York: W. H. Freeman: 2000; p Section 20.3.
18. Eschenfeldt, W. H.; Lucy, S.; Millard, C. S.; Joachimiak, A.; Mark, I. D., A family of LIC vectors for high-throughput cloning and purification of proteins. *Methods Mol Biol* **2009,** *498*, 105-15.
19. Stols, L.; Zhou, M.; Eschenfeldt, W. H.; Millard, C. S.; Abdullah, J.; Collart, F. R.; Kim, Y.; Donnelly, M. I., New vectors for co-expression of proteins: structure of Bacillus subtilis ScoAB obtained by high-throughput protocols. *Protein Expr Purif* **2007,** *53* (2), 396-403.
20. Vonrhein, C.; Flensburg, C.; Keller, P.; Sharff, A.; Smart, O.; Paciorek, W.; Womack, T.; Bricogne, G., Data processing and analysis with the autoPROC toolbox. *Acta Crystallogr D Biol Crystallogr* **2011,** *67* (Pt 4), 293-302.
21. Otwinowski, Z.; Minor, W., [20] Processing of X-ray diffraction data collected in oscillation mode. *Methods Enzymol* **1997,** *276*, 307-326.
22. McCoy, A. J.; Grosse-Kunstleve, R. W.; Adams, P. D.; Winn, M. D.; Storoni, L. C.; Read, R. J., Phaser crystallographic software. *J Appl Crystallogr* **2007,** *40* (Pt 4), 658-674.
23. Dolot, R.; Ozga, M.; Włodarczyk, A.; Krakowiak, A.; Nawrot, B., A new crystal form of human histidine triad nucleotide-binding protein 1 (hHINT1) in complex with adenosine 5'-monophosphate at 1.38 Å resolution. *Acta Crystallogr Sect F Struct Biol Cryst Commun* **2012,** *68* (Pt 8), 883-8.
24. Murshudov, G. N.; Skubák, P.; Lebedev, A. A.; Pannu, N. S.; Steiner, R. A.; Nicholls, R. A.; Winn, M. D.; Long, F.; Vagin, A. A., REFMAC5 for the refinement of macromolecular crystal structures. *Acta Crystallogr D Biol Crystallogr* **2011,** *67* (Pt 4), 355-67.
25. Winn, M. D.; Ballard, C. C.; Cowtan, K. D.; Dodson, E. J.; Emsley, P.; Evans, P. R.; Keegan, R. M.; Krissinel, E. B.; Leslie, A. G.; McCoy, A.; McNicholas, S. J.; Murshudov, G. N.; Pannu, N. S.; Potterton, E. A.; Powell, H. R.; Read, R. J.; Vagin, A.; Wilson, K. S.,

Overview of the CCP4 suite and current developments. *Acta Crystallogr D Biol Crystallogr* **2011,** *67* (Pt 4), 235-42.
26. Adams, P. D.; Afonine, P. V.; Bunkóczi, G.; Chen, V. B.; Davis, I. W.; Echols, N.; Headd, J. J.; Hung, L. W.; Kapral, G. J.; Grosse-Kunstleve, R. W.; McCoy, A. J.; Moriarty, N. W.; Oeffner, R.; Read, R. J.; Richardson, D. C.; Richardson, J. S.; Terwilliger, T. C.; Zwart, P. H., PHENIX: a comprehensive Python-based system for macromolecular structure solution. *Acta Crystallogr D Biol Crystallogr* **2010,** *66* (Pt 2), 213-21.
27. Emsley, P.; Cowtan, K., Coot: model-building tools for molecular graphics. *Acta Crystallogr D Biol Crystallogr* **2004,** *60* (Pt 12 Pt 1), 2126-32.
28. Lebedev, A. A.; Young, P.; Isupov, M. N.; Moroz, O. V.; Vagin, A. A.; Murshudov, G. N., JLigand: a graphical tool for the CCP4 template-restraint library. *Acta Crystallogr D Biol Crystallogr* **2012,** *68* (Pt 4), 431-40.